UC Santa Barbara
UC Santa Barbara Electronic Theses and Dissertations

Title
Aspects of Emergent Geometry, Strings, and Branes in Gauge / Gravity Duality

Permalink
https://escholarship.org/uc/item/8qh706tk

Author
Dzienkowski, Eric Michael

Publication Date
2015

Peer reviewed|Thesis/dissertation

eScholarship.org Powered by the California Digital Library
University of California

University of California
Santa Barbara

Aspects of Emergent Geometry, Strings, and Branes in Gauge / Gravity Duality

A dissertation submitted in partial satisfaction
of the requirements for the degree

Doctor of Philosophy
in
Physics

by

Eric Michael Dzienkowski

Committee in charge:

Professor David Berenstein, Chair
Professor Joe Polchinski
Professor David Stuart

September 2015

The Dissertation of Eric Michael Dzienkowski is approved.

Professor Joe Polchinski

Professor David Stuart

Professor David Berenstein, Committee Chair

July 2015

Aspects of Emergent Geometry, Strings, and Branes in Gauge / Gravity Duality

Copyright © 2015

by

Eric Michael Dzienkowski

To my family, who endured my absense for the better part of nine long years while I attempted to understand the universe.

Acknowledgements

There are many people and entities deserving thanks for helping me complete my dissertation.

To my advisor, David Berenstein, for the guidance, advice, and support over the years. With any luck, I have absorbed some of your unique insight and intuition to solving problems, some which I hope to apply to my future as a physicist or otherwise.

A special thanks to my collaborators Curtis Asplund and Robin Lashof-Regas. Curtis, it has been and will continue to be a pleasure working with you. Additional thanks for various comments and discussions along the way to Yuhma Asano, Thomas Banks, Frederik Denef, Jim Hartle, Sean Hartnoll, Matthew Hastings, Gary Horowitz, Christian Maes, Juan Maldacena, John Mangual, Don Marolf, Greg Moore, Niels Obers, Joe Polchisnki, Jorge Santos, Edward Shuryak, Christoph Sieg, Eva Silverstein, Mark Srednicki, and Matthias Staudacher.

I was very fortunate to have the opportunity to interact with many talented physicists. As such, I would like to thank the members of the Gravity / High Energy Theory group at UCSB and the KITP for their contribution to my education. A particular thanks to Joseph Polchinski and David Stuart for serving on my committee.

I would like to thank my friends and fellow graduate students, especially those who reside with me on the sixth floor of Broida, and in particular, Sebastian Fischetti, Keith Fratus, and Eric Mintun. Thank you for the many useful discussions and insights, and for sharing many working nights.

To my family, for their tremendous amount of support and understanding from

2700 miles away while I accomplished this goal.

Work of E.D. supported by the Department of Energy Office of Science Graduate Fellowship Program (DOE SCGF), made possible in part by the American Recovery and Reinvestment Act of 2009, administered by ORISE-ORAU under contract no. DE-AC05-06OR23100. Work also supported in part by DOE grant DE-FG02-91ER40618, and grant DE-SC0011702. Work also supported in part by the National Science Foundation grant no. Phy05-51164, and grant no. PHYS-1066293. Work additionally supported by the FWO - Vlaanderen, Project No. G.0651.11 and the Odysseus program, by the Federal Office for Scientific, Technical and Cultural Affairs through the Interuniversity Attraction Poles Programme Belgian Science Policy P7/37, the European Science Foundation Holograv Network and by a grant from the John Templeton Foundation. The opinions expressed in this publication are those of the authors and do not necessarily reflect the views of the John Templeton Foundation. The research leading to some of these results has received funding from the European Research Council under the European Communitys Seventh Framework Programme (FP7/2007-2013) / ERC grant agreement no. [247252].

Curriculum Vitæ

Eric Michael Dzienkowski

Education

2015	Ph.D. in Physics (Expected), University of California, Santa Barbara.
2010	M.S. in Physics, Rensselaer Polytechnic Institute.
2010	B.S. in Physics and Mathematics, Rensselaer Polytechnic Institute.

Publications

[1] E. Dzienkowski, *Excited States of Open Strings from* $\mathcal{N} = 4$ *SYM*, arXiv:1507.01595

[2] D. Berenstein, E. Dzienkowski, and R. Lashof-Regas, *Spinning the Fuzzy Sphere*, arXiv:1506.0172.

[3] D. Berenstein and E. Dzienkowski, *Giant gravitons and the emergence of geometric limits in beta-deformations of* $N = 4$ *SYM*, *JHEP* **1501** (2015) 126, [arXiv:1408.3620].

[4] D. Berenstein and E. Dzienkowski, *Numerical Evidence for Firewalls*, arXiv:1311.1168.

[5] D. Berenstein and E. Dzienkowski, *Open spin chains for giant gravitons and relativity*, *JHEP* **1308** (2013) 047, [arXiv:1305.2394].

[6] C. T. Asplund, D. Berenstein, and E. Dzienkowski, *Large* N *classical dynamics of holographic matrix models*, *Phys. Rev.* D**87** (2013), no. 8 084044, [arXiv:1211.3425].

[7] D. Berenstein and E. Dzienkowski, *Matrix embeddings on flat* R^3 *and the geometry of membranes*, *Phys. Rev.* D**86**, 086001 (2012) [arXiv:1204.2788].

Abstract

Aspects of Emergent Geometry, Strings, and Branes in Gauge / Gravity Duality

by

Eric Michael Dzienkowski

We explore the emergence of locality and geometry in string theories from the perspective of gauge theories using gauge / gravity duality.

First, we explicitly construct open strings stretched between giant gravitons in $\mathcal{N} = 4$ SYM. We find that these strings satisfy a relativistic dispersion relation up to three-loop order and conjecture that this should hold to all loop orders. We find the explicit dual solution to the string sigma model and find exact agreement with the geometric nature of the SYM operator and dispersion relation. Using these open strings as probes, we explore the local field theory on the worldvolume of the giant gravitons.

Second, we use classical configurations in holographic matrix models to understand the emergence of geometry from matrix coordinates. We construct an effective Hamiltonian for a probe brane that observes the geometry in a background matrix configuration from which we can construct membranes embedded in three dimensional space. Adding angular momentum to these configurations we are able to observe continuous topology changes. We also study the classical evolution of holographic matrix models to generate a microcanonical ensemble of configurations and study their thermal and chaotic behavior. We argue that these thermal configurations are dual to black holes.

Contents

Curriculum Vitae **vii**

Abstract **viii**

1 Introduction **1**
1.1 Permissions and Attributes 8

Part I Open Strings in AdS / CFT **10**

2 Introduction **11**

3 Anomalous Dimensions of Open Strings **17**
3.1 The $\mathfrak{su}(2)$ Sector 17
3.2 Giant Gravitons and Open Strings 20
3.3 Strings as Cuntz Oscillator Chains 25
3.4 The Cuntz Hamiltonian 30
3.5 Discussion 52

4 Exploring the Ground State **56**
4.1 Finding the Ground State 56
4.2 Geometry from Giant Gravitons and Strings 59
4.3 Correcting the Ground State 65
4.4 A Relativistic Dispersion Relation 80
4.5 The Open String Dual 92
4.6 Discussion 98

5 Emergence of Geometric Limits in $\mathcal{N} = 4$ SYM **102**
5.1 Marginal Deformations of $\mathcal{N} = 4$ SYM 102

5.2 The β-Deformed Cuntz Chain 109
5.3 Geometric Limit Interpretation 113
5.4 Discussion 121

Part II Geometry from Matrix Models 123

6 Introduction 124

7 The Geometry of Membranes 131
7.1 Orbifolding The BFSS and BMN Matrix Models 131
7.2 The Index: Adding a D0-brane Probe 137
7.3 Fuzzy Spheres and Emergent Surfaces 147
7.4 A Linking Number 154
7.5 Discussion 161

8 Classical Dynamics of Holographic Matrix Models 165
8.1 Observables and Symmetry 165
8.2 Numerical Implementation 172
8.3 Thermalization 177
8.4 Power Spectra and Classical Chaos 188
8.5 Factorization 200
8.6 Discussion 206

9 Black Holes From Matrix Models 208
9.1 Gravity From Matrix Models 209
9.2 Aspects of Matrix Black Holes 214
9.3 Exploring the Gapless Region 218
9.4 Locating the Horizon 226
9.5 Discussion 229

10 Adding Angular Momentum 232
10.1 The Hamiltonian and the Ansatz 233
10.2 Symmetry Considerations 240
10.3 The Solutions as a Set of Critical Points 245
10.4 The case of 2×2 matrices 251
10.5 The case of 3×3 matrices 255
10.6 Other Examples 264
10.7 Large N 266
10.8 Topology Change 274

10.9 Discussion 278

11 Conclusions **282**

A Conventions and Relations for the Lie Algebra of $U(N)$ **285**

B Cuntz Algebra and Hamiltonians **288**
B.1 Cuntz Oscillators 288
B.2 Closed Cuntz Hamiltonians 290
B.3 Open Cuntz Hamiltonians 291

C Proof of First Order Ground State Correction **293**

D BFSS and BMN model conventions **295**

E Fermion Decomposition **298**

F Fermionic Modes Between Displaced Fuzzy Spheres **300**
F.1 Diagonal Fermionic Modes 300
F.2 Off-diagonal modes 303

G Measuring the Temperature **306**

Bibliography **308**

Chapter 1

Introduction

Quantum mechanics has been a powerful framework for building physical models of the universe that describe phenomena which occur at length scales comparable to that of an atom. It has a tremendous range of applicability, from the electronics in our mobile devices to processes occurring at the center of our Sun. It has revolutionized the way we understand particles and measurements. We learned that particle and wave like behavior have a unified description called the wave function. The act of measuring once can change the outcome of future measurements. These notions challenge our classical understanding of the world and have truly affected the way we interpret reality.

As we probed nature over the past century, we determined that many of the observed phenomena were due to the following four fundamental interactions: electromagnetic, weak, strong, and gravitational. The first three of these interactions have a very good quantum mechanical description called the Standard Model of particle physics. The Standard Model outlines the fundamental constituents of matter and their dynamics involving the first three of the four fundamental interactions. It is incredibly accurate in predicting what happens in the universe at length scales as small as 10^{-18} m. Gravity, the fourth fundamental interaction, has a different story to tell.

Einstein's theory of general relativity has provided an excellent classical description of gravity for about one hundred years. Like quantum mechanics, it has revolutionized the way interpret our universe. We learned that space and time are not separate entities, but have a unified description as a smooth manifold and should be regarded simply as spacetime. Geometry is encoded in a local gravitational field, the dynamics of which are governed by local energy and momentum densities. Spacetime possesses a curvature which can be measured in the presence of many observers. The successes of general relativity appear at length scales greater than those of quantum mechanics, from Global Positioning Systems (GPS), to the precession of Mercury's orbit around the Sun, and all the way to the configuration of the cosmos.

However, general relativity is not a perfect theory. Solutions to Einstein's equations exist for which the curvature of spacetime is smooth except within some subset of the spacetime for which the curvature diverges. The classical theory of general relativity is incapable of describing the physics at these subsets of diverging curvature, called singularities. Black holes can form when there is enough energy in too small a region of spacetime and some of these solutions have singularities residing at their center. Since we believe to observe black holes in nature, we are obliged to decode the singularity. Singularities are generally characterized by the presence a strong gravitational field occurring at small length scales. Therefore, if we wish to understand the nature of the singularity, we must quantize gravity.

At this point it is important to note which properties of spacetime and gravity we begin to lose when we consider the quantum theory. Suppose we did have a theory of quantum gravity that could describe singularities. We can not recover the metric at the singularity in the classical limit, $\hbar \to 0$, because the metric is not smooth there. Thus the singularity is not geometric. Regions of large curvature near the singularity in the classical theory will then also lose their geometric nature in the quantum theory. We can slowly move away from regions of large curvature to regions of small curvature. We expect the non-geometric nature of the quantum theory to dissipate as we transition from one region to the other. However, this is not guaranteed and thus we lose some notion of geometry in a quantum theory of gravity. Interesting questions arise such as what are the degrees of freedom of quantum gravity, when can we recover geometry from them, and how can we do it?

Black holes pose another interesting problem. The event horizon is a barrier between the interior and exterior of a black hole which prevents light from escaping a black hole. At the horizon spacetime is perfectly smooth, and so it is appropriate to apply the techniques of quantum field theory there. Doing so Hawking showed that black holes radiate [8]; light, and more generally energy, can cross the event horizon and escape from a black hole. This is a contradiction! In particular it violates locality, the idea that events in spacetime which are spacelike separate have no effect on each other. The classical theory of general relativity is a local theory and thus possesses no mechanism by which locality can be violated. We hope that a quantum theory can resolve this issue.

Unlike the electromagnetic, weak, and strong forces, quantizing gravity is a difficult task. The first three forces also have descriptions in terms of local field theories. Infinities appear during the quantization procedure of these field theories, but they can be absorbed into a finite number of counterterms dependent on some energy scale. This is called renormalizing the theory and the process renders calculations finite and useful. General relativity requires an infinite number of counterterms to render the theory finite and is thus non-renormalizable; the theory is only effective up to some energy scale. If we with to understand quantum gravity, we need something else. There are several proposals for describing gravity including, but not limited to, superstring theory [9, 10], loop quantum gravity [11], and causal dynamical triangulation [12]. To date, superstring theory poses the best solution to the problem of quantizing gravity: the theory reproduces Einstein's equations (or some supersymmetric form of them), the theory is finite, and computations are tractable in many scenarios. Unfortunately, superstring theory nor any of its four-dimensional compactifications have yet to be experimentally verified or falsified.

Gauge / gravity duality and holography are developing concepts in recent decades that have either provided us insights into what a quantum theory of gravity should look like or have directly told what the degrees of freedom in quantum gravity are. At the heart of these concepts is a theory of quantum gravity in some number dimensions being 'dual' to a typical quantum field theory in some lower number of dimensions. These quantum field theories are typically conformal field theories, where the spacetime and the fields possess additional symmetries to the usual Poincaré ones. The quantum field theories are also like the ones that describe the electromagnetic, weak, and strong forces; they are gauge theories. The meaning of 'dual' is different with every pair of gauge /

gravity theories, but generally means that the dynamics in one theory have some approximate translation into the dynamics of the other. The exactness of each translation can be quantified in many cases and determines how strong the duality really is.

An explicit example of gauge / gravity duality is the AdS / CFT correspondence [13]. The strongest form of the conjecture is a quantum mechanical one. Quantum Type IIB superstring theory in an asymptotically $AdS_5 \times S^5$ background with background five-form flux (the gravity theory) is dual to the superconformal phase of $\mathcal{N} = 4$ Supersymmetric Yang-Mills (SYM) theory with gauge group $U(N)$ (the gauge theory). Here, dual means that there is an dictionary between objects in the string theory and states (operators) in the gauge theory. The stringy objects and the gauge theory operators should have the same energy. Furthermore, we expect that the dynamics of each theory should preserve the dictionary.

The parameters characterizing the string theory are the AdS radius R, the inverse string tension α', the string coupling g_s, and the amount of five form flux on the sphere N. In the gauge theory we have the rank of the gauge group N, and the Yang-Mills coupling constant g_{YM}. Often we combine the two to form the 't Hooft coupling $\lambda = g_{\mathrm{YM}}^2 N$. The duality relates these parameters through the relations

$$\lambda = \frac{R^4}{\alpha'^2}, \quad \frac{\lambda}{4\pi N} = \frac{g_{\mathrm{YM}}^2}{4\pi} = g_s \tag{1.1}$$

If we keep λ finite and take $N \to \infty$, then $g_s \to 0$ and we recover the weak coupling limit of string theory. The weak coupling limit of string theory is just the classical sigma model on $AdS_5 \times S^5$. The large N limit in the gauge theory allows us to keep only planar Feynman diagrams and is called the planar limit. At this level of the conjecture the duality becomes a statement about the equivalence of the sigma model and the planar gauge theory. After taking the planar limit, we may then take the large λ limit, which corresponds to taking α' small. When α' is small, the massive string states decouple from the massless ones and the string theory dynamics is governed by supergravity. At this level of the conjecture, the duality becomes an equivalence between calculations done perturbatively in $\lambda^{-1/2}$ in the gauge theory and calculations in supergravity with α' corrections. Because large λ corresponds to small α', the AdS / CFT conjecture is example of a strong / weak duality. The strong coupling regime is dual to the weak coupling regime of the other and vice versa.

Although sometimes difficult to work with, gauge theories are well understood. We have many tools to analyze their spectra and dynamics, both analytically and numerically. Furthermore, we can define them in a non-perturbative way through a path integral approach. That is, quantities in the gauge theory do not necessarily have to be computed order by order in the coupling constant $g^2_{\rm YM}$ and the rank of the gauge group N. On the other hand, superstring theory has only been defined perturbatively. Scattering amplitudes are computed order by order in the coupling g_s, and by increasing the complexity of the topology of the string worldsheet. The perspective that we take here is to use the gauge theory to define superstring theory non-perturbatively.

Ordinary general relativity has non-perturbative properties as well. They are characterized by objects which are not small deformations of ordinary flat space; these objects are black holes and singularities. Locality and geometry lose some of their meaning when we consider these objects in the quantum theory. Since string theory is a quantum theory of gravity, we should be able to recover them. However, we can not do this directly in the string theory because it is only defined perturbatively and describes spacetimes which have weak curvatures or and are close to flat space. Gauge / gravity duality provides the only non-perturbative definition of string theory. If wish to understanding locality and geometry in quantum gravity, our only option is to search for these concepts in the gauge theory.

Geometry in string theory has features beyond that of general relativity due to the presence of additional objects. In addition to the geometry of spacetime, string theory contains closed strings, opens strings, and D-branes. Closed strings and open strings are more like particles, but D-branes are large, heavy membranes which have their own unique geometric structure and dynamics.

In Part I we use open strings and D-branes in the planar limit of the AdS / CFT conjecture to understand locality and geometry in the dual string theory. Although many of the calculations are perturbative, we use symmetry arguments to make claims about how these calculations can be extended to all orders in perturbation theory. In Chapters 3 and 4 we construct open strings stretched between a special class of D-branes known as giant gravitons in the gauge theory and find its string theory dual. Using the gauge theory computations we make claims about the nature of locality and geometry on the worldvolume of the D-branes. In Chapter 5 we explore the emergence of the geometric backgrounds of the string dual of the deformed $\mathcal{N} = 4$ SYM.

In Part II we take the approach of using gauge theories generally to understand geometry. The gauge theories we use are matrix models and have well known holographic duals. However, we consider the *classical* dynamics of these gauge theories. In Chapter 7 we use classical matrix configurations to understand the geometry to D-branes and discuss some interesting physics that arises. In Chapter 8 we study the chaotic behavior and thermodynamics of the classical evolution of the gauge theories with specific sets of initial conditions. In Chapter 9 we continue to study the thermal configurations of Chapter 8 and make arguments that these are holographically dual to black holes. In Chapter 10 we consider solutions to the classical gauge theories with angular momentum and study the geometry and topology of those configurations.

1.1 Permissions and Attributes

1. The contents of Chapter 3 and Chapter 4 are the results of work in collaboration with David Berenstein, and has previously appeared in the Journal of High Energy Physics (JHEP) [5]. It has been reproduced here with the permission of the International School of Advanced Studies (SISSA), Trieste, Italy. `http://jhep.sissa.it/jhep/help/JHEP/CR_OA.pdf`

2. The contents of Sections 3.4 and Section 4.3 are partly the results of [1]. (This was all me.)

3. The contents of Chapter 5 are the results of work in collaboration with David Berenstein, and has previously appeared in the Journal of High Energy Physics (JHEP) [3]. It has been reproduced here with the permission of the International School of Advanced Studies (SISSA), Trieste, Italy. `http://jhep.sissa.it/jhep/help/JHEP/CR_OA.pdf`

4. The contents of Chapter 7, Section 9.2, Appendix D, Appendix E, and Appendix F are the results of work in collaboration with David Berenstein, and has previously appeared in Physical Review D (Phys. Rev. D) [7]. It is reproduced here with the permission of the permission of the American Physical Society (APS), College Park, MD, USA. `http://publish.aps.org/info/terms.html`

5. The contents of Chapter 8, Section 9.1, and Appendix E are the results of work in collaboration with Curtis Asplund and David Berenstein, and has previously appeared in Physical Review D (Phys. Rev. D) [6]. It is reproduced here with the permission of the permission of the American Physical Society (APS), College Park, MD, USA. `http://publish.aps.org/info/terms.html`

6. The contents of Sections 9.3 and 9.4 are the results of work in collaboration with David Berenstein [4].

7. The contents of Chapter 10 are the results of work in collaboration with David Berenstein and Robin Lashof-Regas and has previously appeared in [2].

Part I

Open Strings in AdS / CFT

Chapter 2

Introduction

The AdS / CFT correspondence [13] suggests that there should be a relation between the low energy effective field theories of string theory (both with open and closed strings) or M-theory on AdS spaces and the dual gauge theory. These effective field theories in higher dimensions are local and locally Lorentz invariant in the supergravity limit. One of the biggest puzzles in understanding the AdS / CFT correspondence is on exactly how locality and geometry in higher dimensions emerges from lower dimensional physics. If locality and higher dimensional geometry is emergent, then they should be found at the end of some computation.

The integrability of the motion of closed strings propagating on $AdS_5 \times S^5$ [14] is one feature of the $AdS_5 \times S^5$ geometry that can help address the problem of locality, or at least, local Lorentz invariance. It has been argued that integrability shows that local strings moving in $AdS \times S$ are related to certain planar calculations on the boundary, where a similar integrable structure has been found. Thus, one should be able to see how dynamics in higher dimensions can be recovered from a field theory computation. For a review of integrability see [15]. Integrability is very special and does not persist in more general setups like general marginal deformations of $\mathcal{N} = 4$ SYM [16] or the conformal field theory of the conifold where it is known that the string sigma model is not integrable [17]. It also does not explain what happens when conformal invariance is broken. The computation of scattering between string states in the integrability program is still a work in progress.

An alternative way to understand the problem of how locality arises has been by guessing field configurations which could dominate the strong coupling physics [18], at least in the BPS case, and finding an approximation for the perturbative spectrum around such configurations. At the moment this is an uncontrolled approximation, but this setup has the advantage that the conformal symmetry of the theory plays a smaller role. Wthin this approach one can produce different backgrounds for the gravity theory (at least in principle) by expanding around different BPS configurations.

Because probing local physics depends on being able to localize particles on short distances, having objects with a shorter Compton wavelength make better probes of the local geometry those that have a longer Compton wavelength. A successful strategy to tackle the locality problem might start by studying objects that are not strings, but much heavier objects. These heavy objects can not appear in the low energy effective field theory of the AdS supergravity, as all of the supergravity fluctuations are string states. Thus non-perturbative stringy effects might be more amenable to study geometry than supergravity fields. The natural candidates are D-branes (and membranes), which have well defined local effective actions describing their motion. They furnish a well defined local probe of the geometry that can be studied in detail. In order to find such states in the field theory, one needs to be able to control them at weak coupling. Ideally they are BPS states that one can follow from weak coupling to strong coupling.

Giant gravitons [19] and their cousin D-brane excitations of AdS geometries have become a very useful tool to understand geometric aspects of the AdS / CFT duality. They are BPS objects whose quantum numbers are calculable and whose degeneracies can be compared with field theory data [20, 21, 22, 23].

We can examine the local physics with one D-brane probing the geometry, but the physics is much richer if we have multiple D-brane probes because they can help us distinguish 'here from there'. Given the two D-branes, we can measure the distance from here to there by stretching a string between them and computing its energy. Thus the energies of strings start serving as a probe of the metric of the geometry. As we change the coupling constant in the dual CFT, the string tension changes in AdS units, and distances of sub-AdS regions can become very large in string units. We can use this to study how the gap between excitations develops and how these massive string excitations can eventually decouple in various processes.

We can also test if the string motion along the D-branes is compatible with locally Lorentz invariant physics in ten dimensions, or more precisely, along the world-volume of the D-brane. If the motion is locally Lorentz invariant, then in the field theory limit the low lying strings should have a relativistic dispersion relation. This is usually taken for granted in the AdS geometry because this is not given from the beginning of the calculation in the dual field theory. Furthermore the presence of the D-branes breaks conformal invariance, so that dispersion relations in the presence of a D-brane is not just kinematics of the AdS isometry group. It is instead a fully dynamical derived quantity.

The subject of this Part is understanding how geometry is realized in the planar limit from the anomalous dimensions of open strings stretched between two giant gravitons. In Chapter 3 we review how to build open strings states in $\mathcal{N} = 4$ SYM and then translate these states and the action of the dilatation operator into a form more suitable for calculations. We restrict ourselves to states in the $\mathfrak{su}(2)$ sector of the gauge theory for many reasons. First, the space of states can be diagonalized into finite dimensional blocks which in itself immediately simplifies computations. Another is that the dilatation generator is known to very high loop order. Thus we our results to very high order in the 't Hooft coupling and give greater supporting evidence to conjectures. On a practical level, we actually know how to build the giant graviton operators and their stringy excitations in the $\mathfrak{su}(2)$ sector. We have concrete handles on the states we want to study and calculations can be done to any level of precision or abstraction that we desire. Lastly, the string theory dual is known to be that of the string propagating in an $\mathbb{R}_t \times S^3$ subspace of the full $AdS_5 \times S^5$ geometry. Many explicit solutions to the equations of motion exist and can be compared exactly to gauge theory operators.

The main results of Chapter 3 will be a description of the open string states in terms of Cuntz oscillator chains and the effective Hamiltonian governing their dynamics. Armed with this technology, in Chapter 4 we begin studying the dynamics of this system. In particular we solve for the ground state and higher order corrections to its energy and the ground state itself. The computation of the ground state energy is done up to third order in the 't Hooft coupling λ and is compatible with the relativistic dispersion relation we would expect from a locally

Lorentz invariant theory. We discuss the consequences of this dispersion relation in the context of geometry in the string theory and propose from where it originates. Another point to take away from Chapter 4 are the amazing cancellations that take place at higher loop orders that lead to the relativistic dispersion relation itself. In the absense of integrability in the open string sector, in a Bethe ansatz sense, it is not guaranteed that this calculation can be done exactly. Not only can the exact answer be found, but analytic results exist as well.

Other geometries to consider in the context of integrability are β-deformations of $\mathcal{N} = 4$ SYM. This is a continuous family of supersymmetric conformal field theories characterized by two parameters, $\lambda = g_{\mathrm{YM}}^2 N$ and β, which is in turn a subset of the Leigh-Strassler deformations of $\mathcal{N} = 4$ SYM [24]. In some contexts these are known as q-deformations where $q = \exp(2i\beta)$ and β is a real number. The classical weakly coupled string theory on a very large geometry arises as the effective description of the undeformed $\mathcal{N} = 4$ SYM when $g_{\mathrm{YM}}^2 N \to \infty$, and $g_{\mathrm{YM}}^2 \ll 1$. For the case of β deformations, we know that the string theory is integrable which results as a twist of the $AdS_5 \times S^5$ integrable system [16, 25, 26] (see also [27] for a review). As such, we will continue to rely on integrability to give us a recipe for the emergence of geometry. Unfortunately, this does not automatically translate into a large set of states that are easily followed. The corresponding twisted algebraic equations that need to be solved to find these states are hard to solve for analytically, see however [28]. For the purposes of this thesis we will assume that the integrability program has solved the problem of understanding the geometric origin of $AdS_5 \times S^5$ strings, but our goal will be to understand the other geometries that can appear at different values of q. The focus of Chapter 5 is to understand which values of β, and hence q, lead to a well defined classical geometry in this limit using a modification of the open string ground state build in Chapter 4.

Chapter 3

Anomalous Dimensions of Open Strings

Our goal in Part I is to understand geometry from the anomalous dimensions of open strings. In this Chapter we develop the technology for constructing the space of states dual to open strings as well the action of the dilatation generator on that space of states. The answer is written down in a Cuntz oscillator basis suitable for doing typical quantum mechanical calculations.

3.1 The $\mathfrak{su}(2)$ Sector

The theory $\mathcal{N} = 4$ SYM with gauge group $SU(N)$ ($U(N)$) is a superconformal field theory whose spacetime isometries are described by the supergroup $PSU(2,2|4)$ and the corresponding Lie superalgebra $\mathfrak{psu}(2,2|4)$. The field theory contains six real scalars ϕ^I in the $\mathbf{6}$ of the R-symmetry and four Weyl fermions ψ^A_α, $\psi^A_{\dot\alpha}$ in the $\mathbf{4}$ and $\bar{\mathbf{4}}$, all of which live in the adjoint of the gauge group. There is also a gauge field $A_{\alpha\dot\alpha}$ which acts as the connection for the gauge group and is a singlet under the R-symmetry. In the $\mathcal{N} = 1$ formulation of $\mathcal{N} = 4$ SYM, the six scalars are the real components of the lowest component complex scalars of the three chiral superfields. We denote the complex scalars by $X = \phi^1 + i\phi^4$, $Y = \phi^2 + i\phi^5$, $Z = \phi^3 + i\phi^6$. Their complex conjugates will be denoted by $\bar{X}$, $\bar{Y}$, and $\bar{Z}$ when necessary.

The anomalous dimensions of the operators in $\mathcal{N} = 4$ SYM are given by the dilatation generator when the theory is defined on a flat space background, and the Hamiltonian when the theory is defined on $\mathbb{R} \times S^3$. The conformal transformation that relates these two theories is what makes radial quantization possible and leads to the state / operator correspondence. Indeed, we will use the terms ‘state’ and ‘operators’ interchangeably when refering to objects lying in the Hilber space of the field theory.

The Lie superalgebra $\mathfrak{psu}(2,2|4)$ has many sectors closed under renormalization with respect to the dilatation generator. The smallest non-trivial subsector is $\mathfrak{G} = \mathfrak{su}(2) \times \mathfrak{u}(1) \times \mathfrak{u}(1)$ [29]. The states in the $\mathfrak{su}(2)$ subsector are constructed using only two of the three complex scalars. In this thesis, we will use Y and Z. The space of physical states must be gauge invariant. Thus the subsector consists of single and multitrace operators of Y and Z. The first $\mathfrak{u}(1)$ of $\mathfrak{G}$ is just the classical dimension of these operators and counts the total number of Y’s and Z’s. The second $\mathfrak{u}(1)$ of $\mathfrak{G}$ is the anomalous dimension, δD. Regarding each complex field as either spin up or spin down, the Cartan generator of the $\mathfrak{su}(2)$ is just counts the difference between the number of Y and Z fields. Thus, state mixing occurs in the $\mathfrak{su}(2)$ sector between states which have exactly the same number of Y and Z fields. This property aids in block diagonalizing δD and simplifies computations of anomalous dimensions in this sector.

The general problem of solving the spectrum of anomalous dimensions in $\mathcal{N} = 4$ SYM is incredibly difficult, but simplifies in the planar limit. Planar $\mathcal{N} = 4$ SYM is integrable up to one-loop [30] and expected to be integrable to all orders in perturbation theory. The spectrum of anomalous dimensions is characterized by a Bethe ansatz for an integrable $\mathfrak{psu}(2,2|4)$ spin chain [31]. A major success of the integrability program is seen in the thermodynamic limit, where the solutions to the Bethe ansatz become the algebraic curves of the closed string [32].

The integrability of the string sigma model on $AdS_5 \times S^5$ [14] allows direct comparisons to planar $\mathcal{N} = 4$ SYM. In many cases the solutions to the equations of motion and be mapped directly to specific states of the gauge theory. In particular, the string theory dual of the $\mathfrak{su}(2)$ subsector is well known. Operators in this subsector correspond to strings propagating in an $\mathbb{R}_t \times S^3$ background of the $AdS_5 \times S^5$ where $\mathbb{R}_t$ is the time direction in AdS_5 and $S^3 \subset S^5$. A large class of closed string solutions to the equations of motion in this subsector have been found including circular strings, folded strings, spiky strings, and solitonic strings [33, 34, 35, 36]. The solitonic strings are called giant magnons [37]. Bound states of many giant magnons have been found in the gauge theory by studying the asymptotic S-matrix [38]. These giant magnon states will be relevant when we later construct open strings directly in the gauge theory, particularly in Section 4.5.

3.2 Giant Gravitons and Open Strings

D-branes are non-perturbative objects in string theory lacking a full quantum description. Calculations involving D-branes come in the form as BPS solutions to the supergravity equations of motion, classical analysis of the DBI action, or perturbatively in the form of open strings. Using $\mathcal{N} = 4$ SYM as a definition of quantum string theory provides the best approach to formulating D-branes non-perturbatively. The class of D-branes known giant gravitons [19] has been successfully constructed in the gauge theory. In this section we discuss how the giant gravitons appear in the gauge theory and how to build open string excitations on top of them. Much of the language and technology presented here is taken from [39].

The particular giant gravitons we are interested in are D-branes with the world-volume of an S^3 traversing a great circle of the S^5 in $AdS_5 \times S^5$. The radius of the giant graviton is proportional to its velocity, or to its angular momentum around the S^5. They are half BPS whose angular momentum has an upper bound due to the fact that the radius of an S^3 subspace of S^5 is bounded above by that of the S^5. The dual operators in the gauge theory were found in [40] and determined to be subdeterminant operators of the form

$$\det{}_k(Z) = \frac{1}{N!}\binom{N}{k}\epsilon^{a_1\ldots a_k c_{k+1}\ldots c_N}\epsilon_{b_1\ldots b_k c_{k+1}\ldots c_N} Z^{b_1}_{a_1}\cdots Z^{b_k}_{a_k} \tag{3.1}$$

When $k = N$ we just have $\det_N(Z) = \det(Z)$ which is called a maximal giant. The classical upper bound on the angular momenta is directly related to the condition that $k \leq N$.

Attaching open strings to a single subdeterminant was first suggested in [41], following closely the set of states identified for the conifold theory [23]. One can build string excitations, represented as words W_i in $\mathcal{N} = 4$ SYM, on top of maximal giants by contracting the indices of the epsilon symbols with these operators instead of with the identity.

$$\mathcal{O}(W_1, \ldots, W_s) = \frac{1}{N!}\binom{N}{s}\epsilon^{a_1\ldots a_{N-s}c_1\ldots c_s}\epsilon_{b_1\ldots b_{N-s}d_1\ldots d_s}Z^{b_1}_{a_1}\cdots Z^{b_{N-s}}_{a_{N-s}}{W_1}^{d_1}_{c_1}\cdots {W_s}^{d_s}_{c_s} \tag{3.2}$$

The approximate orthogonality of these states when $s \ll N$ was shown in [42]. These operators are given by the generating function equation

$$\mathcal{O}(W_1, \ldots, W_s) = \partial_{\kappa_1,\ldots,\kappa_s} \det\left(Z + \sum_{i=1}^{s}\kappa_i W_i\right)\Bigg|_{\kappa_i=0} \tag{3.3}$$

We find that for one and two excitations

$$\mathcal{O}(W_1) = \det(Z)\mathrm{Tr}(Z^{-1}W_1) \tag{3.4}$$

$$\mathcal{O}(W_1, W_2) = \det(Z)(\mathrm{Tr}(Z^{-1}W_1)\mathrm{Tr}(Z^{-1}W_2) - \mathrm{Tr}(Z^{-1}W_1Z^{-1}W_2)) \tag{3.5}$$

The operator corresponding to a maximal giant can be separated from the excitations reenforcing the idea that we are indeed forming string excitations on maximal giants and not non-maximal ones. Our ability to separate the maximal giant operator can actually be seen by rewriting (3.3) as

$$\mathcal{O}(W_1, \ldots, W_s) = \det(Z)\partial_{\kappa_1,\ldots,\kappa_s} \det\left(1 + \sum_{i=1}^{s}\kappa_i Z^{-1} W_i\right)\Bigg|_{\kappa_i=0} \tag{3.6}$$

The presence of the operator inverse Z^{-1} in the above expressions is purely formal. The generating function (3.3) is polynomial in all of its variables. Taking derivatives can not introduce inverses of these variables. As such, the operators (3.4) and (3.5) are polynomial in its operator variables and completely well defined.

Even though the operator inverses are formal, the serve an important role. We will eventually describe dynamical open strings in the gauge theory. Even at this level of the construction we see that the boundary conditions themselves for the opens string must be present in the operators. Here they are expressed as poles in specially crafted multi-trace operators.

These giant graviton states have definite angular momenta, but are delocalized in position space on the S^5. To establish a connection to the classical string theory, we want operators that are localized in position space and have indefinite angular momentum. This is accomplished by shifting the matrix Z by a complex collective coordinate α, that is, we take $\det(Z) \rightarrow \det(Z-\alpha)$ [39]. Taking inner products of giant gravitons with different collective coordinates yields

$$\langle \det(\bar{Z}-\alpha_2^*)\det(Z-\alpha_1)\rangle \approx N! \exp(\alpha_2^*\alpha_1) \tag{3.7}$$

The geometric interpretation of α being the coordinate of the giant graviton in a complex disk of the S^5 remains valid so long as $\alpha_i < \sqrt{N}$ [39]. Expanding the operator $\det(Z-\alpha)$ in α, we see that the operator looks like a coherent state of giant gravitons with different angular momenta and the exponential approximation of the inner product is in line with this observation. Thus the states $\det(Z-\alpha)$ are in some sense classical.

Dealing with multiple giant gravitons was originally worked out in [43]. The subdeterminant operators (3.1) are Schur polynomials in the matrix Z corresponding to a Young diagram with one column and k boxes. The Young diagram correpsonds to a representation of the symmetric group and dictates how to contract the indices over many occurrences of the matrix Z. The representation can be arbitrary and its interpretation as point-like gravitons, strings, giant gravitons, and dual giant gravitons depends on the number and length of the columns and rows in the correpsonding Young diagrams. In particular, long columns are thought of as the giant gravitons living in S^5 while long rows are thought of as the dual giant gravitons living in AdS_5. To be concrete, if R is a representation of the symmetric group S_n, then the corresponding graviton operator is given by

$$\chi_R(Z) = \sum_{\sigma \in S_n} \chi_R(\sigma) Z^{i_1}_{i_{\sigma(1)}} Z^{i_2}_{i_{\sigma(2)}} \cdots Z^{i_n}_{i_{\sigma(n)}} \tag{3.8}$$

where $\chi_R(\sigma)$ is the character of the group element σ in the representation R and all indices i_j (which range from 1 to N) are summed over. Different representations are orthogonal with respect to free field theory contractions

$$\langle \chi_R(\bar{Z}) \chi_S(Z) \rangle = \delta_{RS} f_R \tag{3.9}$$

with f_R the weight of the Young diagram corresponding to the representation R.

String excitations W_i are added to the giants by introducing restricted characters for representations of the symmetric group. These restrictions fix where the gauge indices are contracted to the rest of the giant graviton operator. The details are beyond the scope of this work and we defer the reader to the review articles

[44, 45, 46]. A consequence of this construction is that each row or column in the Young diagram must have the same number of strings beginning and ending on the corresponding giant. This is a Gauss law constraint for the number of open strings on each of the giants.

Instead of delocalizing bound states of multiple giants expressed as Schur polynomials, we simplify the problem of strings stretched between giant gravitons by considering supersymmetric orbifolds of the $\mathcal{N} = 4$ SYM theory [39]. Multiple giants with collective coordinates α_i can then be expressed as a product of determinant operators

$$\mathcal{O}(\alpha_1, \ldots, \alpha_k) = \det(Z_1 - \alpha_1) \cdots \det(Z_k - \alpha_k) \tag{3.10}$$

with each Z_i belonging to a different sector of the orbifolded theory. We stretch strings between the giant given the schematic of (3.4) and (3.5). That is, a pole in the field $Z_i - \alpha_i$ is introduced when we want to connect strings beginning and ending on the giant graviton α_i. For example, the operator for three giant gravitons with strings stretching from branes $1 \to 2 \to 3 \to 1$ is given by

$$\begin{aligned} &\det(Z_1 - \alpha_1)\det(Z_2 - \alpha_2)\det(Z_3 - \alpha_3)\times \\ &\qquad \mathrm{Tr}\left((Z_1 - \alpha_1)^{-1} W_{12} (Z_2 - \alpha_2)^{-1} W_{23} (Z_3 - \alpha_3)^{-1} W_{31}\right) \end{aligned} \tag{3.11}$$

Up to this point we have chosen to leave the string excitations W_i arbitrary. We restrict the excitations W_i to be composed only of the fields Y and Z. Then the giant graviton operators together with their stringy excitations live in the $\mathfrak{su}(2)$ sector of the gauge theory.

3.3 Strings as Cuntz Oscillator Chains

The operators of Section 3.2 give a concrete handle by which to manage open strings directly in the gauge theory. Of particular interest is the open string ground state and spectrum of excited states above it. These can be acquired by diagonalizing the dilatation generator on this space of states. The action of the dilatation generator in the $\mathfrak{su}(2)$ sector is known to two-loops and in the planar limit up to five-loops. In the planar limit, the dilatation generator acts on single trace operators. The states include single and multi-trace operators of the fields Y and Z. In the planar limit, the action of the dilatation operator simplifies by acting on individual single trace factors.

Individual single traces can be interpreted as closed strings since the cyclicity of the trace can be identified with periodic boundary conditions of the closed string. This space of states can be represented as an $\mathfrak{su}(2)$ spin chain with periodic boundary conditions. Each type of field, Y or Z, represents either spin up or down. The one-loop dilatation generator was recognized as the Hamiltonian of the Heisenberg spin chain and helped kick off the integrability program in the context of the AdS / CFT correspondence.

Another basis has been constructed to represent the space of states in the planar $\mathfrak{su}(2)$ sector. To construct it we fix the number of Y fields in a single trace. Any number of Z fields can be placed between the Y. That is, the Y separate sites at which one can place Z fields. Thus a state is labeled by the number of Y's and the number of Z's between each Y. The cyclic nature of the trace means that we should cyclically identify the states. For example

$$\mathrm{Tr}(ZYZZZYZZY) \to |3,2,1\rangle \equiv |2,1,3\rangle \equiv |1,3,2\rangle \tag{3.12}$$

A general state is represented by some set of occupation numbers $\{n_i\}_{i=1}^{k}$, where k is the number of Y fields. The zero occupation number state is just $\mathrm{Tr}(Y^k)$, which we denote as $|0\rangle_k$. A state with a general set of occupation numbers is represented by $|n_1, \ldots, n_k\rangle_k$.

In spin chain representation of the $\mathfrak{su}(2)$ sector, one use the raising and lowering operators to change a Y field to a Z field and vice versa. In the occupation number basis, we have fix the number of Y's and so it does not make sense to talk about 'raising' or 'lowering' the spin excitation. Instead, we need a means by which to directly insert and delete occurrences of the Z fields.

To do so we introduce a set of Cuntz oscillators [47]. The Cuntz algebra is a q-deformation of the harmonic oscillator algebra in the limit $q \to 0$. One has a lowering operator a and a raising operator $a^\dagger$. There is a zero occupation state $|0\rangle$ satisfying $a\,|0\rangle = 0$. The defining relations are

$$aa^\dagger = I, \quad a^\dagger a = I - P_0 \tag{3.13}$$

and lead to the commutation relation

$$[a, a^\dagger] = P_0 \tag{3.14}$$

with P_0 the projection onto the zero occupation state. Higher occupation states are obtained by acting with the raising operator, $|n\rangle = (a^\dagger)^n |0\rangle$. The commutation relation (3.14) implies the simple action of the ladder operators

$$a^\dagger |n\rangle = |n+1\rangle\,, \quad a|n\rangle = |n-1\rangle \tag{3.15}$$

with $n > 0$ for the second relation. Negative occupation numbers are not allowed.

We can extend these Cuntz oscillators to act on individual sites of our multi-occupation number states by defining $a_i = I^{\otimes^{i-1}} \otimes a \otimes I^{\otimes^{k-i}}$ and likewise for $a_i^\dagger$ and the projection operator P_{0i}. We now have the commutation relation

$$[a_i, a_j^\dagger] = \delta_{ij} P_{0i} \tag{3.16}$$

In the Cuntz language, the state (3.12) can be written as $(a_1^\dagger)^3(a_2^\dagger)^2(a_3^\dagger)^1 |0\rangle_3$ and cyclic identifications thereof. Due to the periodic boundary conditions, we will refer to states of the form (3.12) as closed Cuntz oscillator chains, sometimes dropping the word ‘oscillator.’

Because $aa^\dagger = I$, all operators can (and should) naturally be written as linear combinations of objects in normal ordered form $\hat{S}_{kn} = (a^\dagger)^k a^n$. It is easy to show that $\hat{S}_{nn} = (a^\dagger)^n a^n = 1 - \sum_{m=0}^{n-1} P_m$, where P_m is the projector onto the state with occupation number m. It is clear that $\hat{S}_{nn}|m\rangle = 0$ if $n > m$ and $\hat{S}_{nn}|m\rangle = |m\rangle$ otherwise. Thus the occupation number operator is given by

$$\hat{N} = \sum_{n=1}^{\infty} \hat{S}_{nn} = \hat{N}^\dagger \tag{3.17}$$

One has $[\hat{N}_i, a_i^\dagger] = a_i^\dagger$ and consequently $\hat{N}_i |n_1, \ldots, n_k\rangle_k = n_i |n_1, \ldots, n_k\rangle_k$. It is easy to show that $\hat{N}_{tot} = \sum_{i=1}^{k} \hat{N}$ commutes with the Hamiltonian.

The Cuntz oscillator basis can be used to represent open strings as well. Consider an open string state with strings stretched between two giant gravitons with collective coordinates α_1, α_2. As a reminder, for multiple giants it is simpler to work in the supersymmetric $\mathbb{Z}_n$ orbifold of $\mathcal{N} = 4$ SYM. For $n = 2$, this corresponds to a $U(N) \times U(N)$ quiver theory with $\mathcal{N} = 2$ SUSY in four dimensions. The chiral superpartners of the vector fields will be called $Z_1,\ Z_2$, while the matter hypermultiplets between the two gauge groups will be made of $X,\ Y$ chiral fields. The corresponding state will be given by

$$\det(Z_1 - \alpha_1)\det(Z_2 - \alpha_2)\mathrm{Tr}\left(\frac{1}{Z_1 - \alpha_1} W_{12} \frac{1}{Z_2 - \alpha_2} W_{21}\right) \tag{3.18}$$

The string excitation W_{21} is needed to satisfy the Gauss law constraint. The dilatation generator acts on single trace factors in a multi-trace operator in the planar limit. The analogy for open strings is that the dilatation generator will not act on W_{12} and W_{21} simultaneously without splitting the trace in the planar limit. Thus we can focus our attention on individual strings stretched between giant gravitons instead of the entire cycle, say W_{12}. The string excitation W_{12} is now given in this orbifolded case by

$$W_{12} = Y_{12} Z_2^{n_1} Y_{21} Z_1^{n_2} Y_{12} Z_2^{n_3} \cdots Z_1^{n_k} Y_{12} \tag{3.19}$$

The labels Y_{12} indicate that the Y is a bifundamental in the $(N_1, \bar{N}_2)$ representation of the $U(N_1) \times U(N_2)$ orbifold group (with $N_1 = N_2 = N$ numerically), whereas the Y_{21} is in the $(\bar{N}_1, N_2)$ representation. Thus an open string stretched from α_1 to α_2 can also be represented by a Cuntz oscillator chain with the Y separating the individual sites. We take the open string states to be of the form $\left|\alpha_1, \alpha_2; \{n_i\}_{i=1}^k\right\rangle$ without cyclic identification of the sequence. One should keep in mind that for these states, even though we have only k sites, there are $k+1$ Y fields. This is to separate the giant graviton pole from other Z fields.

If we allowed the monomials to end with occurences of the Z fields, then the poles could be reduced

$$\mathrm{Tr}\left(\frac{1}{Z-\alpha_1}ZYZZ\cdots\right) = \mathrm{Tr}\left(YZZ\cdots\right) + \alpha_1 \mathrm{Tr}\left(\frac{1}{Z-\alpha_1}YZZ\cdots\right) \tag{3.20}$$

The second term can be intrepreted as an open string state, but the end of the open string has detached from the brane in the first term. Such a state may have an interpretation when we are considering string joining and splitting, but it has no place here where we are just looking at strings stretched between two D-branes. Thus we will restrict ourselves to monomials of the form (3.18).

Most useful to us for open strings will be coherent states of the Cuntz oscillators. We introduce a set of complex numbers $\{z_i\}_{i=1}^k$ such that the states satisfy $a_i \left|\alpha_1, \alpha_2; z_1, \ldots, z_k\right\rangle = z_i \left|\alpha_1, \alpha_2; z_1, \ldots, z_k\right\rangle$ For a single Cuntz oscillator we have $a\left|z\right\rangle = z\left|z\right\rangle$ for some complex number z. Solving for $\left|z\right\rangle$ yields

$$\left|z\right\rangle = N_z \sum_{n=0}^{\infty} z^n (a^\dagger)^n \left|0\right\rangle \tag{3.21}$$

Normalizing the coherent states gives the normalization factor

$$N_z = \frac{1}{\sqrt{1-|z|^2}} \tag{3.22}$$

If we want to the coherent states to have finite norm, then z should lie in the complex unit disk. The state $|\alpha_1, \alpha_2; z_1, \ldots, z_k\rangle$ is obtained by tensoring the single Cuntz coherent states with appropriate collective coordinate. These open string states are now described by a collective of numbers in the complex unit disk. We will later see that these locations correspond to the $S^3 \subset S^5$ of the $AdS_5 \times S^5$ geometry.

3.4 The Cuntz Hamiltonian

The technology in the previous section was developed as a simpler means by which to deal with open and closed strings in the gauge theory. To gain a handle on the anomalous dimensions of these operators, we will have to translate the dilatation generator into the basis of Cuntz oscillators. The planar version is useful for dealing with closed string states and the stringy excitations of the open string operators. To deal with the giant gravitons, it will be necessary to use the full non-planar dilatation generator in the $\mathfrak{su}(2)$ sector. Here we discuss both the planar and non-planar versions and how they are translated build a Hamiltonian for the closed and open Cuntz oscillator chains from which one can compute their energies or anomalous dimensions. The results of this section are summarized in Appendix B

3.4.1 Cuntz Hamiltonian for Closed Chains

The Hamiltonian for the closed Cuntz chains (closed strings) can be obtained from the planar version of the dilatation generator. In the planar limit and in the $\mathfrak{su}(2)$ sector, states can be represented as words in the letter Y and Z. Local interactions of the dilatation generator can then be represented as permutations of nearest neighbors, next-to-nearest neighbors, etc. One can rewrite the permutation operators in terms of the so-called chiral functions [48] by shifting the permutation operators by the identity. The chiral functions represent the chiral structure of the underlying Feynman super-graphs that generate them [49]. Let $P_{i,i+1}$ denote the permutation operator which swaps the i^{th} and the $(i+1)^{\text{th}}$ letter in a word in the $\mathfrak{su}(2)$ sector. On a word of length L, the chiral functions are defined by

$$\chi(a_1, a_2, \ldots, a_n) = \sum_{r=1}^{L} \prod_{i=1}^{n} (P - I)_{a_i+r, a_i+r+1} \tag{3.23}$$

with $I_{i,i+1}$ the identity operator on letters i and $(i+1)$. The planar dilatation generator has an expansion in the 't Hooft coupling $\lambda = g_{\text{YM}}^2 N$.

$$D^{\infty} = \sum_{\ell=0}^{\infty} \left(\frac{\lambda}{4\pi^2}\right)^{\ell} D_{\ell}^{\infty} \tag{3.24}$$

where ℓ represents the number of loops. The first four terms of this sequence are given by [49]

$$D_0^{\infty} = \chi() = L \tag{3.25}$$

$$D_1^{\infty} = -\frac{1}{2}\chi(1) \tag{3.26}$$

$$D_2^{\infty} = -\frac{1}{8}[(\chi(1,2) + \chi(2,1)) - 2\chi(1)] \tag{3.27}$$

$$D_3^{\infty} = -\frac{1}{16}[(\chi(1,2,3) + \chi(3,2,1)) + \chi(1,3) - 4(\chi(1,2) + \chi(2,1)) + 6\chi(1)] \tag{3.28}$$

The reason we go to three loop order will be apparent in Section 4.3. The translation of these operators into the Cuntz language was first done in [5] using the full non-planar dilatation generator, but it is easier to start in the basis of chiral functions.

We can understand the chiral functions locally by considering their action on words not cyclically identified whose length is equal to the range of the interaction. For example, the range of $\chi(1)$ is two. It acts non-trivially only on the letter combinations YZ and ZY,

$$\chi(1)(ZY) = YZ - ZY \tag{3.29}$$

$$\chi(1)(YZ) = ZY - YZ \tag{3.30}$$

To convert this to the Cuntz language, we note that the Y's lie on the boundary of sites and so we can label the sites preceding it or after it by i, $i+1$, etc. We can then use the lowering Cuntz oscillators a_i and zero projectors P_{0i} to identify the number of Z's in the input word. To get the output word we use the raising Cuntz oscillators $a_i^\dagger$ to put Z's in the appropriate sites. For the example of $\chi(1)$, let the Z in ZY be at site i. Then the action of $\chi(1)$ is given by the Cuntz operators $(a_{i+1}^\dagger - a_i^\dagger)a_i$. For YZ, we choose the Z to sit at site i and the action of $\chi(1)$ is $(a_i^\dagger - a_{i+1}^\dagger)a_{i+1}$. Adding these contributions and summing over all the sites we have

$$\chi(1) \to -\sum_{i=1}^{k}(a_{i+1}^\dagger - a_i^\dagger)(a_{i+1} - a_i) \tag{3.31}$$

Locally, the chiral functions will vanish on words which are all the same letter. We do not have to consider cases with consecutive Z's. Chains of consecutive Y's are sites with zero occupation which vanish under action of the lowering Cuntz oscillators. Thus, the sum of the length of a word is equivalent to summing over the sites of the corresponding Cuntz chain.

For an example with projectors, we consider the action of the Hermitian combination $\chi(1,2)+\chi(2,1)$ on YZY. One has

$$(\chi(1,2)+\chi(2,1))(YZY) = -(ZYY-2YZY+YYZ) \tag{3.32}$$

In the Cuntz language this becomes

$$-(a_{i+1}^{\dagger}-2a_i^{\dagger}+a_{i-1}^{\dagger})P_{0i}a_i \tag{3.33}$$

The full expression for $\chi(1,2)+\chi(2,1)$ is

$$\begin{aligned}\chi(1,2)+\chi(2,1) \rightarrow -\sum_{i=1}^{k}&(a_i^{\dagger}-a_{i-1}^{\dagger})P_{0i}(a_{i+1}-a_i)+(a_{i+1}^{\dagger}-a_i^{\dagger})P_{0i}(a_i-a_{i-1})\\ &+(a_{i+1}^{\dagger}-a_i^{\dagger})(a_{i+1}^{\dagger}a_i+a_i^{\dagger}a_{i+1})(a_{i+1}-a_i)\end{aligned} \tag{3.34}$$

The functions appearing in (3.25)-(3.28) left to be translated, $\chi(1,2,3)+\chi(3,2,1)$ and $\chi(1,3)$, act on four letter words. Their translation is given by

$$\begin{aligned}&\chi(1,2,3)+\chi(3,2,1) \rightarrow\\ &\quad -\sum_{i=1}^{k}(a_{i+2}^{\dagger}-a_{i+1}^{\dagger})P_{0i+1}P_{0i}(a_i-a_{i-1})+(a_i^{\dagger}-a_{i-1}^{\dagger})P_{0i+1}P_{0i}(a_{i+2}-a_{i+1})\\ &\qquad +(a_{i+1}^{\dagger}-a_i^{\dagger})(a_i^{\dagger}P_{0i}a_{i+1}+a_{i-1}^{\dagger}P_{0i}a_i)(a_i-a_{i-1})\\ &\qquad +(a_i^{\dagger}-a_{i-1}^{\dagger})(a_{i+1}^{\dagger}P_{0i}a_i+a_i^{\dagger}P_{0i}a_{i-1})(a_{i+1}-a_i)\end{aligned}$$

$$+ (a_{i+1}^\dagger - a_i^\dagger)(a_{i+1}^\dagger a_{i+1}^\dagger a_i a_i + a_i^\dagger a_i^\dagger a_{i+1} a_{i+1})(a_{i+1} - a_i) \tag{3.35}$$

$$\chi(1,3) \to \sum_{i=1}^{k} (a_{i+1}^\dagger - a_i^\dagger)(a_i^\dagger - a_{i-1}^\dagger) P_{0i} (a_{i+1} - a_i)(a_i - a_{i-1}) \tag{3.36}$$

Let us begin assembling these pieces into the closed chain Cuntz Hamiltonian. First we write the expansion

$$H_{\text{closed}} = \sum_{\ell=0}^{\infty} \left(\frac{\lambda}{4\pi^2}\right)^{\ell} H_{\text{closed},\ell} \tag{3.37}$$

where D_ℓ^∞ will be translated to $H_{\text{closed},\ell}$. The length of the word L is the total number of Z and Y fields appearing in a single trace. The number of Y fields is given by k for the closed Cuntz chains while the number of Z fields is given by the number operator (3.17). Thus we have

$$H_{\text{closed},0} = \hat{N} + k \tag{3.38}$$

For $\ell = 1$ the result is proportional to (3.31)

$$H_{\text{closed},1} = \frac{1}{2} \sum_{i=1}^{k} (a_{i+1}^\dagger - a_i^\dagger)(a_{i+1} - a_i) \tag{3.39}$$

where the sites are cyclically identified, $i \equiv i + k$.

For $\ell = 2$, we make use of the identity $I = a_i^\dagger a_i + P_{0i}$.

$$\begin{aligned} &(\chi(1,2) + \chi(2,1)) - 2\chi(1) \\ &\to \sum_{i=1}^{k} (-a_i^\dagger + a_{i-1}^\dagger) P_{0i} (a_{i+1} - a_i) + (a_{i+1}^\dagger - a_i^\dagger) P_{0i} (-a_i + a_{i-1}) \end{aligned}$$

$$
\begin{aligned}
&+ (a^\dagger_{i+1} - a^\dagger_i)(a^\dagger_{i+1}(-a_i) + (-a^\dagger_i)a_{i+1})(a_{i+1} - a_i) \\
&+ 2(a^\dagger_{i+1} - a^\dagger_i)(a_{i+1} - a_i) \\
= &\sum_{i=1}^{k} (-a^\dagger_i + a^\dagger_{i-1})P_{0i}(a_{i+1} - a_i) + (a^\dagger_{i+1} - a^\dagger_i)P_{0i}(-a_i + a_{i-1}) \\
&+ (a^\dagger_{i+1} - a^\dagger_i)(a^\dagger_{i+1}(-a_i) + (-a^\dagger_i)a_{i+1})(a_{i+1} - a_i) \\
&+ (a^\dagger_{i+1} - a^\dagger_i)(a^\dagger_{i+1}a_{i+1} + P_{0i+1} + a^\dagger_i a_i + P_{0i})(a_{i+1} - a_i) \\
= &\sum_{i=1}^{k} (a^\dagger_{i+1} - a^\dagger_i)^2(a_{i+1} - a_i)^2 + (a^\dagger_{i+1} - 2a^\dagger_i + a^\dagger_{i-1})P_{0i}(a_{i+1} - 2a_i + a_{i-1}) \quad (3.40)
\end{aligned}
$$

We define

$$
\begin{aligned}
H_{\text{closed},2} = -\frac{1}{8}\sum_{i=1}^{k} &(a^\dagger_{i+1} - a^\dagger_i)^2(a_{i+1} - a_i)^2 \\
&+ (a^\dagger_{i+1} - 2a^\dagger_i + a^\dagger_{i-1})P_{0i}(a_{i+1} - 2a_i + a_{i-1}) \quad (3.41)
\end{aligned}
$$

The translation of D_3^∞ to $H_{\text{closed},3}$ involves nesting the identity $I = a^\dagger_i a_i + P_{0i}$ multiple times. The correct prescription is guided by the finite difference forms of (3.39) and (3.41). We further take advantage of the known Cuntz forms of D_1^∞ and D_2^∞ and replacing $\chi(1)$ and $\chi(1,2) + \chi(2,1)$ with them

$$
D_3^\infty = -\frac{1}{16}[(\chi(1,2,3) + \chi(3,2,1)) + \chi(1,3) + 32D_2^\infty + 4D_1^\infty] \quad (3.42)
$$

Using this particular combination of chiral functions, we insert the identity into D_1^∞ and D_2^∞ as follows.

$$
16D_3^\infty \to
$$

$$\begin{aligned}
&\sum_{i=1}^{k} \Big[(a^\dagger_{i+2} - a^\dagger_{i+1})P_{0i+1}P_{0i}(a_i - a_{i-1}) + (a^\dagger_i - a^\dagger_{i-1})P_{0i+1}P_{0i}(a_{i+2} - a_{i+1}) \\
&\quad + (a^\dagger_{i+1} - a^\dagger_i)(a^\dagger_i P_{0i} a_{i+1} + a^\dagger_{i-1} P_{0i} a_i)(a_i - a_{i-1}) \\
&\quad + (a^\dagger_i - a^\dagger_{i-1})(a^\dagger_{i+1} P_{0i} a_i + a^\dagger_i P_{0i} a_{i-1})(a_{i+1} - a_i) \\
&\quad +(a^\dagger_{i+1} - a^\dagger_i)(a^\dagger_{i+1} a^\dagger_{i+1} a_i a_i + a^\dagger_i a^\dagger_i a_{i+1} a_{i+1})(a_{i+1} - a_i)\Big] \\
&\quad - (a^\dagger_{i+1} - a^\dagger_i)(a^\dagger_i - a^\dagger_{i-1})P_{0i}(a_{i+1} - a_i)(a_i - a_{i-1}) \\
&\quad + \Big[2(a^\dagger_{i+1} - a^\dagger_i)^2(a^\dagger_{i+1} a_{i+1} + P_{0i+1} + a^\dagger_i a_i + P_{0i})(a_{i+1} - a_i)^2 \\
&\quad + 2(a^\dagger_{i+1} - 2a^\dagger_i + a^\dagger_{i-1})(a^\dagger_{i+1} a_{i+1} + P_{0i+1} + a^\dagger_{i-1} a_{i-1} + P_{0i-1})P_{0i}(a_{i+1} - 2a_i + a_{i-1})\Big] \\
&\quad - \Big[(a^\dagger_{i+1} - a^\dagger_i)(a^\dagger_i(a^\dagger_i a_i + P_{0i})a_i + P_{0i}(a^\dagger_{i-1} a_{i-1} + P_{0i-1}))(a_{i+1} - a_i) \\
&\quad + (a^\dagger_{i+1} - a^\dagger_i)(a^\dagger_{i+1}(a^\dagger_{i+1} a_{i+1} + P_{0i+1})a_{i+1} + P_{0i+1}(a^\dagger_{i+2} a_{i+2} + P_{0i+2}))(a_{i+1} - a_i)\Big]
\end{aligned} \tag{3.43}$$

To simplify this expression one has to collect all terms with the same number of projectors and shift indices when needed. The result is

$$\begin{aligned}
H_{\text{closed},3} = \frac{1}{16}\sum_{i=1}^{k} &(a^\dagger_{i+1} - a^\dagger_i)^3(a_{i+1} - a_i)^3 + v^{i\dagger}_a M_{ab} P_{0i} v^i_b \\
&+ (a^\dagger_{i+2} - 3a^\dagger_{i+1} + 3a^\dagger_i - a^\dagger_{i-1})P_{0i+1}P_{0i}(a_{i+2} - 3a_{i+1} + 3a_i - a_{i-1})
\end{aligned} \tag{3.44}$$

$$v^i_a = (a_{i+1}a_{i+1},\ a_{i+1}a_i,\ a_{i+1}a_{i-1},\ a_i a_i,\ a_i a_{i-1},\ a_{i-1}a_{i-1}) \tag{3.45}$$

$$M_{ab} = \begin{pmatrix} 4 & -8 & 2 & 2 & 0 & 0 \\ -8 & 15 & -3 & -3 & -1 & 0 \\ 2 & -3 & 1 & 1 & -3 & 2 \\ 2 & -3 & 1 & 1 & -3 & 2 \\ 0 & -1 & -3 & -3 & 15 & -8 \\ 0 & 0 & 2 & 2 & -8 & 4 \end{pmatrix} \tag{3.46}$$

We will comment on the structure of Cuntz Hamiltonian in Section 3.5.

3.4.2 Cuntz Hamiltonian for Open Chains

The planar dilatation generator acts locally on words composed of Y's and Z's The Cuntz Hamiltonian for closed chains can be determined completely because they are just a single words of composed of many letters. Open Cuntz chains are more complicated; they correspond to states which contain determinants, poles, and string excitations. The string excitations are just words and so the planar dilatation generator is applicable to this part of the state. The boundary of the state, that is, the determinants and poles, complicate the situation and one can no longer use the planar dilatation generator in the basis of chiral functions. In fact, we will see that the non-planar portions of the dilatation generator are necessary for certain cancellations. Thus we need the full non-planar dilatation generator in the $\mathfrak{su}(2)$ sector. The purpose of this section is to use the non-planar operator to compute the boundary contributions to the Cuntz Hamiltonian for open stretched between two giant gravitons.

In the $\mathfrak{su}(2)$ sector the dilatation generator, at finite N, can be written as an expansion in the 't Hooft coupling $\lambda = g_{\rm YM}^2 N$

$$D = \sum_{\ell=0}^{\infty} \left(\frac{\lambda}{4\pi^2}\right)^{\ell} D_\ell \tag{3.47}$$

where ℓ represents the number of loops. The first three terms in this sequence are given by [29]

$$D_0 = :\mathrm{Tr}(Z\check{Z}): + :\mathrm{Tr}(Y\check{Y}): \tag{3.48}$$

$$D_1 = -\frac{1}{2N} :\mathrm{Tr}([Y,Z][\check{Y},\check{Z}]): \tag{3.49}$$

$$\begin{aligned} D_2 = -\frac{1}{8N^2}[&:\mathrm{Tr}([[Y,Z],\check{Y}][[\check{Y},\check{Z}],Y]): + :\mathrm{Tr}([[Y,Z],\check{Z}][[\check{Y},\check{Z}],Z]): \\ &+ :\mathrm{Tr}([[Y,Z],T^a][[\check{Y},\check{Z}],T^a]):] \end{aligned} \tag{3.50}$$

where T^a are generators of $U(N)$ $(SU(N))$, the fields are expanded in these generators $Y = Y^a T^a$, and the checked operators are derivatives with respect to that field, $\check{Z}^B_A Z^D_C = (T^a)^B_A (T^b)^D_C \check{Z}^a Z^b = (T^a)^B_A (T^b)^D_C \delta^{ab} = \delta^B_A \delta^D_C$. The normal ordering indicates that derivatives do not act on other fields inside the normal ordering. Unlike for the planar case, we only have the result up to two loops.

Our goal is here is to translate D to an effective Hamiltonain for the open Cuntz oscillator chain H_{open}. It too has an expansion in the 't Hooft coupling

$$H_{\rm open} = \sum_{\ell=0}^{\infty} \left(\frac{\lambda}{4\pi^2}\right)^{\ell} H_{{\rm open},\ell} \tag{3.51}$$

As already state, the action of D on the word W_{12} is given by the planar portion. We need to compute the boundary contributions.

Let us begin with the tree level translation of $D_0 \to H_{\rm open,0}$. The dilatation operator in the $\mathfrak{su}(2)$ sector does not change the length of the spin chain; the total number of fields is conserved. The Cartan generator of the $\mathfrak{su}(2)$ yields the difference between the number of Y and Z fields. It commutes with the dilatation generator and hence is also conserved. Thus the individual number of Y and Z fields is unchanged. We can choose Z to be a highest weight state of the $\mathfrak{so}(6)$ R-symmetry which is positively charged under one of the angular momenta $\hat{J}_1$. In the $\mathfrak{su}(2)$ sector one can represent $\hat{J}_1 = \mathrm{Tr}(Z\check{Z})$. We can do something similar with Y by choosing an orthogonal momentum $\hat{J}_2 = \mathrm{Tr}(Y\check{Y})$. These are dual to the two orthogonal momenta on the S^3 in the $\mathbb{R}_t \times S^3$ subspace of $AdS_5 \times S^5$. The tree level dilatation operator is then given by $D_0 = \hat{J}_1 + \hat{J}_2$. Although $\hat{J}_2$ is well defined, the determinants contribute order N number of Z fields. Thus $\hat{J}_2$, and hence its anomalous dimension, diverges in the planar limit. We should instead consider the combination $D - \hat{J}_1$ for open strings. In particular we translate the tree level dilatation generator to

$$(D_0 - \hat{J}_1) \to H_{\mathrm{open},0} = k + 1 \tag{3.52}$$

There are various results that need to be put together to calculate the boundary contributions to the anomalous dimension of states of the form (3.18) beyond tree level. In the planar limit, the dilatation generator does not mix the fields of the string excitations W_{12} and W_{21}. Thus we isolate contributions to the anomalous dimension due to W_{12} and the poles. To get the full result, we add another copy of the computation for the W_{21} excitation. We are forced to have an even number of sites because Z_1 and Z_2 alternate between each other in the chain.

However, this does not affect the boundary conditions on the chain that we want to derive and in general we will ignore this condition.

We begin at one-loop order. The object to be computed is

$$\langle \alpha_1, \alpha_2; n'_1, \ldots, n'_k | \, H_{\mathrm{open},1} \, |\alpha_1, \alpha_2; n_1, \ldots, n_k\rangle \tag{3.53}$$

where the states are normalized to have unit norm. The first question, is therefore to compute the norm of the bare states above, to leading order in a $1/N$ expansion.

This answer is given by

$$|||\alpha_1, \alpha_2; n_1, \ldots, n_k\rangle||^2 = N^{k+\sum n_i}(N - \alpha_1\alpha_1^*)(N - \alpha_2\alpha_2^*)\exp(\alpha_1\alpha_1^* + \alpha_2\alpha_2^*) \tag{3.54}$$

which results from combining the results of [39] with planar contractions of the words of the chain. The planar contractions of $(W_{12})^a_b$ and its complex conjugate $(\bar{W}_{12})^{\tilde{b}}_{\tilde{a}}$ in the leading planar approximation give a result proportional to $\delta^a_{\tilde{a}}\delta^{\tilde{b}}_b$. The factor of $N^{k+\sum n_i}$ is this proportionality factor and counts the number of matrix contractions necessary to make the word W_{12}. The result is as if the composite word W_{12} was acting as a single Y, but with a different normalization factor. That other contributions are subleading in powers of $1/N$ was shown in [42]. The reason these factors of N are important is that the effective Hamiltonian changes the number of the n_i at the edges, namely n_1, n_k in such a way that they can exit the region sandwiched between the Y. The results in (3.53) can have different powers of N and this affects the naive planar counting.

To compute the matrix elements of $H_{\mathrm{open},1}$ using unnormalized states we need to divide by the norm of the states carefully. For example, if one has in an unnormalized basis that

$$H_{\text{open},1}\,|a\rangle = \sum_b \tilde{H}_{ba}\,|b\rangle \tag{3.55}$$

Then we have that in a normalized basis

$$H_{\text{open},1}\frac{|a\rangle}{\|\,|a\rangle\|} = \sum_b \frac{\|\,|b\rangle\|}{\|\,|a\rangle\|}\tilde{H}_{ba}\frac{|b\rangle}{\|\,|b\rangle\|} \tag{3.56}$$

So

$$H_{ba} = \frac{\|\,|b\rangle\|}{\|\,|a\rangle\|}\tilde{H}_{ba} \tag{3.57}$$

The orbifolded version of (3.49) is now given by

$$D_{1,\text{orb}} = -\frac{1}{2N} :\mathrm{Tr}\left([\mathbf{Y},\mathbf{Z}]\left[\check{\mathbf{Y}},\check{\mathbf{Z}}\right]\right): \tag{3.58}$$

with

$$\mathbf{Z} = \begin{pmatrix} Z_1 & 0 \\ 0 & Z_2 \end{pmatrix}, \quad \mathbf{Y} = \begin{pmatrix} 0 & Y_{12} \\ Y_{21} & 0 \end{pmatrix} \tag{3.59}$$

$$\check{\mathbf{Z}} = \begin{pmatrix} \check{Z}_1 & 0 \\ 0 & \check{Z}_2 \end{pmatrix}, \quad \check{\mathbf{Y}} = \begin{pmatrix} 0 & \check{Y}_{21} \\ \check{Y}_{12} & 0 \end{pmatrix} \tag{3.60}$$

we can pinpoint various contributions to the anomalous dimension. The first one, is where we take a Z_2 from $Z_2^{n_1}$ and move is to the left of the Y_{12}. We call that a hop-out interaction (following the conventions of [45]). The planar contribution to that term is captured by

$$-:\mathrm{Tr}(Z_1 Y_{12}\check{Z}_2\check{Y}_{12}): \tag{3.61}$$

Acting on the initial state gives a power of N from contractions between the derivatives and the word $Y_{12}Z_2$. Notice that the words go in opposite order than the way derivatives act on them (this is illustrated in [16], particularly the section on matrix models). The state we get after this operation is given by

$$\det(Z-\alpha)\det(Z_2-\alpha_2)\mathrm{Tr}\left(\frac{Z_1}{Z_1-\alpha}Y_{12}Z_2^{n_1-1}Y_{21}Z_1^{n_2}Y_{12}Z_2^{n_3}\cdots Z_1^{n_k}Y_{12}\frac{1}{Z_2-\alpha_2}W_{21}\right) \tag{3.62}$$

Now, in the term with the Z_1 pole in the trace we use the substitution $Z_1 = (Z_1-\alpha_1)+\alpha_1$, generating two terms. One of them is $\alpha_1\,|\alpha_1,\alpha_2;n_1-1,n_2,\ldots,n_k\rangle$, and the other one which has no pole anymore at $Z_1=\alpha_1$ This is considered as a single string state starting from brane two and ending on brane two. Such term counts as changing the number of strings and it is non-planar (this can also be checked by computing norms). The other term counts as planar, but proportional to α_1. Thus, the end result is proportional to $N\alpha_1$. However, when normalizing the states, we see that the norm of the states changes as described in equation (3.54) The result for normalized states with unit norm is actually given by following the recipe in equation (3.53), which involves the ratio of the norms of the states. The result is that for each Z we create we attach a factor of $\sqrt{N}$ and for each Z we annihilate we attach a $1/\sqrt{N}$. When translating to the Cuntz oscillator basis, we can use $(\sqrt{N}a_i^\dagger)$ and $(a_i/\sqrt{N})$ without having to recompute the normalizations of the states; using these replacements instead of $a_i^\dagger$ and a_i takes care of it for us. In this process we have one less Z and so the hop-out interaction from the first element of the chain is given by the following extra contribution

$$H_{\text{hop-out, left}} \simeq -\left(\frac{\alpha_1}{\sqrt{N}}\right) a_1 \tag{3.63}$$

Hermiticity ensures that the hop-in interaction is the adjoint of this operation, so we have that

$$H_{\text{hop-in, left}} \simeq -\left(\frac{\alpha_1^*}{\sqrt{N}}\right) a_1^\dagger \tag{3.64}$$

Finally, there is one extra contribution to the left from acting with the term $:\mathrm{Tr}(Z_1 Y_{12} \check{Y}_{12} \check{Z}_1):$ where the derivative with respect to Z acts on the giant graviton. Such terms are identical to those that were already computed in [39], and these are given by

$$H_{\text{giants}} \simeq \alpha_1 \alpha_1^* \tag{3.65}$$

These terms were called 'kissing interactions' in [45].

Putting it all together, we find that the open Cuntz chain Hamiltonian on the left side of the Cuntz chain is given by

$$H_{\text{open},1} = \frac{1}{2}\left[\left(\frac{\alpha_1}{\sqrt{N}} - a_1^\dagger\right)\left(\frac{\alpha_1^*}{\sqrt{N}} - a_1\right) + (a_1^\dagger - a_2^\dagger)(a_1 - a_2) + \dots\right] \tag{3.66}$$

A similar term shows up in the right hand side, with $\alpha_1 \to \alpha_2$ and $a_1 \to a_k$. Notice that this is a simple generalization of equation (3.39) at the boundaries. This is a nearest neighbor interaction with hopping in and out of the chain at the boundaries. It is important to notice that since the parameter α is complex, there are phases associated to hopping in and out at the boundary. This is a simple generalization of the Cuntz Hamiltonian found in [50, 51]. The Hamiltonian can be made to be the same as the one presented in that work if we choose $\alpha_1 = \alpha_2 = -\sqrt{N(1-p/N)}$ in the notation of [50]. This result ends up having the same information content as the one found in [45] (particularly equations 3.7 and 3.8). We interpret the parameter α_i in our expression in terms of raising and lowering operators associated to the momentum of the giant graviton. Since α_i is a coherent state parameter for a (inverted) harmonic oscillator, as shown in [39], we can think of $\alpha_i \simeq b_i$ and $\alpha_i^* \simeq b_i^\dagger$, for a harmonic oscillator pair. In this case, acting with a lowering operator actually increases the R-charge of the giant, and acting with the raising operator lowers the charge. We also have to be mindful of conventions with respect to signs. When we chose the operators $\det(Z_i - \alpha_i)$ as our giant graviton representatives, we get minus signs in the expansion in terms of subdeterminants. Those minus signs appear in the relative sign between α^* and a_1 in the expressions above. If we would have chosen the operators $\det(Z_i + \alpha_i)$ instead, we would have gotten the result above with various signs changed. Those sign differences would reproduce the results of [45] exactly, while changing from Cuntz oscillators to ordinary oscillators would account for the numerical factors in the square roots appearing in equation (3.7), as well as the equation on page 23 describing the boundary Hamiltonian.

Now we move on to two-loop translation of the dilatation operator into the Cuntz Language, that is, $D_2 \to H_{\text{open},2}$. The full calculation is long and tedious and so here we only point out some qualitative features regarding it leaving further details to Appendix A. The constant of proportionality $-1/8N^2$ will be dropped for the calculation and restored at the end. Again, we will restrict our attention to computing the boundary contributions only, as the contributions from the string excitation alone can be obtained from the planar part of the dilatation operator.

The orbifold trick does simplify things and so we will make use the operator (3.18) for our open Cuntz chain. By symmetry we may focus solely on the left boundary of the open Cuntz chain, that is, the graviton with collective coordinate α_1 and the first site. Thus for explaining this calculation we will take our open Cuntz chain to have the schematic form

$$\det\left(Z_1-\alpha_1\right)\operatorname{Tr}\left(\frac{1}{Z_1-\alpha_1}Y_{12}Z_2^{n_1}W\right) \tag{3.67}$$

where W is a word representing the rest of the Cuntz chain.

The boundary terms coming from the term in D_2 proportional to D_1 have already been computed, but there are subtleties that will be discussed later. The boundary of the Cuntz chain will make a contribution only if one of the Y derivatives in D_2 acts on the first Y in the Cuntz chain. The Z derivatives must act on the determinant, or the first site. However, if the Z derivatives act on a site, then a boundary contribution is made only when we hop out some Z's. Our first example will show how these choices of where the Z derivative acts complicates things, but the orbifold trick makes things simpler.

Consider the action of the following term from D_2 on (3.67)

$$:\operatorname{Tr}\left(Y_{12}Z_2Z_2\check{Z}_2\check{Y}_{12}\check{Z}_1\right): \tag{3.68}$$

Had we not used the orbifold trick, the $\check{Z}_2$ would be a $\check{Z}_1$ and have the option of acting on the determinant or the $(Z_1-\alpha_1)^{-1}$ inside the trace. These terms would have split the oscillator chain and we would have thrown them away, but with the orbifold trick the bookkeeping becomes simpler. Indeed the result is

$$
\begin{aligned}
\det\left(Z_1-\alpha_1\right)\operatorname{Tr}&\left(\frac{1}{Z_1-\alpha_1}Y_{12}Z_2^{n_1}W\right)\to\\
&N\det\left(Z_1-\alpha_1\right)\operatorname{Tr}\left(\frac{1}{Z_1-\alpha_1}\frac{1}{Z_1-\alpha_1}Y_{12}Z_2^{n_1-1+1+1}W\right) &(3.69)\\
&-N\det\left(Z_1-\alpha_1\right)\operatorname{Tr}\left(\frac{1}{Z_1-\alpha_1}\right)\operatorname{Tr}\left(\frac{1}{Z_1-\alpha_1}Y_{12}Z_2^{n_1-1+1+1}W\right) &(3.70)
\end{aligned}
$$

where in the first term $\check{Z}_1$ acted on the determinant and in the second term $\check{Z}_1$ acted inside the trace. We already have made use of the equality $Z_1 = Z_1-\alpha_1+\alpha_1$ and have thrown away terms of lower order. Using the results in Appendix A these terms collect into a nice derivative of α_1:

$$
\begin{aligned}
\det\left(Z_1-\alpha_1\right)\operatorname{Tr}&\left(\frac{1}{Z_1-\alpha_1}Y_{12}Z_2^{n_1}W\right)\to\\
&N\partial_\alpha\left[\det\left(Z_1-\alpha_1\right)\operatorname{Tr}\left(\frac{1}{Z_1-\alpha_1}Y_{12}Z_2^{n_1+1+1-1}W\right)\right] \qquad (3.71)
\end{aligned}
$$

It was explained in [39] how double trace terms will form derivatives, but here we have shown things explicitly to emphasize the care needed to get to the end result. To translate this into the Cuntz language, we note that derivatives of α_1 yield factors of α_1^* (see Appendix of [39]) and we keep track of the normalizations using the results earlier in this section. The contribution to the two-loop Hamiltonian reads

$$N^2\left(\frac{\alpha_1^*}{\sqrt{N}}\right)a_1^\dagger a_1^\dagger a_1 \qquad (3.72)$$

Just as double pole terms generate a single derivative with respect to α_1, we can have triple pole terms and these will generate two derivatives with respect to α_1.

Such a term will appear later on. There are a total of eight terms with two Z derivatives and all three derivatives sitting next to each that contribute to the boundary Hamiltonian. The result of adding these together is

$$N^2\left(a_1^\dagger-\frac{\alpha_1}{\sqrt{N}}\right)\left[\left(-\frac{\alpha_1}{\sqrt{N}}\right)a_1+a_1^\dagger\left(-\frac{\alpha_1^*}{\sqrt{N}}\right)\right]\left(a_1-\frac{\alpha_1^*}{\sqrt{N}}\right) \tag{3.73}$$

Now we deduce which terms with two $\check{Y}$'s can make order N^2 contributions. A term containing $\check{Y}\check{Z}\check{Y}$ can only make a contribution if the $\check{Z}$ acts on the first site. Otherwise a factor of $(Z_1-\alpha_1)^{-1}$ gets inserted and splits the chain. In order to get a contribution from the boundary, we have to hop a Z out of the chain. There is only one such term in D_2.

$$-:\mathrm{Tr}(Z_1Y_{12}Y_{21}\check{Y}_{21}\check{Z}_2\check{Y}_{12}): \tag{3.74}$$

We can pick up at most one factor of N from the $\check{Z}$ in terms with two $\check{Y}$'s. To get the other factor of N, the $\check{Y}$'s must sit next to each other. Although there are four such terms, one of them splits the chain. The three remaining contributing terms are

$$:\mathrm{Tr}\left(Y_{12}Y_{21}Z_1\check{Y}_{21}\check{Y}_{12}\check{Z}_1-Y_{12}Z_2Y_{21}\check{Y}_{21}\check{Y}_{12}\check{Z}_1+Z_1Y_{12}Y_{21}\check{Z}_1\check{Y}_{21}\check{Y}_{12}\right): \tag{3.75}$$

Note that equation (3.74) and the second term of (3.75) couple the second site to the giant graviton. The total contribution from these four terms is

$$N^2\left(\frac{\alpha_1}{\sqrt{N}}P_{01}(a_2-a_1)+(a_2^\dagger-a_1)P_{01}\frac{\alpha_1^*}{\sqrt{N}}\right) \tag{3.76}$$

where P_{01} is the projection onto the zero occupation number state at site one.

The last contribution comes from the two derivative terms in D_2, however, it is just proportional to D_1

$$:\mathrm{Tr}([[Y,Z],T^A][[\check{Y},\check{Z}],T^A]): = 2ND_1 \tag{3.77}$$

The contribution from this operator was determined at one-loop and is given by

$$2N^2\left(a_1^\dagger - \frac{\alpha_1}{\sqrt{N}}\right)\left(a_1 - \frac{\alpha_1^*}{\sqrt{N}}\right) \tag{3.78}$$

For the closed Cuntz chain we were able to complete various squares by inserting two copies of the identity into the quadratic terms, one for each site involved. Here we can not do such a manipulation immediately because one of the two objects involved is not a Cuntz site, it is a giant graviton. We can insert the identity for site one $a_1^\dagger a_1 + P_{01}$. This manipulation only completes the square in the commutator term coupling sites one and two, and the giant graviton. We are still left with an incomplete quartic and some quadratic terms.

$$\begin{aligned}&\left(a_1^\dagger - \frac{\alpha_1}{\sqrt{N}}\right)\left[a_1^\dagger a + \left(-\frac{\alpha_1}{\sqrt{N}}\right)a_1 + a_1^\dagger\left(-\frac{\alpha_1^*}{\sqrt{N}}\right)\right]\left(a_1 - \frac{\alpha_1^*}{\sqrt{N}}\right)\\ &\quad + \left(a_1^\dagger - \frac{\alpha_1}{\sqrt{N}}\right)\left(a_1 - \frac{\alpha_1^*}{\sqrt{N}}\right)\end{aligned} \tag{3.79}$$

The reason we do not have the nice form of the closed Cuntz chain at this point is that we forgot about the contributions of certain non-planar terms. Indeed, since the Z derivatives do not necessarily have to act on a site, we can loosen the requirement that derivatives must sit next to each other. There are four such terms in D_2 that have non-vanishing contribution:

$$
\begin{aligned}
&: \mathrm{Tr}\left(-\check{Z}Y_{12}Z_2\check{Y}_{12}\check{Z}_1Z_1 + \check{Z}_1Y_{12}Z_2\check{Z}_2\check{Y}_{12}Z_1\right.\\
&\qquad \left.+\check{Z}_1Z_1Y_{12}\check{Y}_{12}\check{Z}_1Z_1 - \check{Z}_1Z_1Y_{12}\check{Z}_2\check{Y}_{12}Z_1\right): \qquad (3.80)
\end{aligned}
$$

Consider the action of the first term on the Cuntz chain (3.67). The relevant terms are

$$
\begin{aligned}
&-\det\left(Z_1-\alpha_1\right)\mathrm{Tr}\left(\frac{1}{Z_1-\alpha_1}\frac{1}{Z_1-\alpha_1}\frac{1}{Z_1-\alpha_1}Z_1Y_{12}Z_2^{n_1+1}W\right) && (3.81)\\
&+\det\left(Z_1-\alpha_1\right)\mathrm{Tr}\left(\frac{Z_1}{Z_1-\alpha_1}\right)\mathrm{Tr}\left(\frac{1}{Z_1-\alpha_1}\frac{1}{Z_1-\alpha_1}Y_{12}Z_2^{n_1+1}W\right) && (3.82)\\
&+\det\left(Z_1-\alpha_1\right)\mathrm{Tr}\left(\frac{1}{Z_1-\alpha_1}\right)\mathrm{Tr}\left(\frac{1}{Z_1-\alpha_1}\frac{1}{Z_1-\alpha_1}Z_1Y_{12}Z_2^{n_1+1}W\right) && (3.83)\\
&+\det\left(Z_1-\alpha_1\right)\mathrm{Tr}\left(\frac{1}{Z_1-\alpha_1}\frac{1}{Z_1-\alpha_1}\right)\mathrm{Tr}\left(\frac{1}{Z_1-\alpha_1}Z_1Y_{12}Z_2^{n_1+1}W\right) && (3.84)\\
&-\det\left(Z_1-\alpha_1\right)\mathrm{Tr}\left(\frac{1}{Z_1-\alpha_1}\frac{1}{Z_1-\alpha_1}\frac{1}{Z_1-\alpha_1}Z_1Y_{12}Z_2^{n_1+1}W\right) && (3.85)\\
&-\det\left(Z_1-\alpha_1\right)\mathrm{Tr}\left(\frac{Z_1}{Z_1-\alpha_1}\right)\mathrm{Tr}\left(\frac{1}{Z_1-\alpha_1}Y_{12}Z_1^{n_1+1}W\right) && (3.86)
\end{aligned}
$$

where we have not made use of the expansion $Z_1 = Z_1 - \alpha_1 + \alpha_1$. Making use of the expansion, we see that equations (3.81), (3.83), (3.84), and (3.85) pick up a factor of α. The factor of 1 from expanding $Z_1/(Z_1-\alpha_1)$ usually ends up reducing at which order of N the corresponding term contributes. In (3.82) and (3.86), however, we have a trace over the 1 and thus pick up a factor of N. These terms come in at order N^2 but are only quadratic in α_1 and Cuntz operators. The remaining six terms contain triple pole terms which all combine to give a single second derivative with respect to α_1. The contribution to the Hamiltonian from

(3.80) is

$$\begin{aligned}&N^2\left(a_1^\dagger-\frac{\alpha_1}{\sqrt{N}}\right)\left(-\frac{\alpha_1}{\sqrt{N}}\right)\left(-\frac{\alpha_1^*}{\sqrt{N}}\right)\left(a_1-\frac{\alpha_1^*}{\sqrt{N}}\right)\\&-N^2\left(a_1^\dagger-\frac{\alpha_1}{\sqrt{N}}\right)\left(a_1-\frac{\alpha_1^*}{\sqrt{N}}\right)\end{aligned}\tag{3.87}$$

Note that the sign on the quadratic term is exactly opposite that of (3.79) providing a nice cancellation.

The final result after summing everything up and putting back the numerical factors is

$$\begin{aligned}H_{\text{open},2}=-\frac{1}{8}\Bigg[&\left(\frac{\alpha_1}{\sqrt{N}}-a_1^\dagger\right)^2\left(\frac{\alpha_1^*}{\sqrt{N}}-a_1\right)^2+\sum_{i=1}^{k-1}(a_{i+1}^\dagger-a_i^\dagger)^2(a_{i+1}-a_i)^2\\&+\left(a_k^\dagger-\frac{\alpha_2}{\sqrt{N}}\right)^2\left(a_k-\frac{\alpha_2^*}{\sqrt{N}}\right)^2+\left(\frac{\alpha_1}{\sqrt{N}}-2a_1^\dagger+a_2^\dagger\right)P_{01}\left(\frac{\alpha_1^*}{\sqrt{N}}-2a_1+a_2\right)\\&+\sum_{i=2}^{k-1}(a_{i+1}^\dagger-2a_i^\dagger+a_{i-1}^\dagger)P_{0i}(a_{i+1}-2a_i+a_{i-1})\\&+\left(a_{k-1}^\dagger-2a_k^\dagger+\frac{\alpha_2}{\sqrt{N}}\right)P_{0k}\left(a_{k-1}-2a_k+\frac{\alpha_2^*}{\sqrt{N}}\right)\Bigg]\end{aligned}\tag{3.88}$$

The boundary terms have the same structure as the internal terms of the open Cuntz Hamiltonian. We define the c-number operators

$$a_0\equiv\xi_1=\frac{\alpha_1^*}{\sqrt{N}},\quad a_0^\dagger=\xi_1^*=\frac{\alpha_1}{\sqrt{N}}\tag{3.89}$$

$$a_{k+1}\equiv\xi_2=\frac{\alpha_2^*}{\sqrt{N}},\quad a_{k+1}^\dagger=\xi_2^*=\frac{\alpha_2}{\sqrt{N}}\tag{3.90}$$

The ξ_i coordinates are the complex conjugates of similar named variables in [39].

It is then convenient to rewrite the one and two-loop open Cuntz Hamiltonians as

$$H_{\text{open},1} = \frac{1}{2}\sum_{i=0}^{k}(a_{i+1}^\dagger - a_i^\dagger)(a_{i+1} - a_i) \tag{3.91}$$

$$H_{\text{open},2} = -\frac{1}{8}\sum_{i=0}^{k}(a_{i+1}^\dagger - a_i^\dagger)^2(a_{i+1} - a_i)^2 - \frac{1}{8}\sum_{i=1}^{k}(a_{i+1}^\dagger - 2a_i^\dagger + a_{i-1}^\dagger)P_{0i}(a_{i+1} - 2a_i + a_{i-1}) \tag{3.92}$$

We see that at one and two-loops the closed Cuntz Hamiltonian (3.39), (3.41) can be modified very simply to obtain their open versions. One breaks the period of the closed Cuntz chain and adds two boundary 'sites' that are ordinary c-numbers. These c-numbers are scaled versions of the giant graviton collective coordinates.

We would also like the Cuntz Hamiltonian at three-loops for the open Cuntz chain. Understanding the action of the dilatation operator at one and two-loops on delocalized giants $\det(Z-\alpha)$ [39, 5] and expanding in the collective coordinate α, we see that the subdeterminants can be realized as a truncated representation of the harmonic oscillator algebra. Denote the states by $|n\rangle = \det_n(Z)$ and operators b and $b^\dagger$ that act as $b\,|n\rangle = N^{-1/2}\sqrt{n}\,|n\rangle$, $b^\dagger\,|n\rangle = N^{-1/2}\sqrt{n+1}\,|n\rangle$. The delocalized giant graviton operators can be realized as a coherent state of this truncated algebra $|\alpha\rangle = \det(Z-\alpha)$ which satisfy $b\,|\alpha\rangle = \frac{\alpha}{\sqrt{N}}\,|\alpha\rangle$ [52]. Then the one-loop Cuntz Hamiltonian should be written as

$$\sim (b_2^\dagger - a_k^\dagger)(b_2 - a_k) + \sum_{i=1}^{k-1}(a_{i+1}^\dagger - a_i^\dagger)(a_{i+1} - a_i) + (a_1^\dagger - b_1^\dagger)(a_1 - b_1) \tag{3.93}$$

where the subscript on b denotes which giant graviton the operator acts on. The one-loop open Cuntz chain Hamiltonian (3.91) is then realized as (3.93) in a background of coherent state giant gravitons. This approximation is valid because because we are taking the planar limit where the D-branes are rigid objects and the open strings do not back react. We will assume that the giant gravitons can be inserted into the Cuntz chain as ordinary harmonic oscillators happens at three-loops as well. Realizing we are taking the planar limit then allows us to replace the operators with ordinary c-numbers. The open Cuntz Hamiltonian at three-loops is then given by

$$\begin{aligned} H_{\text{open},3} = \frac{1}{16}\sum_{i=0}^{k}(a_{i+1}^{\dagger}-a_i^{\dagger})^3(a_{i+1}-a_i)^3 + \frac{1}{16}\sum_{i=1}^{k} v_a^{i\dagger}M_{ab}P_{0i}v_b^i \\ + \frac{1}{16}\sum_{i=1}^{k-1}(a_{i+2}^{\dagger}-3a_{i+1}^{\dagger}+3a_i^{\dagger}-a_{i-1}^{\dagger})P_{0i+1}P_{0i}(a_{i+2}-3a_{i+1}+3a_i-a_{i-1}) \end{aligned} \tag{3.94}$$

with v_a^i and M_{ab} defined by (3.45) and (3.46) and the boundary operators given by (3.89).

3.5 Discussion

We devoted this Chapter to setting up the technology to be used for Chapters 4 and 5. We described states lying in the $\mathfrak{su}(2)$ sector of $\mathcal{N} = 4$ SYM dual to open strings stretched between giant gravitons. Collective coordinates for the giant gravitons introduce a generating series for giant graviton states of definite R-charge and make them more semiclassical. In Section 4.5, the coordinates will be an explicit realization of the boundary of the open strings we wish to attach to the giant gravitons. The string excitations between the D-branes come in the form of spin chains. These spin chain states and the dilatation operator in this sector were translated into a Cuntz oscillator basis. Diagonalizing the open Cuntz Hamiltonian will yield the anomalous dimensions of open strings in the planar limit. Of particular interest is the ground state of the open Cuntz Hamiltonian and will be the subject of the next chapter. The Cuntz Hamiltonians for the open and closed chains are summarized in Appendix B.

A few comments on the structure of the Cuntz Hamiltonians (3.91), (3.92), and (3.94) are in order. The first term of each Hamiltonian takes the form

$$\sum_{i=0}^{k}[(a_{i+1}^{\dagger}-a_i^{\dagger})(a_{i+1}-a_i)]^{\ell} \tag{3.95}$$

with ℓ the loop order. This is the magnitude squared first order finite difference between consecutive sites raised to a power equal to the loop level at which we are operating. These terms can also been seen as self-energy and hopping terms [5]. The consistent appearance of this terms leads us to conjecture that it will appear at higher loop orders as well. Further evidence for this will be seen when we compute higher order corrections to the energy of open string ground state in Section 4.3. The energy of the state at each loop order receives contributions proportional to $(|\xi_1-\xi_2|^2)^{\ell}$. We will conjecture with symmetry arguments that all contributions at ℓ-loops are proportional to $(|\xi_1-\xi_2|^2)^{\ell}$. These contributions to the ground state energy will appear in perturbation theory due to the expectation values $\langle H_{\text{open},\ell}\rangle$ if a term of the form (3.95) appears in $H_{\text{open},\ell}$. The ground state itself will be corrected as well, but this is accounted for by other terms in the

Hamiltonian.

The last terms of (3.92) and (3.94) are the magnitude squared of a second and third derivative finite difference operator, respectively. Each contains a number of projection operators necessary for $SU(2)$ invariance. They take into account consecutive sites with low occupation number. These are operators where the Y fields are separated by at most one Z at two loops and two Z at three loops. These last terms is also symmetric about the sites on which they operate. For example, switching $i+2 \leftrightarrow i-1$ and $i+1 \leftrightarrow i$ for the three-loop Hamiltonian is a symmetry of this term. At ℓ-loops we expect a similar term to occur; the magnitude squared of an ℓ-order finite difference with $\ell-2$ projectors in the middle

$$\sim \sum_{i=1}^{k} \left(\sum_{m=0}^{\ell} \binom{\ell}{m} a^{\dagger}_{i+m-\lfloor \ell/2 \rfloor} \right) \left(\prod_{n=1}^{\ell-1} P_{0,i+n-\lfloor \ell/2 \rfloor} \right) \left(\sum_{p=0}^{\ell} \binom{\ell}{p} a_{i+p-\lfloor \ell/2 \rfloor} \right) \tag{3.96}$$

The second term of (3.94) is mysterious and has no analog at a lower order. Despite numerous attempts by the author, a simple finite difference form of the operators quartic in the Cuntz oscillators could not be found. Given the nature of the other terms, one would expect it to be a mixture of first and second order finite differences. However, we will see that its expectation value against the open string ground state is non-vanishing, $\left\langle \Omega^{(0)} \right| (v^i_a)^\dagger M_{ab} P_{0i} (v^i_b) \left| \Omega^{(0)} \right\rangle \neq 0$ with $\left| \Omega^{(0)} \right\rangle$ the open string ground state. Thus it can not be rewritten so that every term contains a second or higher order finite difference term. The non-vanishing of the expectation value implies that the ground state *must* get corrected at higher orders in perturbation theory. The second term, however, does have the same reflection symmetry as the others. The exchange $i+1 \leftrightarrow i-1$ is a site-by-site symmetry.

This can be seen by the fact that the matrix (3.46) remains unchanged after flipping it over the horizontal and vertical axes and then swapping the middle two columns and rows. The final swap is necessary because the exchange $i+1 \leftrightarrow i-1$ does not swap $a_{i+1}a_{i-1}$ and $a_i a_i$ in v_a^i.

The reflection symmetry is a consequence of the existence of a parity symmetry at the planar level. Thus we expect this to be a local symmetry of the Cuntz Hamiltonian to all orders in perturbation theory. That is, the Cuntz Hamiltonian should have a normal ordered form such that every term exhibits the reflection symmetry at the site level.

Another universal property of all the terms in the Cuntz Hamiltonian at all loop levels here is that they contain the same number of Cuntz oscillators. Recalling that $P_0 = [a, a^\dagger]$ is quadratic in the Cuntz oscillators, we see that all terms have 2ℓ Cuntz oscillators at ℓ-loop order. Even thought the different kinds of interactions have different range, they all have the same number of Cuntz oscillators when we fix the loop level. This is different than the spin chain picture where the range of individual interactions can be different than the loop level (although the maximum range is bounded by the loop level). We currently do not have an explanation for why the same number of Cuntz oscillators appear, we do predict that the Cuntz Hamiltonian can always be written in a form in which this is true at all loop orders.

Chapter 4

Exploring the Ground State

Using the technology of Chapter 3 developed for open strings stretched between giant gravitons, we solve for the open string ground state and make inferences about the geometry in which it lives. In particular, we conjecture that the open string satisfies a relativistic dispersion relation to all loop orders whose origin is a central charge extension of a $\mathfrak{su}(2|2)$ symmetry left unbroken by the giant gravitons. The central charge is given by the distance between the collective coordinates of the giant gravitons between which the string is stretched.

4.1 Finding the Ground State

We use coherent states of open strings described at the end of Section 3.3 to find the ground state of the lowest order non-trivial open Cuntz Hamiltonian (3.91). The procedure is to minimize the expectation value of the Hamiltonian against a single coherent state. We will fix the giant gravitons to have collective coordinates α_1 and α_2 for the remainder of this chapter and so we will omit these labels when writing coherent states of open strings. That is, we will write

$|z_1, \ldots, z_k\rangle$ instead of $|\alpha_1, \alpha_2; z_1, \ldots, z_k\rangle$. One obtains a simple quadratic function of the z_i

$$\left\langle z_1^0, \ldots, z_k^0 \right| H_{\text{open},1} \left| z_1^0, \ldots, z_k^0 \right\rangle = \frac{1}{2}\left[\left|\xi_1 - z_1^0\right|^2 + \sum_{i=1}^{k-1} |z_i^0 - z_{i+1}^0|^2 + \left|z_k^0 - \xi_2\right|^2\right] \tag{4.1}$$

When we minimize with respect to the z_i^0 parameters we find that

$$\xi_1 - z_1^0 = z_1^0 - z_2^0 = \cdots = z_i^0 - z_{i+1}^0 = \cdots = z_k^0 - \xi_2 \tag{4.2}$$

Adding these together we have

$$\xi_1 - \xi_2 = (k+1)(z_i^0 - z_{i+1}^0) \tag{4.3}$$

Solving for the individual collective coordinates we have

$$z_i^0 = \frac{1}{k+1}[(\xi_1 - \xi_2)i + (k+1-i)\xi_1] \tag{4.4}$$

Here we let $i = 0, \ldots, k+1$ so that $z_0^0 = \xi_1$ and $z_{k+1}^0 = \xi_2$. For convenience, we make the notational identification

$$\left|\Omega^{(0)}\right\rangle \equiv \left|z_1^0, \ldots, z_k^0\right\rangle \tag{4.5}$$

Using $z_i^0 - z_{i+1}^0 = \frac{1}{k+1}(\xi_1 - \xi_2)$ we find that the expectation value of the Hamiltonian against this state is

$$E_0^{(1)} \equiv \frac{1}{2}\frac{|\xi_1 - \xi_2|^2}{k+1} \tag{4.6}$$

Here the superscript indicates that we are doing a one-loop computation, and the subscript indicates the ground state energy. To show consistency with the previous evaluation using the collective coordinate approach, we note that when $k = 0$ (a chain with no sites), we reproduce the energy of the configurations calculated in [39]. Additionally, if $\alpha_1 = \alpha_2$ (and hence $\xi_1 = \xi_2$), we get the same ground state with zero energy first deduced in [50].

Let us show that the state we have found is not only an eigenstate of the Hamiltonian, but the true ground state. We begin with the following operator identity

$$\sum_{i=0}^{k}(a_{i+1} - a_i) = \xi_2 - \xi_1 \tag{4.7}$$

Applying the Hamiltonian (3.91) to $\left|\Omega^{(0)}\right\rangle$ we have

$$H_{\text{open},1}\left|\Omega^{(0)}\right\rangle = \frac{1}{2}\frac{\xi_2 - \xi_1}{k+1}\sum_{i=0}^{k}(a_{i+1}^\dagger - a_i^\dagger)\left|\Omega^{(0)}\right\rangle = \frac{1}{2}\frac{|\xi_1 - \xi_2|^2}{k+1}\left|\Omega^{(0)}\right\rangle \tag{4.8}$$

which shows $\left|\Omega^{(0)}\right\rangle$ is an eigenstate. Let $|\psi\rangle$ denote an abitrary state and $|\psi\rangle_i = (a_{i+1} - a_i)|\psi\rangle$ including $i = 0$ and $i = k$. Using (4.7) we have

$$\sum_{i=0}^{k}|\psi\rangle_i = (\xi_2 - \xi_1)|\psi\rangle \tag{4.9}$$

Using the inequality between the quadratic mean and the arithmetic mean (suitably generalized to complex vector spaces), we have

$$\frac{1}{k+1}\sum_{i=0}^{k}|||\psi\rangle_i||^2 \geq \left|\left|\frac{1}{k+1}\sum_{i=0}^{k}|\psi\rangle_i\right|\right|^2 = \frac{|\xi_1 - \xi_2|^2}{(k+1)^2}\langle\psi|\psi\rangle \tag{4.10}$$

The inequality follows from convexity of the function $|| \, |\psi\rangle \, ||^2$ on a complex vector space. It is saturated only if the $|\psi\rangle_i$ are all the same vector. For a normalized state $\langle\psi|\psi\rangle = 1$ and we can translate this into the following inequality

$$\langle\psi| \, H_{\text{open},1} \, |\psi\rangle = \frac{1}{2}\sum_{i=0}^{k} || \, |\psi\rangle_i \, ||^2 \geq \frac{1}{2}\frac{|\xi_1 - \xi_2|^2}{k+1} = E_0^{(1)} \tag{4.11}$$

which shows that the energy for any other state is higher than the one for the coherent state we found. The only thing left to show is that the state $\left|\Omega^{(0)}\right\rangle$ has finite norm. As explained in Section 3.3, this requires $|z_i^0| < 1$ for $1 \leq i \leq k$. The α are required to have norm less than $\sqrt{N}$ [39], it follows that $|\xi| \leq 1$. Since the z_i^0 are lie in the convex hull of ξ_1 and ξ_2, it follows that each of the z_i^0 have norm less than one as well. Thus all of the z_i are in the unit disk and the state is normalizable.

4.2 Geometry from Giant Gravitons and Strings

What we see is that the z coordinates are very closely related to the α coordinates characterizing giant gravitons. The geometric layout of the ground state collective coordinates is displayed in Figure 4.1 The expectation value of the energy for a general coherent state with arbitrary collective coordinates z_i in the unit disk, with $z_0 = \xi_1$ and $z_{k+1} = \xi_2$ is evaluated to a sum of squared distances in the complex plane,

$$E(z_0, \ldots, z_{k+1}) = \frac{1}{2}\left(\frac{\lambda}{4\pi^2}\right)\sum_{i=0}^{k} |z_{i+1} - z_i|^2 \tag{4.12}$$

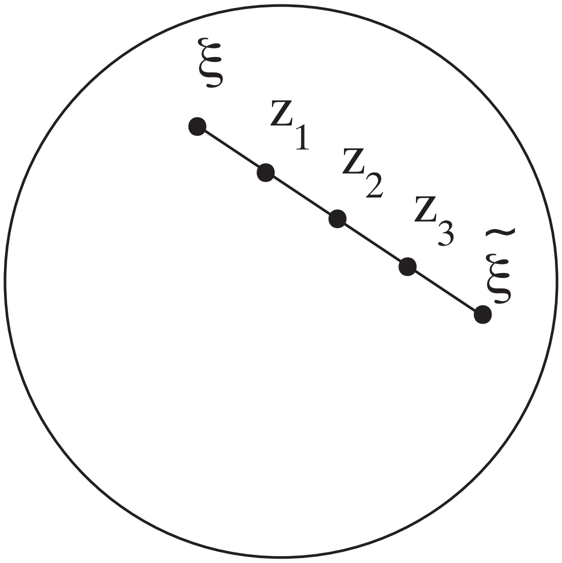

Figure 4.1: Geometric layout of the z_i^0 in the ground state, as an interpolating chain of complex numbers between ξ_1 and ξ_2.

which is a geometric equation and we have restored the 't Hooft coupling. Although z_0 and z_{k+1} are the giant graviton coordinates, the energy of the state does treat them differently than the other z_i. We can reverse the logic and state that all the z_i could be treated as if they are D-brane coordinates of some sort. The formula for the mass squared then looks like a sum over contributions of impurities stretched between successive D-branes with gauge invariance requiring that for each incoming string to a brane there is an outgoing string. This interpretation gives further evidence to the idea that geometry at strong coupling can be understood in terms of open strings stretching between gases of eigenvalues (D-branes) as espoused originally in [18]. This also makes contact with the calculations in [53, 54] which required a saddle point integral to obtain a geometric interpretation. It improves on these concepts by allowing specific D-brane endpoints. Indeed, we find for the ground state an exact calculation at one-loop, rather than an approximation.

We can write an effective action for the Cuntz chain with Hamiltonian (4.12) to make further contact with the geometric interpretation of giant gravitons described in [39]. The effective action for coherent states in the standard representation is

$$S_{\text{eff}} = \int dt \, \langle \vec{z}(t) | \, i\partial_t \, | \vec{z}(t) \rangle - \int dt \, \langle H_{\text{open}} \rangle \tag{4.13}$$

The first term is the Berry phase for the coherent states. This was originally computed in [50], but the result was written in a different coordinate system. To compute the Berry phase in our coordinates, we need the following result for unnormalized Cuntz coherent states

$$\langle \tilde{z} | z \rangle = \sum_{k=0}^{\infty} (\tilde{z}^* z)^k = \frac{1}{1 - \tilde{z}^* z} \tag{4.14}$$

Then we can take the limit

$$\lim_{\tilde{z} \to z(t)} \frac{1}{\langle \tilde{z} | z(t) \rangle} i\partial_t \, \langle \tilde{z} | z(t) \rangle = \frac{i\bar{z}\dot{z}}{1 - \bar{z}z} \tag{4.15}$$

This gives us a Berry connection on the set of states parametrized by $|z\rangle$. If we choose to work with normalized states, we use the following definition for the

Berry phase

$$\lim_{\tilde{z}\to z(t)} \frac{1}{\sqrt{\langle \tilde{z}|\tilde{z}\rangle}} \partial_t \left(\frac{1}{\sqrt{\langle z(t)|z(t)\rangle}} \langle \tilde{z}|z(t)\rangle \right) = \frac{i}{2} \frac{\bar{z}\dot{z} - \dot{\bar{z}}z}{(1-\bar{z}z)} \tag{4.16}$$

which differs from the above by a total derivative. The Berry connection associated to the holomorphic variable z gives rise to a metric for the z coordinate, which turns out to be the metric of the Poincaré disc.

Apart from the one-loop correction Cuntz Hamiltonian, there is a tree level contribution to the energy of the Cuntz chain which we have ignored. In Section 3.4.2 we made the translation $D_0 - \hat{J}_1 \to k+1$. We subtracted out $\hat{J}_1$, which counts the number of Z fields in a field theory operator, because in the large N limit the graviton operators yield an infinite contribution. Here we will add $\hat{J}_1$ back to the open Cuntz Hamiltonian and compute its expectation value for open Cuntz chains for the purpose of building an effective Hamiltonian.

The contribution to $\langle \hat{J}_1 \rangle$ from the giant gravitons was computed in [39] and we will freely include it later being careful with the fact that ξ is now defined to be the complex conjugate of the variable ξ defined in that paper. The contribution to $\langle \hat{J}_1 \rangle$ from the open string is $\langle \hat{N} \rangle$, the expectation value of the occupation number operator. Noting that equation (4.14) is a generating series for the amplitudes of the different $|n\rangle$ states in a coherent state parametrized by z, the expectation value can be easily computed as

$$\langle \hat{N} \rangle = \lim_{\tilde{z}\to z} (\langle \tilde{z}|z\rangle)^{-1} z\partial_z \langle \tilde{z}|z\rangle = \frac{\bar{z}z}{(1-\bar{z}z)} \tag{4.17}$$

The coherent state effective action to one-loop order, including the effects of the giant graviton and the string stretching back from ξ_2 to ξ_1, is

$$
\begin{aligned}
S_{\text{tot}} &= S_{\text{gg}} + S_{\text{cc}} + S_{\text{return}} \qquad (4.18) \\
S_{\text{gg}} &= N \int dt \left[\frac{i}{2}(\xi_1 \dot{\bar{\xi}}_1 - \bar{\xi}_1 \dot{\xi}_1) - (1 - \bar{\xi}_1 \xi_1) \right] \\
&\qquad + N \int dt \left[\frac{i}{2}(\xi_2 \dot{\bar{\xi}}_2 - \bar{\xi}_2 \dot{\xi}_2) - (1 - \bar{\xi}_2 \xi_2) \right] \qquad (4.19) \\
S_{\text{cc}} &= \int dt \left(\frac{i}{2} \sum_{i=1}^{k} \frac{\bar{z}_i \dot{z}_i - \dot{\bar{z}}_i z_i}{(1 - \bar{z}_i z_i)} \right) - \sum_{i=1}^{k} \frac{\bar{z}_i z_i}{1 - \bar{z}_i z_i} \\
&\qquad - (k+1) - \frac{1}{2} \left(\frac{\lambda}{4\pi^2} \right) \sum_{i=0}^{k} |z_{i+1} - z_i|^2 \qquad (4.20) \\
S_{\text{return}} &= - \int dt \left(1 + \frac{1}{2} \left(\frac{\lambda}{4\pi^2} \right) |\xi_1 - \xi_2|^2 \right) \qquad (4.21)
\end{aligned}
$$

The action S_{return} is from the return string previously labeled by W_{21}. Here we have let $W_{21} = Y$, that is, it is a Cuntz chain with zero sites.

Let us look at the equations of motion of the z_i and $\xi_1,\ \xi_2$ in the case $\lambda = 0$

$$\dot{\xi}_1 = -i\xi_1, \quad \dot{\xi}_2 = -i\xi_2 \tag{4.22}$$

$$\dot{z}_i = -iz_i \tag{4.23}$$

The collective coordinates ξ_1, ξ_2, and z_i all rotate at the same angular speed. This means that in the free field theory limit $|z_i - z_{i+1}|^2$ is constant. When we minimize the one-loop term with respect to the z_i, we find a correction to the equations of motion. On the ground state of the Cuntz chain this correction vanishes for the z_i^0. The only corrections to the equations of motion in this case are the corrections to the equations of motion of $\xi_1,\ \xi_1$. This correction is suppressed by $1/N$, so it can be considered as back-reaction of the brane to the presence of strings attached to it. If we consider small fluctuations of the z_i^0 around their ground state, the fact that the ξ motion can only be corrected to order $1/N$ means that we can treat it as a Dirichlet boundary condition, namely $z_0,\ z_{k+1}$ have a fixed motion described by the free giant graviton solution to the equations of motion.

Although the coordinates $\xi_1,\ \xi_2,\ z_i$ parametrize the same disk, appear on similar footing in the interacting Hamiltonian, and share the equations of motion in the free field limit, the associated phase space for the variables is different. The Berry connection for the variables $\xi_1,\ \xi_2$ gives rise to a flat metric in the ξ coordinate, while the Berry phase in the z coordinate lead to a Poincaré disk metric. This indicates that in the end the ξ and the z are representing different objects: D-branes and pieces of strings. When we take the D-branes to the edge of the disk we recover exactly the one loop dispersion relation for giant magnons and their bound states made of $k+1$ defects [38]. This will be important in Section 4.5, when we explicitly construct the open string dual to the ground state $\left|\Omega^{(0)}\right\rangle$. We also find that the wave function characterized by the z_i is exactly of the Bethe ansatz type at complexified momentum and where the S-matrix coefficients for various re-orderings of the momenta vanish. It is natural to identify $z \simeq \exp(ip)$ at complex values of p to make this identification.

We can try to apply this result to other setups. For example, consider the problem of open spring theory, where at the end of a long computation to one loop order in a basis of operators made of Schur polynomials [43] with string decorations [55], one obtains an effective Hamiltonian which is similar to a discretized hopping on a lattice [56]. Diagonalizing this problem leads to an effective theory of free harmonic oscillators [57]. The springs are made of a string stretching between two giants with a single Y (a Cuntz chain with zero sites). The main advance of [39] was to simplify these computations by introducing the collective coordinate approach. In this section we see that for strings (Cuntz chains) made with $k+1$ Y's stretching between the giants, where we get a Cuntz chain with k sites, the one loop computation of the spring energy is reduced by $1/(k+1)$ relative to the case with a single Y defect. This is similar to taking $k+1$ springs and connecting them in a series configuration. To connect them in parallel one would use many strings stretching between the giants. Thus we see that these computations generate more configurations for the open spring theory program that lead to a system of harmonic oscillators in the one loop approximation of anomalous dimensions.

4.3 Correcting the Ground State

So far we have studied the one-loop effective Hamiltonian for strings stretching between giant gravitons and computed their ground state. We have seen that the energy of the state can be understood geometrically. It is interesting to consider the higher loop computation for various reasons. Consider for example the case of the higher loop computation of BMN states [58, 59]. The goal there was to show that the higher loop order corrections matched the string theory result for energies [60] and to show that a low energy effective field theory on the worldsheet would appear. One can follow the same rationale here, and ask what is the effective Hamiltonian to higher loop orders and try to understand how the Hamiltonian and its ground state are organized.

It is simple to understand the giant magnon dispersion relation as arising from saturating a BPS constraint for a centrally extended $\mathfrak{su}(2|2)$ algebra [61] This also applies for their bound states [38]. In general setups, like strings in flat space, one notices that the central charge extension of supersymmetry vanishes for closed string states on trivial topologies, that is, those that have no fundamental group. This is not generally so for open strings. If one considers D-branes in a flat background, the position separation between D-branes is a central charge. The separation vector between two D-branes can be thought of as being T-dual to momentum [62]. Momentum appears as a central charge for supersymmetry, as seen in dimensional reduction. The central charges of excitations in general can be physical in the open string sector even if they are confined for closed strings. One can check that this central charge extension property applies to solitons as well as fundamental particles in field theory [63]. This understanding is the basis for dualities in $\mathcal{N} = 2$ theories in four dimensions [64]. The fact that the spectrum of closed (long) string excitations is characterized by building blocks that carry a central charge suggests that the spectrum of open strings might actually measure this charge directly in the ground state of the open string. Looking at the results we found in the previous section, the string central charge is computed exactly by the difference of the coordinates of the end D-branes in the droplet plane. Obtaining additional evidence to identify $\alpha_1 - \alpha_2$ as a central charge is important because then we can really start thinking of the giant gravitons as collective objects in the field theory in a way that resembles the Coulomb branch of $\mathcal{N} = 4$ SYM more precisely. This is, after all, the expected low energy theory on the worldvolume of the giant gravitons themselves when they coincide. It would also tell us that the ground state of these strings might be computed by a BPS formula and extrapolating to strong coupling might be possible not only in principle, but in practice as well.

Consider also the problem of understanding the origin of this central charge from the point of view of string motion in $AdS_5 \times S^5$. For giant magnons this was understood in [37] where the relation between the central charges of the spin chain and the geometric formulation in gravity became clear; the giant magnon was identified as a particular geometric configuration. It is important that relativistic effects play a very important role in making the match between the sigma model and the magnon dispersion relation possible. The geometric picture found this way is very similar to the one that was argued for earlier in field theory [53, 54] using a saddle point approximation on a background made of a gas of eigenvalues. Obtaining further evidence for this geometric interpretation in field theory, and more precisely, the interpretation of geometries as being approximately described by eigenvalues forming some sort of quantum gas [18] whose excitations are bits of strings stretching between the eigenvalues is worthwhile. Finding exactly how this intuition ends up working in detail might give us a better understanding of how higher dimensional geometry emerges in field theory.

Finally, consider the problem of integrability of the spin chain. The integrability in the closed string sector has been argued in [65, 14], and perhaps a one parameter family of integrable systems interpolate between these [66]. A review of this program can be found in [15]. For open strings, one generally expects that general boundary conditions of the spin chain will not be integrable, but that for special boundary conditions the integrability might be preserved. It has been suggested that integrability is preserved for general giant gravitons [67]. Only in the special case of the maximal giant graviton, however, is there enough evidence for this (see for example [68]) where one can argue that the system might be solvable with a Bethe ansatz. In the case that the general giant graviton boundary condition is not integrable, understanding the structure of the Hamiltonian to higher loop orders will help us understand the detailed dynamics of the strings better. We can compare it directly to the effective action of a string in a particular geometry (with α' corrections), rather than to the very special properties that make the system fully solvable in an integrable setup. Also, even if the system with giant graviton boundary conditions is not integrable, one might still be able to find some exact eigenstates of the spin chain, or in our case, the Cuntz Hamiltonian.

Given the Cuntz Hamiltonians in Section 3.4.2, we can correct the ground state to first order in perturbation theory and the correction to the energy up to second order. The equations to second order in perturbation theory require sums over the eigenvalues of the Hamiltonian. It is unexpected that we could obtain the spectrum for any number of sites due to the lack of integrability or a Bethe ansatz for general boundary conditions of the giant gravitons. Regardless, we will need a handle on the excited states of the Cuntz Hamiltonian.

4.3.1 Shifted Cuntz Operators

We would like to construct a Fock space of states identifying the open string ground state as the vacuum. Consider a single Cuntz excitation at site i, $a_i^\dagger \left|\Omega^{(0)}\right\rangle$. It is not orthogonal to the ground state. We substract off the projection and find that

$$\left\langle \Omega^{(0)} \right| \left[(a_i^\dagger - \bar{z}_i^0) \left| \Omega^{(0)} \right\rangle \right] = 0 \tag{4.24}$$

We think of $(a_i^\dagger - \bar{z}_i^0) \left| \Omega^{(0)} \right\rangle$ as a one particle state. The process for constructing an n-particle state is just the Gram-Schmidt process beginning with the state $(a_i^\dagger)^n \left| \Omega^{(0)} \right\rangle$. The result is that the n-particle states are given by

$$(a_i^\dagger)^{n-1} (a_i^\dagger - \bar{z}_i^0) \left| \Omega^{(0)} \right\rangle \tag{4.25}$$

They are mutually orthogonal, but not yet normalized. We define the site operators

$$A_i^{(n)} = \begin{cases} 1 & n = 0 \\ (a_i)^{n-1} (a_i - z_i^0) & n > 0 \end{cases} \tag{4.26}$$

We include the $n = 0$ case for convenience. The operators (4.26) annihilate the ground state for all $n > 0$, $A_i^{(n)} \left| \Omega^{(0)} \right\rangle = 0$. We think of $A_i^{(n)\dagger}$ as the creation operator for an n-particle state at site i.

One can show by induction that the site operators satisfy the commutation relations

$$[A_i^{(m)}, A_j^{(n)\dagger}] = \delta_{ij} \sum_{i=1}^{\min(m,n)} A_i^{(n-i)\dagger} P_{0i} A_i^{(m-i)} \tag{4.27}$$

Using (4.27) we find that the states $A_i^{(n)^\dagger} \left| \Omega^{(0)} \right\rangle$, $n > 0$, have norm squared

$$\left| \left| A_i^{(n)\dagger} \left| \Omega^{(0)} \right\rangle \right| \right|^2 = \left\langle \Omega^{(0)} \right| A_i^{(n)} A_i^{(n)\dagger} \left| \Omega^{(0)} \right\rangle = \left\langle \Omega^{(0)} \right| P_{0i} \left| \Omega^{(0)} \right\rangle = 1 - |z_i^0|^2 \tag{4.28}$$

To fully normalize a state with particles created at multiple sites, one should divide by $(1 - |z_i^0|^2)^{1/2}$ for each $A_i^{(n)\dagger}$ present. Although for $m = n = 1$ we have

$$[A_i^{(1)}, A_j^{(1)\dagger}] = \delta_{ij} P_{0i} \tag{4.29}$$

the single excitation site operators do not form a Cuntz algebra. This can be seen from the relation $a_i a_i^\dagger = I$. For the single excitation site operators we have

$$A_i^{(1)} A_i^{(1)\dagger} = (I - |z_i^0|^2) - \bar{z}_i^0 A_i^{(1)} - z_i^0 A_i^{(1)\dagger} \tag{4.30}$$

As a consequence, if we choose to work in the basis of n-particle states instead of the occupation number basis, we can not simply make the replacement $a_i \to A_i^{(1)}$, $a_i^\dagger \to A_i^{(1)\dagger}$. To translate from the Cuntz oscillators to the site operators, one must undo the transformation that takes a_i^n to $A_i^{(n)}$. For $n > 0$ one has

$$a_i^n = \sum_{\ell=0}^{n} (z_i^0)^\ell A_i^{(n-\ell)\dagger} \tag{4.31}$$

The site operators have the property that they do not form an $\mathbb{N}$ homomorphism [1]. That is, $A_i^{(m)} A_i^{(n)} \neq A_i^{(m+n)}$. The composition rule for $m,\ n > 0$ is $A_i^{(m)} A_i^{(n)} = A_i^{(m+n)} - z A_i^{(m+n-1)}$. The site operators thus do not build a true Fock space. Regardless, these operators do generate excitations above the open string ground state and we will continue to refer to them as particles.

Lastly we can extend the site operators to boundary of the open Cuntz chain by defining $A_0^{(1)} = b_1 - \xi$, $A_{k+1}^{(1)} = b_2 - \tilde{\xi}$. It only really makes sense to introduce the giant graviton collective coordinates when we are talking about coherent states.

---

[1] Thinking of $\mathbb{N}$ as a monoid, not a group.

Using the arguments of Section 3.4.2, we should then think of these operators in coherent state giant graviton backgrounds. Then we have $A_0^{(1)} = A_{k+1}^{(1)} = 0$.

We can reexpress the one-loop Cuntz Hamiltonians (3.91) in terms of the site operators. We define the difference between the string collective coordinates $\Delta z \equiv z_{i+1}^0 - z_i^0 = (\xi_2 - \xi_1)/(k+1)$. The one-loop energy of the ground state has already been computed to be

$$E_0^{(1)} = \frac{1}{2}\frac{|\xi_1 - \xi_2|^2}{k+1} \tag{4.32}$$

The sum $\sum_{i=0}^{k}(A_{i+1} - A_i)$ telescopes and hence vanishes. One has

$$\begin{aligned} H_{\text{open},1} &= \frac{1}{2}\sum_{i=0}^{k}(A_{i+1}^{(1)\dagger} - A_i^{(1)\dagger} + \Delta\bar{z})(A_{i+1}^{(1)} - A_i^{(1)} + \Delta z) \\ &= E_0^{(1)} + \frac{1}{2}\sum_{i=0}^{k}(A_{i+1}^{(1)\dagger} - A_i^{(1)\dagger})(A_{i+1}^{(1)} - A_i^{(1)}) \end{aligned} \tag{4.33}$$

Writing the Hamiltonian in this form directly isolates the ground state energy from the energy of the excited states. That is, since $A_i^{(1)}\left|\Omega^{(0)}\right\rangle = 0$, it is immediate that $H_{\text{open},1}\left|\Omega^{(0)}\right\rangle = E_0^{(1)}\left|\Omega^{(0)}\right\rangle$.

The system with one site, $k = 1$, is actually solvable. The Hamiltonian takes the simple form

$$H_{\text{open},0} = E_0^{(0)} + A_1^{(1)\dagger}A_1^{(1)} \tag{4.34}$$

The spectrum was solved in [67] in the case of $\xi_1,\ \xi_2 \in \mathbb{R}$ with their $\alpha = -z_1^0 = -(\xi_1 + \xi_2)/2$. The adjustment to account for complex giant graviton coordinates is simple. The excited states and their energies above the ground state are given by

$$|\Psi(p)\rangle = \sum_{n=1}^{\infty} \sin(pn) e^{in\mathrm{Arg}(z_1^0)} A_1^{(n)\dagger} |0\rangle_1 \tag{4.35}$$

$$E_1(p) = (1 + |z_1^0|^2 - 2|z_1^0|\cos(p)) = (1 - |z_1^0|)^2 + 4|z_1^0|\sin^2\left(\frac{p}{2}\right) \tag{4.36}$$

where p is a quasi-momentum defined in the range $0 \leq p \leq \pi$ and $|0\rangle_1$ is the zero occupation state for the one site Cuntz chain. We immediately see that there is a gap between the ground state and the first excited state given by $(1 - |z_1^0|)^2$. These states are delta function normalizable

$$\langle\Psi(p)|\Psi(p')\rangle = \frac{\pi}{2}(1 - 2|z_1^0|\cos(p) + |z_1^0|^2)\delta(p - p') \tag{4.37}$$

The states (4.35) are not written in terms of the n-particle states described earlier. However, they can be written in that basis using

$$\sqrt{1 - |z_i^0|^2}\, |0\rangle_k = P_{0,i} \left|\Omega^{(0)}\right\rangle = (1 - z_i^0 a_i^\dagger) \left|\Omega^{(0)}\right\rangle \tag{4.38}$$

and $a^\dagger A_i^{(n)\dagger} = A_i^{(n+1)\dagger}$. Then (4.35) becomes

$$|\Psi(p)\rangle = \frac{1}{\sqrt{1 - |z_1^0|^2}} \sum_{n=1}^{\infty} \left(\sin(pn) - |z_1^0|\sin(p(n-1))\right) e^{in\mathrm{Arg}(z_1^0)} A_1^{(n)\dagger} \left|\Omega^{(0)}\right\rangle \tag{4.39}$$

where we have used $|z_1^0| = z_1^0 \exp(-i\mathrm{Arg}(z_1^0))$. Equation (4.35) suggests that the states $A_i^{(n)\dagger} P_{0i} \left|\Omega^{(0)}\right\rangle$ might be a more natural candidate for the n-particle states than the $A_i^{(n)\dagger} \left|\Omega^{(0)}\right\rangle$, each contributing n units of p momentum. The one site states take the form of a Bethe ansatz for a semi-infinite lattice and so we conclude some form of integrability.

The solution for the two site chain when $\xi_1 = \xi_2 = 0$ was given in [67]. For this case of giant gravitons, the site operators are the usual Cuntz oscillators and the ground state is the zero occupation number state, $A_i^{(n)} \to (a_i)^n$, $\left|\Omega^{(0)}\right\rangle \to |0\rangle_k$. The two site open Cuntz chain is related to a two site closed chain (the hopping terms have a different normalization) and is integrable. The solution for the excited states can be solved using a Bethe ansatz and is given by

$$|n, q\rangle = \sum_{\ell=0}^{n} [2\sin(q\ell) - \sin(q(\ell+1))](a_1^\dagger)^\ell (a_2^\dagger)^{n-\ell} |0,0\rangle_2 \tag{4.40}$$

where q is a complex momentum subject to the constraint

$$4\sin(qn) - 4\sin(q(n+1)) + \sin(q(n+2)) = 0 \tag{4.41}$$

The energy of these states is given by

$$E_2(n, q) = 2 - \cos(q) \tag{4.42}$$

The appearance of the integer n reflects the fact that the Hamiltonian commutes with the total occupation number operator. For each n there are finitely many solutions to (4.41). The spectrum of the excited states is then countable, although the solution space for real q should be dense in some subset of $[0, \pi]$. As we move ξ_1, ξ_2 away from zero, the spectrum will deform but maintain this non-trivial structure.

Another special case to consider is $\xi_1 = \xi_2$. This implies that the string collective coordinates are equal as well and there is only one free parameter $z \equiv z_1^0 = z_2^0$. The site operators will produce factors of z when acting on states

$$A_i^{(1)}(A_i^{(n)\dagger}|0\rangle_k) = (A_i^{(n-1)\dagger} - zA_i^{(n)\dagger})|0\rangle_k \tag{4.43}$$

$$A_i^{(1)\dagger}(A_i^{(n)\dagger}|0\rangle_k) = (A_i^{(n+1)\dagger} - zA_i^{(n)\dagger})|0\rangle_k \tag{4.44}$$

Even though the particle number changes indefinitely under these operators, the same factor z is produced at all sites Thus for some states, it should be easier to relate the amplitudes of different particle excitations. As a concrete example we consider the eigenstate

$$|1,\pi/3\rangle_z = \sum_{n=1}^{\infty}(-z)^{n-1}(A_1^{(n)\dagger} - A_2^{(n)\dagger})|0\rangle_2\,, \quad E_{2,z}(n,\pi/3) = \frac{3}{2}(1+|z|^2) \tag{4.45}$$

This state is the deformation of the two site excited state (4.40) with $n = 1$ and $q = \pi/3$, which we obtain as we take $z \to 0$. Note that this state does not contain terms with particles excited at site one and site two. The cancellation happens that makes this possible is

$$A_2^{(1)\dagger}(A_2^{(1)} - \tfrac{1}{2}A_1)\sum_{n=1}^{\infty}(-z)^{n-1}A_1^{(n)\dagger}|0\rangle_2 \tag{4.46}$$

$$= A_2^{(1)\dagger}((-z) - \tfrac{1}{2}A_1)\sum_{n=1}^{\infty}(-z)^{n-1}(A_1^{(n)\dagger}|0\rangle_2) \tag{4.47}$$

$$= A_2^{(1)\dagger}\left(\sum_{n=1}^{\infty}(-z)^n A_1^{(n)\dagger} - \frac{1}{2}\sum_{n=1}^{\infty}(-z)^{n-1}A_1^{(n-1)\dagger} - \frac{1}{2}\sum_{n=1}^{\infty}(-z)^n A_1^{(n)\dagger}\right)|0\rangle_2 \tag{4.48}$$

$$= -\frac{1}{2}A_2^{(1)\dagger} \tag{4.49}$$

There is another term with $1 \leftrightarrow 2$ that allows (4.45) to be an exact eigenstate. Similar cancellations occur where $\sum_{n_1=1}^{\infty}(-z)^{n-1}A_1^{(n_1)\dagger}A_2^{(n_2)\dagger}$ will only generate terms $A_1^{(m_1)\dagger}A_2^{(m_2)\dagger}$ with $m_1,\ m_2 < n_2$. Summing states of this type and solving the constraints for low particle number might lead to new exact eigenstates, although their exact form is beyond the scope of this work.

As for integrability, we note that the space of states characterized by the site operators $A_1^{(n_1)\dagger}A_2^{(n_2)\dagger}$ can be parametrized by the sum and difference of n_1 and n_2. When $\xi_1 = \xi_2 = 0$, the space factorizes with $n_1 + n_2$ being a conserved number and a Bethe ansatz exists for the subspace parametrized by $n_1 - n_2$. When $\xi_1 \neq 0$ and $\xi_2 \neq 0$, this is no longer the case. It is not clear one could implement a Bethe ansatz which also takes into account the dimension parametrized by $n_1 + n_2$ as well. The state $\left|1, \pi/3\right\rangle_z$ could be interpreted as a Bethe asantz with complex momentum $\log(-z)$, but at the same time looks like a Cuntz oscillator coherent state. In particular we have that

$$(a_1 + a_2)\left|1, \pi/3\right\rangle_z = (-z)\left|1, \pi/3\right\rangle_z \tag{4.50}$$

We note that the eigenstate $\left|1, \pi/3\right\rangle_z$ is antisymmetric under the interchange, $1 \leftrightarrow 2$. There is another state that is symmetric under $1 \leftrightarrow 2$ which is the deformation of the second eigenstate with $n = 1$ at $\xi_1 = \xi_2 = 0$. We found numerically that the deformed symmetric eigenstate has particle excitations at both sites simultaneously without any kind of truncation occurring. It is not obvious that this state is the result of a Bethe ansatz and so it may just be the case that a Bethe ansatz describes only a subset of states.

4.3.2 The Calculation

Although the full spectrum of the open Cuntz Hamiltonian is out of our hands for now, one can still find the first order correction to the ground state $\left|\Omega^{(0)}\right\rangle$. We begin with the expansions of the full Hamiltonian H_{open} [2], the full ground state $|\Omega\rangle$, and its exact energy E_0,

$$H_{\text{open}} = \sum_{i=0}^{\infty}\left(\frac{\lambda}{4\pi}\right)^{i} H_{\text{open},i+1}, \quad |\Omega\rangle = \sum_{i=0}^{\infty}\left(\frac{\lambda}{4\pi}\right)^{i}\left|\Omega^{(i)}\right\rangle, \quad E_0 = \sum_{i=0}^{\infty}\left(\frac{\lambda}{4\pi}\right)^{i} E_0^{(i+1)} \tag{4.51}$$

where $H_{\text{open},1}\left|\Omega^{(0)}\right\rangle = E_0^{(1)}\left|\Omega^{(0)}\right\rangle$. To second order in perturbation theory, the equation $H_{\text{open}}|\Omega\rangle = E_0|\Omega\rangle$ yields

$$E_0^{(2)} = \left\langle\Omega^{(0)}\right| H_{\text{open},2}\left|\Omega^{(0)}\right\rangle = -\frac{1}{8}\frac{|\xi_1-\xi_2|^4}{(k+1)^3} \tag{4.52}$$

$$(H_{\text{open},1} - E_0^{(1)})\left|\Omega^{(1)}\right\rangle = -(H_{\text{open},2} - E_0^{(2)})\left|\Omega^{(0)}\right\rangle \tag{4.53}$$

$$E_0^{(3)} = \left\langle\Omega^{(0)}\right| H_{\text{open},3}\left|\Omega^{(0)}\right\rangle - \left\langle\Omega^{(1)}\right|(H_{\text{open},1} - E_0^{(1)})\left|\Omega^{(1)}\right\rangle \tag{4.54}$$

To arrive at the expectation value (4.52) we need a couple of ingredients. One is the relation $(a_{i+1}^{\dagger} - a_i^{\dagger})\left|\Omega^{(0)}\right\rangle = \Delta z\left|\Omega^{(0)}\right\rangle$. A great simplification then arises since the second term of (3.92) vanishes on the ground state by virtue of the linearity of the string collective coordinates, $(a_{i+1} - 2a_i + a_{i-1})\left|\Omega^{(0)}\right\rangle = (\Delta z - \Delta z)\left|\Omega^{(0)}\right\rangle = 0$. Thus we have

$$\left\langle\Omega^{(0)}\right| H_{\text{open},2}\left|\Omega^{(0)}\right\rangle = -\frac{1}{8}\sum_{i=0}^{k}|\Delta z|^4 = -\frac{1}{8}\frac{|\xi_1-\xi_2|^4}{(k+1)^3} \tag{4.55}$$

---

[2] We exclude tree level contribution and drop an overall factor of the coupling $\lambda/4\pi^2$.

Next we solve (4.53) to get the first order correction to the ground state $\left|\Omega^{(1)}\right\rangle$. We expand the right hand side in the basis of n-particle states. Lastly we have to rewrite the Cuntz oscillators in terms of the site operators. The non-vanishing terms become

$$(a_{i+1}-a_i)^2 = A^{(2)}_{i+1} - 2A^{(1)}_i A^{(1)}_{i+1} + A^{(2)}_i + A^{(1)}_{i+1}(2\Delta z - z_{i+1}) - A^{(1)}_i(2\Delta z + z_i) + (\Delta z)^2 \tag{4.56}$$

The right hand side of (4.53) is then

$$\begin{aligned}-(H_{\text{open},1} - E^{(1)}_0)\left|\Omega^{(0)}\right\rangle = \frac{1}{8}(\Delta z)^2 \sum_{i=0}^{k} (&A^{(2)\dagger}_{i+1} - 2A^{(1)\dagger}_i A^{(1)\dagger}_{i+1} + A^{(2)\dagger}_i + A^{(1)\dagger}_{i+1}(2\Delta\bar{z} - \bar{z}_{i+1}) \\ &- A^{(1)\dagger}_i(2\Delta\bar{z} + \bar{z}_i) + (\Delta\bar{z})^2)\left|\Omega^{(0)}\right\rangle\end{aligned} \tag{4.57}$$

$$= \frac{1}{4}(\Delta z)^2 \left(\sum_{i=1}^{k} A^{(2)\dagger}_i - \sum_{i=1}^{k-1} A^{(1)\dagger}_i A^{(1)\dagger}_{i+1} - \sum_{i=1}^{k} \bar{z}_i A^{(1)\dagger}_i \right) \left|\Omega^{(0)}\right\rangle \tag{4.58}$$

We expect that $H_{\text{open},2}\left|\Omega^{(0)}\right\rangle$ contains two particle states because the nonvanishing terms contain two Cuntz oscillators. The appearance of one particle states is caused by the site operators containing an indefinite number of Cuntz oscillators. Admittedly, we do not have a way to brute force solve equation (4.53). The solution was obtained using `Mathematica` by truncating the Hilbert space, solving the linear system numerically, and realizing a pattern. The result is

$$\left|\Omega^{(1)}\right\rangle = \frac{1}{4}(\Delta z)^2 \sum_{i=1}^{k} \sum_{n=2}^{\infty} z_i^{n-2} A^{(n)\dagger}_i \left|\Omega^{(0)}\right\rangle \tag{4.59}$$

Regardless, the analytic proof that (4.59) solves (4.53) exists and is given in Appendix C. The state $\left|\Omega^{(1)}\right\rangle$ is normalizable, implying that the ground state remains normalizable to this order in perturbation theory,

$$\left\langle\Omega^{(1)}\middle|\Omega^{(1)}\right\rangle = \frac{k}{16}|\Delta z|^2 \tag{4.60}$$

Note that when the giant gravitons are on top of each other, $\Delta z = 0$ and the ground state receives no corrections.

To finish the computation of $E_0^{(3)}$ we need the expectation values $\left\langle\Omega^{(0)}\right| H_{\text{open},3} \left|\Omega^{(0)}\right\rangle$ and $\left\langle\Omega^{(1)}\right| (H_{\text{open},1} - E_0^{(1)}) \left|\Omega^{(1)}\right\rangle$. The expectation value of first order finite difference term in (3.94) is simple to compute and yields

$$\frac{1}{16}(k+1)|\Delta z|^6 \tag{4.61}$$

The expectation value of the third order finite difference term in (3.94) vanishes due to the linear nature of the string collective coordinates, $(a_{i+2} - 3a_{i+1} + 3a_i - a_{i-1}) \left|\Omega^{(0)}\right\rangle = (\Delta z - 2\Delta z + \Delta z) \left|\Omega^{(0)}\right\rangle = 0$. The expectation value of $\sum_i (v_a^i)^\dagger M_{ab} v_b^i$ in (3.94) is not as simple to compute because it has no immediate interpretation in terms of finite differences. To simplify the computation we make use of the relations $z^0_{i+1} = z^0_i + \Delta z$ and $z^0_{i-1} = z^0_i - \Delta z$ and write

$$\begin{pmatrix} a_{i+1}a_{i+1} \\ a_{i+1}a_i \\ a_{i+1}a_{i-1} \\ a_i a_i \\ a_i a_{i-1} \\ a_{i-1}a_{i-1} \end{pmatrix} \left|\Omega^{(0)}\right\rangle = \begin{pmatrix} z^0_{i+1}z^0_{i+1} \\ z^0_{i+1}z^0_i \\ z^0_{i+1}z^0_{i-1} \\ z^0_i z^0_i \\ z^0_i z^0_{i-1} \\ z^0_{i-1}z^0_{i-1} \end{pmatrix} \left|\Omega^{(0)}\right\rangle = \begin{pmatrix} 1 & 2 & 1 \\ 1 & 1 & 0 \\ 1 & 0 & -1 \\ 1 & 0 & 0 \\ 1 & -1 & 0 \\ 1 & -2 & 1 \end{pmatrix} \begin{pmatrix} (z^0_i)^2 \\ z^0_i \Delta z \\ (\Delta z)^2 \end{pmatrix} \left|\Omega^{(0)}\right\rangle \tag{4.62}$$

The expectation value is now just a product of matrices localized at a single site and we have

$$\frac{1}{16}\sum_{i=1}^{k} \left\langle\Omega^{(0)}\right| (v^i_a)^\dagger M_{ab} P_{0i} v^i_b \left|\Omega^{(0)}\right\rangle = \frac{1}{16}|\Delta z|^4 \sum_{i=1}^{k}(1 - |z^0_i|^2) \tag{4.63}$$

where the factors of $(1 - |z^0_i|^2)$ come from the projectors. Using the orthogonality of the n-particle state, we have for the second expectation value

$$\left\langle\Omega^{(1)}\right| (H_{\text{open},1} - E^{(1)}_0) \left|\Omega^{(1)}\right\rangle$$

$$= -\left\langle\Omega^{(1)}\right| (H_{\text{open},2} - E^{(2)}_0) \left|\Omega^{(0)}\right\rangle \tag{4.64}$$

$$= \frac{1}{4}(\Delta z)^2 \left\langle\Omega^{(1)}\right| \left(\sum_{i=1}^{k} A^{(2)\dagger}_i - \sum_{i=1}^{k-1} A^{(1)\dagger}_i A^{(1)\dagger}_{i+1} - \sum_{i=1}^{k} \bar{z}_i A^{(1)\dagger}_i \right) \left|\Omega^{(0)}\right\rangle \tag{4.65}$$

$$= \frac{1}{16}|\Delta z|^4 \sum_{i=1}^{k}(1 - |z^0_i|^2) \tag{4.66}$$

This cancels exactly with (4.63) and we have

$$E_0^{(2)} = \frac{1}{16}(k+1)|\Delta z|^6 = \frac{1}{16}\frac{|\xi_1-\xi_2|^6}{(k+1)^5} \tag{4.67}$$

Including the tree level contribution to the energy of the open string, we have for the energy of the ground state to three-loops

$$\begin{aligned} E_0 = (k+1) &+ \frac{1}{2}\left(\frac{\lambda}{4\pi^2}\right)\frac{|\xi_1-\xi_2|^2}{(k+1)} - \frac{1}{8}\left(\frac{\lambda}{4\pi^2}\right)^2\frac{|\xi_1-\xi_2|^4}{(k+1)^3} \\ &+ \frac{1}{16}\left(\frac{\lambda}{4\pi^2}\right)^3\frac{|\xi_1-\xi_2|^6}{(k+1)^5} + O(\lambda^4) \end{aligned} \tag{4.68}$$

This agrees with the relativistic dispersion relation

$$E_0 = \sqrt{(k+1)^2 + \frac{\lambda}{4\pi^2}|\xi_1-\xi_2|^2} \tag{4.69}$$

and will be the subject of the next section.

4.4 A Relativistic Dispersion Relation

So far, we have done our calculations without trying to understand the interpretation of the results from the point of view of $AdS_5 \times S^5$ in detail. The purpose of this section is to do this and to use the $AdS_5 \times S^5$ geometric intuition to conjecture how the higher loop order corrections might look like to all orders in perturbation theory in detail. There are two important things we need to consider. First, we saw evidence for being able to measure a central charge for open strings in terms of a difference of coordinates of the end-points of the strings. We need to try to understand the significance of this observation on $AdS_5 \times S^5$. The existence of a central charge suggests that there is a BPS formula that would characterize the answer for the all loop result. The second thing we need to do is to try to understand how our perturbative results relate to local ten dimensional physics on $AdS_5 \times S^5$. Indeed, this is the obvious starting point for studying D-branes in $AdS_5 \times S^5$, but since in the dual field theory the geometric concepts are emergent, we need to ask ourselves, exactly, what is emerging from our answers?

The first thing we will do therefore is to make an educated guess for the answer of the energy of the ground state of the string stretching between two such giants. Our first observation is that when we take the D-brane to the edge of the BPS quantum droplet, we seem to recover the dispersion relation for giant magnons [61] and their bound states [38]. Indeed, such an expression would be of the form

$$\Delta - J_1 = \sqrt{(k+1)^2 + \frac{\lambda}{\pi^2}\sin^2\left(\frac{p}{2}\right)} \tag{4.70}$$

where we have a bound state of $k+1$ constituents, and the BMN momentum is p. We have denoted the eigenvalue of the dilatation operator by Δ and that of $\hat{J}_1$ by J_1. The formula for the energy of the giant magnon relation depends on having a centrally extended $SU(2|2)$ symmetry on the worldsheet for which the giant magnon produces a short representation. Although in principle one could have a more general function of λ appearing in the square root, this form matches both the weak coupling expansion, as well as the $AdS_5 \times S^5$ sigma model limit [37]. This suggests that this is the exact formula for all λ, suggesting a particular non-renormalization theorem. One can make other field theory arguments that suggest that this is the only result that is compatible with S-duality [69].

In the case where we send $\xi_1,\ \xi_2$ towards the boundary, we have that both become unitary $\xi_1 = \exp(ip_1)$, $\xi_2 = \exp(ip_2)$, and then

$$\xi_1 - \xi_2 = 2ie^{i(p_1+p_2)/2}\frac{e^{i(p_1-p_2)/2} - e^{-i(p_1-p_2)/2}}{2i} \tag{4.71}$$

$$= 2ie^{i(p_1+p_2)/2}\sin\left(\frac{\Delta p_{12}}{2}\right) \tag{4.72}$$

so that

$$|\xi_1 - \xi_2|^2 = 4\sin^2\left(\frac{\Delta p_{12}}{2}\right) \tag{4.73}$$

If we identify $\Delta p_{12} = p$ and we assume compatibility with the giant magnon dispersion relation we conclude that in this limit

$$\Delta - J_1 = E_0 = \sqrt{(k+1)^2 + \frac{\lambda}{4\pi^2}|\xi_1 - \xi_2|^2} \tag{4.74}$$

would give the correct energy of the string to all orders in perturbation theory. The results of Section 4.3.2 agree with this conjecture up to third order in the 't Hooft coupling. Strong evidence is provided by the fact that non-trivial cancellations occurred at higher orders in perturbation theory to make this happen.

If ξ_1 and ξ_2 compute the central charge associated to each end-point of the string, then we must conclude that this result should be valid for all ξ and not just for those special ξ that are unitary and live at the edge of the quantum droplet. To test this conjecture, let us look at the special case when the giant gravitons are on top of each other $\xi_1 = \xi_2$. The excitations stretching between the two giants should have the same spectrum as the excitations of a giant to itself. After all, when the D-branes are on top of each other, there is an enhanced (gauge) symmetry of coincident D-branes [62]. Such a dispersion relation would give us $\Delta - J_1 = k + 1$ which indeed saturates a BPS inequality. The corresponding state would belong to the chiral ring of the $\mathcal{N} = 4$ SYM theory and can be compared to the DBI fluctuations of giant gravitons finding an exact match [70]. The spectrum of such fluctuations is independent of the size of the giant graviton and here we find a match to those results.

The giant graviton background is made of Z fields, and this background breaks the $SO(6)$ R-symmetry to an $SO(4)$ unbroken subgroup. The Y can be considered the highest weight of a vector representation of this unbroken $SO(4)$. This $SO(6)$ R-symmetry is related to the isometry rotations of the S^5 into itself. The $SO(4)$ is the little group unbroken by the giant graviton, and it performs rotations of the giant graviton into itself (this is an $S^3_{GG} \subset S^5$ rotating in S^5 [19]). We identify the S^3_{GG} of the giant graviton as a different S^3 than the one that determines the radial quantization of the $\mathcal{N} = 4$ SYM theory where the computations are made. A state with the quantum numbers of Y^{k+1} has angular momentum $k + 1$ along this $SO(4)$. We should thus think of our string ground state as a state with angular momentum $k + 1$ (this is in the same way that momentum is carried for closed strings [53]).

Let us assume that the conjecture (4.74) does indeed capture the full result to all orders for the lightest string with angular momentum k stretching between two giant gravitons. The result is a square root and this suggests that we interpret it as a relativistic dispersion relation for a massive particle in curved space.

Let us consider first the case of branes in flat space. When two D3-branes come close to each other, the low energy effective field theory on their worldvolume is $\mathcal{N} = 4$ SYM on the Coulomb branch [71] [3]. In the Coulomb branch, the vacuum expectation values of configurations that describe vacua consist of commuting matrices, which can be diagonalized. The positions of the D-branes are the eigenvalues themselves. Given the positions of two D-branes $\vec{X}_1$ and $\vec{X}_2$ in the transverse direction to the branes, the W bosons have masses proportional to $|\vec{X}_1 - \vec{X}_2|$ and these are not renormalized. The massive vector multiplets of $\mathcal{N} = 4$ SYM are short representations with a central charge proportional to $\vec{X}_1 - \vec{X}_2$ itself. This intuition should also apply if we embed the D-branes in a curved manifold and we make the D-branes parallel to each other (in a curved manifold, where the two D-branes are BPS states we take this to mean that the shortest distance between the branes can be computed anywhere and the results don't depend on where we do this due to a group symmetry).

In the short distance limit between the branes, the same intuition should hold, because we should be able to take a low energy field theory limit where the masses and the geometry are fixed, but the string scale is taken to the $\alpha' \to 0$ limit, just as in the seminal AdS / CFT paper [13]. If there is a notion of a position transverse to the brane, so that $\vec{X}_1 - \vec{X}_2$ makes sense, the mass of a W boson should be proportional to the distance between the branes. The effective distance can be computed using the central charge. If we have a constant mass for a W boson independent of the position along the brane, then the problem of computing the spectrum of W bosons should reduce at low energies to the problem of computing a relativistic dispersion relation for $\mathcal{N} = 4$ SYM on the Coulomb branch in curved space. In this calculation the curved space is along the worldvolume of the nearby branes themselves. These W bosons can be of spin one or zero depending on the details of the state, but they will all belong to the same representation of supersymmetry in flat ten dimensional space.

---

[3] This is because the ground state D-brane configuration breaks half of the supersymmetries of flat space, and the only low energy field theory with 16 supersymmetries and spin content with spin less than or equal to 1 is the $\mathcal{N} = 4$ SYM itself.

In our example, the central charge is $|\xi_1 - \xi_2|$, and the worldvolume of the D-brane is a curved S^3_{GG}, the worldvolume of the giant gravitons themselves. In the limit $\xi_1 - \xi_2 = 0$, the Y fluctuations can be thought of as changing the orientation of the brane embedding into the S^5, so it is natural to think of them as affecting the Goldstone modes that result from breaking $SO(6)$ down to $SO(4)$ on the D-brane worldvolume. As such, when we turn on the separation between the branes it makes sense to identify the W boson states we get as those that arise from Goldstone bosons in the presence of spontaneous gauge symmetry breaking. Since these are eaten up by the longitudinal component of the massive W bosons, the states for which we have computed the mass are part of the massive vector particle, rather than a scalar particle in the W multiplet. If we identify the number of Y as a momentum, we see that there is no obvious string ground state at zero momentum; in that case there is no Y connecting the two giants. This is expected because fluctuations of the Goldstone boson at zero momentum can be gauged away. This suggests that out of the $k + 1$ Y fields, only k of them should be counted as momentum, and the last one should come from the spin of the W particle.

Consider a free conformal field theory in four dimensions compactified on a sphere of radius R times time. If such a field theory has a free scalar field, the scalar field will couple to the background curvature of the sphere with a non-minimal conformal coupling. This is, one would need to solve for the spectrum of the second order differential operator

$$\partial_t^2 - \nabla_{S^3}^2 - aR^{-2} \tag{4.75}$$

where aR^{-2} is the term with the Ricci scalar of the background metric. The energy levels of such a conformally coupled scalar on the sphere will be

$$E_\ell = \frac{\ell + 1}{R} \tag{4.76}$$

starting at $\ell = 0, \dots,$ where ℓ is the principal quantum number for spherical harmonics on the sphere. For a massive scalar field of mass m, with a conformal coupling, we would instead derive that

$$E_\ell = \sqrt{\left(\frac{\ell + 1}{R}\right)^2 + m^2} \tag{4.77}$$

If we set $R = 1$, we get that

$$E_\ell = \sqrt{(\ell + 1)^2 + m^2} \tag{4.78}$$

The effective Laplacian gets a shift that makes it into a square. We have found a similar equation, but we would need to identify $k + 1 \to \ell$, whereas we seem to be getting instead $k + 1 \to \ell + 1$. Such a difference can be accounted by a unit of spin.

The $AdS_5 \times S^5$ and $\mathcal{N} = 4$ SYM on S^3 themselves have 32 supersymmetries. The superconformal group $SU(2,2|4)$ admits no central extension. The only way that we get a central extension to have non-zero values in $\mathcal{N} = 4$ SYM is by spontaneously breaking the scaling symmetry, but keeping the flat space supersymmetry. Indeed, the central charge extension is necessary to keep the spin to be smaller than or equal to one. Only half the supersymmetry of the original system survives when we do this, and this is done by going to the Coulomb branch.

By the same token, the presence of the giant gravitons breaks the conformal symmetry of $SU(2,2|4)$ so that only half of the supersymmetries are unbroken. Given that supersymmetry was broken to half, one can now argue that a central charge extension can appear for the open strings stretching between giants in a similar way to what happens in flat space. Moreover, there are 16 supersymmetries acting on the system that do not act on the D-brane system, which is considered a ground state. To only have particles of spin less than or equal to one survive as W bosons in the presence of so many supersymmetries, it must be the case that there is a central charge extension. Otherwise one would have long representations of supersymmetry (they would have 2^8 states, rather than 2^4) which include particles of spin higher than one and this would be inconsistent with the expectations of low energy physics of D-branes. All of the other states in the multiplet should therefore be accessible by acting with the unbroken supersymmetries. Some of these commute with the twisted Hamiltonian $H_{BMN} = D - \hat{J}_1$ and should produce degeneracies with other states that have different spin. Thus, in a formula like (4.74), the $SO(4)$ charge could change by one unit, but the spin could also change in such a way that a (massive) particle of spin zero on the S^3 has the same energy as a vector particle with the right polarization, but where the splitting of quantum numbers into momentum versus spin is different.

Further evidence for this identification of the coordinates of the quantum hall droplet as giving rise to a central charge comes from considering the so called dual giant gravitons (those that grow into AdS_5 rather than on the S^5 sphere [72, 73]). In the quantum hall droplet picture, these states are interpreted as an eigenvalue of the Z matrix acquiring a large expectation value and spontaneously breaking the original $U(N)$ gauge symmetry of the $\mathcal{N} = 4$ SYM to $U(N-1) \times U(1)$ [73, 74]. This is a constant field configuration on the S^3 of the original theory, and the dual giant is also of the shape of an S^3 which now is ‘parallel’ to the boundary S^3. The classical configurations of the Z that satisfy the corresponding BPS conditions are exactly points on the Coulomb branch of $\mathcal{N} = 4$ SYM, and one can extend this idea to 1/8 BPS states [18]. Indeed, this idea that the configurations on moduli space can be turned to dual giants is applicable for fairly general $AdS \times X$ geometries and one can also argue that this is enough to reproduce plane wave limit spectra and supergravity spectra from field theory [75, 76]. For this setup, the eigenvalues of Z themselves determine the position of the branes on the Coulomb branch and serve as the X coordinates, as well as the central charge. If we take a scaling limit of large eigenvalues, the effective mass of all the W bosons can be made arbitrarily large, much larger than the scale of compactification of the original field theory on the S^3, so that a flat space limit can be taken by going to intermediate energies (momentum of order the mass, which correspond to wavelengths much shorter than the S^3 inverse radius) and we can really think of the system as $\mathcal{N} = 4$ SYM on the Coulomb branch in flat space. This is seen also by taking appropriate limits in supergravity solutions [77].

Perhaps a more convincing argument is to follow the work of [61, 78] more closely. In that work Beisert argues that the central charge on the spin chain with a ferromagnetic Z background corresponds to adding (or subtracting) a Z at the left and right of asymptotic excitations (this only works on the infinite chain limit). In our case, we would want to produce such a central charge extension for a finite open string in such a way that it is compatible with the asymptotic prescription. On each excitation we want to replace $Y \to [Y, \check{Z}]$, or $Y \to [Z, Y]$, just like in the infinite chain so that we can add or subtract a Z from the chain around each Y. This is realized by the Cuntz chain operators $\sqrt{N}(a_i^\dagger - a_{i+1}^\dagger)$, or $(a_i - a_{i+1})/\sqrt{N}$ (the additional normalization factor of $\sqrt{N}$ is due to the change in the norm of the state with a different length of the spin chain). To add a Z to the left of the chain, in our notation for operators, we would use the identity $(Z-\alpha)^{-1}Z = 1 + \alpha(Z-\alpha)^{-1}$ to show that we get a factor of α (the term with the one would be non-planar and would remove the boundary of the string on the left, joining it with another string). Thus we would get that the asymptotic central charge for each Y is either $\sqrt{N}(a_i^\dagger - a_{i+1}^\dagger)$ or $\alpha - \sqrt{N}a_1^\dagger$ and a similar term for the right boundary. For the case where we subtract a Z, we would identify $\xi_1 - a_1, a_1 - a_2, \ldots, a_k - \xi_2$ as the values of the central charge for each Y defect. The total central charge is then

$$(\alpha_1 - \sqrt{N}a_1^\dagger) + \sqrt{N}\sum_{i=1}^{k-1}(a_i^\dagger - a_{i+1}^\dagger) + (\sqrt{N}a_k - \alpha_2) = \alpha_1 - \alpha_2 \tag{4.79}$$

Obviously, we see then that the condition to get a short multiplet of the centrally extended $SU(2|2)$ would correspond to the equation (4.74) exactly, and the identification of $\xi_1 - \xi_2$ as the central charge of the full string is inevitable.

All our arguments so far are in order to make the claim that equation (4.74) is correct to all orders in perturbation theory. We are claiming that this equation should be interpreted as a relativistic dispersion relation for a (local) field theory on S^3_{GG}, the worldvolume of the giant gravitons themselves. The fact that we can reproduce this to third order in λ suggests that we are actually probing properties associated to local Lorentz invariance in higher dimensions. From the boundary field theory it is natural to assume that time and the original S^3 are related by locality and causality, but that does not make it automatic for S^3_{GG}, since this $S^3_{GG} \subset S^5$ is emergent itself. The new local Lorentzian structure would mix an $SO(4)_R$ symmetry with time, rather than the $SO(4) \subset SU(2,2) \simeq SO(4,2)$ which is also unbroken by the giant graviton. This relativistic dispersion relation is also compatible with the usual way of thinking about the Higgs mechanism arising from D-branes in string theory.

Having this relativistic dispersion relation has consequences for our understanding of locality on the sphere in the directions transverse to the D-brane, not only along its worldvolume. So long as the gap in anomalous dimensions is typically large, taking k large but finite and varying $\alpha_1 - \alpha_2$ to be small enough so that $g_{YM}^2 N|\alpha_1 - \alpha_2| \simeq k^2$, one can see that at large 't Hooft coupling one can corner oneself so that $|\xi_1 - \xi_2| \ll 1$ which means we have probed the geometry of the sphere on distances much smaller than the AdS radius R transversely to the D-branes, and on distances of order R/k along the giant graviton worldvolume.

The limit where both terms are of the same size is of the order of the Compton wavelength of the string as a W boson in the directions along the D-brane. This is much smaller than the AdS radius, so it provides evidence for locality on much smaller scales than the AdS radius in all directions along the sphere. One can also argue that this extends to the AdS geometry itself; the giant gravitons are localized at the origin of AdS in global coordinates. In principle we can move them so that they can be at different positions in the AdS radial direction by giving the giant gravitons some angular momentum (these are the result of superconformal transformation on the different giant graviton states). Presumably one can find evidence in such a case that the corresponding W bosons would also get a mass from the AdS displacement which would also indicate local physics along all of the AdS directions together with the sphere.

One can also consider the so called dual giant gravitons, which grow into AdS but are point like on the sphere. The dual states to those D-branes growing into the AdS directions are known but not their precise collective coordinate description in the full quantum theory. To zeroth order one thinks of them as spontaneous symmetry breaking of the original $U(N)$ gauge field theory to $U(N-1) \times U(1)$ by a particular time dependent vev. For that case, the mass of W bosons is determined from the classical physics of this symmetry breaking. One should then realize these states in the geometry, as branes in the free fermion droplet [74, 77]. Since these states break the same symmetries of the conformal group as the ordinary giant gravitons, one expects that the string attached to them would also measure a central charge which is measured by the coordinate of the giant graviton in the quantum hall droplet plane geometry. The details of such a calculation are beyond the scope of the present work but progress has been made in [52].

4.5 The Open String Dual

In previous sections we found the ground state of the open string stretched between two giant gravitons in $\mathcal{N} = 4$ SYM and that the energy satisfied a relativistic dispersion relation. In this section we find the dual of the open string states in the string theory itself. We solve the equations of motion for the open string sigmal model on $AdS_5 \times S^5$ with the boundary conditions that the strings end on giant gravitons with fixed angular momentum on the S^5. The identification between the open string ground state in the gauge theory and the string theory is supported by matching relativistic dispersion relations and the underlying geometry of both objects.

Since our open Cuntz chains are BPS, their dual string states should correspond to solutions of the sigma model that have this property, albeit modified to include the effects of the new boundary conditions. The BPS states in $\mathcal{N} = 4$ SYM with large angular momentum in the infinite chain limit are bound states of elementary excitations as shown by Dorey [38] called giant magnons. Each state is characterized by the quantum numbers

$$\Delta - J_1 = \sqrt{Q^2 + \frac{\lambda}{\pi^2}\sin^2(p/2)} \tag{4.80}$$

$$J_2 = Q \tag{4.81}$$

with Q the number of magnon excitations, J_i the Cartan generators of the $SO(6)$ R-charge, and p the quasi momentum of the bound state. In particular, J_1 is the R-charge of the half-BPS ground state which is infinite in the infinite chain limit. The corresponding classical string solutions were found in [79, 80] (see also [36]). There, the J_i correspond to the angular momenta of the string on the S^5 and p is the geometric angle subtended by the string stretched between two points on the edge of a maximal disk in the S^5. Like their spin chain dual, these strings have infinite length. Thus we take our ansatz to be these classical string solutions but truncated so that the endpoints fall on the giant gravitons.

We verify that these truncated solutions are dual to the open Cuntz chain ground state in three parts. First we need to relate the positions of the giants gravitons in the S^5 to the collective coordinates of the giant gravitons in the open Cuntz chain. Otherwise we could not compare the energy and angular momentum of the string to that of the open Cuntz chain. Then we need to check that the infinite string can be truncated so that the ends follow the positions of the giant gravitons (this is, the string ends don't fall from the giant graviton). Lastly, we need to relate $\Delta - J_1$ and J_2 for the truncated solutions and get the relation (4.74), namely

$$\Delta - J_1 = \sqrt{Q^2 + \frac{\lambda}{4\pi^2}|\xi_1 - \xi_2|^2} \tag{4.82}$$

$$J_2 = Q \tag{4.83}$$

where $\xi_1,\ \xi_2$ are coordinates on a unit disc.

First we need to find a relation between $\xi_1,\ \xi_2$ and the positions of the giant gravitons. Let us label the coordinates on the sphere by z_i, $i = 1, 2, 3$ with the constraint $\sum_i \bar{z}_i z_i = 1$. These should not be confused with the collective coordinates of the open string Cuntz chains. The corresponding angular momenta are the J_i. If we have a giant graviton with angular momentum L, wrapping an S^3 inside S^5 (it is a point in the z_1 coordinate), then it moves with angular velocity equal to one and sits at $|z_1| = \sqrt{1 - L/N}$ [19]. In the dual CFT, in terms of the description based on fermion droplets and coherent states of the dual field theory, these also sit on a disk which can be normalized to have radius one [74, 39], and have energy

$$E = L = N(1 - |\xi|^2) \tag{4.84}$$

Fixing L, we see that $|\xi| = |z_1|$. Furthermore, both notions of the angle direction between field theory and gravity are the same; the angle is related to the conjugate variable to angular momentum.

In order to impose the truncated boundary conditions, we need to make sure that the string solutions can end on the giant gravitons and that they rotate with angular speed equal to one in the z_1 plane. This follows because the ends of the infinite string classical solution travel at the speed of light and moreover they reside at the edge of the disk. Traveling at the speed of light in this case means that they move with angular velocity one and if we cut the solutions, they actually end on the giant gravitons.

Using the variable definitions of [79], we recall the classical infinite string solution. The worldsheet coordinates are called t, x. The time on the world sheet is identified with the external time variable. The solution depends on two auxiliary variables γ, θ. They are related to the magnon excitation number Q

and quasi momentum p by

$$\cot(\gamma) = \frac{2r}{1-r^2}\sin\left(\frac{p}{2}\right) \tag{4.85}$$

$$\tan(\theta) = \frac{2r}{1+r^2}\cos\left(\frac{p}{2}\right) \tag{4.86}$$

where r is a function of the energy, angular momenta, quasi momentum, and boundary conditions. The classical solution for the infinite string is then given by

$$u = (x\cosh(\theta) - t\sinh(\theta))\cos(\gamma) \tag{4.87}$$

$$v = (t\cosh(\theta) - x\sinh(\theta))\sin(\gamma) \tag{4.88}$$

$$z_1 = e^{it}\left(\cos\left(\frac{p}{2}\right) + i\sin\left(\frac{p}{2}\right)\tanh(u)\right) \tag{4.89}$$

$$z_2 = e^{iv}\frac{\sin\left(\frac{p}{2}\right)}{\cosh(u)} \tag{4.90}$$

where $u,\ v$ are auxiliary functions. Notice that at $t = 0$ the real part of z_1 is constant.

As we can see from equation (4.89), the string moves at constant angular velocity equal to one. In these solutions, the range of u is infinite. For our case, we want to cut the string so that the range of x (or u for that matter) is finite.

To find our string, we need to fix the boundary conditions by restricting the range of the variables so that $z_1(u_1, t) = \xi_1 \exp(it)$ and $z_1(u_0, t) = \xi_2 \exp(it)$ and then solving for $u_0,\ u_1$. Since we need the real part of z_1 constant at $t = 0$, we choose $\xi_1,\ \xi_2$ to have the same real part, which can be achieved by a global rotation of the D-brane configuration. The boundary conditions now read

$$\cos\left(\frac{p}{2}\right) + i\sin\left(\frac{p}{2}\right)\tanh(u_1) = \xi_1 \tag{4.91}$$

$$\cos\left(\frac{p}{2}\right) + i\sin\left(\frac{p}{2}\right)\tanh(u_0) = \xi_2 \tag{4.92}$$

The quasi momentum p is found from the real part of ξ_1 or ξ_2. Consequently we have

$$\tanh(u_1) = \frac{\xi_1 - \cos(p/2)}{i\sin(p/2)}, \quad \tanh(u_0) = \frac{\xi_2 - \cos(p/2)}{i\sin(p/2)} \tag{4.93}$$

so that $\xi_1,\ \xi_2$ are enough to determine p and the values of $u_0,\ u_1$. We also have the relation

$$\sin\left(\frac{p}{2}\right)(\tanh(u_1) - \tanh(u_0)) = |\xi_1 - \xi_2| \tag{4.94}$$

which will be imporant when computing $\Delta - J_1$.

The energy and the angular momentum are given by

$$\Delta - J_1 = \frac{\sqrt{\lambda}}{2\pi}\int dx\,(1 - \Im(\bar{z}_1\partial_t z_1)) \tag{4.95}$$

$$J_2 = \frac{\sqrt{\lambda}}{2\pi}\int dx\,\Im(\bar{z}_2\partial_t z_2) \tag{4.96}$$

over the appropriate range. This is evaluated at $t = 0$ for convenience, where $u,\ x$ are proportional to each other.

After some lengthy algebraic computation, one shows that

$$\Delta - J = \frac{\sqrt{\lambda}}{2\pi}\frac{1+r^2}{2r}\sin\left(\frac{p}{2}\right)\cosh(\theta)\cos(\gamma)\int dx\,\mathrm{sech}^2(u) \tag{4.97}$$

$$= \frac{\sqrt{\lambda}}{2\pi}\frac{1+r^2}{2r}\sin\left(\frac{p}{2}\right)\int du\,\mathrm{sech}^2(u) \tag{4.98}$$

$$= \frac{\sqrt{\lambda}}{2\pi}\frac{1+r^2}{2r}\sin\left(\frac{p}{2}\right)(\tanh(u_1)-\tanh(u_0)) \tag{4.99}$$

Similarly, one finds that the J_2 angular momentum is given by

$$J_2 = \frac{\sqrt{\lambda}}{2\pi}\sin\left(\frac{p}{2}\right)\cosh(\theta)\cos(\gamma)\int dx\,\mathrm{sech}^2(u) \tag{4.100}$$

$$= \frac{\sqrt{\lambda}}{2\pi}\frac{1-r^2}{2r}\sin\left(\frac{p}{2}\right)\int du\,\mathrm{sech}^2(u) \tag{4.101}$$

$$= \frac{\sqrt{\lambda}}{2\pi}\frac{1-r^2}{2r}\sin\left(\frac{p}{2}\right)(\tanh(u_1)-\tanh(u_0)) \tag{4.102}$$

We now want to fix $J_2 = Q$. Since we know $p,\ u_0,\ u_1$, this determines the value of r.

Notice that apart from the r dependence, $\Delta - J_1$ and J_2 are essentially identical. Call $A_\pm = \frac{1\pm r^2}{2r}$.One then sees that $A_+^2 - A_-^2 = 1$. It follows that

$$(\Delta - J)^2 - J_2^2 = \left(\frac{\sqrt{\lambda}}{2\pi}\right)^2\left|\sin\left(\frac{p}{2}\right)(\tanh(u_1)-\tanh(u_0))\right|^2(A_+^2 - A_-^2) \tag{4.103}$$

$$= \left(\frac{\sqrt{\lambda}}{2\pi}\right)^2\left|\sin\left(\frac{p}{2}\right)(\tanh(u_1)-\tanh(u_0))\right|^2 \tag{4.104}$$

$$= \left(\frac{\lambda}{4\pi^2}\right)|\xi_1 - \xi_2|^2 \tag{4.105}$$

So we find that

$$\Delta - J_1 = \sqrt{Q^2 + \frac{\lambda}{4\pi^2}|\xi - \tilde{\xi}|^2} \tag{4.106}$$

As mentioned in Section 4.4, we should identify Q with $k+1$ to complete the matching of the open Cuntz chain ground state to this open string solution to the equations of motion.

4.6 Discussion

In this Chapter we solved for the ground state of the open Cuntz Hamiltonian (3.91). In doing so we have solved for the open string ground state stretched between a special class of giant gravitons and found its anomalous dimension. We were able to correct the ground state energy to three-loop order in the gauge theory. The energy is consistent with a relativistic dispersion relation which we conjecture to hold to all loop orders. The energy in perturbation theory matches the Taylor expansion of (4.74) in the mass squared $|\xi_1 - \xi_2|^2$ and not the momentum $k+1$.

Our conjecture is supported by the existence of a central charge extension of the unbroken supersymmetry algebra that leaves the giant gravitons invariant. The central charge is proportional to the distance between the giant gravitons $|\xi_1 - \xi_2|$. This quantity is often seen as the Higgs mass of W bosons in the Coulomb branch of supersymmetric field theories. The distance between D-branes typically gives masses to open strings stretched between them and we are seeing this effect in our open Cuntz chains.

The effective action (4.18) is of a nearest neighbor type. This is reminiscent of geometries being built by string bits stretching between D-branes that form a non-trivial quantum gas. The nearest neighbor interactions would be the energies of these string bits, and the higher order terms that are missed would deal with the interactions between these string bits. Because the expansion seems to be written in terms of multiple discrete derivative operators, as mentioned in Section 3.5, one can imagine that in the continuum limit these might fully restore the string sigma model in a particular gauge, where one can also recover higher derivative

α' corrections of the string propagation on $AdS_5 \times S^5$. There might be issues with this story at three loops where the middle term of (3.94) has no immediate interpretation as finite differences. Noting that the projection operators yield factors of the inverse metric, it is possible that this term is realized as derivatives of the metric if one shifts around the site indices a bit. To further understand this issue one necessarily has to go to higher loop orders.

As we have argued in this paper, string states stretched between D-branes give us some insight into how geometry is realized. Although this is not a new point of view, understanding its realization in the AdS / CFT correspondence setup is important because it can lead to a much better understanding as to how classical geometry is replaced by a quantum realization of geometry, or when geometry stops making sense. This is in keeping with the idea that the CFT is actually a definition of quantum gravity. Following this train of thought we have been able to get a glimpse of how locality in higher dimensions can emerge in the AdS / CFT context from a field theory computation. Particularly important for this question is how the gap in anomalous dimensions is generated between different states: those that remain massless in the supergravity limit, and those that become stringy. In our example, the distance between the branes emerges as a measurement of this gap. Indeed, we have found evidence that in the full $AdS_5 \times S^5$ geometry giant graviton D-brane defects break the conformal field theory in such a way that they give rise to a central charge extension of the unbroken SUSY algebra, extending previous ideas of this central charge extension that are related to the integrable structure of the $\mathcal{N} = 4$ spin chain model. The simple interpretation of this central charge is that it is expected from trying to understand the emergent $\mathcal{N} = 4$ SYM for a stack of D-branes in the Coulomb branch (the D-branes in question are the giant gravitons, and the effective $\mathcal{N} = 4$ SYM is the dynamics on their worldvolume). A non-zero value for such a central charge in principle gives a lower bound for operator dimensions and helps further explain this gap. Furthermore, such a central charge can be thought in some instances to provide a natural notion of position, like in the case of flat D-branes in flat space.

D-branes carry non-trivial gauge fields on their worldvolume. This implies that open string joining and splitting necessarily takes place along the worldvolume of the D-brane. Thus interactions are local in the directions transverse to the D-brane. This only makes sense so long as we can argue that the D-branes are actually local in some geometry in the first place. Presumably, consistency of locality between different such probes requires that physics is local in the geometry. Since the D-branes can be moved closer or father apart from each other, one can argue that so long as the gap is sufficiently large, one has probed locality on distances longer than a Compton wavelength for a W boson. These distances are much smaller than an AdS radius and thus one is finding locality on sub-AdS lengths.

Although we have not studied this process yet, the fact that there is an effective gauge theory on giant graviton states is understood because one can see that there is a Gauss' law constraint for counting string states between giants [55] (see also [81, 39]). This is intimately tied to the gauge invariance of the original $\mathcal{N} = 4$ SYM and generalizes to other field theories. To nail the case of locality one would need to show that interactions are polynomial in momenta. There are setups where constituents can have relativistic dispersion relations, but the interactions do not respect Lorentz invariance, such as in noncommutative field theory, which can appear as limits of string theory (see [82] for a review). We believe that understanding the precise role that the central charge plays is crucial to understanding locality in ten dimensions. Understanding exactly how this central charge extension might control the effective field theory generated on the D-brane would be very interesting.

Chapter 5

Emergence of Geometric Limits in $\mathcal{N} = 4$ SYM

In this Chapter we study a one parameter family of supersymmetric marginal deformations of $\mathcal{N} = 4$ SYM with $U(1)^3$ symmetry, known as β-deformations, to understand their dual $AdS \times X$ geometry, where X is a large classical geometry in the $g^2_{\mathrm{YM}} N \to \infty$ limit. The geometry is infered by studying the spectrum of open strings stretched between giant gravitons developed in the previous chapters.

The number-theoretic properties of β are very important. When $\exp(i\beta)$ is a root of unity, the space X is an orbifold. When $\exp(i\beta)$ close to a root of unity in a double scaling limit sense, X corresponds to a finite deformation of the orbifold. Finally, if β is irrational, sporadic light states can be present.

5.1 Marginal Deformations of $\mathcal{N} = 4$ SYM

The $\mathcal{N} = 4$ SYM admits a three parameter (complex) family of deformations that preserves $\mathcal{N} = 1$ super conformal invariance [24]. If we use $\mathcal{N} = 1$ SUSY notation, the $\mathcal{N} = 4$ SYM has three chiral fields $\tilde{X}, \ \tilde{Y}, \ \tilde{Z}$ in the adjoint representation of the gauge group. We will be interested in the case where the gauge group is $SU(N)$ Then $\tilde{X},\ \tilde{Y},\ \tilde{Z}$ are $N\times N$ are traceless Hermitian matrix superfields. We will reserve the letters $X,\ Y,\ Z$ without tildes for the lowest component of the corresponding superfields, in the following manner:

$$\tilde{X}(x,\theta)=X(x)+\sqrt{2}\theta\psi_X(x)+\theta^2F_X(x) \tag{5.1}$$

The three parameter family is characterized by the superpotential

$$W=\lambda_1\mathrm{Tr}([\tilde{X},\tilde{Y}]\tilde{Z})+\lambda_2\mathrm{Tr}(\{\tilde{X},\tilde{Y}\}\tilde{Z})+\lambda_3\mathrm{Tr}(\tilde{X}^3+\tilde{Y}^3+\tilde{Z}^3) \tag{5.2}$$

where $\lambda_1,\ \lambda_2,\ \lambda_3$ are arbitrary complex parameters. The gauge coupling constant is determined from $\lambda_1,\ \lambda_2,\ \lambda_3$ by requiring that the beta function of the gauge coupling constant vanish. This amounts to the vanishing of the anomalous dimension of the fields $X,\ Y,\ Z$. Because the superpotential has enough discrete symmetries to cyclically replace $\tilde{X}\to\tilde{Y}\to\tilde{Z}\to\tilde{X}$, the anomalous dimensions of $\tilde{X},\ \tilde{Y},\ \tilde{Z}$ are identical and they need to be set to zero. This requires the R-charge of $\tilde{X},\ \tilde{Y},\ \tilde{Z}$ be equal to one. In this case the beta function vanishes. The requirement of vanishing anomalous dimension is enough to determine g_{YM} in terms of $\lambda_1,\ \lambda_2,\ \lambda_3$. When $\lambda_3=0$, the superpotential has a $U(1)^3$ symmetry, where $\tilde{X},\ \tilde{Y},\ \tilde{Z}$ can be independently rotated from each other, a linear combination of these rotations, combined with spinor rotations is the $U(1)_R$ charge. The $\mathcal{N}=4$ theory is obtained when $\lambda_2=\lambda_3=0$, and in that case $\lambda_1=g_{\mathrm{YM}}$ (this convention requires the $X,\ Y,\ Z$ fields to be canonically normalized). We are interested in the case where we turn on both λ_1 and λ_2. It is convenient to rewrite the superpotential as follows

$$W = G_{\rm YM}\left[{\rm Tr}(\tilde{X}\tilde{Y}\tilde{Z}) - h{\rm Tr}(\tilde{X}\tilde{Z}\tilde{Y})\right] \tag{5.3}$$

where $G_{\rm YM}$ is a function of $g_{\rm YM}$ and h. When $h^*h = 1$, we call $h = \exp(2i\beta)$, and in this case $G_{\rm YM} = g_{\rm YM}$. For the particular case of roots of unity, these result from orbifolds with discrete torsion of the $\mathcal{N} = 4$ SYM theory itself [83, 84]. In that case, planar diagrams match those of the $\mathcal{N} = 4$ SYM. This can be conveniently understood by noticing that the corresponding spin chain can be obtained by twisting the original spin chain of $\mathcal{N} = 4$ SYM theory [16]. Results to various loop orders when $|h| \neq 1$ were obtained in [85]. At one loop order one has that $g^2_{\rm YM}(1+|h|^2) = 2G^2_{\rm YM}$. This is easy to obtain by requiring that the one loop planar anomalous dimension of X be equal to zero. The study of general h, although rather interesting, is beyond the scope of the present Chapter. As argued in [16], the model fails to be integrable. For us this means that we can not control the results of calculations to all orders in perturbation theory.

In this Chapter we will be mostly interested in the generalized $\mathfrak{su}(2)$ sector. This is spanned by gauge invariant operators made of Y, Z alone which for $h = 1$ corresponds to a sector of operators that is closed under perturbation theory and that moreover has an $SU(2)$ symmetry of rotations of Y into Z. This $SU(2)$ is part of the $SU(4)$ R-charge of $\mathcal{N} = 4$ SYM. For general h, operators with these quantum numbers can only mix with each other as there are no other states with the same quantum numbers (this necessarily includes the bare dimension of the operator). We have already discussed the $\mathfrak{su}(2)$ in the case of $\beta = 0$ which has important consequences for the BPS states of the theory. What is important to us here is that the half BPS giant gravitons [19] remain half BPS for all β. The giants are characterized by coordinates which live on a disk in the S^5, which is selected upon choosing which half of the supersymmetries we wish to preserve.

Let us identify the $U(1)^3$ symmetry charges of the theory. In our conventions the θ, $\bar{\theta}$ variables of superspace have $U(1)_R$ charge equal to $\mp 3/2$ respectively, and $\tilde{Z}$ has R-charge equal to one. Thus, a superpotential term in the action of the form

$$\int d^2\theta \mathrm{Tr}(\tilde{Z}^3) \tag{5.4}$$

has net R-charge equal to zero. Also, for the vector superfields we use $W_\alpha \simeq \psi_\alpha + \theta(F + D)_\alpha + \theta^2(\bar{\partial\!\!\!/}\bar{\psi})_\alpha$. We can classify our fields by the $U(1)^3$ charges. This is depicted in Table 5.1. For the conjugate fields we reverse all the charges, except the dimension Δ. We also introduce the charge J in analogy with the corresponding charge for $\mathcal{N} = 4$ SYM [60]. Fields other than Z in the field theory have $\Delta - J > 0$.

A particular subclass of operators is the set that are made of the single field

Field	$U(1)_R$	$U(1)_1$	$U(1)_2$	Δ	$(\Delta - J)$
X	1	0	$-1/2$	1	1
Y	1	$-1/2$	$1/2$	1	1
Z	1	$1/2$	0	1	0
ψ	$3/2$	0	0	$3/2$	1
θ	$-3/2$	0	0	-1/2	0

Table 5.1: List of charges of the fields under the $U(1)^3$ symmetry and the dimensions of the fields. For other fields they are determined by the charge of the superspace variables and requiring that superfields have definite charges. We have also defined $J = (1/3)Q_R + (4/3)Q_1 + (2/3)Q_2$.

Z. Any polynomial of Z that is gauge invariant is identical in algebraic form to those of the half-BPS sector of $\mathcal{N} = 4$ SYM that would be built out of Z. These are multitraces of Z. If the degree of the polynomial is n, then the R-charge of such an operator is n, and the $U(1)_1$ charge is $n/2$. All of these operators have $\Delta - J = 0$. Thus, this subsector does not mix with any other (all other sectors have fields with $\Delta - J > 0$). We also have that these operators can not have any anomalous dimension either. These operators are the lowest component of a scalar chiral superfield $f(\tilde{Z})$, so $\bar{D} f(\tilde{Z}) = 0$. These equations imply that either the lowest component of the multiplet $f(\tilde{Z})$ is a primary field, invariant under half of the supersymmetries whose dimension is entirely controlled by the $U(1)_R$ charge, or that $f(\tilde{Z})$ is a descendant of the form $f(\tilde{Z}) = \bar{D} U$ for some other superfield U that is not chiral. Remember that $\bar{D}$ acts without changing the value of $\Delta - J$. The right hand side would need to be an operator with $\Delta - J = 0$, of the same class as the ones we are studying. Since these operators are chiral, no such U superfield can give a non-zero right hand side. The only possibility is that the operator has a protected dimension. This is independent of how many traces make up the operator. This is also true for arbitrary values of h, not only those where $|h| = 1$. This means that this entire sector is protected by supersymmetry, no matter the trace structure of the operator.

The set of half BPS operators can be classified in the free field theory limit by studying Young tableaux [43]. The arguments in [74] show that the collection of these objects can also be visualized in terms of a quantum hall droplet (free fermions on a magnetic field). We can also interpret the corresponding particle and hole states as analogous to dual giant gravitons and giant gravitons. Configurations can have one such giant graviton or many. Also, the collective coordinate formalism of [39] can be adapted to this problem without any modifications. Hole states will be associated to a point inside a fermion droplet of radius $\sqrt{N}$ [1].

As described before, we are interested in the analogue of the $SU(2)$ sector. These are operators built of $Y,\ Z$. The operator $\Delta - J$ will count the number of Y fields, which we will call m. Also, the $U(1)_2$ charge of this operator is equal to $m/2$. There are not many other operators that carry those quantum numbers for $\Delta - J$ and $U(1)_2$. The only candidate that also carries positive values of $U(1)_2$ is $\bar{\psi}_Z$. Such a field contributes also one to $\Delta - J$ and $1/2$ to $U(1)_2$. However, it has a smaller R-charge than Y, namely, its R-charge is equal to $1/2$, rather than one, so it can not mix with the operators we have described (all three conserved quantum numbers would need to match for mixing to occur). This means that the $SU(2)$ sector survives as a sector for all values of h, and not just for $h = 1$.

We will first consider single trace operators in the asymptotic limit where we take

$$\mathcal{O} \simeq \sum_{[n_i]} a^{[n_i]} \mathrm{Tr}(Z^{n_1} Y Z^{n_2} \dots Z^{n_k} Y) \tag{5.5}$$

in the planar limit with k fixed and very high occupation numbers n_i. We are interested in the value of $\Delta - J$ for the operator $\mathcal{O}$ and when it exists. This requires that $\sqrt{N} \gg \sum_i n_i \gg k$. We can take $\sum_i n_i \sim N^{1/a}$ with $a > 3$ for example to ensure that we can stick to planar diagrams. In this limit the Y defects are dilute, and we can treat them independently of each other on a first approximation. The spin chain has translation invariance of the Y relative to the position of the Z, essentially because of the cyclic property of the trace [60]. The vacuum $\mathrm{Tr}(Z^n)$ is a ferromagnetic ground state with minimal $\Delta - J$. A single Y defect is an impurity. In the free field theory limit $G_{\mathrm{YM}}^2 N \to 0$, Y contributes to $\Delta - J$ by one. When there is more than one Y, the n_i labels matter and serve to measure the distance between the defects. At large separation we have approximate translation invariance. Thus, it is natural that asymptotically we have that $a^{[n_i]} \simeq \exp(i(q_1 n_1 + q_2 n_2 \cdots + q_k n_k))$, so that each defect carries some quasi momentum equal to $\phi_i = q_{i+1} - q_i$. In the planar limit, at each given loop order s, the Y can move at most s steps to the left or to the right, so the energy (this is the same as the anomalous dimension) of a defect can be computed locally and should depend only on $\phi_i = q_{i+1} - q_i$. We therefore expect to have a dispersion relation $\Delta - J = \sum_i E(\phi_i)$, where each defect contributes $E(\phi_i)$ to the energy.

---

[1] This is the radius of the droplet for a particular normalization of the collective coordinate, it can also be rescaled to be of order 1

An important question for us is what is the form of $E(\phi_i)$ for arbitrary $h = \exp(2i\beta)$ and g_{YM}. This has been answered for $h = 1$ in a variety of ways [59, 53, 78]. The main result is that

$$E(\phi) = \sqrt{1 + \frac{g_{\mathrm{YM}}^2 N}{\pi^2} \sin^2\left(\frac{\phi}{2}\right)} \tag{5.6}$$

In the notation of [59], the quantity $4\sin^2(\phi/2) = -\alpha = \exp(i\phi) + \exp(-i\phi) + 2 = -(1 - \exp(i\phi))(1 - \exp(-i\phi))$ is determined by the equations of motion. The same calculation in the presence of β leads to

$$E(\phi) = \sqrt{1 + \frac{g_{\mathrm{YM}}^2 N}{\pi^2} \sin^2\left(\frac{\phi}{2} - \beta\right)} \tag{5.7}$$

One effectively shifts the quasi momentum of each particle excitation in the spin chain from $\phi \to \phi - 2\beta$. This is in accordance with the fact that the associated spin chain is just a twist of the original one [16]. The associated superpotential can be written in terms of a generalized star product [25]. Thus one can guarantee that the planar diagrams of the β-deformed theory coincide with the planar diagrams of $\mathcal{N}=4$ SYM, to all orders, up to the point where we care about the periodicity conditions of the various fields on the spin chain. A calculation for those giant magnons based on the sigma model can be found in [86, 87]. For general $|h| \neq 1$, there is no integrability at one loop level [16], and one can not argue that a deformed $\mathfrak{su}(2|2)$ symmetry survives that would protect the result on the right hand side.

Our goal in this Chapter will be to understand the corresponding energy of the $\mathfrak{su}(2)$ ground state with n copies of Y and arbitrary Z, for an open string whose ends attach to a giant graviton made of Z. This energy is interpreted as a dispersion relation for a fluctuation between the D-branes with n units of momenta.

5.2 The β-Deformed Cuntz Chain

Following the calculations of [16] it is easy to write down the Cuntz Hamiltonian for the one-loop $\mathfrak{su}(2)$ sector in the Cuntz oscillator basis for arbitrary h. The answer is

$$H^{h}_{\text{closed},1} = \frac{1}{2}\left(\frac{G^2_{\text{YM}}N}{4\pi^2}\right)\sum_n (a^\dagger_n - h a^\dagger_{n+1})(a_n - h^* a_{n+1}) \tag{5.8}$$

$$H^{\beta}_{\text{closed},1} = \frac{1}{2}\left(\frac{g^2_{\text{YM}}N}{4\pi^2}\right)\sum_n (e^{-i\beta} a^\dagger_n - e^{i\beta} a^\dagger_{n+1})(e^{i\beta} a_n - e^{-i\beta} a_{n+1}) \tag{5.9}$$

the second line is specific to $h = \exp(2i\beta)$. This is directly derived from the superpotential. Roughly, the cost to switch $YZ \to ZY$ in the equations of motion of Z is a factor of h. At this loop order, only the square of the superpotential shows up. In this form the Hamiltonian is also a sum of squares, and in the $SU(2)$ sector for arbitrary h it corresponds to the XXZ chain.

The Hamiltonian (5.9) is obtained by replacing ordinary commutators in the dilatation operator by q-deformed commutators. Define $[A,B]_q \equiv AB - qBA$ and make the replacement $[A,B] \to [A,B]_q$. Dropping constants of proportionality, the one-loop dilatation operator becomes

$$:\mathrm{Tr}([Y,Z][\check{Z},\check{Y}]): \to :\mathrm{Tr}([Y,Z]_q[\check{Z},\check{Y}]_{q^*}): \tag{5.10}$$

Because we are working in the β-deformed theory with gauge group $SU(N)$ and not $U(N)$, there is an additional term that needs to be added.

$$:\mathrm{Tr}([Y,Z][\check{Z},\check{Y}]): \to :\mathrm{Tr}([Y,Z]_q[\check{Z},\check{Y}]_{q^*}): - :\mathrm{Tr}([Y,Z]_q)\mathrm{Tr}([\check{Z},\check{Y}]_{q^*}): \tag{5.11}$$

The added term yields an additional contribution to the anomalous dimension in the planar limit only for the operator $\mathrm{Tr}(YZ)$, in which case the anomalous dimension vanishes entirely. In [88] it was argued that the only state affected in the $SU(2)$ sector by these finite size effects, called prewrapping, is $\mathrm{Tr}(YZ)$. Additionally it was shown that this state is protected to all loop orders. Integrability, which we have assumed captures both sides of the AdS / CFT correspondence in the planar limit, predicts a divergent anomalous dimension for $\mathrm{Tr}(YZ)$ [89]. Later on we will only be considering operators with large R-charge and so these finite size corrections unaccounted for by integrability for very short closed strings are not a concern to us. We do not need to make any modifications to $H^{\beta}_{\text{closed},1}$.

To add the boundary conditions, we follow the calculations in [39] and Chapter 3. The way this works with the giant graviton collective coordinates amounts to adding phases to the collective coordinates α for the boundary contributions. We get that

$$\begin{aligned} H^{\beta}_{\text{open},1} = \frac{1}{2}\left(\frac{g^2_{\text{YM}}N}{4\pi^2}\right)\Big[\left(e^{-i\beta}\xi_1 - e^{i\beta}a^{\dagger}_1\right)\left(e^{i\beta}\bar{\xi}_1^{-} e^{-i\beta}a_1\right) + \dots \\ + \left(e^{i\beta}\xi_2 - e^{-i\beta}a^{\dagger}_k\right)\left(e^{-i\beta}\bar{\xi}_2 - e^{i\beta}a_k\right)\Big] \end{aligned} \tag{5.12}$$

The twist to turn the theory to the previous Cuntz chain is easier to explain in the open Cuntz chain. We just replace $a_s = \exp(-2is\beta)\tilde{a}_s$. Notice that this is an automorphism of the Cuntz algebra, if at the same time we take $a^{\dagger}_s = \exp(2is\beta)\tilde{a}^{\dagger}_s$. We can then easily check that the phases cancel in the Cuntz chain Hamiltonian after this replacement. This should be thought of as a local field redefinition of the local fields $a_n,\ a^{\dagger}_n$. To include the boundary conditions, we just need to take the result in equation (3.91) and make the replacement

$$\alpha_2 \to q^{k+1}\alpha_2 = \exp[2i(k+1)\beta]\alpha_2 \tag{5.13}$$

From here, it is easy to find the energy of the open string ground state with angular momentum $n = k + 1$ to all orders. We just copy the result in equation

(4.74) with the appropriate substitutions. We find that

$$\Delta - J = \sqrt{n^2 + \frac{g_{\rm YM}^2 N}{4\pi^2}|\xi_1 - q^{-n}\xi_2|^2} \tag{5.14}$$

The power of $q^{-n} = q^{-k-1}$ arises because α_i and ξ_i are related to each other by complex conjugation. This result follows from putting together two observations. The first is based on integrability of the spin (Cuntz) chain and that equation (4.74) is correct due to the central charge extension symmetry of the all loop spin chain. The other is that the field theory dynamics predict planar equivalence (with a twist) of the $\mathcal{N} = 4$ SYM spin chain for the β-deformed version. This is the usual statement that noncommutative field theories and regular field theories have the same planar diagrams, which in this case results from a $*$-product deformation [25]. These statements can be made entirely within quantum field theory and do not require additional insight from string theory.

Consider the operators of the $SU(3)$ sector with ℓ_1 Y and ℓ_2 X defects against an Z background. In $\mathcal{N} = 4$ SYM at one loop order, these operators can be obtained by an $SO(4)$ rotation of the ground state with only Y defects. In the twisted theory, the net twist of the boundary condition is proportional to $q^{\ell_1 - \ell_2}$. The equations of motion of the Leigh-Strassler theory are cyclic in X, Y, Z. Thus the cost in phase for a X to get past an Z ends up being opposite in phase to the cost of having a Y jump past an Z.

For this more general case we find that

$$\Delta - J = \sqrt{(\ell_1 + \ell_2)^2 + \frac{g_{\rm YM}^2 N}{4\pi^2}|\xi_1 - q^{-\ell_1 + \ell_2}\xi_2|^2} \tag{5.15}$$

We can also understand similar $SO(4)$ rotations of Y into $\bar{X}$ and X into $\bar{Y}$, and the corresponding twists. For our purposes, the difference between $X,\ Y$ is enough.

5.3 Geometric Limit Interpretation

In this section we consider various space-time configurations of D-branes, choosing suitable values of $\alpha_1,\ \alpha_2$ (or ξ_1, ξ_2), and ask what happens to the spectrum in the limit $g_{\text{YM}}^2 N \to \infty$ using expressions (5.14) and (5.15). The main question we will ask is which states remain light in this limit. We will call states light if their energy is below the typical string scale $\Delta - J < \ell_s^{-1} = (g_{\text{YM}}^2 N)^{1/4}$. Even though $\Delta,\ J \simeq O(N)$ for the giant graviton ground state, it always remains light in this sense since $\Delta - J = 0$. The appearance of ℓ_s makes sense because we are measuring energies in units of the AdS radius in the gravity theory. As such, ℓ_s can be thought of as a dimensionless ratio of the string length to the AdS radius.

As a warm up to analyze this problem, let us start in the undeformed $\mathcal{N} = 4$ SYM with a giant graviton at ξ_1, and another one at ξ_2. Equivalently we are considering the case where $q = 1$. The spectrum of states between them will contain light states if

$$\Delta - J = \sqrt{n^2 + \frac{g_{\text{YM}}^2 N}{4\pi^2}|\xi_1 - \xi_2|^2} < (g_{\text{YM}}^2 N)^{1/4} \tag{5.16}$$

Unpacking the inequalities, we need that both

$$n^2 < (g_{\text{YM}}^2 N)^{1/2} \tag{5.17}$$

and that

$$\frac{g_{\rm YM}^2 N}{4\pi^2}|\xi_1 - \xi_2|^2 < (g_{\rm YM} N)^{1/2} \tag{5.18}$$

because the term in the square root is a sum of squares.

The first term tells us that the momentum of the state is below the string scale, that is, $n < \ell_s^{-1}$ which is usually what we mean by a low energy limit. This condition is satisfied for all fixed n when we take the limit $g_{\rm YM}^2 N \to \infty$. This shows that the volume of the five sphere is becoming infinite in string units; more modes become available below the string scale as we take the geometric limit.

The second term essentially tells us that

$$|\xi - \tilde{\xi}| < \ell_s \tag{5.19}$$

so that the two D-branes have to be closer to each other than the string scale. This is a standard way to extract the low energy field theory in the Maldacena limit [13]. In this case all field theory modes survive (there is one state per angular momentum n, up to the degeneracy expected from supersymmetry). Moreover, this second term in the sum of squares can be thought of as the Higgs mass that results when we separate two D-branes by a distance $|\xi_1 - \xi_2|$.

The simplest way to understand the geometric location of these states is to consider maximal giant gravitons first, and to consider the standard fibration structure of the 5-sphere as a circle bundle over the complex projective plane, $S^1 \hookrightarrow S^5 \to \mathbb{CP}^2$. This fibration determines a choice of an $\mathcal{N} = 1$ superspace R-charge. BPS chiral ring states have their energy equal to the angular momentum along the S^1, which means that in the geometric optics limit they are at a fixed position in $\mathbb{CP}^2$ (they are null geodesic in $AdS_5 \times S^5$). The little group of such fixed position determines a fixed $SU(2) \times U(1) \subset SU(3)$ decomposition. The state carries no $SU(2)$ quantum numbers, so that it can be interpreted as a highest weight of $SU(3)$ with respect to this geometric decomposition. This is one way to think of building $\mathbb{CP}^2$ in terms of coherent states.

In the presence of a maximal giant graviton, which is a maximal S^3 that shares its S^1 fiber with that of the S^5, the allowed positions for such an open string lie in a $\mathbb{CP}^1 \subset \mathbb{CP}^2$, and similarly can be interpreted as a highest weight of $SU(2)$. Seen from the point of view of the Hopf vibration of S^3, an object that carries n units of angular momentum on S^3 along the Hopf fiber can be thought of as a highest weight state for a monopole spherical harmonic of charge n on the base. These highest weight states are localized on $\mathbb{CP}^1$ because the effective magnetic field is proportional to n and the Landau level classical orbits are circles centered around some position on the sphere. The angular momentum is along the direction of the point on the $\mathbb{CP}^1$.

A similar statement can be made for the other giant gravitons. These end up moving at constant speed on the S^1 fiber of S^5, and the string is moves along with them. It also moves inside the S^3, and the $SU(2)$ chiral symmetry preserved by the giant graviton determines a similar Hopf fibration of this S^3. The statement results from looking at the $x_3, \dots x_6$ coordinates of the S^5 as a $\mathbb{C}^2$, and then we choose the standard complex structure on this $\mathbb{C}^2$ to pick the $SU(2)$ we need.

The next case we want to look at are the orbifolds with discrete torsion, where q is no longer equal to one, but instead is a fixed root of unity. Let us say $q^s = 1$ is a primitive root of unity for some integer $s > 1$ implying that β is rational. These orbifolds are interesting because the geometry is given by a $S^5/\mathbb{Z}_s \times \mathbb{Z}_s$ quotient [83, 84]. A giant graviton at fixed ξ will correspond to a brane wrapping a $S^3/\mathbb{Z}_s$ We think of it as the corresponding S^3 in the covering space S^5 and act by the corresponding quotient group that maps the position of the brane to itself. We can also think of this scenario by the method of images a la Douglas-Moore [90].

Let us ask what happens at generic values of $\xi_1 = \xi_2 \equiv \xi$, that is, what happens to the spectrum of fluctuations of a single brane. To have a light state will require that

$$n < \ell_s^{-1} \tag{5.20}$$

and that

$$g_{\mathrm{YM}}^2 N |\xi|^2 |1 - q^{-n}|^2 < (g_{\mathrm{YM}}^2 N)^{1/2} \tag{5.21}$$

For generic $|\xi| \simeq 1$, we will need that $|1 - q^{-n}| \to 0$, or equivalently, that n is a multiple of s Only fluctuations with s units of angular momentum will survive the low energy limit. More precisely, if we go to the $SU(3)$ sector, we will require that $|1 - q^{-\ell_1 + \ell_2}|$ survive, which shows that $\ell_1 - \ell_2$ is a multiple of s. This is exactly what we expect from the optical limit on a $S^3/\mathbb{Z}_s$ space, which decomposes as a Hopf vibration with a $\mathbb{CP}^1/\mathbb{Z}_s$ base. The other heavy states can be thought of as long strings stretching between ξ and its images $q^k\xi$.

Similarly, we can ask what happens if we take $\xi_2 = q^m \xi_1$, that is, we try to locate a second brane in one of the image points of ξ under the $\mathbb{Z}_s$ action that can act on a complex coordinate of the S^5. We find that a light spectrum of states between the branes survive as long as n differs from m by a multiple of s. This spectrum of states has fixed differences in momenta, plus a shift from zero. The natural interpretation is that the two D-branes are on top of each other, but they differ in the choice of discrete electric Wilson lines between them, in a similar vein to [91]. This means that the coordinate ξ contains both the position and the Wilson line information. The position is uniquely determined by ξ^s. We can also take limits where $|\xi_2 - q^{-n}\xi_1| < \ell_s$ to have such setups, and the interpretation in terms of a relative discrete Wilson line does not change.

A natural question is to ask how we can deal with magnetic Wilson lines, along the lines of [91]. This would be important to understand S-duality on the set of states. It is hard to understand the S-dual magnetic strings between branes. See however [69], where it is argued that the D-strings and (p, q)-strings have the same world sheet sigma model as the ordinary strings, except for their tension. We would expect that the BPS central charge argument is extended to these as well, with the tension of the string making an appearance inside the square root formula. However, a field theory computation for these states is beyond what can be done with perturbation theory. The action of S-duality on the Leigh-Strassler deformations is also complicated [92]. For us, the D3-branes with magnetic flux need to be at the same location, so they must have the same value of ξ^s. Hence they should be linear combinations of the branes at the values of ξ and its images. It is natural to assume that such branes with magnetic Wilson lines will have fixed values of the R-charge modulo s and are related to the ones with fixed ξ by a discrete Fourier transform. Understanding S-duality in detail is beyond the scope of the present paper.

Now let us ask also about the special limit where $|\xi| \to 0$. In this case all of these states can survive. We ask that $|\xi| < \ell_s$ and we get a construction where the images of a brane are separated from a brane itself by distances that are sub-stringy. The spectrum is then the same as that of a single maximal giant graviton. We can think of it as an S^3 world volume, or as a $U(s)$ theory on $S^3/\mathbb{Z}_s$ in a ground state where there is a discrete nonabelian Wilson line given by

$$W \simeq (1, q, q^2, \ldots, q^{s-1}) \tag{5.22}$$

All we need is that $W^s = 1$ as a matrix. Both of these give the same spectrum of states. Which is more appropriate will then depend on the nature of the local interactions; if they are local on S^3, or on $S^3/\mathbb{Z}_s$. We will not answer this question here.

Now let us consider β to be close to zero, that is $q \to 1$, and $\xi_1 = \xi_2$. Again, we are asking about fluctuations of a single brane. In this case we can Taylor expand in β around $q = 1$.

$$q^n \simeq 1 + 2i\beta sn + O(n^2) \tag{5.23}$$

Again, just as before, we ask that $n < \ell_s^{-1}$, and that

$$g_{\rm YM}^2 N |\xi|^2 \beta^2 n^2 < (g_{\rm YM}^2 N)^{1/2} \tag{5.24}$$

One simple way to do this is to take $\beta^2 (g_{\rm YM}^2 N)$ finite. It can even be made very large in a double scaling limit sense so long as we allow ourselves to restrict n to be smaller.

What we find is that the energy is proportional to n, and more generally, to the square root of a quadratic form involving $\ell_1,\ \ell_2$. This is the dispersion relation of a squashed sphere, where different directions have been squashed differently. Keeping $\beta^2(g_{\rm YM}^2 N)$ gives a finite squashing; the sphere is still of a size comparable to the AdS radius.

In this case, if we also separate the branes slightly, taking $\xi_1 \neq \xi_2$, we notice that the dispersion relation becomes a square root of a quadratic form involving $\ell_1,\ \ell_2$ plus a constant term, and more crucially, a linear term will arise. One can even fix ξ_2 as being related to ξ_1 by a phase such that the factors of q cancel for some n. Such a linear term is like a position dependent relative Wilson line. This will need to be interpreted as having a non-trivial H-flux in the geometry (this follows similar reasoning to [93]). These should end up matching the Lunin-Maldacena geometries when we explore them in more detail [25], where the squashing of the sphere and the H flux is known. This problem of reading the flux can also be analyzed using other techniques with D-brane instantons [94].

The next question we need to ask is what happens for irrational β. At least naively, nothing survives. This is because the numbers $1 - q^{-n}$ will typically never be close enough to zero at finite n. However, if we let $\xi_1 = \xi_2 \equiv \xi$ with $|\xi|$ close to zero, we can have states for which $|\xi|^2|1 - q^{-n}|^2 < \ell_s^2$. If we use a continuous fraction approximation to β/π, we can find integers $r,\ t$ such that $|\beta/\pi - r/t| < 1/t^2$. We then find that $|\xi|$ can be larger than ℓ_s by a factor of roughly t. The states whose momenta are multiples of t will then survive to low energies so long as the first order Taylor expansion of the exponential in $1/t$ is still a reasonable approximation. Thus, for sufficiently small values of $|\xi|$, even if they are larger than the string scale by a factor of t they look similar to orbifolds with discrete torsion $S^5/\mathbb{Z}_t \times \mathbb{Z}_t$. The value of t changes as we go away from the fixed point $|\xi| = 0$. In this case we jump between geometric duality frames depending on the distance from the origin $|\xi| = 0$. Even if the full result is not geometric, certain classes of questions could be asked in the corresponding orbifold with discrete torsion.

If $\ell_1 = \ell_2$, the states always survive. This means that we should think of the brane as having at least one large circle of radius one in AdS units, with the other directions forming a stringy geometry. The general structure of states is very similar to what happens in the study of Melvin models [95], where the different rational approximations to an irrational number play an important role. In our case we are dealing with open strings stretched between D-branes, rather than with the closed string spectrum. It is natural to imagine that the closed string sector in these β-deformed theories will also have a list of sporadic light states that depend on the number theoretic properties of β. A natural difference is that in the work [95] the light states came from wrapped strings on a small circle, while in our case they carry angular momentum. Momentum versus wrapping are T-dual to each other, so exploring these issues further is very interesting.

A natural question to ask is how much of this picture could be obtained from a stringy computation? Given the Lunin-Maldacena geometries, the corresponding giant graviton states are known [96, 97] and in even more general deformations where they become unstable [98]. Seeing as our classical solutions stretching between branes correspond to cutting well known solutions of the sigma model on S^3, it should be possible to produce these from solutions in the TsT transformations that generate the Lunin-Maldacena backgrounds and the work [99] These should also be applied to the orbifolds with discrete torsion. These details are beyond the scope of the present work.

5.4 Discussion

In this Chapter we have analyzed the spectrum of open strings between giant gravitons in both the $\mathcal{N} = 4$ SYM theory at strong coupling and in the β-deformations of $\mathcal{N} = 4$ SYM theory. We argued that this set of open string states can be understood as a set of BPS states for the central charge extension of the infinite spin chain discovered by Beisert [61] that determines their energy.

The results for the open string ground state of Chapter 4 can be ported over to the β-deformed theories because the Cuntz chain is almost the same as in $\mathcal{N} = 4$ SYM; there is a twist which only affects the boundary conditions of the open strings in a simple way based on the quantum numbers of the string states. The energies of these strings are encoded simply in equations (5.14) and (5.15) which makes it possible to take limits and understand geometry very simply. We argue that physics can be interpreted geometrically in the strong coupling limit if there is a rich set of open string states with low energies (low compared to the string scale) that survives.

This strong coupling limit with a large set of states depends very strongly on the number theoretic properties of β, and the notion of geometry jumps discontinuously as we move in β at infinite coupling, in a way that is very reminiscent of Melvin models [95]. In general, we expect a similar structure as a function of β for all toric quivers, since their dual geometries can also be deformed by the

Lunin-Maldacena method [25]. It would also be interesting to understand other marginal deformations of $\mathcal{N} = 4$ SYM and which of them are geometric. A lot less is known about such cases (see however [100, 101], where examples with dual geometries are expected).

It would be interesting to explore this issue further in other orbifolds of $\mathcal{N} = 4$ SYM. This again results in the same Cuntz chain, but the twistings that need to be done are different [102] and it would be interesting to see how this can affect the study of giant graviton states. It is also interesting to explore $\mathcal{N} = 2$ theories, where we also expect a central charge extension to control the allowed energies of the states, but where we do not expect integrability [103].

We also discovered that in the orbifolds with discrete torsion, the giant gravitons carried electric Wilson lines on their world volume. This suggests interesting questions regarding how S-duality acts on those states. Considering that the action of S-duality is complicated when looking at different questions [92] for β-deformed theories, this suggests that resolving these issues might be very non-trivial.

Part II

Geometry from Matrix Models

Chapter 6

Introduction

The AdS / CFT dictionary is a one-to-one map between objects in certain string theories and operators in $\mathcal{N} = 4$ SYM in four dimensions. In addition to open and closed strings, we expect to be able to describe D-branes [62]. Without a non-perturbative definition of string theory, calculations involving D-branes come in the form as BPS solutions to the supergravity equations of motion, classical analysis of the Dirac-Born-Infeld (DBI) action, or perturbatively through open strings. In the limit of vanishing string coupling, the D-branes become rigid membranes in some embedding space which act as boundary conditions for open strings. The coordinate positions of D-branes were first suggested to be matrices in [104]. If we treat the matrix variables classically and they all commute, then their eigenvalues give the exact positions of the individual D-branes in the embedding space. When the matrices no longer commute, the geometric information about the membranes becomes encrypted and the ensemble is considered fuzzy. Extracting the membrane information from this fuzziness is an important step in understanding how full quantum D-branes emerge when we move away from non-vanishing string coupling.

Describing membranes as non-commuting coordinates also comes from the lightcone quantization of the membrane [105]. The coordinates that do not commute describe the internal degrees of freedom of the membrane itself. In the lightcone quantization, the supermembrane acquires a non-degenerate Poisson structure on its spatial worldvolume. One can consistently truncate the space of functions on which the Poisson structure acts. The embedding coordinates become Hermitian matrices and the Poisson structure is replaced with a $\mathfrak{u}(N)$ Lie bracket. The truncation acts as a UV regulator for the membrane on the lightcone. The same story can be repeated for the supermembrane, a membrane with bosonic and fermionic coordinates [106]. The dynamics of the full supermembrane should be recovered as $N \to \infty$.

The truncation of the supermembrane results is the BFSS matrix model [107]. The BFSS matrix model was originally argued to be a candidate for the strongly coupled dynamics of D0-branes with some momentum in the lightcone direction. Its connection to the supermembrane means it has the capacity to describe membranes, at least in the large N limit, and lead to the conjecture that the matrix model is the discrete lightcone quantization (DLCQ) of M-theory in flat space. At finite N, the BFSS matrix model should describe M-theory with one direction compactified to a circle of radius R. If M-theory is a theory of membranes, then they should exist at finite N in the BFSS matrix model as well! All considerations of membranes as matrices so far holds in a classical context. There is no need for a full quantum treatment in terms of solving the spectrum of the BFSS Hamiltonian and extracting membranes from the eigenstates. This is the subject of Chapter 7: how can we extract classical surfaces in some embedding space using classical complex valued matrices at finite N? We will not ignore quantum mechanics completely, as it is the governing dynamics of the system, but it will guide us in building an effective Hamiltonian for extracting membranes from matrices.

The BFSS matrix model is a gauged quantum mechanics. It has nine scalar matrices ϕ^i and sixteen fermionic matrices living in the adjoint of $U(N)$. The action is given by

$$\begin{aligned} S_{\text{BFSS}} = \int dt\, \text{Tr} \Bigg[&\sum_{j=1}^{9} \frac{1}{2(2R)} (D_0 \phi^j)^2 + \frac{i}{2} \Psi^\dagger D_0 \Psi + \frac{(2R)}{4} \sum_{j,k=1}^{9} [\phi^j, \phi^k]^2 \\ &+ \sum_{j=1}^{9} \frac{1}{2} (2R) (\Psi^\dagger \gamma^j [\phi^j, \Psi]) \Bigg] \end{aligned} \tag{6.1}$$

with the time covariant derivative $D_0 \phi^i = \partial_t \phi^i - i[A_0, \phi^i]$ and A_0 a non-dynamical $U(N)$ gauge connection. The parameter R can be scaled away showing that the BFSS matrix model has no intrinsic scale. See Appendix D for more details.

Another important model we will consider is the BMN matrix model [60]. Its action is given by

$$S_{\text{BMN}} = S_{\text{BFSS}} + S_{\text{mass}} \tag{6.2}$$

$$\begin{aligned} S_{\text{mass}} = \int dt\, \text{Tr} \Bigg[&\frac{1}{2(2R)} \left(- \left(\frac{\mu}{3}\right)^2 \sum_{j=1}^{3} (\phi^j)^2 - \left(\frac{\mu}{6}\right)^2 \sum_{j=4}^{9} (\phi^j)^2 \right) \\ &- \frac{i}{2} \left(\frac{\mu}{4}\right) \Psi^\dagger \gamma_{123} \Psi - i \frac{\mu}{3} \sum_{j,k,l=1}^{3} \epsilon_{jkl} \phi^j \phi^k \phi^l \Bigg] \end{aligned} \tag{6.3}$$

where μ is a new mass scale. The BMN matrix model is a massive deformation of the BFSS matrix model. The scalars and fermions both acquire a mass due to the presence of a background four form flux and the Myers effect [108]. This has some major consequences, both classically and quantum mechanically. The BMN potential is unbounded in all directions of the coordinate space whereas the BFSS potential has flat directions. These flat directions lead to the classical instability of the supermembrane. Quantum mechanically these flat directions lead to non-normalizable modes, in the same way that occurs for a free particle, and leads to a continuous spectrum. The BMN model, on the other hand, behaves more like a quantum harmonic oscillator and the spectrum is discrete.

To arrive at the BMN matrix model, one considers a fast spinning particle on a sphere in an $AdS_{4,7} \times S^{7,4}$ geometry. After taking a double scaling limit, the particle sees the geometry of a parallel-plane wave with background four form flux. One obtains the matrix model by performing the appropriate DLCQ for the superparticle. The BMN matrix model should describe the DLCQ of M-theory in a plane-wave background with background four form flux. This is very similar to the BFSS matrix model. Indeed, the BMN matrix model contains a mass parameter μ which in the limit $\mu \to 0$ turns off additional interactions and leaves the BFSS matrix model. Holographically the plane-wave becomes ordinary flat space and the four form flux turns off. Another similarity these models share is that they can both be obtained by dimensional reduction. The BFSS matrix model can be realized as the dimensional reduction of $\mathcal{N} = 4$ SYM on flat four dimensional space. For the BMN matrix model, one starts with $\mathcal{N} = 4$ SYM on $\mathbb{R} \times S^3$ and takes the singlet sector of one of the $SU(2)$'s of the sphere [109].

At some level of the AdS / CFT correspondence, we expect to find full geometries in addition to stringy objects hiding in the states of the gauge theory. After all, string theory should be considered as a single theory that describes all geometric backgrounds [9]. Solving strongly coupled gauge theories in general is a very difficult problem, especially the one relevant to the full correspondence, $\mathcal{N} = 4$ SYM. We can alleviate this issue in two ways: one is to consider these theories classically, and the other is to use matrix models.

Before searching for the geometries hiding in classical gauge theories, we should comment on the success of holography in computing transport coefficients. Beginning with the work of [110], the problem of large N (high dimensional gauge group), finite temperature, strongly coupled quantum gauge theory dynamics is replaced by the much simpler problem of analyzing classical Green's functions in various black hole backgrounds with boundary conditions that reflect our understanding of response theory. The calculation in [110] and subsequent work is, to leading order and when properly normalized [111], completely independent of N and all the precise details of the field theory. These are classical gravity computations in AdS black hole backgrounds. Corrections appear when the gravitational theory suffers quantum corrections, i.e., when the curvature is large somewhere in Planck units, or when the truncation to gravity breaks down, as when the black hole has curvature radii of order the string scale. In the dual field theory, this corresponds to finite N or weak coupling.

In Chapter 8 we consider the opposite scenario of extracting gravitational and geometric information using classical gauge theories. The strong non-linearities will cause chaotic dynamics. The large N limit should be understood as a thermodynamic limit, where the number of degrees of freedom grows as N^2 even though some aspects of the dynamics are N-independent. We will also look for collective modes to emerge, akin to hydrodynamic variables, that indicate collective time dependent dynamics also roughly independent of N.

Classical non-linear field theories have an infinite number of degrees of freedom and suffer from the ultraviolet (UV) catastrophe. The UV catastrophe is cured by introducing the Planck constant, which originally gave birth to quantum mechanics. This would seem to stop this idea of studying classical non-linear field theory dynamics in its tracks. However, thinking of a field theory expanded in Fourier modes, a finite $\hbar$ freezes the dynamics of most of the modes to be in their ground state. The frozen modes are exist above some cutoff determined by the dynamics and the initial conditions. One is only dealing with finitely many active degrees of freedom and the initial problem of an infinite number of degrees of freedom in field theory can be solved. By studying matrix models, we begin with finitely many degrees of freedom and avoid the UV catastrophe completely.

Chapter 8 is devoted to building classical equilibrium configurations of matrices through the real time simulations of the BMN and BFSS matrix models and analyzing their chaotic dynamics. We study both equilibrium configurations with their associated equations of state, and also simple transport processes, or more precisely, out of equilibrium relaxation. We study the latter via fluctuations of the appropriate variables and by invoking the fluctuation-dissipation theorem.

In Chapter 9 we begin our search for geomtries in this classical regime of holography. We discuss whether such classical models can be used to study holographic dualities, where we also have some gravitational information. We use the techniques and tools developed in Chapter 7 to explore the extent to which the matrix configurations developed in Chapter 8 can be called black holes.

We conclude the study of geometry in the context of holography in Chapter 10.

The BMN matrix model has exact, supersymmetric solutions with zero energy [60]. These matrix configurations are characterized by all adjoint representations of $\mathfrak{su}(2)$ and are called fuzzy spheres. It is expected that adding angular momentum to the fuzzy sphere states can induce topology changes from a sphere to a torus [112]. The purpose of Chapter 10 is to investigate this topology transition with a special family of matrix solutions at finite angular momentum. Once the solutions are found, the geometry of the corresponding fuzzy membrane is analyzed using the techniques of Chapter 7.

Chapter 7

The Geometry of Membranes

The coordinate positions of D-branes [62] are realized as matrices [104]. If we treat the matrix variables classically and they all commute, then their eigenvalues give the exact positions of the individual D-branes in the embedding space. When the matrices no longer commute, the geometric information about the membranes becomes encrypted and the ensemble is considered fuzzy.

In this Chapter we investigate how to decode the fuzziness of classical matrix coordinates to obtain information about the membranes hiding inside them, and eventually the D-branes themselves. We work in the context of the BFSS matrix model and its massive deformation, the BMN matrix model.

7.1 Orbifolding The BFSS and BMN Matrix Models

The simplest version of the BFSS and BMN matrix models are obtained by setting $N = 1$. In this case we are working with 1×1 matrices. The classical configurations are given by their positions in $\mathbb{R}^9$. The fermions add degeneracy to these states and give the correct counting for the number of degrees of freedom for a graviton supermultiplet in eleven dimensions [107]. The $\mathbb{R}^9$ describes the transverse directions to the lightcone and the rank of the matrices is the amount of lightcone momentum. The lonely 1×1 matrix model describes a single D0-brane. The lowest energy configurations in the classical theory in general correspond to configurations of commuting matrices, where N such D0-branes are located on $\mathbb{R}^9$.

An important aspect about the BFSS matrix model is its capability to describe extended objects. One can describe configurations of D-branes of varying orders. These are easy to see in the infinite N limit [113], as central charges in the supersymmetry algebra become activated which encode objects of infinite extent. These solutions lead to effective noncommutative field theories. A modern introduction to the geometric interpretation of these developments can be found in [114].

One can also check that matrix configurations source the various supergravity fields at long distances and that the couplings to weakly curved backgrounds give us a way to compute the currents and the multipoles with respect to the brane charges of the configurations. This was very systematically developed in the works of Taylor and collaborators [115, 116, 117]. A review of the BFSS matrix model where all of this is very clearly addressed is in [118].

Finite matrix configurations can also behave like extended D-branes. The simplest example are fuzzy spheres [119], where three of the matrices are proportional to angular momentum matrices, that is, the irreducible representations of $\mathfrak{su}(2)$. The BFSS matrix model can in principle describe all types of D-branes in type

IIA string theory. However, a random configuration of matrices would very complicated and encode somewhat random extended D-branes of the type IIA theory. It is important to ask if these geometries survive at finite N, or if they are only well defined strictly when $N \to \infty$. In this chapter we show that a description for precise geometries exists even at finite N. We begin by reducing the problem to studying surfaces in three dimensions, where three of the ϕ matrices matter and the other six are eliminated somehow.

One way of doing this begins with the realization that the BFSS matrix model can be obtained by dimensionally reducing $\mathcal{N} = 4$ SYM in $3+1$ dimensions down to $0+1$ dimensions. By reducing the supersymmetry from $\mathcal{N} = 4$ SYM to just $\mathcal{N} = 1$ SYM, we only have to deal three of scalar matrices instead of all nine. These arise from the dimensional reduction of the gauge field connection. In this situation, the D0-branes are confined to an $\mathbb{R}^3$ instead than an $\mathbb{R}^9$. We might expect that we can only describe D2-branes, as any higher dimensional even brane would have too high a dimension to fit in three dimensions.

To achieve this truncation and keep a full geometric interpretation of the system in terms of string theory we consider the supersymmetric orbifold $\mathbb{C}^3/\mathbb{Z}_k$. These are described by quiver theories which can be constructed by the techniques developed by Douglas and Moore [90]. What matters for us is that we can end up with a theory where only the dynamics of $\mathcal{N} = 1$ SYM matter.

This would be the theory of N identical fractional branes at the orbifold singularity. A explanation of how those field theories can be built and studied is found in [120]. The geometric interpretation in terms of fractional branes and intersection theory of those objects can be found in [121].

For simplicity we can choose a $\mathbb{Z}_k$ action that gives rise to chiral theories where between any two nodes in the quiver there is at most one chiral field connecting them. If we add a probe for a different fractional brane, we can get a single chiral multiplet worth of fields connecting the probe to the configuration. In particular, we choose the orbifold given by $\mathbb{C}^3$ with coordinates $\alpha_1,\ \alpha_2,\ \alpha_3$ and whose action of $\mathbb{Z}_k$ is defined by the identifications $\alpha_1 \to \omega\alpha_1,\ \alpha_2 \to \omega^2\alpha_2,\ \alpha_3 \to \omega^{-3}\alpha_3$, and $\omega = \exp(2\pi i/k)$ is a primitive root of unity. Many other orbifolds will have similar properties and the precise details of the orbifold are not important at this stage. All that we need can be visualized by a simple subquiver diagram

$$U(N) \bullet \longrightarrow \bullet\ U(1) \text{ Probe} \tag{7.1}$$

where the arrow indicates a single chiral multiplet.

The advantage of having a single chiral field is that the fermions are represented by a two component Weyl spinor, and the gamma matrices appearing in the BFSS matrix model reduce to the four dimensional gamma matrices, that is, the Pauli matrices. The details of the reductions are shown in Appendix E. Chiral fields have the additional advantage in that they carry anomalies in four dimensions. Thus they might encode topological information even in the reduction to $0 + 1$ dimensions.

Upon reduction, the fermion terms involve only four dimensional gamma matrices. Indeed, if we reduce to a single chiral multiplet, then we can think of the gamma matrices themselves as Pauli matrices. The effective action is then

$$S_{\text{orb}} = \int dt\, \mathrm{Tr}\left[\sum_{j=1}^{3} \frac{1}{2(2R)}(D_0\phi^j)^2 + \frac{i}{2}\Psi^\dagger D_0 \Psi + \frac{(2R)}{4}\sum_{j,k=1}^{3}[\phi^j, \phi^k]^2 \right.$$
$$\left. + \sum_{j=1}^{3}\frac{1}{2}(2R)(\Psi^\dagger \sigma^j [\phi^j, \Psi])\right] \tag{7.2}$$

where if ψ is chiral, then $\psi^\dagger$ is antichiral. Again, R is meaningless as it can be redefined away, and the classical symmetries of S_{orb} have the same properties as those for S_{BFSS}. The action above is a shorthand; it is the same action of the BFSS matrix model, but the matrices are restricted by the orbifold conditions [90] [1].

We have thus achieved our goal of only having to deal with three (Hermitian) matrices instead of nine. Additionally, the Pauli matrices are easier to handle than the nine dimensional gamma matrices.

Now we ask the physically meaningful quesiton: can we associate a collection of D2-branes in a specific geometric configuration in $\mathbb{R}^3$ to the three Hermitian matrices $\phi^{1,2,3}$? To the extent that we can, we may then uplift any gained intuition to nine dimensions and understand better how membrane geometries arise in the BFSS matrix model.

Another useful matrix model to consider is the BMN matrix model [60]. This model describes M-theory on a plane wave in the discrete lightcone quantization.

---

[1] In practice this can be done keeping the form of the action fixed and adding information about the matrix restrictions by using a crossed product algebra [122]. This will produce a set of orthorgonal projectors for each node of the quiver, and the commutation relations with these projectors will recover all the information of the quiver diagram. For example the traces of the projectors will recover the rank of the gauge groups on each node.

Its action is given by

$$S = S_{\text{BFSS}} + S_{\text{mass}} \tag{7.3}$$

$$S_{\text{mass}} = \int dt\,\text{Tr}\left[\frac{1}{2(2R)}\left(-\left(\frac{\mu}{3}\right)^2\sum_{j=1}^{3}(\phi^j)^2 - \left(\frac{\mu}{6}\right)^2\sum_{j=4}^{9}(\phi^j)^2\right)\right.$$
$$\left. - \frac{i}{2}\left(\frac{\mu}{4}\right)\Psi^\dagger\gamma_{123}\Psi - \frac{\mu}{3}i\sum_{j,k,l=1}^{3}\epsilon_{jkl}\phi^j\phi^k\phi^l\right] \tag{7.4}$$

which is a mass deformation of the BFSS matrix model. Again, if we look at the $N = 1$ case, the configuration space is $\mathbb{R}^9$. However, there are no flat directions due to the quadratic potential in the Hamiltonian. This is expected and just reflects the presence of the gravitational potential in the plane wave geometry. The BMN model can be obtained by a dimensional reduction of $\mathcal{N} = 4$ SYM to $0 + 1$ dimensions. In this reduction, however, the four dimensional gauge theory is placed on $\mathbb{R} \times S^3$ and fields invariant under one of the two $SU(2)$'s of the sphere remain [109]. Again, we can get simplify the situation to three matrices by playing the same orbifold trick to get rid of the matrices $\phi^{4\ldots9}$. We can get rid of R and choose units where $\mu = 3$, but then we are not free to rescale $\hbar$ to be whatever we want any longer. Thus the BMN matrix model does have a parameter $\hbar$, even when we orbifold. As we move to the classical regime, we can ask the same question as above: can we associate a collection of D2-branes in a specific geometric configuration in $\mathbb{R}^3$ to the three Hermitian matrices $\phi^{1,2,3}$?

We answer this question in the affirmative in both the BFSS and the BMN matrix models. The surfaces will be slightly different in the two models for a given set of matrices ϕ^{123} because the fermions have mass in BMN. This reflects the fact that in the eleven dimensional maximally supersymmetric plane wave background there is a non trivial background flux. Such a contribution changes slightly the shape of the branes that one associates to the configurations and this is essentially due to the Myers effect [108]; branes are polarized in the presence of RR backgrounds. In particular a D0-brane can polarize into a sphere.

The remainder of this chapter is to look in detail at the fermion degrees of freedom to understand the geometry of branes. We relabel the matrices $\phi^{1,2,3} \to X,\ Y,\ Z$ or $\vec{X}$ when appropriate. From the point of view of the fermion degrees of freedom we ask the question, what would a probe point like D0-brane see in the constant background $\vec{X}$?

7.2 The Index: Adding a D0-brane Probe

As described previously, the geometry in the BFSS and BMN matrix models is encoded in matrices of dimension one. In this section we work exclusively in the context of the BFSS matrix model and only add some passing remarks at the end. To understand how a generic object of the model looks geometrically (a general matrix configuration), we add a point-like probe. That is, we extend a matrix configuration by taking a direct sum with a zero-brane probe. We embed an $N \times N$ matrix configuration into an $(N+1) \times (N+1)$ matrix in the upper left corner and add an eigenvalue in the rightmost bottom corner with zeros everywhere else.

We have a new auxiliary configuration with

$$\tilde{X} = \begin{pmatrix} X & 0 \\ 0 & x \end{pmatrix}, \quad \tilde{Y} = \begin{pmatrix} Y & 0 \\ 0 & y \end{pmatrix}, \quad \tilde{Z} = \begin{pmatrix} Z & 0 \\ 0 & z \end{pmatrix} \tag{7.5}$$

with $X,\ Y,\ Z$ three Hermitian matrices of one of the orbifolded matrix models.

The geometric characterization of the auxiliary matrices are then encoded in the observations of the spectator brane. The spectator brane can only ask questions related to the dynamics of the matrix models themselves and in particular of the degrees of freedom that connect the extra eigenvalue to the matrix configuration. There are two classes of modes that connect the extra eigenvalue to the configuration: the bosonic degrees of freedom and the fermionic degrees of freedom. Here we will restrict ourselves to the fermionic degrees of freedom and the questions we ask depend on the position of the extra eigenvalue probe.

We decompose the fermionic degrees of freedom as

$$\tilde{\psi} = \begin{pmatrix} 0 & \psi \\ 0 & 0 \end{pmatrix} \tag{7.6}$$

where our goal now is to ask what are the energies associated to the modes $\tilde{\psi}$. Notice that we picked very particular components of the fermions and not others. This can be justified completely in orbifold models, as we discussed previously, but orbifolds are not really required to make this argument. All we need is the subquiver diagram that enforces the restrictions of the matrices defined by equations (7.5) and (7.6). To do this carefully, we are choosing the probe to be a different fractional brane than the matrices $\vec{X}$ represent. The chirality of these modes indicates that if the branes were four dimensional fractional branes and we think of fractional branes as higher dimensional branes wrapped on collapsed cycles, then they would definitely intersect. The intersection properties of the fractional branes represent the intersection properties of the collapsed cycles [121]. Also notice that we did not put fermions in the bottom leftmost corner; this is our chirality assumption for the arrow.

The first question we ask is if there is a definition of distance from the eigenvalue probe to the matrix configuration. The way to answer that question is to look at the spectrum of fermions connecting the probe eigenvalue to the matrix configuration. The eigenvalue probe is located at $x,\ y,\ z$ in a background of the three Hermitian matrices $X,\ Y,\ Z$. The dynamics are described by the following effective Hamiltonian

$$H_{\text{eff}} = (X - xI_N) \otimes \sigma_x + (Y - yI_N) \otimes \sigma_y + (Z - zI_N) \otimes \sigma_z \tag{7.7}$$

where I_N is the $N \times N$ identity matrix which we will omit in the future. The origin of this Hamiltonian comes from the Yukawa terms in the full Hamiltonian given by

$$\text{Tr}(\Psi^\dagger \gamma^i [X_i, \Psi]) \tag{7.8}$$

and evaluated in the configuration $\tilde{X},\ \tilde{Y},\ \tilde{Z}$. The Hamiltonian above describes the mass term for the off diagonal modes of the fermion ψ that are charged under the gauge group of the extra eigenvalue probe. The structure of how the Pauli matrices appear for chiral multiplets is derived in Appendix E. The dependence on the bosonic variables comes directly from the commutators.

We can think of this as a Hamiltonian in a tensor product space $\mathcal{H}_{\text{big}} = \mathcal{H}_N \otimes \mathcal{H}_{\uparrow\downarrow}$ of an $N-$ dimensional Hilbert space times a spin one half object (a single q-bit). The Hamiltonian H_{eff} is covariant under unitary transformations of $\mathcal{H}_N$. A transformation $U \in \text{Aut}(\mathcal{H}_N)$, induces an automorphism of $\mathcal{H}_{\text{big}}$ via $U \otimes 1$. The automorphism takes $X \to UXU^{-1}$, $Y \to UYU^{-1}$, $Z \to UZU^{-1}$ and $H_{\text{eff}} \to (U \otimes 1)H_{\text{eff}}(U^{-1} \otimes 1)$ which shows that the spectrum of H_{eff} is invariant under such rotations. This is inherited from the gauge transformations of the original matrix model. What is important is that the spectrum of H_{eff} is gauge invariant.

As is usual in string theory, the off diagonal modes connecting a subconfiguration to another are considered to be strings, once they are quantized. The typical energy of a string of length ℓ is given by $\alpha'\ell$ where α' denotes the string tension [2]. Hence, in our effective Hamiltonian, we can denote the distance from the probe brane located at $(x,\ y,\ z)$ to the configuration by the eigenvalues of the effective Hamiltonian H_{eff}. The reason to look at fermions is that fermionic Hamiltonians do not have tachyons. Thus technically all energies are positive and thus the notion of distance is positive. This is also true for string states; open string fermions in the NSR superstring appear in the Ramond sector for open strings. The zero point energy of the fields cancels between bosons and fermions on the worldsheet because they have the same boundary conditions Thus the only contribution to the energy of the string is from the classical stretching between the ends of the strings.

---

[2] The units of α' are energy per unit length, althoug in natural units it is inverse length squared.

The eigenvalues of H_{eff} themselves can be positive or negative. As such, we interpret the positive eigenvalues as the frequencies of creation operators, and the negative eigenvalues as frequencies of lowering operators upon second quantization. The absolute value of the spectrum of H_{eff} is then the list of distances from the probe brane to the object when interpreted as strings. Obviously, if we have more than one distance, the object with respect to which we are measuring distances should be considered to be an extended object. The minimal eigenvalue of the spectrum obtained should give us the minimal distance to the extended configuration.

The Hamiltonian H_{eff} is covariant under rotations and translations. These symmetries are inherited from the original BFSS Lagrangian. More importantly, the Hamiltonian is also covariant under rescalings: if we rescale $X,\ Y,\ Z$ and the coordinates $x,\ y,\ z$ by the same common factor, the entries of the matrix rescale with the same power and thus the eigenvalues scale as well.

First let us solve the spectrum in the asymptotic regime, where $(x,\ y,\ z) \to \infty$ along a determined direction in $\mathbb{R}^3$ keeping the X, Y, Z matrices fixed. By convenience, we can use rotation invariance to take $z \to \infty$ keeping $x,\ y$ equal to zero. We then have that

$$H_{\text{eff}} = -z \otimes \sigma_z + (Z \otimes \sigma_z + X \otimes \sigma_x + Y \otimes \sigma_y) \tag{7.9}$$

We can compute the eigenvalues of H_{eff} by considering it as a perturbation theory of $H_{\text{eff}} \simeq -z\sigma_z$. The eigenvalues of this matrix are degenerate. There are N eigenvalues of values $+z$ and N eigenvalues of value $-z$. These are very large.

Since the spectrum is degenerate, to first order we need to resolve the splitting among the degenerate subset. This is done by looking at the perturbation terms in H_{eff} that commute with σ_z. The term that does that is $Z\sigma_z$ itself. So the transformation that diagonalizes H_{eff} along the two degenerate subsets is the same transformation that diagonalizes Z. We find that the leading order spectrum is given by

$$\mathrm{Eig}(H_{\text{eff}}) = \pm(z - \lambda_i^z) + O(1/z) \tag{7.10}$$

where λ_i^z are the eigenvalues of Z. The extra corrections of order $1/z$ result from the 'energy denominators' in perturbation theory and involve the components of X, Y.

We find the familiar theme that the eigenvalues of the matrices X, Y, Z describe the positions of objects (distances) as viewed from infinity. Since the eigenvalues are continuous functions of the matrices, we find that the notion of distance by taking the minimum eigenvalue is a continuous function of the position.

Let us now ask what happens when we are at distance zero from a configuration. This can happen in two ways: an eigenvalue of H_{eff} crosses zero, or the eigenvalues just grazes zero and keeps its sign. We will define an index that counts possible crossings of zero from infinity. At infinity, the spectrum of H_{eff} is paired into positive and negative eigenvalues and to first order in perturbation theory they are equal to each other up to sign, obviously this implies that they both have the same number of eigenvalues. If an eigenvalue goes from positive to negative, the number of positive eigenvalues decreases by one, and the number of negative eigenvalues increases by one. Similarly in the other direction. We want the index to be zero at infinity and changes by one at each crossing. The definition of the index is given by

$$I((x,y,z))_{X,Y,Z} = \frac{n_+ - n_-}{2} \tag{7.11}$$

where n_+ the number of positive eigenvalues of H_{eff}, and n_- is the dimension of the space of negative eigenvalues of H_{eff}. The index is a locally constant function (after all, eigenvalues of matrices are continuous functions of the entries) that can only change values at locations where H_{eff} has null eigenvalues. If for a configuration we have that $I(x,y,z) \neq 0$, we know that on any path connecting $x,\ y,\ z$ to infinity there are crossings of zero and thus the location (x,y,z) is surrounded by the noncommutative object characterized by $X,\ Y,\ Z$.

Such an index was defined in [123] for the position $x,\ y,\ z = 0$ called a Bott index. In their formulation, they dealt with approximations to a sphere, where $X^2 + Y^2 + Z^2 \simeq 1$ and the introduction of Pauli matrices was an auxiliary construction in mathematics. The matrices $X,\ Y,\ Z$ represented observables in a quantum system where only finitely many states were allowed and hence position observables became finite matrices. They were also restricted to small commutators. The operator H_{eff} in that case would square to something that was very closed to the identity, so that all eigenvalues of H_{eff} were very close to ±1. Counting positive and negative eigenvalues is an invariant under small deformations that prevent the eigenvalues from getting too far from ±1. The index was interpreted in that case as an obstruction to localizing states on a sphere (making $X,\ Y,\ Z$ strictly commute). Demanding that $||X^2+Y^2+Z^2-r^2|| < \delta$ by deformations of $X,\ Y,\ Z$ imposes a bound on their commutators. The spectrum of the operator $\vec{X}\cdot\vec{\sigma}$ is also used in numerical studies of noncommutative field theories (see [124] for a recent example). One can also use the operator $\vec{X} \cdot \vec{\sigma}$ to define a fuzzy sphere by studying a single matrix model of $2N \times 2N$ matrices with a constraint [125].

In the case we have described, the index is dictated by the dynamics of fermionic degrees of freedom on D-branes. There are no restrictions on the size of commutators. These ideas can be extended further to higher dimensions and matrices with various restrictions following the ideas in [126]. Such a generalization is beyond the scope of the present paper.

Here are basic properties of the Index function (some of these already appear in the work [123]):

1. The index is an integer. At infinity the index vanishes (as we computed already). The index changes by ± 1 if a single eigenvalue crosses zero. It changes by integers if many eigenvalues cross zero.

2. The index defines a collection of oriented closed surfaces. The surfaces are the locus of where the index changes value. The orientation is defined by going from larger values to smaller values of the index (this includes the sign, thus $-1 > -2$ etc). The surface set itself is obtained from the zero locus of a polynomial in $(x,\ y,\ z)$ obtained by taking determinants. These surfaces will be called membranes or D-branes interchangeably.

3. The index has an additive property. Given two configurations $X_1,\ Y_1,\ Z_1$ and $X_2,\ Y_2,\ Z_2$, we can consider a new configuration given by taking direct sums $X_3 = X_1 \oplus X_2$, $Y_3 = Y_1 \oplus Y_2$, $Z_3 = Z_1 \oplus Z_2$. Under such constructions

we have

$$I((x,y,z))_{X_3,Y_3,Z_3} = I((x,y,z))_{X_1,Y_1,Z_1} + I((x,y,z))_{X_2,Y_2,Z_2} \tag{7.12}$$

and the set of surfaces with orientation is also additive under this operation.

4. The index possesses Orientation reversal. We can reverse the orientation of a surface without affecting its shape. To do so, we consider the complex conjugate of the matrices $X,\ Y,\ Z$. In equations, we have that

$$I((x,y,z))_{X,Y,Z} = -I((x,y,z))_{X^*,Y^*,Z^*} \tag{7.13}$$

The proof is as follows. A matrix and its transpose have the same eigenvalues. Then $(\vec{X}-\vec{x})\otimes\vec{\sigma}$ has the same eigenvalues as $(\vec{X}-\vec{x})^T\otimes\vec{\sigma}^T$. Since $\vec{X}$ is Hermitian, we can exchange $\vec{X}^T$ for $\vec{X}^*$. However, for Pauli matrices we have that $\vec{\sigma}^T \simeq -\vec{\sigma}$ after a unitary transformation in the spin one half subspace. Thus we have that the eigenvalues of $(\vec{X}-\vec{x})\otimes\vec{\sigma}$ are equal to the eigenvalues of $(\vec{X}^*-\vec{x})\otimes(-\vec{\sigma})$. That is, the matrix $(\vec{X}^*-\vec{x})\otimes\vec{\sigma}$ has the same eigenvalues as $(\vec{X}-\vec{x})\otimes\vec{\sigma}$ but with signs changed. This exchanges n_+ and n_- and reverses the index.

5. If $X,\ Y,\ Z$ are real, then $I((x,y,z)) = 0$ everywhere. This is a corollary of the orientation reversal property. For such configurations we have that $I((x,y,z))_{X,Y,Z} = -I((x,y,z))_{X^*,Y^*,Z^*} = -I((x,y,z))_{X,Y,Z}$. In particular this holds for collections of zero branes which are direct sums of one dimensional problems.

6. The index is covariant under rotations, translations, and dilatations of the system. This follows from the similar properties that H_{eff} has.
7. The index is not trivial. In the next section we will explore matrix configurations (X, Y, Z) for which $I((x, y, z))_{X,Y,Z} \neq 0$.

If we instead work with the BMN matrix model, we get an effective Hamiltonian given by

$$H_{\text{eff}} = (X - xI_N) \otimes \sigma_x + (Y - yI_N) \otimes \sigma_y + (Z - zI_N) \otimes \sigma_z + \frac{3}{4} I_N \otimes \sigma^x (-i\sigma^y) \sigma^z \quad (7.14)$$

The extra term ruins some of the properties above. In particular, the scaling the surfaces no longer holds, as does the ability to change the sign of the eigenvalues by complex conjugation. Translation and rotation covariance do remain. The index still vanishes when a probe is at infinity, but one can check that even for 1 × 1 matrices, the index changes when the probe used to define the index is on top of the D0-brane that described the configuration. This is the Myers effect in action [108]. As far as fermions are concerned, the presence of a background RR flux changes the Dirac equation, and an computed example can be found in [93]. In that example the displacement of the location of the fermion zero modes was required in order for configurations to form tori that were BPS. In the present case, the structure of the gamma matrices follows the background flux in the BMN model [60].

On the other hand, in this case many fuzzy spheres are ground states of the system and one expects that these solutions survive as time independent configurations. Also, many of these can be made to oscillate slightly so the membranes can persist indefinitely.

7.3 Fuzzy Spheres and Emergent Surfaces

7.3.1 Fuzzy spheres

Now that we have defined an index, let us consider some special examples of the index computation. We will start with a fuzzy sphere and ask about the index at the center of the sphere. The fuzzy sphere is defined as follows. Let $L^{1,2,3}$ be the angular momentum matrices of an irreducible representation of $SU(2)$ of spin j. These satisfy the identities

$$[L^i, L^j] = i\epsilon^{ijk}L^k \tag{7.15}$$

The maximum eigenvalue of L^3 are $\pm j$. Consider the following set of 3 matrices built by the following combinations:

$$X = \frac{r}{j}L^1, \quad Y = \frac{r}{j}L^2, \quad Z = \frac{r}{j}L^3 \tag{7.16}$$

We call this a fuzzy sphere. The maximum eigenvalue of Z is $|r|$. One could then argue that the sphere has radius $|r|$ as seen from infinity using our large distance computation in the previous section. On the other hand, $X^2+Y^2+Z^2 = \frac{j(j+1)}{j^2}r^2$. Thus one could also argue that the radius of the sphere is given by $\tilde{r} = \sqrt{1+\frac{1}{j}}|r|$. These two become identical in the large j limit, but at finite j there is some discrepancy. However, it is natural to believe that there is a well defined surface near this radius that surrounds the origin and that is our candidate for a locus where an eigenvalue changes sign.

Let us prove this assertion by computing the index in the center of the configuration, at $x = y = z = 0$. The effective Hamiltonian we have to deal with is then given by

$$H_{\text{eff}} = \frac{r}{j}\vec{L} \cdot \vec{\sigma} \tag{7.17}$$

This is the same type of problem that shows up in spin-orbit coupling in the hydrogen atom. The important thing is that this is spherically symmetric, so it makes sense to decompose the Hilbert space $\mathcal{H}_{\text{big}}$ into irreducible representations of $SU(2)$. The big Hilbert space is given by

$$\mathcal{H}_{\text{big}} \simeq (j) \otimes \left(\frac{1}{2}\right) \simeq \left(j + \frac{1}{2}\right) \oplus \left(j - \frac{1}{2}\right) \tag{7.18}$$

and it decomposes into two irreducible representations of $SU(2)$. For each of them, we have a common eigenvalue of H_{eff}. Moreover, H_{eff} is traceless. This can be proved in general because the Pauli matrices themselves are traceless. Thus, the two possible eigenvalues of H_{eff} have the opposite sign. One is positive, and the other is negative. This depends on the sign of r. Let us choose the sign of r so that $n_+ > n_-$. The number of eigenvalues of the bigger representation of $SU(2)$ is $n_+ = 2j + 2$, while those of the smaller representation are $n_- = 2j$. These are the dimensions of the two irreducible representations of $SU(2)$ appearing in the tensor product. We obtain that

$$I((0,0,0))_{\text{Fuzzy Sphere}} = \frac{n_+ - n_-}{2} = 1 \tag{7.19}$$

We already knew that the index was an integer, and that the typical change should be by ±1. Here we find an explicit example where the index changed by one somewhere between the origin and infinity. Because of spherical symmetry, the index changes value at a fixed sphere radius. A direct computation carried out in Appendix F shows that the radius at which it happens is given exactly by $|r|$. We thus find that the radius is governed by the maximum eigenvalue, rather than by the value of $X^2 + Y^2 + Z^2$. Indeed, if we use the definition of distance from the origin that is obtained from the spectrum of H_{eff} we find that the distance is equal to $|r|$. Indeed, with the spectral definition of distance we used, we find that the distance from any point in space to the sphere is the one that is obtained by elementary geometry.

We can also set up direct sums of concentric fuzzy sphere configurations of various radii, so we can get configurations where the index is arbitrarily large. For such configurations the index counts the (minimal) number of sphere layers that need to be crossed to get out of the center. Since the index counts with sign, surfaces (which we call membranes) of different orientations can be present and the index itself represents a lower bound on the number of layers that need to be crossed.

7.3.2 From a Sphere to a Torus

Here we detail how to make configurations that lead to a fuzzy torus embedded in three dimensions. The idea is to begin with a fuzzy sphere and to deform the matrices in the simplest way to get to a fuzzy torus. We follow the construction of the giant torus as described in [112] (other examples of embeddings of Riemann surfaces in $\mathbb{R}^3$ can be found in [127], and in [128] one can also find a different example that interpolates between sphere and tori). In the case of the giant torus, one is supposed to add strings with maximal angular momentum to a sphere until the geometry transitions to a torus. To do this, it is convenient to use matrices defined by

$$X^{\pm} = X \pm iY \tag{7.20}$$

and in the other direction

$$X = \frac{1}{2}(X^{+} + X^{-}), \quad Y = \frac{1}{2i}(X^{+} - X^{-}) \tag{7.21}$$

The matrices $X^{\pm}$ in the fuzzy sphere of spin j case are rescaled ladder operators for spherical harmonics and are adjoints of each other. In a natural basis for a sphere, we have that

$$X^{+}_{ba} = r\sqrt{j(j+1) - a(a+1)}\, \delta_{b,a+1} \tag{7.22}$$

The labels $a,\ b$ range from $j, \ldots, -j$.

If we quantize fluctuations of the fuzzy sphere (see for example [129]), one can check that the different diagonals of the matrix X^{+} carry different amounts of angular momentum in the z direction. They differ by one unit, and the diagonal where X^{+} has entries carries no angular momentum in the z direction. When we condense these fluctuations, we replace them by an expectation value which becomes a number multiplying the appropriate fuzzy tensor harmonic. Since we are looking to maximize the angular momentum of the fluctuations, the deformation we seek is given by

$$X^+_{ba} = r\sqrt{j(j+1) - a(a+1)}\,\delta_{b,a+1} + r\beta\delta_{b,j}\delta_{a,-j} \tag{7.23}$$

and take $X^- = (X^+)^\dagger$. We are using the index convention for the matrices that is associated to the L_z spin of the $SU(2)$ representation of spherical harmonics. The self-adjoint matrices X, Y are built from the same linear combinations as above, after the deformation. The parameter r just rescales the full solution, so we can ignore it. The parameter β then controls the geometry. For $\beta = 0$ we have a sphere. Indeed, the sphere topology is preserved for some values of β around zero. Numerically we have seen that the topology changes at the precise value $\beta = j$, although this is not essential for our discussion.

The presence of β also breaks the rotational symmetry of the surface to $\mathbb{Z}_{2j+1}$, where $2j + 1 = N$ is the rank of the matrices. It is the unbroken symmetry associated to condensing the state with highest spin along the z axis. Thus the torus shape is not invariant under full rotations along the X, Y plane. The simplest case where the family of surfaces we get seems to contain a torus is for 4×4 matrices. A figure for the case of 6×6 matrices is presented in Figure 7.1.

We should also notice that in our case it is obvious we have a torus. Determining the genus of the surface in other setups is more involved. One may use an approximation to Morse theory on the surface [130], but the result is inherently more fuzzy or explicitly requires taking a limit of large matrices. One can also obtain more standard fuzzy tori as zero energy configurations in higher dimensions by studying beta deformed matrix models [131].

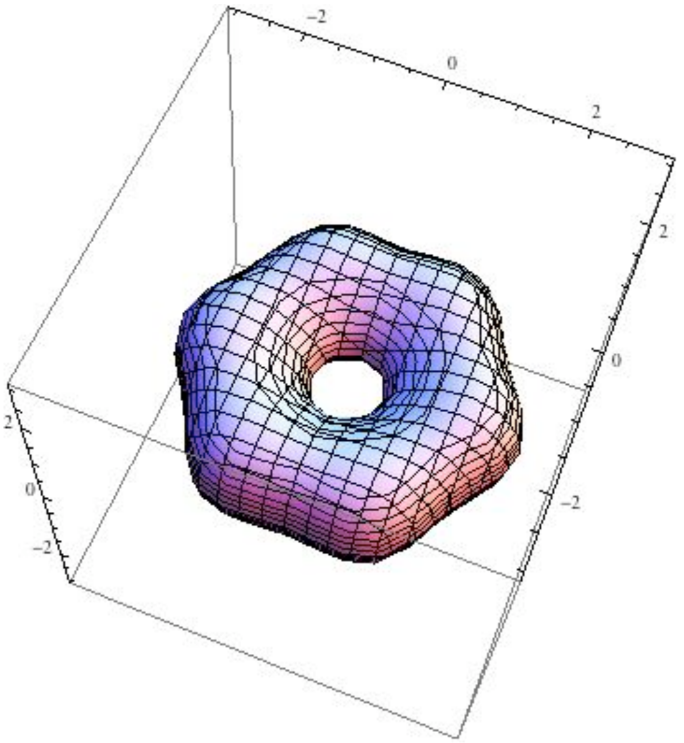

Figure 7.1: A fuzzy torus, for $r = j = 5/2$, $\beta = 2.55$. The $\mathbb{Z}_6$ symmetry is easily visible.

7.3.3 D2-branes

The intriguing feature of D-branes is that they carry a connection on their worldvolume. We see this in the open string sector, where a massless spin one particle exists on the D-brane worldvolume. Here, we want to show the geometry we deduced for these surfaces carries the information of a line bundle on it.

The surfaces are defined by the vanishing of an eigenvalue of H_{eff}, as calculated from equation (7.7). For a single zero eigenvalue there is a corresponding eigenvector, call it $\psi_0(x, y, z)$. The eigenvector ψ_0, normalized to unity, is well defined up to a $U(1)$ phase. This is the familiar symmetry for states in a Hilbert space in quantum mechanics; a global phase for the full wave function is not measurable, as physical states are rays in the Hilbert space. Since the eigenvectors are smooth functions of the matrix elements, they change continuously as we change our location on the surface. One can construct a bundle from the eigenvectors $\psi_0(x,y,z)$ and thus build sections over that bundle. One may further introduce patches over the bundle and a phase multiplying $\psi_0(x,y,z)$ on each patch with a transformation rule on patch intersections.

The tranformation rules can be supplemented by defining a connection. We use the familiar Berry phase, defined by

$$v^\mu A_\mu = -iv^\mu \psi_0^*(x,y,z)\partial_\mu \psi_0(x,y,z) = -iv^\mu \langle \psi_0|\partial_\mu|\psi_0\rangle \tag{7.24}$$

where v^μ is a vector tangent to the surface. This completes the definition of the connection of a line bundle on the worldsheet. Thus the membrane behaves exactly as we would expect a D2-brane to behave. At this stage, it is not clear the Berry connection that one would compute this way is just the connection that open strings feel, or if this is further twisted by the tangent bundle on the surfaces that were defined as we prescribed.

The full exploration of the curvature on these bundles and the precise connection to D-branes is beyond the scope of the present paper. We will show later that there is further evidence for physical states feeling a connection on the membrane worldsheet when we intersect two of these objects.

7.4 A Linking Number

Now that we have defined a geometric object for a collection of three Hermitian matrices, let us take two such objects and ask how they are related to each other. In the matrix model setups, each of them would be a configuration of branes. The spectrum of strings stretching between them becomes interesting from a dynamical point of view. In particular, one can define a linking number that for a D0-brane at position $\vec{x}$ reduces to the index we defined in previous sections.

We take matrices $X_1,\ Y_1,\ Z_1$ of rank r_1, matrices $X_2,\ Y_2,\ Z_2$ of rank r_2, and define a matrix analog the Hamiltonian $H_{\text{eff}}(x, y, z)_{X_1,Y_1,Z_1}$, where we replace (x, y, z) by Hermitian matrices (X_2, Y_2, Z_2). If the matrices commute with one another, we want the H_{eff} operator to give us an operator that acts as H_{eff} on the direct sum over the eigenvalues of $X_2,\ Y_2,\ Z_2$. The Hamiltonian that does the trick is

$$H^{(1)}_{\text{eff}}(\vec{X}_1, \vec{X}_2) = (X_1 \otimes I_{r_2} - I_{r_1} \otimes X_2) \otimes \sigma_x + (y \leftrightarrow x) + (z \leftrightarrow x) \tag{7.25}$$

Once $H^{(1)}_{\text{eff}}$ is defined this way, it does not matter anymore that the $X_2,\ Y_2,\ Z_2$ matrices commute with each other.

The definition of our linking number is given by

$$L^{(1)}[(X_1, Y_1, Z_1), (X_2, Y_2, Z_2)] = \frac{n^1_+ - n^1_-}{2} \tag{7.26}$$

The linking number $L^{(1)}$ is antisymmetric in its entries because tensor product spaces $A \otimes B$ are equivalent to $B \otimes A$ as Hilbert spaces. If we think of these spaces in tensor notation, the equivalence is a reordering of the indices and the Hamiltonian $H^{(1)}_{\text{eff}}$ changes sign More precisely, $H^{(1)}_{\text{eff}}(\vec{X}, \vec{X}')$ is unitarily equivalent to $-H^{(1)}_{\text{eff}}(\vec{X}', \vec{X}))$ when we exchange the triples $\vec{X}_1$ and $\vec{X}_2$.

There is a second linking number that one can define by changing a brane to an antibrane, that is, by reversing the orientation:

$$H^{(2)}_{\text{eff}} = (X_1 \otimes 1_{r_2} - 1_{r_1} \otimes X_2^*) \otimes \sigma_x + (y \leftrightarrow x) + (z \leftrightarrow x) \tag{7.27}$$

Again, if $X_2,\ Y_2,\ Z_2$ commute with each other and are diagonal, we can not distinguish $H^{(2)}_{\text{eff}}$ from $H^{(1)}_{\text{eff}}$. If the matrices do not commute with each other, we can distinguish them. The definition of the second linking number is

$$L^{(2)}[(X_1, Y_1, Z_1), (X_2, Y_2, Z_2)] = \frac{n_+^2 - n_-^2}{2} \tag{7.28}$$

This is symmetric in the exchange of $(X_1,\ Y_1,\ Z_1)$ and $(X_2,\ Y_2,\ Z_2)$. This uses the antisymmetry of $L^{(1)}$ combined with the change in sign of the index upon complex conjugation discussed in previous sections. It turns out that when considering the dynamics of fermions as given in the BFSS matrix model, it is the spectrum of $H^{(2)}_{\text{eff}}$ that controls the physics [132]. This is because the matrix multiplication rules on commutators translate to needing to take the transpose of the matrices $X_2,\ Y_2,\ Z_2$, which is equivalent to using their complex conjugates. This is also equivalent to saying that the fermions transform as a fundamental under one set of branes and an antifundamental with respect to the other set of branes.

Note that if we take one of the objects to infinity (say by adding multiples of the identity matrix), then at infinity both of the linking numbers are zero. If we shrink one object until it is point-like (by making $X_2,\ Y_2,\ Z_2$ proportional to the identity matrix, with coefficients x_2, y_2, z_2), then the linking number is r_2 times the index $I(x_2, y_2, z_2)_{X_1,Y_1,Z_1}$.

One can also use the Hamiltonians $H^{(1)}_{\text{eff}}$ and $H^{(2)}_{\text{eff}}$ to define a spectral distance between two such configurations, again by taking the eigenvalues closest to zero and taking absolute values. For infinite membranes touching each other in the IKKT matrix model one finds zero modes [133]. The effective Hamiltonian for fermions in that case takes a similar form to the BFSS matrix model. This is as expected from the mode spectrum of brane intersections at angles [134]. When the intersections are extended and compact, the low lying modes at the intersection need to be quantized carefully and zero modes are not guaranteed. One would expect that the spectral distance then gives an upper bound for a geometric distance between the brane configurations.

We now provide an application of the linking numbers. We will show that the linking numbers contain information about the connections on the line bundles of the surfaces defined in the previous section which couple to physical states. This provides further evidence that the surfaces are actually behaving as D2-branes. This is easiest to check from the calculations in Appendix F.

To show this, we take two fuzzy spheres and displace them relative to each other. For simplicity, we have normalized them so that their radii are equal to j and j', the spin of the corresponding representations of $SU(2)$. Let the displacement between the fuzzy sphere centers be characterized by the parameter b. Due to the high amount of symmetry, one can actually compute the index analytically and follow the crossings of the zero fermion eigenvalues in great detail.

If the displacement is b along the z axis and the fermions are decomposed into fuzzy spherical harmonics with respect to both fuzzy spheres, one finds that the eigenvalues cross zero sequentially when $b = j - j' + \ell$, where ℓ is an integer between 0 and $2j'$ inclusive. The index of the configuration where the big fuzzy sphere surrounds the smallest is exactly equal to $2j' + 1$, which is the dimension of the representation of the spin j' set of matrices. We expect this as the small fuzzy sphere is made of $2j' + 1$ D0-branes so that when they are all inside the big fuzzy sphere, we expect the index to be $2j' + 1$ times the index of the smallest representation.

The first zero mode appears when the spheres touch each other for the first time, at displacement $b = j - j'$. As b advances further, the two fuzzy spheres touch each other along a circle. We expect the lightest fermions to be localized in this circle. The problem effectively reduces to one dimension. As can be seen from the results of Appendix F, the fermion modes with maximal angular momentum in each $SU(2)$ representation of fuzzy spherical harmonics do not mix with other states, and their frequencies are given exactly by

$$j - j' + \ell - b \tag{7.29}$$

with ℓ an integer. These states are evenly split in energy, creating effectively a Kaluza-Klein tower of finitely many states. This is very similar to the Kaluza-Klein tower of tachyons between such spheres computed in the BMN model for such crossings in [135]. Such a Kaluza-Klein tower is an approximation to a quantum field theory for zero mass fermions on a circle in the presence of an holonomy. The fermions can be either leftmoving or right-moving depending on the positivity of the energy mode and the holonomy can be accommodated through quasi-periodic boundary conditions on the fermions. The fermions can have zero eigenvalues if the holonomy is a multiple of 2π. This can be removed by a large gauge transformation and redefines the notion of momentum on said circle. The important thing to note is that if the corresponding intersecting surfaces have the properties of D-branes, in that each carries a connection $\mathcal{A}_1$, $\mathcal{A}_2$, then the fermions that stretch between them feel the connection $\mathcal{A}_1 - \mathcal{A}_2$. Because of spherical symmetry, this connection can be computed from Gauss' law by calculating the area of the region of the sphere that the circle where the fermions lie enclose $\oint \mathcal{A}_1 = \int_{S_1} F_1$. The area of a sphere slice is proportional to the height of the slice, hence $\int_{S_1} F_1 \propto A$ which is linear in the vertical height of the slice.

Hence, shifts of 2π in the holonomy are equally spaced in b. Indeed, if the sphere is made of n D0 branes, we expect the total flux through the sphere of this bundle to be equal to $n = 2j + 1$. However, we can also expect a curvature correction. If we think of the matrices as describing a lowest Landau level of endpoints on each sphere and the endpoints as monopole spherical harmonics, in order to have n states we need a monopole flux equal to $n - 1$. This extra one is the contribution of the curvature of the sphere. One can check this way that the net flux for this connection through each sphere is $2j$ and $2j'$ respectively, as opposed to $2j + 1$ and $2j' + 1$. Thus the net flux through a slice is proportional to the area, which is $2\pi j(2j - t)$ where t is the height of the slice. Since the total flux through each sphere is $2j$, and the area is $4\pi j^2$ for each sphere, we get that the flux per unit height is constant and the same for both spheres. Thus, the flux

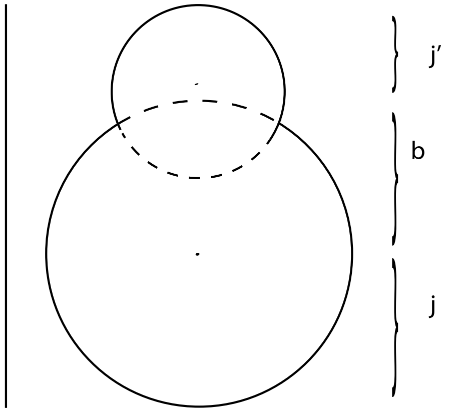

Figure 7.2: Illustration of two intersecting spheres. The net connection seen by the fermions stretching between can be computed by calculating the net flux through the solid lines.

for each sphere is linear in height with the same coefficient. This is visualized in Figure 7.2. As seen in the figure, the net flux that we need to compute is the one associated to the surface that has not been dashed in the graphic. This is proportional to $j + j' + b$ as a function of the displacement. This number needs to be an integer to get the correct holonomy. Thus the geometric argument matches the matrix computation. We should mention, however, that this is a simplified computation where the flux per unit height on each sphere is the same.

The setup shows that the surfaces we make are indeed compatible with the idea of having a curvature of a line bundle on them for physical states that thread between them. Another way to think about this, which we have already discussed, is that on the locus of positions where an eigenvalue vanishes there is a preferred fermion wavefunction for the Hamiltonian $H_{\rm eff}$; the zero eigenvector itself. This is only well defined up to a phase. If we want to patch these together to form a vector bundle over the surface, we need a line bundle connection so that this phase ambiguity is resolved on parallel transport. This is the generic case, but we can set it up so that the null eigenspaces are degenerate (thereby giving us multiple branes on top of each other). Thus, in general one will need a bundle connection to resolve these issues. Since the structure that we are analyzing involves the symmetries of a Hilbert space under change of basis, the connection in general will be $U(n)$ valued for n coinciding branes.

Lastly in this section we would like to give a more physical interpretation of these zero modes. The main idea, which we have hinted at already when we defined the index function, is that a crossing by zero represents a raising operator becoming a lowering operator and vice versa. If we follow a ground state continuously past this change, the ground state is defined by $a\left|0\right\rangle = b\left|0\right\rangle = 0$, where a is the lowering operator for particles with positive frequency, and b is the lowering operator for the particles with negative frequency, i.e., the antiparticles. After a zero crossing, the state $\left|0\right\rangle$ no longer remains a ground state. Instead, one of the lowering operators becomes a raising operator. The state on the other side of the barrier will have a non-zero occupation number for a single fermion in the Hilbert space. That is, on a zero crossing, a fermion is created. This is the Hanany-Witten effect (and its various generalizations discussed in [136, 137]).

The linking number we defined then encodes the number of strings that are created (with orientation) when separating two objects that are partially inside each other. Equivalently it describes the number of strings that were created on bringing the objects together from infinity as they cross one another. We see this by following a vacuum adiabatically until the point where the transition happens exactly. Creation operators become annihilation operators and vice versa, and so strings are either created or destroy at each transition. The resulting vacuum will then have a net string number associated to the number of these transitions.

This interpretation in terms of the Hanany-Witten effect explains why the geometry is so sharp. The presence or not of strings connecting the two surfaces is easy to test We check if the fermionic ground state is gauge invariant or not. The Hanany-Witten effect has the property that the fermionic ground state is not always gauge invariant, so the presence of the strings is protected by topology.

7.5 Discussion

We have orbifolded the BFSS and BMN matrix model to reduce the number of supersymmetries from sixteen down to four. Consequently, three of the nine bosonic matrices remain which capture some of the dynamics of the full theory. Chiral fermions arise if the orbifold is chosen with respect to a $\mathbb{Z}_k$ action. By adding a D0-brane probe to classical bosonic background configurations, the Yukawa terms in each matrix model yield an effective Hamiltonian for the chiral fermions, seen as fractional branes, which allowed us to examine some of the topological informaiton carried by the fermions.

The eigenvalues, being porportional to the string length, provide an effective distance to the background matrix configuration. The positivity of the eigenvalues determine whether the corresponding fermionic operators are of creation or annihilation type and we defined an index encoding this information. As one crosses a membrane from a higher to lower index, a fermion creation operator is transformed into a fermion annihilation operator. In the BFSS matrix model we can view this as a generalization of the Hanany-Witten effect. In the BMN matrix model, the dynamics of flux changes the results and many of the properties of the index are modified. We were also able to generalize this index to a linking number between two configurations. The linking number can also be interpreted as a Hanany-Witen effect in that it counts how many such strings are created when trying to separate the two configurations.

The locus of zero eigenvalues defines a surface in $\mathbb{R}^3$. We showed configurations that correspond to both spheres and tori. We were also able to show that the surfaces carry the information of a line bundle on them with connection (which can be calculated using Berry phase arguments). This shows that the membranes we found really behave like D2-branes. Our exploration of this issue was very sketchy, so finding how to make this correspondence precise requires more work. Indeed, we would need to see if the connection we computed also includes information of the tangent bundle of the surface or not and how to separate that part from the D-brane worldvolume spin one excitations. For recent investigations, see [138, 139, 140].

After solving the problem of embeddings into three dimensions, it would be interesting to understand how this same story plays out in higher dimensions. One of the ways in which extended objects are understood is in terms of Berry phase dynamics [141] (for a more recent discussion see [142] and references therein). The Berry phase can lead to a non-trivial vector bundle structure of fermion excitations connecting a probe to a brane. If topology requires that this structure becomes degenerate at various loci, then these loci probably describe extended objects. One has to look for fermion zero modes depending on position and at least in principle it should be possible to predict that there are degenerations in some setups. However, the story might be more complicated, as we might need to have more than one fermion zero mode simultaneously to describe this locus. The Berry phase dynamics associated to that setup would then be non-abelian, which might also require using extended probe branes to see the effects. The general question will then be to understand generalized versions of the Hamiltonian (7.7) and the general structure of degenerations. Our construction also suggests that in these general setups there can be a similar linking number so long as one can guarantee crossings of zero of the eigenvalues of H_{eff}. One can show that for even dimensions (an even number of matrices) the spectrum of fermions starting from a D0-brane probe to a configuration is mirrored; for every positive eigenvalue there is a negative one. This is because one can find a matrix similar to γ^5 in four dimensions that anti-commutes with H_{eff} as given by the generalization of equation (7.7). This suggests that ideally we should work with an odd number of matrices to make the existence of zero modes plausible for somewhat general configurations.

The inverse problem is also interesting to study. Given a surface, and perhaps some additional information, how can one recover the matrices and their rank? One could also ask if the surfaces we obtained move in a way that closely resembles the membrane dynamics once we turn on the dynamics. This might be important to understand $1/N$ effects in matrix theory. We found that in general we could reverse orientations of branes by using complex conjugation. It would be nice to understand if a brane-antibrane pair in these models generally leads to tachyons on their worldvolume and it would be interesting to analyze how tachyon condensation would progress in these setups. It would also be interesting to understand this issue with a probe D0-brane on top of a D2-brane, that is, do we always get tachyons in this way?

Additionally, the ideas found in [126] suggest various generalizations to different types of matrices. These ideas have applications in condensed matter physics and the connections we found with string theory ideas might provide ways of analyzing the condensed matter systems and their dynamics. Such changes of the structure of matrices are natural when considering orientifolds. Thus our arguments should generalize to those setups as well.

Chapter 8

Classical Dynamics of Holographic Matrix Models

In this Chapter we accept our inability to solve strongly coupled quantum theories directly, drop the adjective 'quantum,' and study 'strongly coupled classical theories.' We simulate the real time classical dynamics of the BFSS and BMN matrix models, which have well known holographic dual descriptions. The non-linearity of these theories will induce chaotic dynamics. In the large N limit good thermodynamic and hydrodynamic variables will emerge. Along the way we will make connections to holography, but leave a larger portion of the gravitational intrepretation to Chapter 9.

8.1 Observables and Symmetry

The regime where the four dimensional $\mathcal{N} = 4$ SYM theory is dual to a semi-classical (super) gravity theory is large N and strong 't Hooft coupling [13]. This regime involves $\hbar$ in a crucial way because the strong coupling regime implies that $g_{\mathrm{YM}}^2 N\hbar \gg 1$. We should be careful interpreting this relation. In dimensions other than four, like our $0+1$ dimensional matrix models, the Yang-Mills coupling constant has units. Thus the left hand side can not be compared to the right hand side without choosing a state and multiplying by the appropriate quantum numbers to obtain a dimensionless ratio.

If we choose a thermal state at temperature T for an oscillator degree of freedom with angular frequency ω, we can ask if thermal fluctuations are larger than quantum fluctuations for that degree of freedom. This happens when $k_{\mathrm{B}}T \gg \hbar\omega$ and so $\hbar$ can be small if the temperature is high enough. For relativistic quantum field theories there is always some ω where $k_{\mathrm{B}}T < \hbar\omega$. Such degrees of freedom would be responsible for the UV catastrophe. On the other hand, for oscillators with small ω the left hand side is much larger than the right hand side and the corresponding oscillators are at high occupation quantum numbers. The dynamics of these low frequency modes is controlled by classical physics. The classical world meets the quantum world in the intermediate regime. Roughly speaking, the correspondence principle in quantum mechanics should let us interpolate between the classical and the quantum regimes. In the BMN and the BFSS matrix model we only have a finite number of degrees of freedom, so the UV catastrophe issue is avoided However, we can still try to push the system to the correspondence limit, which we describe below.

Typical quantum states are superpositions of position eigenstates, so if we are to match various physical quantities of the quantum system we should either average over positions or smear the classical states to a volume of $\hbar$ for each canonical pair of variables. If the system is chaotic, most energy eigenstates behave as if they are thermal for sufficiently small subsystems [143] (one has to make allowances if there are conserved quantities which don't thermalize), so the correspondence principle suggests that we should study the statistical properties of the thermal ensemble to study the coarse grained properties of the quantum states. In this paper we do not calculate anything in the regime where quantum effects start making a difference, but we keep in mind that in the end we want to understand the system in the quantum regime.

Let us return to the BMN and BFSS matrix models. The regime of interest for us is the large N regime, as dictated by holography. In this regime, the number of degrees of freedom grows like N^2. We will see that the large N limit is not only a thermodynamic limit but that we also observe a kind of hydrodynamics. Here we do not mean thermodynamic limit in a formal, rigorous sense, but simply that we find various state variables that remain finite as N grows. Ideally, we should be able to show local equilibrium and transport to claim hydrodynamic behavior. Unfortunately, we do not know how to make such a formulation from first principles, as the degrees of freedom in these matrix models are essentially non-local. If we take one of the matrices of the matrix model, we can interpret the eigenvalues as positions of D-branes [62, 71], while the off-diagonal elements are strings stretching between the branes. In the classical regime we are studying, all the off-diagonal modes are excited, so it is hard to define local quantities that could play the role of, e.g., densities of D-particles.

Instead we can add a probe far away and determine what it sees. In the BFSS matrix model such a formulation leads to an effective potential for the probe. The effective potential can be computed from traces of the configuration [107] convolved with some Green's functions that decay polynomially in the distance

[132]. This is a quantum computation where one integrates out the off-diagonal degrees of freedom connecting the probe to the configuration under study. This gives rise to gravitational interactions between general D-brane objects and gravitons (the interactions between gravitons by integrating off-diagonal models is part of the original formulation of the BFSS matrix model [107] [1]). The natural candidates for hydrodynamic variables are these traces of various products of matrices appearing in the effective potential. They act as moments of the distributions of matter in the effective potential for a faraway probe.

We need to show that the dynamics of these collective modes are roughly independent of N to justify calling their dynamics hydrodynamic. Note that we only make claims about these collective degrees of freedom in a statistical sense as if we were considering the hydrodynamic variables of a system of molecules. Since we will be studying mostly equilibrium configurations, all we have access to are the fluctuations of these variables. The results of this chapter will show that these fluctuations have some dynamical properties independent of N.

Specifically, we will study time dependent correlation functions of certain single trace observables. Consider first a single trace operator

$$\mathcal{O}_{[i]} = \mathrm{Tr}\left(X^{i_1}X^{i_2}\ldots\right), \tag{8.1}$$

where $[i]$ is a multi-index. In the brane picture this will be a source for some gravity field, or more generally a closed string field. We usually find that

---

[1] The simplest one loop computation was done in [144, 145], while a two loop result was obtained in [146]. Higher order results require information on the wave functions of the graviton states one is scattering.

$$\mathcal{O}_{[i]} \simeq \int d^d x\, \rho_\alpha(x) f(x), \tag{8.2}$$

where ρ_α would be the local source of the field (if such a notion makes sense) with its corresponding spin labels and f is some polynomial function of x, which can also carry angular momentum labels. Together these would combine into a multipole expansion labeled by the multi-index $[i]$. We can decompose the product into spherical harmonics, and then symmetry considerations will tell us that if the configuration is spherically symmetric the averages of objects whose spin is non-zero vanishes. For many interesting observables the time average should vanish

$$\langle \mathcal{O}_{[i]} \rangle_t = 0, \tag{8.3}$$

even though it does not do so for each configuration.

Given two such observables $\mathcal{O}_i(t)$, we can consider averages of the form

$$S_{ij}(a) = \langle \mathcal{O}_i(t) \mathcal{O}_j(t+a) \rangle_t \tag{8.4}$$

where we average over a trajectory (or a collection of such trajectories with the same energy and conserved quantities). The correlation function $S_{ij}(a)$ will describe the statistical properties of the time dependent correlations between the observables and encode fluctuation-dissipation information. These correlation functions can be different from zero, even if the individual expectation values of the $\mathcal{O}_i$ vanish. This is similar to studying sound modes for gas in a cavity.

If the individual harmonics are not excited, then their average is zero, but there will be thermal fluctuations. These fluctuations, when properly normalized, will have a good thermodynamic limit, but away from this limit there can be finite size effects that are sensitive to the number of particles.

We will say the system behaves hydrodynamically if a collection of the $S_{ij}(a)$ properly normalized has a large N limit where the collection $S_{ij}(a)$ converges to a single function of a for fixed ij, and for a reasonable interval of time that is short compared to the Poincaré recursion time, but that can be much longer than any thermalization time (or scrambling or relaxation time) for near equilibrium dynamics.

On the other hand, this may be too narrow a definition. Consider a toy model of gas in a box with a somewhat random shape that is temperature dependent (like a rubber balloon filled with an ideal gas). We would say that the hydrodynamic behavior there is independent of the box. However, let us imagine that we want to study hydrodynamics by looking at the normal modes of sound in the box, or other such decomposition into normal modes. If we change the temperature, we would change the shape of the box somewhat because the added pressure would deform the walls of the container. This would deform the harmonics of the box, and the collection of harmonics of the box would be temperature dependent. These changes can not be done while preserving the spectrum (even after rescaling time). Additionally, if we change the number of particles inside the box in such a way that the pressure stays the same, the shape of the box would not change. The temperature of the gas, however, would change depending on the number of particles. In such a case, the modes of sound on the box would be independent of the temperature only after a rescaling of time, and the ratios of the different frequencies would be invariant, but not the frequencies themselves.

Our systems are somewhat analogous to this. After thermalization, the matrices will relax to an approximately spherically symmetric configuration about the center of mass. This is in the absence of angular momentum for the initial conditions. We will consider the addition of angular momentum in Chapter 10. These spherical configurations grow in size if we increase the temperature. In the BMN system, the geometry of the plane wave in which the configuration is embedded acts like a box, similar to how AdS acts like a mirror. If we increase the temperature the configuration grows in size and the external pressure changes. There is also an internal pressure that makes the system want to collapse. Excitations of the off-diagonal modes between the branes act like a glue that makes the system shrink. If these are treated as harmonic oscillators, one would expect that each such harmonic oscillator has an energy of $k_{\mathrm{B}}T$ and that the energy stored in these configurations is independent of the position. However, as we move a D-particle far away from the system, the effective frequency of these modes goes up, and there is a corresponding shrinkage of the available phase space for these modes. Thus, there is an entropy cost to move a D-particle away from the configuration and the internal pressure to hold the system together is an entropic force. It has been argued that this type of entropic effect leads to the gravitational force near the horizon of a black hole [147].

At the same time, thermal pressure makes the system expand. These two forces can reach an equilibrium. In the very high temperature limit we expect that the internal pressure dominates over the external pressure so that the shape of the container matters less. However, we will not be able to guarantee that the system is hydrodynamic without fine tuning. To do so we would need to match the box shapes between different values of N. Doing this carefully requires a fairly detailed understanding of the phase diagram of the system.

All of this is much simpler to study in the BFSS matrix model. The classical dynamics of the BFSS model has a scaling property. Any configuration at a given energy can be rescaled to any other energy by a rescaling of time and the matrix components. Thus, it does not matter at what energy we study the system as the dynamics is essentially the same. Thus in BFSS we can get rid of the temperature dependent shape parameters. Then the dynamics of the thermal system depends only on N and we can explore that singular dependence. For of this reason, we analyze the large N limit primarily in the BFSS matrix model.

8.2 Numerical Implementation

The numerical implementation of these simulations has been discussed previously in [148]. We work with a leapfrog algorithm and we indicate how to implement the constraints in the initial conditions. Here we reiterate the algorithm.

In Appendix D we list the BFSS and BMN matrix models. In this Chapter we relabel the fields to explicitly indicate the breaking of the $SO(9)$ symmetry in the BFSS matrix model to $SO(3)\times SO(6)$ in the BMN case. Here we label the bosonic matrices $X^i = \phi^{i+1}$, $i = 0, 1, 2$, and $Y^a = \phi^{a+3}$, $a = 1, \ldots, 6$. Additionally the dynamics in this chapter are Hamiltonian and so we have the conjugate momenta to X^i and Y^a denoted by P_i and Q_a, respectively. Because we are only beginning to explore the classical dynamics, we completely ignore the fermions.

The bosonic part of the Hamiltonian can be written as

$$H = \frac{1}{2}\mathrm{Tr}\left(P_i^2 + Q_a^2 + (\alpha X^i + i\epsilon^{ijk}X^jX^k)^2 \right.$$
$$\left. + \frac{\alpha}{4}(Y^a)^2 - [X^i, Y^a]^2 - \frac{1}{2}[Y^a, Y^b]^2\right) \tag{8.5}$$

The potential is written to emphasize that the $SO(3)$ part can be written as a sum of squares. For $\alpha = 0$ we get the BFSS matrix model. When $\alpha \neq 0$ we have the BMN matrix model, but for convenience we set $\alpha = 1$. We have rescaled the variables so that the classical equations of motion are independent of $\hbar$ and all of the quantum mechanics is hidden in the initial conditions. We have also normalized the mass of X to one, i.e., we measure time by the oscillation period of one of the X modes. Along with the $U(N)$ gauge symmetry comes the Gauss' law constraint

$$G = \sum_{i=0}^{2}[X^i, P_i] + \sum_{a=1}^{6}[Y^a, Q_a] = 0 \tag{8.6}$$

To integrate the equations of motion we use a leapfrog algorithm. This has the virtue of preserving the constraints. The discretized matrix equations of motion read

$$X_{t+\delta t} = X_t + P_{t+\frac{\delta t}{2}}\delta t, \qquad P_{t+\frac{\delta t}{2}} = P_{t-\frac{\delta t}{2}} - \left.\frac{\partial V}{\partial X}\right|_t \delta t \tag{8.7}$$

and similarly for the Y modes. Since we have the X^i, P_i evaluated at different times, we need to be a little careful with the constraint. We define

$$G(t) = [X^i(t), P_i(t+\delta t/2)] + [Y^a(t), Q_a(t+t/2)] \tag{8.8}$$

and will set it to zero in the initial conditions. We also define the constraint at half intervals to be given by

$$G(t+\delta t/2) = [X^i(t+\delta t), P_i(t+\delta t/2)] + [Y^a(t+\delta t), Q_a(t+\delta t/2)] \tag{8.9}$$

To show that the constraints are satisfied notice that when we evolve the constraint by using the equation of motion (8.7), after one half step in t we get that

$$\begin{aligned} G(t+\delta t/2) - G(t) &= \sum_i [\delta X^i(t), P_i(t+\delta t/2)] + \dots \\ &= \sum_i [P_i(t+\delta t/2), P_i(t+\delta t/2)]\delta t + \dots = 0 \end{aligned} \tag{8.10}$$

which vanishes term by term. For the second half step we need to work harder, but so long as V is a sum of traces of products of X and Y matrices (or functions of such traces), one can prove that the contribution from each such trace vanishes by summing cyclically over the letters making the word in the trace. Hence, $G(t+\delta t) - G(t) = 0$ and this tells us that $G(t)$ is a constant of motion of the discrete evolution. Incidentally, the same arguments work for angular momentum conservation laws. Our initial conditions are those for (near) zero angular momentum. The only place where constraint violations might appear is from rounding errors, so we need to check that we don't suffer from this problem. To improve numerical stability we use double precision numbers. To check for numerical errors, we record the absolute value of the constraint $CV = |\mathrm{Tr}(G^2)|$ as a check for the code. We find that the constraint is well satisfied for the runs we perform, so we do not need to implement constraint damping. The equations of motion evolve Hermitian matrices into Hermitian matrices. Truncation errors in matrix multiplication can also take us away from that locus. We found that we needed to enforce hermiticity of the matrices every few steps, by taking $X \to (X + X^\dagger)/2$ and similarly for all other matrices. We do this every time we write the matrix configurations.

The main sources of difficulty in the setup are the initial conditions. For this paper, we have used the following initial classical configurations:

$$X^0 = \begin{pmatrix} L_n^0 & 0 \\ 0 & 0 \end{pmatrix}, \quad X^1 = \begin{pmatrix} L_n^1 & \delta x_1 \\ \delta x_1^\dagger & 0 \end{pmatrix}, \quad X^2 = \begin{pmatrix} L_n^2 & \delta x_2 \\ \delta x_2^\dagger & 0 \end{pmatrix},$$

$$P_0 = \begin{pmatrix} 0 & 0 \\ 0 & v \end{pmatrix}, \quad P_{1,2} = 0 = Q_{1,\ldots,6}, \quad Y^a = \delta y^a \tag{8.11}$$

in the BMN matrix model. These are the same initial conditions that were used in [148]. The δx and δy are generated by Gaussian distributions with a width proportional to $\sqrt{\hbar/(N-1)}$. This is a classical estimate of the quantum uncertainty of the modes. The parameter $\hbar$ is only used in the initial conditions and is similar to the standard practice in molecular dynamics simulations [149].

To generate matrix configurations in the BFSS matrix model, we first evolve in the BMN matrix model, set $\alpha = 0$ at some time later, and then continue the evolution of the system. As mentioned at the end of the previous section,

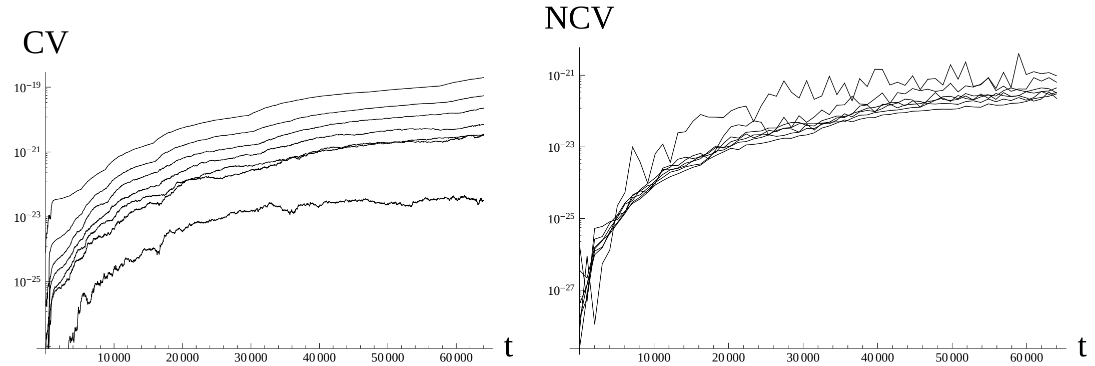

Figure 8.1: Constraint violation and normalized constraint violation as a function of machine time. The constraint violation stays very low through the computation. The graph indicates values at $N = 4,\ 7,\ 10,\ 13,\ 18,\ 27,\ 47$, and after normalization it shows larger fluctuations for smaller N. These are due to the statistical fluctuations of $\mathrm{Tr}(X^2)\mathrm{Tr}(P^2)$, which are an integral part of the dynamics. In the plot to the right we have selected larger intervals in machine time to aid visualizing the different values of N.

the classical BFSS matrix model enjoys a scaling symmetry and the only free parameter is N. Thus we can test the convergence of quantities as we increase N in a temperature independent way.

We store the full configurations of the matrices every few steps in δt (for the data sets present here we set this number to ten unless otherwise stated), and we store other information for faster processing at different intervals. This is especially important for long simulations. We will call machine time the total run in the simulation in units of the smallest time step that is recorded.

Our results for the constraint violation can be seen in Figure 8.1. The constraints have units and so we need to normalize them. We define the normalized constraint violation to be $NCV = -N\mathrm{Tr}(G^2)/(\mathrm{Tr}(X^2)\mathrm{Tr}(P^2))(t)$ (we randomly chose X^2, P_1) with N the size of the matrices. In the simulations depicted in Figure 8.1 we set $\alpha = 0$ after machine time $t = 2000$.

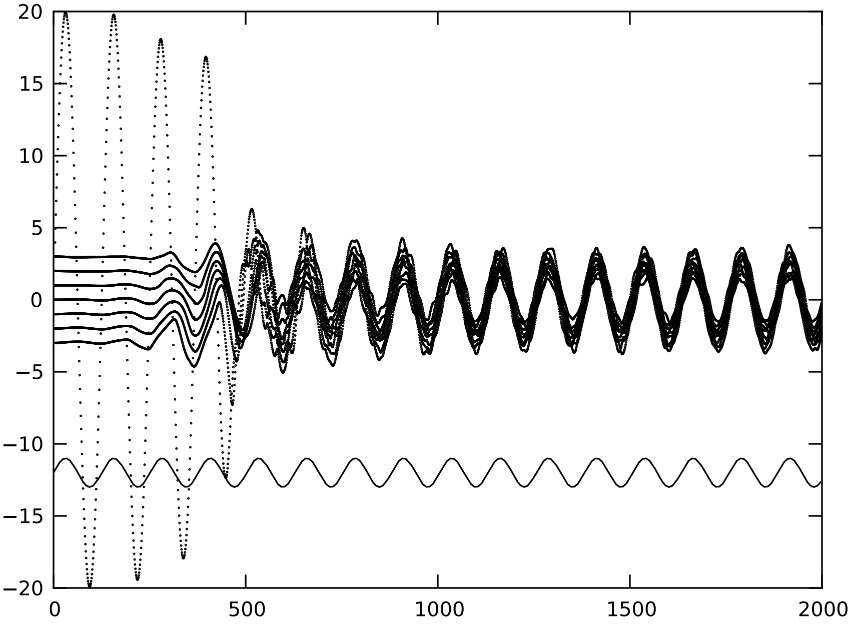

Figure 8.2: Eigenvalues of X^0 as a function of time for a simulation of rank 8 matrices with $\delta t = 0.001$, $v = 20.0$, and $\hbar = 0.001$. The abscissa measures discrete time units between recordings. The sinusoidal curve at the bottom is the trace of X^0 which serves as a clock due to its equations of motion.

8.3 Thermalization

In [148] it was shown that the initial conditions (8.11) generate configurations of eigenvalues which coalesce into a uniformly oscillating blob, for example see Figure 8.2. The system was argued to have thermalized in that time averaged distributions of the momentum degrees of freedom follow a Gibbs ensemble $dP\,dQ\,\exp(-\beta H)$ for some inverse temperature β. The Gibbs distribution factors into a product of Gaussians because the BFSS and the BMN Hamiltonians depend quadratically on the momenta. It was shown that the binned eigenvalues collected over time follow the semicircular distribution for random matrices, as is expected for random Gaussian matrices in the large N limit. Here we explore in more detail the nature of the thermalization, the appropriate finite N Gibbs distribution, and the design of a correctly calibrated thermometer.

One thing to note is that the equations of motion for the traces of the coordinates and their momenta are those of a harmonic oscillator. The traces of the X^i and P^i oscillate with period 2π while those of Y^a and Q^a oscillate with period 4π. Although this property of the BMN system can be used to generate a clock for the system (as in Figure 8.2), it is undesired here. The trace is a protected degree of freedom that does not thermalize. To describe the thermalized system in a statistical manner, we must remove the trace degree of freedom from our Gibbs distribution. The matrices are Hermitian, and so we must also enforce that on our Gibbs distribution. What we are left with is the Traceless Gaussian Unitary Ensemble (TGUE), a means by which to select random traceless Hermitian matrices. The trace of the matrices represents the center of mass motion of the system and thus our partition function really only describes the internal degrees of freedom that can thermalize.

In order to study ensemble quantities of the system, we must coarse grain the dynamics leaving only gauge invariant quantities to be studied. We can study our Gibbs distribution in a gauge invariant manner by focusing on eignvalues and traces. Integrating over the unitary degrees of freedom gives the joint probability distribution for the eigenvalues. This result is well known for the GUE and is simple to modify for the traceless case in which we are interested. The trace is invariant under a unitary transformation, and thus we may enforce tracelessness by inserting a delta function without affecting the removal of the unitary degrees of freedom. We define the following partition function as the integral of the joint probability of the eigenvalues for the TGUE

$$\mathcal{Z}_\lambda = \int d^N\lambda\, \delta(\mathrm{Tr}(\Sigma_i \lambda_i)) \prod_{1\leq i<j\leq N} |\lambda_i - \lambda_j|^2 \exp\left(-\frac{\beta}{2}\sum_{i=1}^{N}\lambda_i^2\right) \tag{8.12}$$

where N is the rank of the matrices of interest and β is a parameter analogous to the standard deviation for normal distributions. For us β is physically the inverse temperature of our system. Note that the polynomial in the integrand is the square of the Vandermonde determinant of the eigenvalues.

Before moving on to the thermodynamics, we would like to point out something about the dynamics of the eigenvalues. We can move the Vandermonde determinant into the exponential

$$\mathcal{Z}_\lambda = \int d^N\lambda\, \delta(\mathrm{Tr}(\Sigma_i \lambda_i)) \exp\left(-\frac{\beta}{2}\sum_{i=1}^{N}\lambda_i^2 + 2\sum_{i<j}\log|\lambda_i - \lambda_j|\right) \tag{8.13}$$

The exponential describes a quadratic potential with a logarithmic term. Thus the eigenvalues should always repel each other and do not cross. Although the rogue eigenvalue in Figure 8.2 appears to pass through the others at early times, it actually just transfers energy to the adjacent eigenvalue, like a Newton's cradle. This behavior can be realized in plots like Figure 8.2 with a sufficiently small time step, a large enough sampling rate, and enough zooming. An example of such is shown in Figure 8.3.

To determine if our system has thermalized, the first step is to match our eigenvalue distribution to the distribution predicted by the partition function $\mathcal{Z}_\lambda$. The Vandermonde determinant becomes exponentially complex with increasing

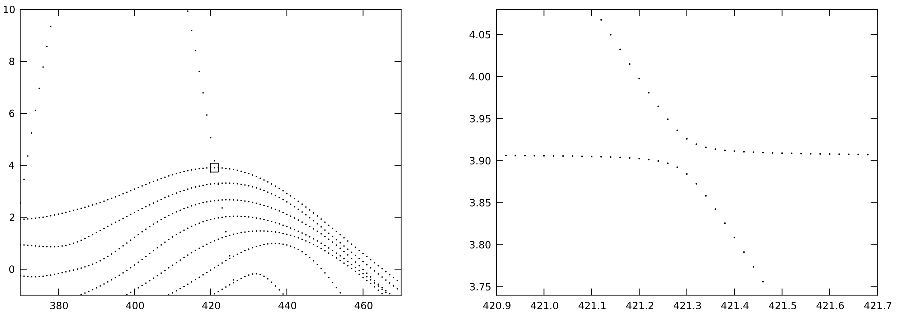

Figure 8.3: In the left figure we have zoomed in on the time interval $[370, 470]$ in Figure 8.2. In the right figure we have blown up the small rectangle in the left figure to observe more closely a crossing between the two largest eigenvalues. The sampling rate was increased 50 fold to obtain the right figure, however the time scales between the two figures have been kept in sync to avoid confusion.

N and so a direct comparison is time expensive. Instead we use the probability distribution obtained by integrating the partition function over all but one eigenvalue, i.e., the eigenvalue probability density or level density function. An explicit form of the level density for the TGUE for arbitrary N has been found in [150] [2]. Figure 8.4 shows that the eigenvalues of the traceless momentum matrices sampled over time after thermalization do indeed fit the predicted function.

In order to make these comparisons, we need to know the temperature β. If we consider the tracelessness of the matrices as a constraint, then we can apply the proof in Appendix G to a single traceless matrix and obtain

$$T = \frac{\langle \mathrm{Tr}(P^2) \rangle_0}{N^2 - 1} \tag{8.14}$$

---

[2] We thank John Mangual for his discussions about random matrices and for his pursuit of a formula for the level density for the TGUE at arbitrary N. This led to a discussion on the website `mathoverflow.net` and the answer of F. Bornemann [151], which ultimately resulted in the formula reported in [150].

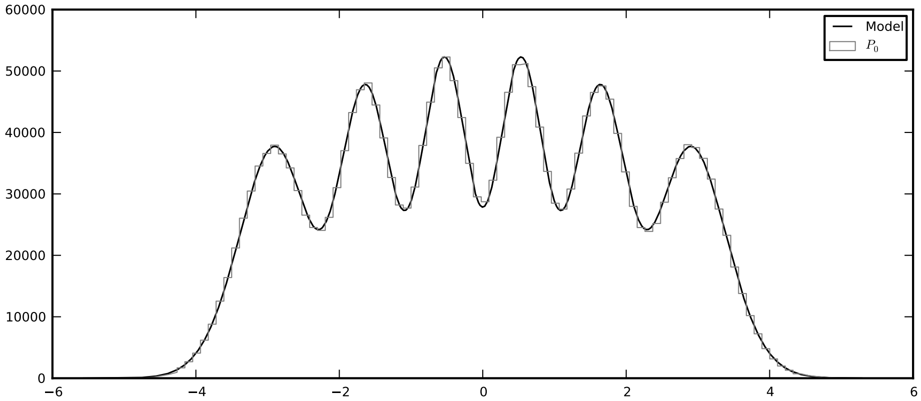

Figure 8.4: A histogram of the eigenvalues of P^0 for a simulation of rank 6 matrices sampled after thermalization. A total of 4×10^5 configurations were sampled meaning we fitted using 2.4×10^6 eigenvalues. By computing the second moment, we can fit the distribution to the level density of the TGUE. The level density has been normalized to the total number of samples times the bin size. The fit has an R^2 value of 0.999904.

where P is any single momentum matrix and the zero subscript indicates we take the expectation value with respect to the TGUE. For numerical measurements, the zero subscript indicates averaging only over the traceless part of the matrices. The momentum contribution to the Hamiltonian is invariant under an $SO(9)$ transformation and one would expect that we could use any momentum matrix and obtain the same temperature. The numerical data of Table 8.1 shows that this is not the case.

What we have forgotten in developing our thermometer are the constraints. If we read directly from the table under our naive assumptions, we would conclude that the system has two different temperatures even though the isotropy exists along the relevant directions in phase space. It would seem that either the system is not thermal or the thermometers are broken. To solve this puzzle, we note that

N	$\langle \mathrm{Tr}(P_0^2)\rangle_0$	$\langle \mathrm{Tr}(P_1^2)\rangle_0$	$\langle \mathrm{Tr}(P_2^2)\rangle_0$
4	23.2 ± 0.6	23.3 ± 0.4	23.2 ± 0.5
11	26.9 ± 0.3	27.2 ± 0.2	27.0 ± 0.3
23	32.2 ± 0.3	32.2 ± 0.2	32.1 ± 0.2

N	$\langle \mathrm{Tr}(Q_1^2)\rangle_0$	$\langle \mathrm{Tr}(Q_2^2)\rangle_0$	$\langle \mathrm{Tr}(Q_3^2)\rangle_0$	$\langle \mathrm{Tr}(Q_4^2)\rangle_0$	$\langle \mathrm{Tr}(Q_5^2)\rangle_0$	$\langle \mathrm{Tr}(Q_6^2)\rangle_0$
4	21.3 ± 0.5	21.3 ± 0.5	21.2 ± 0.6	21.2 ± 0.4	21.3 ± 0.4	21.0 ± 0.4
11	26.6 ± 0.2	26.5 ± 0.3	26.6 ± 0.2	26.6 ± 0.3	26.6 ± 0.2	26.5 ± 0.2
23	31.9 ± 0.2	31.9 ± 0.2	31.9 ± 0.2	31.9 ± 0.2	31.9 ± 0.2	32.0 ± 0.2

Table 8.1: Time average samples of the trace of the square of the traceless momenta for various N with $v = 20.0$, $\hbar = 0.001$, and $\delta t = 0.001$. For each expectation value, 20 samples were used but the number of configurations varies with N due to limited hard disk space. The differences between the values in the disjoint groups of $\langle \mathrm{Tr}(P_i^2)\rangle_0$ and $\langle \mathrm{Tr}(Q_a^2)\rangle_0$ are smaller compared to the differences of the values in the union of these two groups indicating the breaking of the $SO(9)$ symmetry between the momenta that is present the Hamiltonian.

the naive Gibbs ensemble is over all P, Q matrices, but the full ensemble should be over P, Q, X, Y matrices. There is a constraint associated to the $U(N)$ gauge symmetry. Additionally there are $3 + 15 = 18$ angular momentum constraints associated to the $SO(3) \times SO(6)$ symmetry of the model. In particular, the $SO(9)$ symmetry is broken by the X and Y matrices in the potential. When we integrate out the X and Y fields, the momenta will have different weights in the gauge constraint because of this broken symmetry. Consequently, the distributions for the individual momentum matrices will be different for in the $SO(3)$ and $SO(6)$ parts of the model and explains the discrepancy in Table 8.1.

Putting everything together, our true Gibbs distribution is the GUE for nine matrices with the constraint of tracelessness, the gauge constraint, and the total amount of angular momentum set to zero. Each of these constraints is linear in the momenta. We may thus apply the result in Appendix G, which is just a generalized equipartition theorem, to obtain an absolute normalization of the temperature.

$$\begin{aligned}\sum_{i=0}^{2}\langle \mathrm{Tr}(P_i^2)\rangle_0 + \sum_{a=1}^{6}\langle \mathrm{Tr}(Q_a^2)\rangle_0 &= \left(9(N^2-1)-(N^2-1)-\frac{3\cdot 2}{2}-\frac{6\cdot 5}{2}\right)T \\ &= (8N^2-26)T \qquad (8.15)\end{aligned}$$

The lowest rank matrix which can exhibit thermalization behavior nontrivially is $N = 2$ and so we do not run into an issue of negative temperature. Otherwise this would indicate we have not taken into account relations between the constraints.

We would also like to ensure that temperature measurements are independent of the time step parameters in our numerical implementation, that is, δt. The BMN matrix model exhibits chaos. Shrinking the time step does not cause the numerical solution to converge to a solution of the equations of motion as small differences grow exponentially for large times. We still expect that each of the trajectories computed this way would lead to the same ensemble since we should be sampling the phase space according to the dynamically invariant measure, in a manner typical of numerical simulations of chaotic dynamical systems.

In order to measure the temperature we need to measure $\langle \mathrm{Tr}(P^2)\rangle_0$ for all momenta matrices. We can determine the accuracy of our measurements by dividing the configurations into groups to obtain several sample measurements of $\langle \mathrm{Tr}(P^2)\rangle_0$. The expectation value is independent of the grouping of configurations due to its linearity, but now we can obtain a standard deviation. Consecutive configurations are correlated, so some care must be taken when grouping configurations to make a sample. To minimize correlations between samples, we group configurations consecutively. Each sample will be correlated with itself, but different samples

	N		
δt	4	14	23
0. 005	1.932 ± 0.014	0.16235 ± 0.00050	0.06845 ± 0.00018
0. 003125	1.932 ± 0.014	0.16234 ± 0.00043	0.06844 ± 0.00017
0. 0025	1.932 ± 0.014	0.16235 ± 0.00047	0.06843 ± 0.00016
0. 002	1.932 ± 0.016	0.16234 ± 0.00048	0.06843 ± 0.00018
0. 00125	1.932 ± 0.013	0.16234 ± 0.00050	0.06843 ± 0.00016
0. 001	1.932 ± 0.014	0.16234 ± 0.00048	0.06843 ± 0.00016
0. 000625	1.932 ± 0.015	0.16234 ± 0.00053	0.06843 ± 0.00016
0. 0005	1.932 ± 0.017	0.16234 ± 0.00051	0.06843 ± 0.00017
0. 0004	1.932 ± 0.015	0.16234 ± 0.00051	0.06843 ± 0.00015

Table 8.2: Measured temperatures of thermalized system for rank 4, 14, and 23 matrices for several δt using the same initial conditions for each N. The sampling rate is chosen such that the time separation between recorded configurations is kept constant, in particular (sampling rate) $\times$ (δt) $= 0.05$. A total of 20 samples were used for each measurement, however, the number of configurations per sample was decreased with increasing N.

will only be correlated at their boundaries. This sampling process provides a way to measure $\langle \mathrm{Tr}(P^2) \rangle_0$ with some degree of accuracy. The temperature is computed using equation (8.15) and the standard deviation is computed by summing the standard deviations of the $\langle \mathrm{Tr}(P^2) \rangle_0$ in quadrature.

Table 8.2 lists the temperatures of simulations for various N and various δt with the same initial conditions for each N. The temperatures are equal to several significant figures and the error bars intersect a common average value. Furthermore we find that the coefficients of variation are less than 1%. To claim our comparison among different δt is reasonable, the sampling rate is chosen such that the time between recorded configurations is constant. We conclude that the temperature is a well defined quantity regardless of how far apart trajectories in phase space become due to changing the time step.

Some simple observables that are also natural thermodynamic variables are the sizes of the distributions of X and Y matrix eigenvalues. We can determine how they scale with the temperature and N using the virial theorem. For our case, a virial can be computed for each X and Y matrix. Consider, for simplicity, the expression

$$\frac{d}{dt}\mathrm{Tr}(X^i P_i) = \mathrm{Tr}(P_i^2) + \mathrm{Tr}(X^i \dot{P}_i) = \mathrm{Tr}(P_i^2) - \mathrm{Tr}(X^i \partial_{X^i} V) \tag{8.16}$$

where we are only using the traceless parts of the matrices (we subtract the trace modes, which are decoupled) and we don't sum over i. We then integrate over a period of time τ and average to obtain

$$\frac{1}{\tau}(\mathrm{Tr}(X^i P_i)(\tau) - \mathrm{Tr}(X^i P_i)(0)) = \left\langle \mathrm{Tr}(P_i^2) - \mathrm{Tr}(X^i \partial_{X^i} V)\right\rangle_\tau \tag{8.17}$$

If the trajectories are bounded then the left hand side asymptotes to zero as $\tau \to \infty$ and we obtain a relation between the kinetic energy and various derivatives of the potential energy. This is simplest in the BFSS matrix model. We find after summing over the X_i that

$$\sum_i \mathrm{Tr}(P_i^2) + \sum_{ij} \mathrm{Tr}([X^i, X^j][X^i, X^j]) = 0 \tag{8.18}$$

This is, we find that the kinetic energy is twice the potential energy $2E_{\mathrm{kin}} = 4E_{\mathrm{pot}}$. We have already argued that the left hand side grows like $(8N^2 - 26)T$, so we find

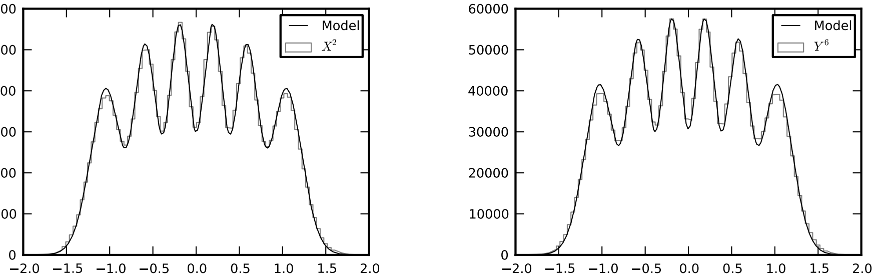

Figure 8.5: A histogram of the eigenvalues of X^2 and Y^6 for a simulation of rank 6 matrices sampled after thermalization. A total of 4×10^5 configurations were sampled meaning we fitted using 2.4×10^6 eigenvalues. Each fit has an R^2 value of 0.99925 and 0.9988 respectively.

that the right hand side takes the same value. The total energy in that case is

$$E_{tot} = \frac{3}{4}(8N^2 - 26)T \tag{8.19}$$

At large N, we get that the energy as a function of the temperature is $\frac{3}{4}(8N^2)T$. The specific heat is essentially the same as that of $6N^2$ harmonic oscillators and is constant. Notice that this result also matches the Monte-Carlo lattice simulations in the matrix model, as seen in Figure 3 of [152]. Other such simulations [153] do not cover the high temperature regime.

Another means of getting at the size of the X and Y matrices is to look at the distribution of the eigenvalues. The elements of any single coordinate matrix appear at most quadratically in the Hamiltonian. Integrating the Gibbs distribution $\exp(-\beta H)$ over all momenta and all but one coordinate matrix will be a Gaussian distribution in the remaining coordinate matrix elements. The standard deviation will be modified due to the constraints, but the form of the integrand will remain unchanged. The only constraint left over is the tracelessness

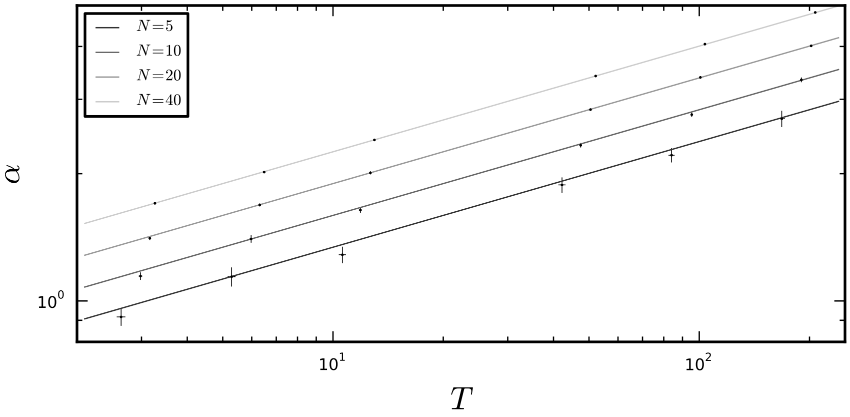

Figure 8.6: A plot of the size of X^0, measured as $\alpha = \sqrt{\langle \mathrm{Tr}(X^2)\rangle/N}$, as a function of temperature for various N. The error bars for larger N are smaller than the point size and thus may not be visible in the plot. The lines are given by $\alpha = cN^{1/4}T^{1/4}$ for constant N. Doing a least squares fit gives the constant $c = 0.504$. Plots for the other coordinate matrices give identical results.

of the matrices. Thus we expect that the eigenvalues follow the level density of the TGUE. Observing Figure 8.5 this is exactly what we see.

We can also estimate the commutator squared term if we assume that the X and Y matrices are random. If the eigenvalues of X are of order α (we call this the size of the matrix), then the eigenvalues of $[X^i, X^j][X^i, X^j]$ grow like α^4, and we get that $N\alpha^4 \simeq N^2T$. Thus the size of the matrices grows like $\alpha \simeq N^{1/4}T^{1/4}$. This is also true for the BMN matrix model at high temperature. In that case, the cubic and quadratic terms in the potential are subleading when the size of the matrices gets large and one asymptotically matches the BFSS matrix model. A test of our prediction is shown in Figure 8.6 with remarkable agreement. Our claims hold for large N and so we see larger deviations for smaller N.

8.4 Power Spectra and Classical Chaos

As we have seen, there is evidence for thermalization in the BMN matrix model. Similar considerations show that the BFSS matrix model thermalizes (this has been studied for different initial conditions in [154]). This should not be surprising. Both the BFSS and BMN matrix models result from dimensional reduction of $\mathcal{N} = 4$ SYM to constant configurations on either flat space or the sphere, respectively. The dynamics of translation invariant configurations of Yang-Mills theories generally exhibit chaos [155, 156] and therefore the BFSS matrix model exhibits chaos (this was reiterated in [157]). Because of classical scale invariance of the Yang-Mills action, chaotic behavior extends all the way to infinitesimal configurations of the fields. Chaos is also present if a mass term is added [158], but to access the chaotic region requires finite field configurations. The BMN matrix model is effectively a massive version of the BFSS matrix model, so it should also exhibit chaos for field configurations where the fields are sufficiently large, but can display integrable behavior for small oscillations around vacuum states.

In this section we analyze chaos in both the BFSS and BMN matrix models and show how we can use this information to study holography. For this purpose, let us pretend that a configuration in our classical system represents a thermal equilibrium state in a quantum system. Then we would be interested in various response functions and correlation functions of observables in order to understand the dynamics of the thermal state.

A typical gauge invariant observable would be a trace. The simplest traces are those of the matrices X^i and P_i. However, we do not gain much from studying these as they decouple and either work as a harmonic oscillator (this is the center of mass motion in the BMN matrix model), or they give free non-relativistic motion on flat space (this is the center of mass motion in the BFSS matrix model). Instead, we should look at traces of composite objects. Remember that we are studying configurations with zero angular momentum. This means we are looking for spherically symmetric configurations in ten dimensions (nine spatial plus the lightcone time). In the BMN model, these configurations are only approximately spherically symmetric. Perturbations of these configurations may be characterized by their angular momenta. The matrices X^i form a $\mathbf{9}$ of $SO(9)$ in the BFSS matrix model, so it is convenient to study configurations that are highest weight states of $SO(9)$ multiplets.. In BMN the appropriate group is $SO(3) \times SO(6)$, which is only slightly more complicated to analyze. Spherical symmetry then predicts that the one point correlation functions of $SO(9)$ non-singlets in a thermal state would be zero, but two point functions could be non-zero if there is a singlet in the tensor product of the two $SO(9)$ representations.

Consider the $SO(9)$ highest weight state $Z = X^1 + iX^2$ and operators of the form $\mathcal{O}_L = \mathrm{Tr}(Z^L)$. These operators will be highest weight states of symmetric traceless combinations of the X with angular momentum L. In the context of $\mathcal{N} = 4$ SYM, modes constructed from scalars at zero temperature are protected states [43] and are dual to gravitational excitations in AdS space. At zero temperature these states already display incompressible and dissipation free hydrodynamic behavior, in the form of a quantum hall droplet [74]. Collective excited states can be put in one to one correspondence with gravity states [77] and the shape of the gravity configuration is directly determined by the expectation values of these traces. We expect that these simplest traces are also closely related to gravity modes of a black hole in the dual of $\mathcal{N} = 4$ SYM at finite temperature. We are further lead to believe that these dynamical variables are also related to gravity modes in both the BFSS and BMN matrix models at finite temperature. For example, they could describe how gravitational or dilaton partial waves (see, e.g., [159, 160]) are absorbed or emitted from such systems. Regardless, these variables are important for understanding these configurations in detail and could help us to ultimately learn about emergent black hole phenomena like Hawking radiation, or whatever corresponds to it in the regime we are studying.

Consider the conjugate operators are $\bar{\mathcal{O}}_L = \mathrm{Tr}(\bar{Z}^L)$ and the two point function

$$\left\langle \mathcal{O}_L(t)\bar{\mathcal{O}}_L(t')\right\rangle = S_L(t-t') \tag{8.20}$$

The dependence on the time difference $t - t'$ is due to the time translation invariance of the thermal density and the Hamiltonian. One can also study the Fourier transform of this correlator $\tilde{S}_L(\omega) = \int S_L(a)\exp(-i\omega a)\,da$, which is how frequency dependent transport coefficients are usually defined. Closely related quantities can be calculated in gravitational setups by using the holographic dictionary in a perturbed black hole geometry with infalling boundary conditions at the horizon. This ultimately yields a relation between the quasinormal modes of asymptotically AdS black holes and CFT response functions (see [161, 162, 163] for reviews). To compute these quantities in the classical dynamics we note that in quantum chaotic regimes we expect $S_L(t-t')$ to be roughly independent of the microstate we choose, even if it is a pure state, so long as it is a typical state of the thermal system [3]. Indeed, we expect most correlation functions of energy eigenstates $|E_i\rangle$ to be approximately thermal

---

[3] This expectation is an extension of the idea that all energy eigenstate behave as if they

$$\big\langle E_i \big| \mathcal{O}_L(t)\bar{\mathcal{O}}_L(t') \big| E_i \big\rangle \simeq S_L(t-t') \tag{8.21}$$

with the dependence on the difference $t-t'$ guaranteed by time translation invariance of the matrix elements of the energy eigenstates. Here thermalization means that S_L decays to zero (usually exponentially) with some thermalization time τ, and that the left hand side approximates the right hand side on time scales that are short compared to Poincaré recurrence times.

We extend this to more typical states, which are superpositions of energy eigenstates around some energy value, by averaging over t keeping $t-t'$ fixed. We then expect

$$\big\langle \big\langle \psi \big| \mathcal{O}_L(t)\bar{\mathcal{O}}_L(t+a) \big| \psi \big\rangle \big\rangle_t \simeq S_L(a) \tag{8.22}$$

where $|\psi\rangle$ is some typical state and we average over time. The quantum theory should match the classical theory for these correlation functions in the correspondence limit. That is, at very large quantum numbers the answer in the classical and quantum theory should be very similar so long as the time scales involved are relatively small compared to the Poincaré recurrence time. For our large N matrix models, all time scales considered are much smaller than the recurrence time.

We compute the left hand side of (8.22) by using a typical state of the microcanonical ensemble and averaging over its trajectory. We obtain these from our simulations by first waiting until the system thermalizes then averaging over

---

are thermal states for time independent questions [143]. Some evidence of this behavior can be found in examples [164].

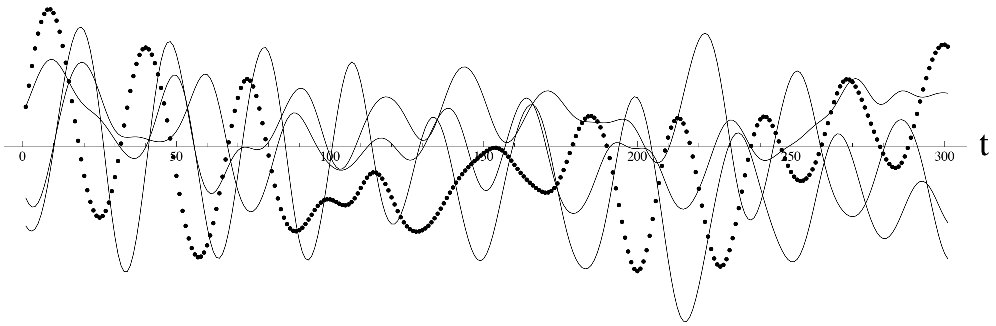

Figure 8.7: Time series of the function $\mathrm{Re}(\mathrm{Tr}(Z^2(t)))$. We show four different time series obtained by rotations of the Z by $SO(9)$ action. They all look similar, showing approximate rotation invariance of the time average. We showcase the discrete data we have in one of them, so show that the time dependent features are well covered by our time slicing. The sample shown here is for 18×18 matrices.

various configurations. The functions $S_L(a)$ are the autocorrelation functions of the system. Let us first consider the time series of $\mathcal{O}_L(t)$ for some L after thermalization. We display this in Figure 8.7. From the figure we see oscillations of a typical frequency, but they are not regular nor centered on zero. Rather, they appear to be superposed on waves of a much longer period than the time period shown.

To extract information from the time series, we compute $\tilde{S}_L(\omega)$ by taking the Fourier transform of $\mathcal{O}_L(t)$ and averaging over many configurations. In our case, rotation invariance tells us that we did nothing special by choosing $(X^1 + iX^2)$ as our highest weight state. Since all tensor representations of $SO(n)$ are real, $(X^1 - iX^2)$ can be obtained from a rotation of $(X^1 + iX^2)$. This means that the right hand side of (8.22) only depends on the absolute value of a and therefore the power spectrum $P(\omega) = \tilde{S}(|\omega|)$ is an even real function of ω. Thus we only have to display the answer for $\omega \geq 0$. We show power spectra for $L = 2$, 3, 4 in

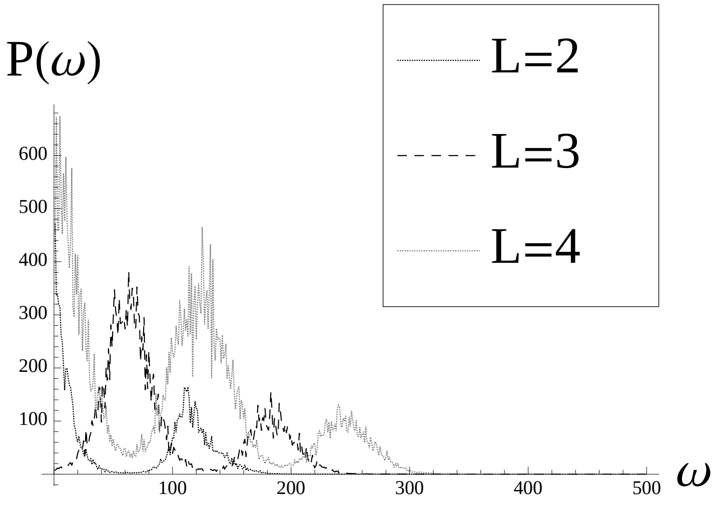

Figure 8.8: The power spectrum of $S(a) = \langle \mathrm{Tr}(X^1{+}iX^2)^L(t)\mathrm{Tr}(X^1{-}iX^2)^L(t{+}a)\rangle$ for various L in random units. Results shown are for 13×13 matrices in the BFSS matrix model after thermalization. The results are averaged over 15 runs of the same length, taken from splitting a single time series in 15 equal parts. The jiggling of the data should be interpreted as an estimate of the statistical error bars for each frequency.

Figure 8.8.

The first observation we make from these plots is that the power spectra are those of a chaotic system. If a system is integrable, we expect it to be solvable in terms of action-angle variables. The angle variables are multivalued, with period 2π or 1 depending on conventions, but possess the simple time dependence $\phi_\alpha(t) = \phi_\alpha(0) + \omega_\alpha t$. Any single valued function on phase space can then be represented by its Fourier series in the angle variables. Its time dependence is that of a quasi-periodic function of time with characteristic frequencies determined by all integer linear combinations of the ω_α. Thus, the power spectrum of a time series in an integrable system should display delta-function peaks at the characteristic frequencies of the system. The series we observe is better described by broad band noise than delta-functions peaks. This is one of the standard criteria to distinguish chaotic from non-chaotic systems [165].

Let us return to Figure 8.7 to make more sense of it. For $L = 2$ there seem to be two peaks, one near zero and another one at a characteristic frequency ω_0. We may then describe the signal approximately as oscillating with some characteristic frequency while riding on a very low frequency envelope. There is information present in the other modes as well. For $L = 4$ we observe broader peaks located in roughly the same places as well as a frequency doubling of the ω_0 peak. For $L = 3$ we observe peaks at 'half period' spacings relative to $L = 2$. The reader may have concern that in Figure 8.7 we used 18×18 matrices, whereas in Figure 8.8 we studied 13×13 matrices. The natural way to understand this is to look at how the power spectrum depends on N, the size of the matrices. This is shown in Figure 8.9.

We see from Figure 8.9 that the power spectrum of all $L = 2$ modes for various values of N are actually very similar to each other. Each has a large peak at zero, which is more noticeable in a log-linear plot. We also see a second peak at some characteristic frequency which depends on the energy of the system and N. We compare various values of N by finding the location of the peak and rescaling the power to make the plots lie on top of each other. To find the location of the peak we do a fit of the $\log(P(\omega))$ to a quadratic function of ω in a small interval around the visual maximum. We then extract the value of ω that corresponds to the maximum and we scale each axis of frequency to the corresponding ω_N found for each N. The main systematic error comes from the choice of the interval. The result is shown in Figure 8.10. The data have collapsed to a single graph.

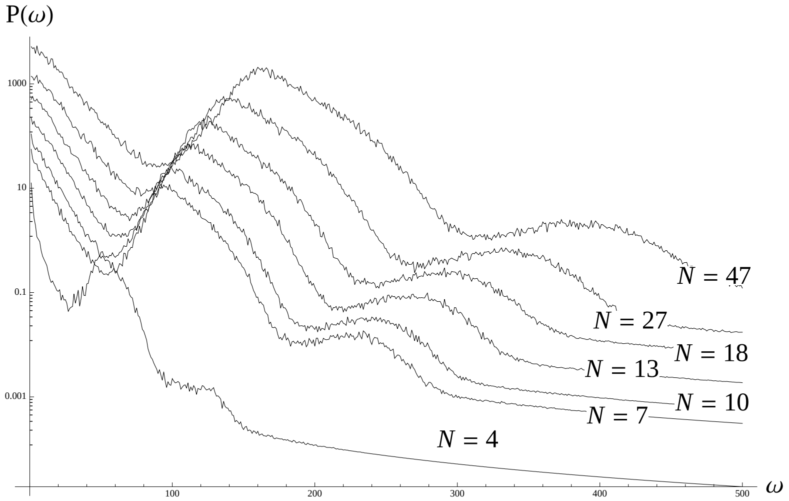

Figure 8.9: The power spectrum of $\mathrm{Tr}((X^1+iX^2)^2)(t)$ for various sizes of $N\times N$ matrices in arbitrary units (its Fourier transform is $S(a)$). Results shown are for the BFSS matrix model after thermalization. The results are averaged over 15 runs of the same length, taken from splitting a single time series in 15 equal parts. We also average further over 8 rotations of the variables to increase the statistics. The jiggling in the curves gives a measure of the statistical error bars of the data sets.

As shown suggestively in Figure 8.10, the logarithm of the power spectrum seems to have rather distinct features characterized by straight lines. We can numerically compare the different values of N to get an idea of how closely the curves match by considering the width of the peak near zero, relative to ω_N. The dimensionless width can be parametrized by the slope

$$\gamma_N = -\left(\omega_N \frac{d}{d\omega_N} \log(P(\omega)_N)\right)^{-1} \tag{8.23}$$

which is evaluated near zero and with a cutoff slightly below $0.4\omega_N$. Larger γ_N corresponds to a larger width. This is a dimensionless number that can be used to quantify how close the curves at different N are to each other. We show this in

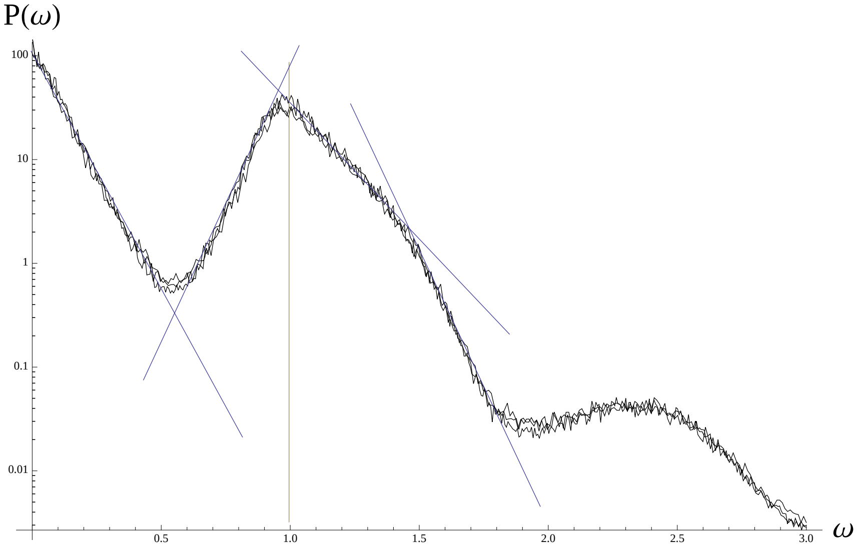

Figure 8.10: The power spectrum of $\mathrm{Tr}(X^1+iX^2)^2(t)$ for various sizes of $N\times N$ matrices. The axis of frequency has been rescaled for each N, to the frequency ω_N, and we have also rescaled the power spectrum. The reference frequency for each N is located at 1 in the graph. Results shown for $N = 7,\ 10,\ 47$. We also have drawn additional suggestive straight lines superposed on the graph that serve as distinctive features of the power spectrum.

Figure 8.11. As seen in the figure, all values of $N > 4$ have similar behavior and differences are controlled by the systematics of the fit, which are dominated by the choice of interval over which we compute the slope. This matching is necessary to have a well defined large N limit for these time dependent correlation functions. We have checked that the graphs are very similar for other simple operators and so they all seem to have a good large N limit.

How should we interpret these results? We would like to conclude that the system is behaving hydrodynamically as described in Section 8.1. There are some large N collective variables whose time dependent characteristics are independent of N, up to some rescalings of the variables by the natural frequency of the dynamics. We checked the simplest angular momentum mode with $L = 2$, but we

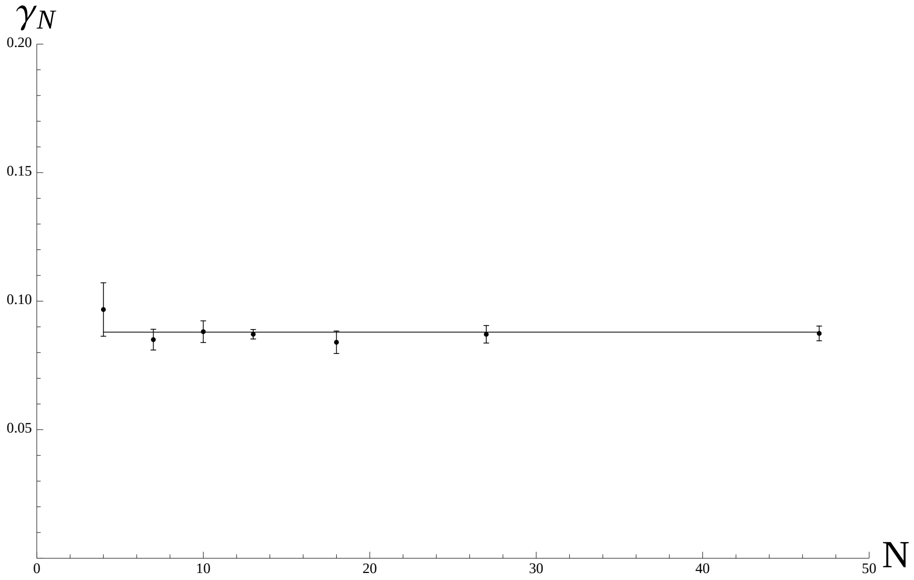

Figure 8.11: The dimensionless quantity γ_N versus N. The error bars indicate systematic errors from choosing the fitting intervals. A fit to a single number has been done ignoring $N = 4$ which is an outlier by inspection. All of the different values of $N > 4$ align within the systematic errors.

can do the analysis for $\mathrm{Tr}(Z^L)$ for various L. The plot of the power spectrum for various L can be seen in Figure 8.12. As the reader can see, the patterns observed for low L in Figure 8.8 persist. Notice that the logarithmic scaling of the power spectrum makes the pattern more regular. To investigate this in more detail we need to address further how the different N are related to each other.

We can also look at what happens when we deform the system from the BFSS matrix model to the BMN matrix model. It is interesting to see how symmetry breaking is implemented in the power spectra. In Figure 8.13, the power spectrum of $\mathrm{Tr}(X^1 + iX^2)^2$ acquires a new bump near where the power spectra of the BFSS matrix model had a local minimum. The bump is less pronounced in the $\mathrm{Tr}(XY)$ channel and seems absent in the $\mathrm{Tr}(Y^1 + iY^2)^2$ channel. There is also

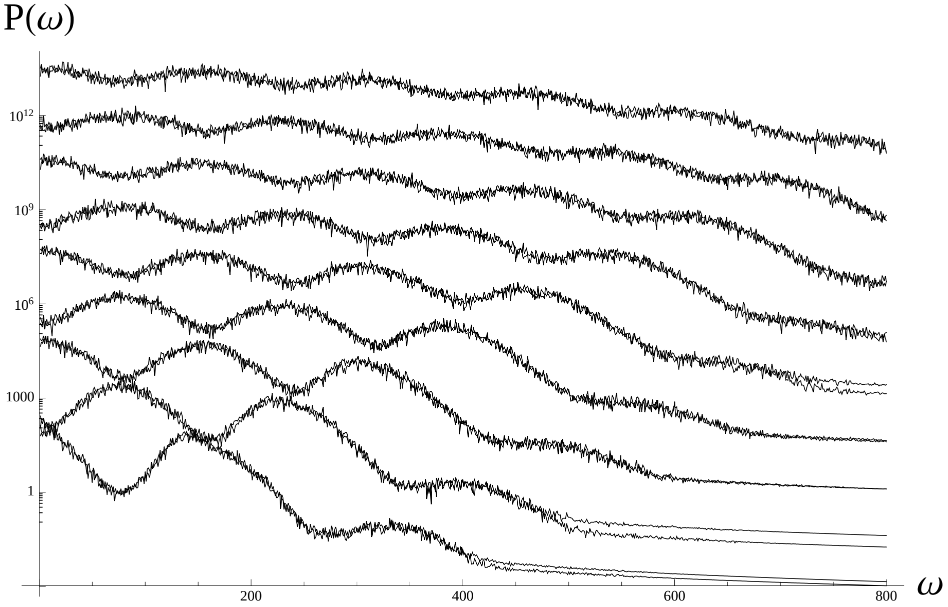

Figure 8.12: Power spectrum in arbitrary units for $\mathcal{O}_L$, with $L = 2, \ldots 10$, with values of L increasing from bottom to top in the graph. The plots are vertically separated so they can be easily distinguished. For each L we show two such sets. These data are from $N = 27$.

a deformation of the $\mathrm{Tr}(XY)$ bump near the second minimum. This shows that three objects that had the same symmetry properties in the BFSS matrix model exhibit the broken symmetry of the BMN matrix model in their dynamics. If we zoom in near the bump at zero, we can also see small differences. The size of these bumps depends on the strength of the mass term in the BMN matrix model. A full analysis of these deformations would consider the mixing between modes in different symmetry classes and provide some understanding of response theory beyond the linear level. We made a finite deformation of the Lagrangian and the response to the deformation can be measured in dynamical quantities, or at least in this case, in power spectra.

Understanding how the bump size depends on N and the effective mass while

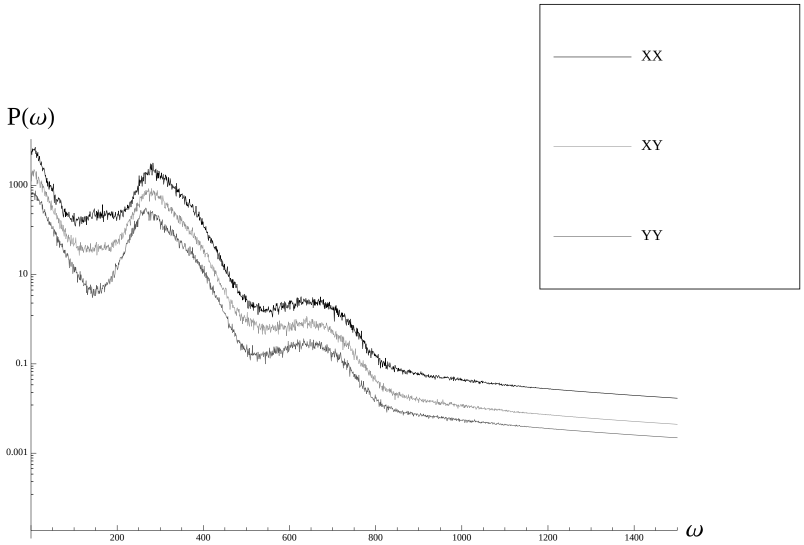

Figure 8.13: Power spectra in arbitrary units for $\mathcal{O}_2$ for various matrix combinations. The plots are artificially separated so they can be easily distinguished. In most of these plots the net normalization of $\mathrm{Tr}(X^2) \simeq \mathrm{Tr}(Y^2)$ is very close to each other, as shown previously. These arise from 40×40 matrices with initial velocity in our initial conditions set to $v = 100$.

keeping the temperature fixed could give us a better understanding of the phase diagram of the BMN matrix model. We would also be able to fine tune the system to obtain an appropriate large N limit. This requires the effects of the mass term and cubic term deformations to be compatible with the large N scaling we obtained in Section 8.3. We can analyze this in terms of their expected contributions to the free energy. The corrections to the free energy from the mass terms should be of order $N\mu^2 N^{1/2} T^{1/2}$, as compared to $N^2 T$. If we want the ratios of these two contributions to the free energy to stay fixed (so that we get a proper large N counting of the free energy), we need to scale $\mu^2 \simeq N^{1/2} T_0^{1/2}$ for some reference temperature T_0. Performing such an analysis is beyond the scope of the present work.

8.5 Factorization

A crucial aspect of large N physics is factorization. This states that correlators have a large N expansion in powers of $1/N$, where the leading power of N arises from planar diagrams [166] and subleading corrections arise from higher genus Feynman diagrams. For the simplest observables, the leading expectation value of a product of observables is the product of the expectation values, so long as these expectation values do not vanish in the first place. Planarity and the idea that large N physics is approximately free with interactions governed by $1/N$ corrections is an integral part of gravitational holography [13] (see [167] for a nice description of this physics).

The classical dynamics we have factorizes in a trivial sense. The value of a product of any set of observables at time t is the product of the values. What we would like to check is that expectation values averaged over time have this property as well. That is, the simple degrees of freedom can be converted into approximately 'free' constituents. The thermal fluctuations in observables are independent of each other for the factorized degrees of freedom. Because the degrees of freedom are approximately free, the fluctuations should be Gaussian. In the quantum theory near the vacuum, there is a standard way to understand that this leads to a consistent large N classical dynamics [168]. Here we want to check that there are also classical thermodynamic (or more precisely hydrodynamic) variables on which one can do a similar type of analysis.

Imagine that the simulations we are doing with time evolution in the BFSS or

BMN matrix model can be reinterpreted as a matrix model calculation

$$\langle \mathcal{O}(t)\rangle_t \simeq \frac{\int \mathcal{O}(X)\exp(-\beta V(X))_{\mathrm{MM}}}{\int \exp(-\beta V(X))_{\mathrm{MM}}} \tag{8.24}$$

where MM denotes an integration measure with respect to some matrix model. If the right hand side factorizes, then so does the left hand side. The algorithm we are following would compute the right hand side using a hydrodynamic Monte Carlo code. As long as the trajectories in the system we have mix sufficiently well, equation (8.24) should hold for large times t.

Interestingly, the right hand side of equation (8.24) in the BFSS matrix model has no terms quadratic in the X variables. Hence the usual arguments based on planar diagrams do not hold. In the BMN matrix model at large β the quadratic terms matter very little and it is instead the quartic term that dominates. Moreover, the BFSS potential has flat directions. Both of these observations combined could conceivably produce anomalous powers of N in the final answer, so it is worth checking that factorization holds.

We proceed in two steps. First, we will check some consequences of factorization at some large value of N. For example, consider the matrix model correlators (as in equation (8.24)) of the following form

$$\langle \mathcal{O}_L^n \bar{\mathcal{O}}_L^m \rangle = A_{m,n}^L \tag{8.25}$$

where $Z = X^1 + iX^2$ (or any of its rotations), $\mathcal{O}_L = \mathrm{Tr}(Z^L)$, and $\bar{\mathcal{O}}_L = \mathrm{Tr}(\bar{Z}^L)$. Rotational invariance of the ensemble implies that $A_{m,n} = A_m \delta_{m,n}$. Our goal is to understand the A_m^L at large N. Notice that $\langle \mathcal{O}_L \rangle = 0$, so this is exactly one of the cases where the naive large N factorization does not apply. Instead, we can consider A_1^L as our first non-trivial value, and use it to normalize the answers. Because the potential in the BFSS matrix model is a scaling function, the ratios A_m^L/A_1^L should be independent of the effective coupling constant β. Arguing analogously to [60], we can think of $\mathrm{Tr}(Z^L)$ as a raising operator for a composite field (an *in* single string state), and $\mathrm{Tr}(\bar{Z}^L)$ as the corresponding lowering operator (an *out* single string state). The effective propagator for raising and lowering would be just A_1. This is the naive argumentation if planar diagrams were applicable. Then we would find that

$$A_m = m!(A_1)^m \tag{8.26}$$

from all the free contractions between raising and lowering operators. This would be the leading diagram for closed string propagation without interactions, and furthermore, other diagrams with interactions would be suppressed by $1/N^2$. Thus the statistical distribution of $\mathrm{Tr}(Z^L)$ would be that of a random Gaussian variable. A simple check is to bin the results of sampling the real part of $\mathrm{Tr}(Z^L)$, divide by its normalization (which in this case is $A_1^L/\sqrt{2}$), and compare it to a Gaussian model for the distribution normalized to the number of samples. This is independent of L. We can see the results of this procedure in Figure 8.14. The results of the test are that the different $\mathcal{O}_L$ have Gaussian statistics and we conlcude that the correlators do factorize in this sense. We did this for $N = 87$, but the results are very similar for other values of N.

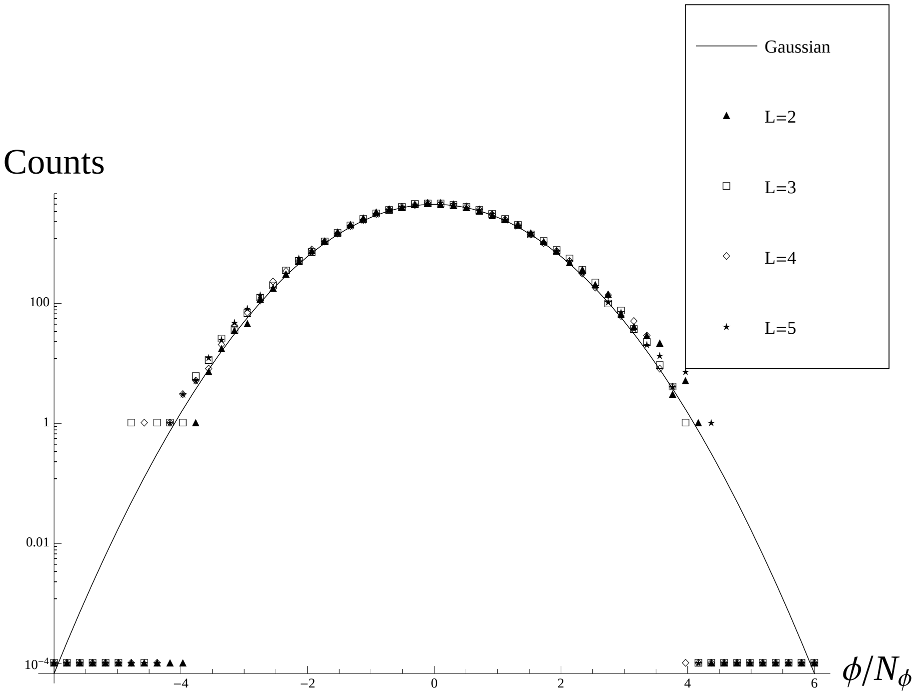

Figure 8.14: Test of factorization for $N = 87$. We bin the samples of $\mathrm{Re}(\mathcal{O}_L(t))$ for various L obtained from the time series after thermalization. We compare to a Gaussian model of the data. Using logarithmic scaling in the counts permits us to check the tails of the distribution. We put measured counts of zero at 10^{-4}.

We also consider correlators such as

$$\frac{\langle \mathcal{O}_L \mathcal{O}_M \bar{\mathcal{O}}_{L+M} \rangle}{\sqrt{A_1^L A_1^M A_1^{L+M}}} \sim \frac{C_{L,M,L+M}}{N} + O(1/N^3) \tag{8.27}$$

which should give rise to the structure constants $C_{L,M,L+M}$ that have a well defined large N limit. If we ignore the $1/N^3$ corrections, then the $C_{L,M,L+M}$ should be independent of N up to statistical uncertainties. Since $\bar{Z}$ can be obtained by an $SO(9)$ rotation of Z, the above correlators are real.

Note that this correlator decays only $1/N$ and not as $1/N^2$. This is important

	$N=10$	$N=13$	$N=18$	$N=87$
$C_{2,2,4}$	4.97 ± 0.51	4.54 ± 0.15	4.94 ± 0.8	4.97 ± 1.2
$C_{3,3,6}$	6.97 ± 0.86	6.9 ± 0.4	7.58 ± 0.5	8.36 ± 1.4

Table 8.3: Values of $C_{L,M,L+M}$ at various values of N

for understanding the large error bars of the measurement [4]. The value of an instantaneous measurement on the left is of order one while the expectation value is of order $1/N$. Thus the various measurements must cancel each other most of the time, leaving a small residual. A non-zero average could be also called a "violation of Gaussianity" if we think of the $\mathcal{O}_L$ as statistically independent variables. A simple test for two possible $C_{L,M,L+M}$ is shown in Table 8.3, where we can see that the $C_{L,M,L+M}$ are indeed N independent given the error bars. This gives us confidence that the standard large N counting is applicable.

We can generalize equation (8.27) to include time dependence and check that

$$\frac{\langle \mathcal{O}_L(t)\mathcal{O}_M(t)\bar{\mathcal{O}}_{L+M}(t+a)\rangle_t}{\sqrt{A_1^L A_1^M A_1^{L+M}}} \sim \frac{C_{L,M,L+M}(a)}{N} + O(1/N^3) \tag{8.28}$$

where now the $C_{L,M,L+M}(a)$ indicate nonlinear correlations with time dependence. If the matrix model and gravity are to be matched, these powers of N should be robust. We expect that the right hand side will decay with time a, as correlations typically do in chaotic systems. A plot of the correlation function $C_{2,2,4}(a)N^{-1}$ can be seen in Figure 8.15, where it decays as expected. The statistical error band that one should associate to the graph is similar in size to the error bars seen in Table 8.3.

---

[4] Similar issues appeared in [169], where an object similar to $C_{L,M,L+M}$ had a theory prediction that was being tested against a model.

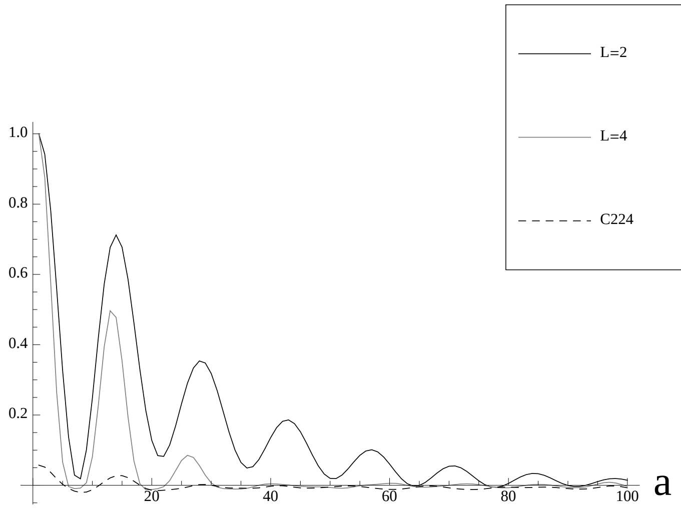

Figure 8.15: Correlation function $C_{2,2,4}(a)/N$ compared to the normalized autocorrelations $A_1^{2,4}(a) = \langle \mathrm{Tr}(Z^{2,4}(t))\mathrm{Tr}(\bar{Z}^{2,4}(t+a))\rangle_t$. The normalization is $A_1^{2,4} = A_1^{2,4}(0)$ for $L = 2, 4$ respectively. The statistical error band on $C_{2,2,4}$ should be roughly at 25% of the maximum around the value at zero. The graph shows data from a run at $N = 87$.

Note how the correlation between the different variables $\mathcal{O}_L(t)$ peaks when the autocorrelation of the variables also peaks and that the correlations between different variables roughly decay as the autocorrelation function decays. This is consistent with naive expectations. The purpose of this check is to show that large N counting is also applicable to general dynamical questions. If the initial non-Gaussianity is of order $1/N$ and it bounds the time dependent non-Gaussianity, then these can not be larger than $1/N$.

8.6 Discussion

There are strong indications that the BFSS and BMN are chaotic and thermalize given the appropriate intial conditions. Most prominently, the momentum and position matrix variables behave as random matrices from the traceless Gaussian unitary ensemble at late times. This is expected for the momentum matrices because the Hamiltonian is quadratic in the relevant degrees of freedom, but because of the nonlinearities in the potential we would not immediately guess this for the position matrices. We showed how the presence of constraints alters the naive arguments about the appropriate random matrix ensembles for these systems.

We have also seen that certain observables behave hydrodynamically, i.e., their power spectra at equilibrium are approximately independent of the total number of degrees of freedom and they have approximately Gaussian statistics. Large N counting applies to time correlation functions between observables, so that violations of Gaussianity scale like $1/N$, i.e., there is factorization of these degrees of freedom. This $1/N$ scaling is associated with quantum corrections under the usual AdS/CFT power counting arguments.

This was not guaranteed. Hydrodynamics usually requires a geometric coarse graining of degrees of freedom confined to small regions. Holographic systems are usually made of D-branes. The holographic degrees of freedom are the strings stretching between the branes, which are extended objects that generally do not localize to small volumes. In the case of AdS bulk geometries, even small regions on the AdS boundary have infinitely large volumes in AdS, so this issue does not apply directly. One does hydrodynamics on the boundary of AdS and not in the bulk, as in [110]. In the case of the BMN matrix model, the conformal boundary of the dual plane wave geometry has no spatial extent [170, 171] and so one cannot have transport there. Hence, hydrodynamic behavior was not an obvious possibility in this case. However, the membrane paradigm for black holes suggests that there should be transport phenomena for the degrees of freedom in the near horizon limit of our thermal matrix configurations.

We seek to further investigate the dissipation and other transport properties. For example, the time autocorrelation functions of various observables, such as those displayed in Figure 8.15, can be integrated to compute the associated transport coefficients, via the Green-Kubo relations. We could investigate how these depend on the temperature, N, or other variables, and see whether the behavior can be interpreted holographically and meets our expectations from gravity. We note that these transport phenomena are related to the chaotic dynamics of the system, characterized by quantities such as the Lyapunov exponents, Pollicot-Ruelle resonances, and Kolmogorov-Sinai entropy (see, e.g., [172] for a review). These quantities also control the far from equilibrium dynamics. In that vein, we may be able to profitably study other non-equilibrium phenomena by applying further techniques and results from non-equilibrium statistical mechanics.

Chapter 9

Black Holes From Matrix Models

Simulations have been carried out in matrix models to understand various aspects of the dynamics of black holes in holographic setups. The main idea so far has been to compare the numerical simulations in the BFSS matrix model with black holes as described in [137]. The numerical approach was initiated in the works [173, 174] and a lot of the thermodynamic static properties of the black holes have been matched in the quantum mechanics. The most impressive such agreement is in [153]. The BFSS matrix model has an infinite moduli space of vacua, so the thermal ensemble of these models is not well defined and contributes systematic errors to these calculations. The BMN matrix model has a well defined ensemble that avoids these complications. Numerical simulations using lattice techniques were carried out in [175].

We additionally have the numerical simulations of the BMN matrix model of Chapter 8 which themselves were a continuation of the work [148]. In this Chapter we explore the holographic interpretation of the thermalized classical dynamics of Chapter 8 using gravitational arguments and some of the techniques developed in Chapter 7.

9.1 Gravity From Matrix Models

Let us begin with the D-brane background geometries in the absence of excitations. They are characterized by the supergravity solutions found in [176]. In the string frame, the ten dimensional metric is given by

$$ds^2 = H^{-1/2}(r)(dx_{\|}^2) + H^{1/2}(r)(dr^2 + r^2 d\Omega_{8-p}^2) \tag{9.1}$$

where $dx_{\|}$ are the $p+1$ coordinates that run along the worldvolume of the p-brane, r is a radial direction, and Ω_{8-p} is an $8-p$ dimensional sphere The harmonic form H is given by

$$H(r) = 1 + \frac{Na}{r^{7-p}} \tag{9.2}$$

where a is a constant that depends on p, but not on N or r.

We start with a few comments on string theory in this geometry. For $p \leq 3$ these metrics produce a long throat near $r = 0$, in that $\lim_{r\to 0} \int_r^R H^{1/4}(r')\, dr'$ diverges. If not for the time warping, a string that stretches to the brane from the origin would have infinite mass. Thus the region near $r = 0$ can be considered a large volume (in string units), and we are justified in dropping the 1 in (9.2). As noted in [137], the string coupling remains finite as we take the near horizon, decoupling limit. For $p = 0$, which is the case of interest given the $SO(9)$ symmetry of the BFSS system, the effective curvature becomes large for large r, and is small near $r = 0$.

Imagine adding energy to this system and creating a black hole with the same asymptotics as this background. These black holes have positive specific heat. If the temperature is low, the curvature of the black hole near the horizon is small in string units [137]. Because the dilaton runs in these geometries towards small coupling in the UV, the effective string scale depends on the position, and the curvature becomes large in string units in the UV. Correspondingly, the curvature will be large in string units if the temperature is high, so the high temperature black hole is stringy. The regime of interest for us is high temperature, where the curvature near the putative back hole is large and where stringy corrections must be important. In the spirit of [177], we should be able to describe that region by replacing the black holes by configurations of D-branes, because we are in the stringy regime. The classical dynamics we studied in Chapter 8 are the microscopic, classical dynamics of the D-brane configurations. These configurations with D-brane sources are horizonless in the sense of classical gravity, but when the system cools enough we recover a black hole. This notion that we recover a black hole when we cool the system down is the reverse of the scenario in [177], where the authors argued that a black hole that becomes small enough to become stringy is replaced by a set of strings and possibly D-branes. We assume that this philosophy is applicable in this case as well, as there is no reason to expect a phase transition and we can corroborate this by examining the scalings of various quantities with respect to N and T.

From our calculations via the virial theorem in Section 8.3 we know that the radius of the brane configurations in the classical system grows as $R \simeq N^{1/4}T^{1/4}$, so the effective (codimension two) size covered by the brane system scales as $R^8 \simeq N^2T^2$. The energy is of order N^2T whereas the entropy of the D-brane gas is of order $N^2 \log(T/T_0)$, where T_0 is some reference temperature whose precise value does not concern us here. As computed in [173], the entropy at low temperatures scales as $S \simeq N^2 T^{9/5}$ and the free energy scales as $E \simeq N^2 T^{14/5}$. The smooth transition to the brane gas occurs near $T \simeq 1$ in their units. Since for the black brane we have the usual area law for the entropy $S \simeq r^8$, for $T \simeq 1$ we have $R^8 \simeq r^8$. Hence the brane gas extends all the way to where we would imagine the black hole horizon to be. The entropy in both cases is of order N^2, as is their energy, so there is no gap between the energy or entropy scalings that would suggest a phase transition. This is the essence of the argument in [177] for smooth interpolation between strings and black hole physics. Furthermore, that the configuration reaches the same radius as where the black hole horizon would be located is very similar to the fuzzball geometries (see [178] for a review). This suggests that the system can be described both as a black hole and as a collection of D-branes. We will have further comments on this in Section 9.4. If the transition between the descriptions is smooth, we can choose one or the other depending on the question we want to ask.

Now we want to consider the dissipation we observe, in the sense of decaying correlations, in our simulations. As shown in Figure 8.10, we get a very similar power spectrum of fluctuations for all N. Applying fluctuation-dissipation relations, we can use these to characterize response functions. Matching to gravity, which should be valid at lower temperatures, we would expect dissipation to arise as the presence of quasinormal modes associated with a black hole horizon.

We expect the point of comparison between both descriptions to be the analytic structure of correlation functions and power spectra, such as those shown in Figure 8.10. As shown in the Figure, there are many suggestive straight lines that describe the logarithm of the power spectrum. Remember also that the power spectrum is symmetric about $\omega = 0$. The most naive fit to the graph near $\omega \simeq 0$ is

$$P(\omega) \simeq \exp(-\beta|\omega|) \tag{9.3}$$

The absolute value is not an analytic function of the complex variable ω and the Fourier transform of equation (9.3) only decays polynomially at large times. An analytic function of ω could replace $|\omega|$ to smooth out the singularity near $\omega = 0$. A simple function that does the job is $f(\omega) = \sqrt{\omega^2 + \epsilon}$. When $\epsilon \to 0$ we recover the above result. The presence of ϵ suggests a pair of branch cuts beginning near $\omega \simeq 0$ along the imaginary axis. If these are the closest singularities to the real axis, then the function decays exponentially in time. Thus, even if the ultimate late time fate of the system has correlation functions that decay exponentially in time, there can be a long transient where the decays of the correlation functions are only polynomial.

A square root branch cut can be approximated by a density of poles (this is often seen in matrix models [179]). Since we only have the analytic function on the real numbers, extrapolating to find the poles requires a very good understanding of the analytic structure of the function and the pattern of pole locations. For comparison, another similar function would be given by

$$P(\omega) \simeq \exp\left(-\sqrt{\beta\omega^2 + \epsilon} - \sqrt{\beta^*\omega^2 + \epsilon^*}\right) \tag{9.4}$$

where β, β^* are complex conjugates of each other. This is real on the real axis and has four branch cuts near the origin starting at $\omega = \pm i\sqrt{\epsilon/\beta}$ and $\omega = \pm i\sqrt{\epsilon^*/\beta^*}$.

Such branch cuts could indicate a series of poles along straight lines, starting from the brach cut endpoints and going towards infinity. Such patterns of quasinormal modes aligning on fairly straight curves have been observed in Schwarzschild and AdS black holes [161, 162, 163]. A particularly nice set of examples can be found in [180], Figure 4, and [181]. In gravity setups such patterns are interpreted in terms of the membrane paradigm [182].

Our results suggest that there is agreement between our analytics and the existence of a large collection of quasinormal modes for each L near $\omega = 0$. We might eventually be able to interpret them as shear or sound modes once we understand the details of how these modes are mapped into each other. As we increase L, as in Figure 8.12, the curves become flatter near $\omega = 0$ for even L. This suggests that the corresponding poles nearest to the origin are moving away from the real axis. It is possible that there is a dispersion relation for the frequencies $\omega(L)$ of these poles such that $\mathrm{Im}(\omega(L))$ increases with L. Since L is the angular momentum about the sphere of the spherical black hole geometry, such a dispersion relation could be interpreted geometrically. However, without an model predicting the locations of the poles and branch cuts, any match to a specific dispersion relation would remain speculation.

The analytic structure of the power spectra of observables in a chaotic dynamical system is generally controlled by poles off the real axis known as Pollicot-Ruelle resonances. The locations of these are known for some simple systems, but finding them in general, even for very low dimensional systems, is difficult (see, e.g., [183]). For large systems with many degrees of freedom there are expected to be accumulations of poles and also branch cuts [184], in line with our discussion above. More detailed information on the analytic structure may be difficult to obtain, but we plan to analyze this in more detail in the future. We also note the other lines drawn in the Figure 8.10. They suggest similar interpretations for the other peaks as modes whose frequencies begin with a non-zero real part.

We do not have a theory for the analytic structure of the power spectra, but based on the data and our general understanding of dissipative phenomena, we speculate that there are branch cuts in the analytically continued spectra. Given the behavior of black hole horizons, as in the membrane paradigm and as characterized by the quasinormal modes, we think our numerical data are consistent with having a smooth transition from the matrix configurations to a black hole at low temperatures. That is, our thermal matrix configurations are holographically dual to black holes and we will refer to each with the other in mind.

9.2 Aspects of Matrix Black Holes

The constructions of Chapter 7 permit us to ask very geometric questions about matrix configurations in a thermal ensemble. For example, understanding how to count the number of membranes inside one of these holographic black holes might help us understand black hole entropy. The general consideration of black hole entropy for non-extremal black holes currently suggests that they are made of a gas of brane anti-brane pairs [185] and their excitations.

As explained in the previous section, the numerical matrix configurations of Chapter 8 are holographically dual to black holes. We can ask what these look like

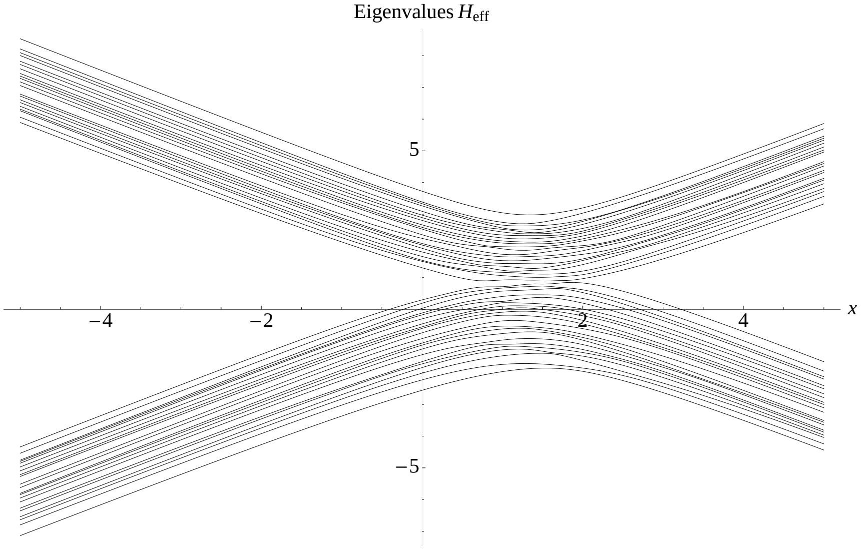

Figure 9.1: Eigenvalues of $H_{\text{eff}}(x,0,0)_{X,Y,Z}$ from a typical configuration of matrices after thermalization, when varying x. The matrices have rank 21.

in the matrix variables. We truncate the data to the three matrices $X,\ Y,\ Z$ generated by these simulations and compute the spectrum of $H_{\text{eff}}(x,y,z)_{X,Y,Z}$. Here we use the BMN effective Hamiltonian (7.14). We fix the matrix configuration and set $y,\ z=0$. A typical result is shown in Figure 9.1.

What we should notice is that there are various crossings of zero, and that there is a region in the center of the configurations where the eigenvalues of H_{eff} do not seem to have a gap in them. That is the black hole region of the configuration. For large x we see that the eigenvalues behave as parallel lines and this matches our expectations based on perturbation theory from equation (7.10). We clearly see various crossings of zero, mostly because of the shift of flux. Also, in the region without a gap the eigenvalue distribution appears to have a well defined density of eigenvalues. In Section 9.3 we will continue this analysis in the context of the BFSS matrix model to better understand the location of the horizon in these holographic blackholes.

As explained in Section 8.3 and reiterated in the previous section, the eigenvalues of the X matrices grow approximately as $N^{1/4}T^{1/4}$ when the temperature T is large. Consequently, the eigenvalues of H_{eff} grows as $N^{1/4}$ as well. If we assume the in the ungapped region the Hamiltonian H_{eff} has a well defined density of eigenvalues in the $N \to \infty$ limit, that is, it behaves like a random matrix, then since we have $2N$ eigenvalues, the eigenvalue density near the black hole region near zero grows like $N^{3/4}$. The flux contribution to the fermion mass displaces the center of the eigenvalue distribution from zero; in our units it is $3/4$ (see Appendix D). Far away from the center of the matrix configuration, half the eigenvalues are above the x axis and half are below. We roughly have that $\rho(0) \simeq O(N^{3/4})$ eigenvalues cross zero. This means the inside of the black hole is full of branes that have been polarized, all with the same orientation. As the temperature is increased, the eigenvalue distribution becomes wider and fewer eigenvalues cross zero. The N dependence is still correct, but there is also a temperature dependence. This polarization into D-branes is mostly because of the Myers effect. Remember that we have truncated to three matrices and are actually working with an orbifold. The true fermion Hamiltonian in the BMN matrix model uses all nine matrices and will have different characteristics. Thus, if we truncate this way we are working with something that resembles more a brane-world black hole (we can not move it away from some locus).

An important characteristic of black holes is that if one throws matter at them, then the matter does not come out at the other side. Let us throw a fractional D0-brane at such a (orbifold) black hole. Note that we need to do so in the orbifold of the BMN geometry. We can require the fractional D0-brane to be at a large distance from the black hole, say k times the size of the black hole itself. The energy of such a D0-brane in the BMN matrix model that starts at rest is of order $k^2N^{1/2}$. To estimate this we just look at the quadratic potential term for the $X^{1,2,3}$ matrices.

If we throw a fractional D0-brane to the black hole as described above, at each zero eigenvalue crossing a string is created due to the Hanany-Witten effect we discussed in Section 7.4. This is identical to the creation of strings observed in the one dimensional model for D-brane scattering studied in [144]. There are about $N^{3/4}$ such strings per D0-brane that are created; there are as many going in as out. When we reach the end of the matrix configuration, these strings have a length of order $N^{1/4}$, so the energy stored in these strings is of order $\hbar N$. As long as $\hbar N \gg k^2N^{1/2}$, we find that the D0-brane does not have enough energy to come out the other side; some of the energy gets transfered to the strings. Note that this depends on $\hbar$. When we take $N \to \infty$, it is clear that the strings win over the initial energy of the D0-brane. Thus we find that the thermal matrix configuration becomes a very good absorber; every fractional D0-brane that is thrown at it is eaten. If we throw bigger objects at the thermal ensemble, say a collection of fractional D0-branes, then the effect is proportional to the number of fractional D0-branes making the object and this will be reflected in the linking number. All objects are absorbed with the same efficiency. This is very similar to how we currently think black holes operate.

Usually in these dynamical setups, if fermions are created by dynamics, then so are bosons. The accounting might be different, but they usually follow each other somewhat. In the BMN model alone, the presence of tachyons in some regions of the dynamics can generate large numbers of bosons [135]. Thus one should also expect bosonic modes to be created by dynamical mechanisms (the modes become non-adiabatic) rather than by a simple topological argument in general.

This simple accounting of how objects are absorbed that we found is different than other approaches that presume the formation of a tachyon in an ensemble [186]. Maybe an effective tachyon can be thought of as a collective effect of all these fermions and bosons.

We remind the reader that we should not take the arguments above based on generalizations of the Hanany-Witten effect very seriously for the full BMN matrix model. There the dynamics of the other matrices might change the physics substantially, as we expect these D2-branes to fluctuate in the transverse directions. Thus, the topology of the Hanany-Witten effect would only be available for D8-branes, rather than D2-branes, so that there is no background flux to polarize D8-branes in large numbers.

9.3 Exploring the Gapless Region

Figure 9.1 reveals a gapless region in the truncated data of our thermal matrix configurations. In this Section we explore the transition that occurs as one moves from the gapped region to the gapless region using all of the matrix data. The truncated data is valid only in the orbifolded BMN theory and so we should check that a similar effect happens in the full matrix model.

In the next section we will analyze the effective field theory of the fermions near the transition. We will see that it breaks down at the transition and the local physics changes. We know that local quantum field theory is valid far away from a black hole, while the physics at the singularity is expected to be highly non-geometric. Thus somewhere between infinity and the singularity the effective local physics has to drastically change. This implies that in some sector of the dual gauge theory the effective local physics must also change. There is an ongoing debate as to where in spacetime this change occurs on the gravity side [187, 188], but here it does not matter. We can first search for some signature of changing physics in the gauge theory and ask later where this is happening in the gravity theory. All questions will be addressed within the dynamics of the gauge theory. Even though the black holes in question are *hot and stringy*, we will give robust arguments that our conclusions should extend to *cold* semiclassical black holes as well.

We first extend the notions of Chapter 7 to the full BFSS Hamiltonian, not just some orbifolded version of it. The fermionic part of the BFSS Hamiltonian [107]

$$H_{\text{ferm}} \sim \operatorname{Tr}\left(\Psi^\dagger \Gamma^i [X^i, \Psi]\right) \tag{9.5}$$

where $1 \leq i \leq 9$, the Ψ are $SO(9)$ spinors, and Γ^i the nine dimensional gamma matrices. The constant of proportionality depends on the normalization of the fields and $\hbar$ (see Appendix D for notes on scalings). The matrices X^i and Ψ are in the adjoint of $U(N)$, that is, they are Hermitian. Just as we did for the orbifold, we can construct an $N+1 \times N+1$ configuration $\tilde{X}^i$ from an $N \times N$ configuration of X^i by adding a single D0-brane probe with coordinates $x^i \in \mathbb{R}^9$ in the lowest right corner. We only want to consider the fermion modes connecting the background and the brane probe.

$$\tilde{X}^i = \begin{pmatrix} X^i & 0 \\ 0 & x^i \end{pmatrix}, \quad \tilde{\Psi} = \begin{pmatrix} 0 & \psi \\ 0 & 0 \end{pmatrix} \tag{9.6}$$

where ψ is an $N \times 1$ column vector (it is in the fundamental of $U(N)$). The effective Hamiltonian for the configuration $(\tilde{X}^i, \tilde{\Psi})$ is analogous to (7.7)

$$H_{\text{eff}}^{(9)} \sim \sum_{i=1}^{9} \psi^\dagger([X^i - x^i I_N] \otimes \Gamma^i)\psi \tag{9.7}$$

This effective Hamiltonian can be considered at each instant of time and for each position of the probe. Furthermore, we can choose to make the probe fully dynamical or not. If we make it dynamical, we can call it an ‘observer’ and choose a set of initial conditions, that is, the initial position and velocity of the probe. If the probe is not dynamical, we can scan over $\mathbb{R}^9$ with the position of the probe and label each point by the properties of the fermion spectrum of eigenvalues in equation (9.7).

We consider the spectrum of $H_{\text{eff}}^{(9)}$ for our thermal matrix configurations. Without loss of generality we may take the matrices to be traceless. By rotational invariance (the configurations do not have angular momentum), we need only consider moving the brane probe in a single direction, say x^1, and we choose to go through the center of the configuration. The spectrum of $H_{\text{eff}}^{(9)}$ for a typical configuration is plotted in Figure 9.2. Since the nine dimensional gamma matrices are 16×16 the spectrum of fermions for a rank N configuration has $16N$ modes. The

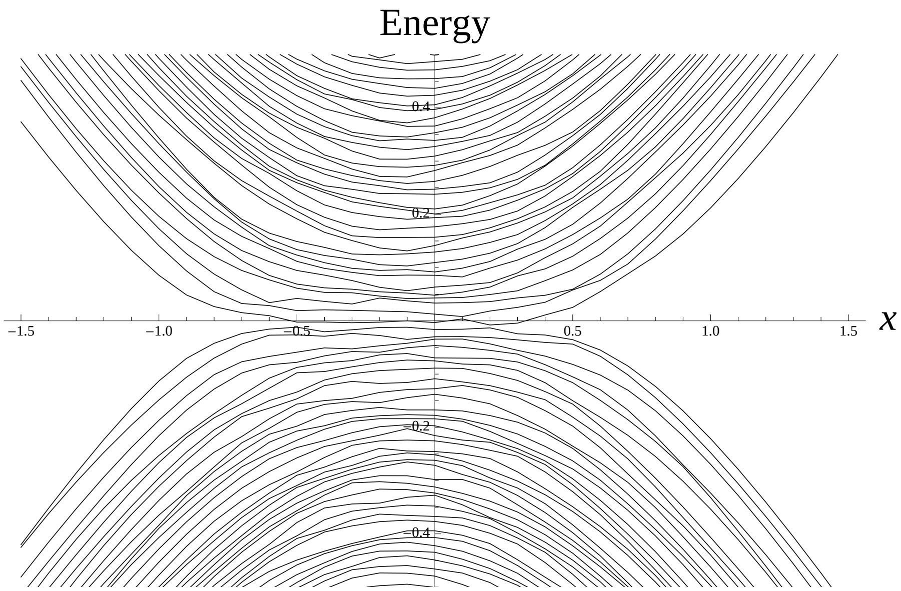

Figure 9.2: Fermionic eigenvalue spectrum for a typical configuration of matrices with $N = 47$ after thermalization. The units are arbitrary.

spectrum is typically non-degenerate and there are crossings of zero; a fermion becomes massless at such loci. Recall from Section 7.4 that the number of strings created when the probe is moved to the bulk from infinity is a generalization of the Hanany-Witten process [136].

Adding the remaining matrix data did not ruin qualitative nature of the different regions of Figure 9.1. Figure 9.2 shows a clean separation of two regions. In the first region, the eigenvalues of the fermions are well separated from zero; there is a gap which can be used to measure the distance from the probe to the configuration. There is a second region where the typical eigenvalue separation of the fermion spectrum from zero is similar to the separation of the eigenvalues from each other. We call this region gapless. Remember that the simulated matrix configurations are thermal. The temperature gives a thermal activation energy kT. So long as the modes near zero have energies below kT, they can become thermally active. At large N and fixed temperature, the size of the matrix configuration X^i scales as $N^{1/4}$ and so the number of fermions in the band of energy kT grows as $N^{3/4} \simeq NN^{-1/4}$. Thus, in a large N setup there are a lot of fermion states that could in principle get activated. In this sense, there is no gap.

9.3.1 Spectral Dimension and Nonlocality

We wish to understand the nature of the physics inside the gapless region, and in particular if we can understand this information geometrically or not. One step in this direction is knowing the effective dimension of spacetime that the matrix configuration describes. Since we are exploring $\mathbb{R}^9$, it is natural to suspect that the matrix configuration in the gapless region is $9+1$ dimensional. In massless free field theories in $d+1$ dimensions, the density of states near zero follows a power law $\rho(\epsilon) \sim \epsilon^{\gamma-1}$ where ϵ is the energy and $\gamma = d$. We call γ the spectral dimension of a configuration and argue that using a probe to measure γ yields the local spatial dimension of standard configurations.

Consider a toy model for matrix black holes in which the matrices X are essentially commuting and describe a gas of D0-branes (this has been argued recently for example in [189, 190] and references therein). The matrices can be diagonalized simultaneously, and we can talk about the positions of the D0-branes as the common eigenvalues in $\mathbb{R}^9$. More importantly, we can think of a density of eigenvalues in some region of $\mathbb{R}^9$, call it $\rho(r)$. The energy of the fermions connecting a probe at x to an eigenvalue at r will be $\epsilon \simeq |x-r|$. The number of such states at fixed $|x-r| = s$ for small s is $n(s) = \int d^9r\, \rho(r)\delta(|x-r|-s) \simeq \rho(x)s^8 \simeq \rho(x)\epsilon^8$. So in a region where $\rho(x) \neq 0$ we expect to measure a spectral dimension of $\gamma = 9$. Similarly, we can consider a D2-brane background obtained from a fuzzy sphere configuration. If we put the D0-brane probe in contact with the fuzzy sphere, it is easy to show that one gets a spectral dimension $\gamma = 2$, the dimensionality of the sphere as a geometric object. This coincides with approximating the D2-brane as a collection of D0-branes uniformly distributed on the surface of the fuzzy sphere. The spectral dimensionality captures the dimension of extended objects, or equivalently of the smearing of D0-branes in some region. It is natural to expect that if the matrix configuration can be pictured as some extended D-brane contorted to fill the gapless region, one would measure $\gamma = 9$ just from smearing into a density of D0-branes. We check if this is true or not numerically. If it does coincide with $\gamma = 9$, we would be giving evidence in favor of the toy model of black holes as a gas of D0-branes or an extended brane filling the region. We find a completely different result.

We define

$$\gamma \equiv \lim_{\epsilon \to 0} \frac{d \ln(\rho(\epsilon))}{d \ln(\epsilon)} + 1 \tag{9.8}$$

The difficulty with this definition is that we can not take the limit on a configuration of finite size matrices, where we only have finitely many eigenvalues in the effective Hamiltonian. What we need is a fit to a power law by choosing a few points near $\epsilon \simeq 0$. The precise way in which we choose to do this can give slightly different answers. To reduce such problems, we average over many configurations so that we can measure γ statistically.

We also need to compare the spectra of eigenvalues of the effective Hamiltonian at different values of N. This way we can extrapolate to large N and find a value of γ that is valid in the thermodynamic limit. This helps to show that our result is robust. To put different values of N on top of each other we take advantage of the scaling symmetry of the classical BFSS matrix model and scale the X^i by some N-dependent factor that is also temperature dependent. Since the X^i approximately follow the Gaussian Unitary Ensemble for traceless Hermitian matrices (TGUE), as explained in Section 8.3, we can scale the matrices such that their distributions of eigenvalues can be analyzed in terms of the limits of the TGUE which are semicircle distributions. This is done by fixing the second moment. The width of the associated semicircle is given by $2\sqrt{N}\sigma$ where σ is the width of the TGUE. The value of σ is given by

$$\sigma = \sqrt{\frac{\langle \sum_{i=1}^{9} \mathrm{Tr}(X^i) \rangle}{9(N^2-1)}} \tag{9.9}$$

where we have averaged over all nine bosonic matrices which is allowed by the $SO(9)$ invariance.

The spectral dimension of the field theory when the probe is at the center of the gapless region is $\gamma = 1.0$. This can be seen from Figure 9.3 where the density of states is flat at zero energy. As we move away from the center of the gapless region the spectral dimension stays approximately constant. Near the edge of the gapless region, the spectral dimension shoots up to about $\gamma = 1.3 \pm 0.1$. The density of states at the edge shown in Figure 9.3 shows the cusp at zero energy. It is difficult to pin down exactly where the gapless transition occurs due to a finite bin size and limited statistics, but log-log plots indicate a qualitative change at around $|x| = 0.33 \pm 0.03$ for the rescaled matrix configurations. For reference, the matrices are scaled so that average maximum eigenvalue of the X^i

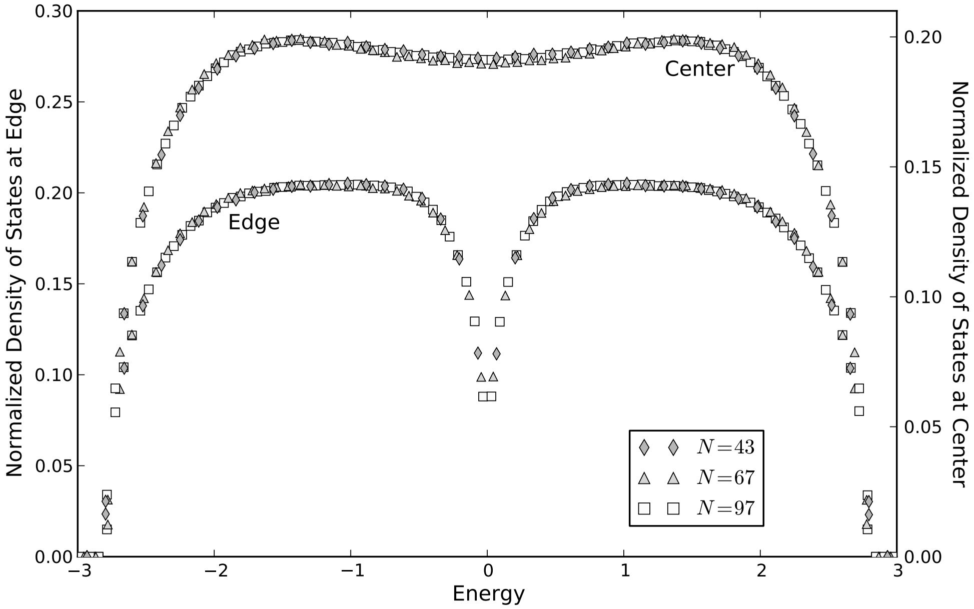

Figure 9.3: A plot of the density of states as a function of energy at the center and edge of the gapless region for various values of N averaged over 1000 configurations. Each function is normed such that $\int \rho(\epsilon)\, d\epsilon = 1$.

approaches one as $N \to \infty$. Even with numerical errors the spectral dimension at the boundary is far from nine. In the BFSS matrix model it is believed that there is no finite temperature phase transition between the high temperature regime and the low temperature regime. Thus if we include quantum corrections, the value of γ should stay close to the classical physics value. The lack of a phase transition has been verified numerically as the free energy curves as a function of the temperature are smooth [174, 152, 153]. Also, the thermal states in the BFSS model are deconfining for arbitrary small temperatures in the dual supergravity setup [190].

How should we interpret this result? The authors of [191] consider a class of theories with fermions defined on a fully connected lattice whose links are weighted. They argue that the typical configuration is maximally connected giving rise to a theory on one maximally non-local infinite-dimensional simplex; all sites are adjacent to each other. When the weights are Gaussian distributed, the spectrum of the Hamiltonian follows a cumulative semicircle distribution (in the large N limit). Near zero energy the spectrum is linear, the density of states is flat, and they conclude that the non-local fermion theory has an effective description in $1 + 1$ spacetime dimensions, in the sense that the density of states is the same as the one of a $1+1$ dimensional theory. We also find a spectral dimension of one and thus consider ourselves to be in the same universality class as the models in [191], which is also the universality class of a random Hamiltonian. By analogy to the fully connected lattices, we believe that the probe brane is in an environment where is it effectively equally far from the D0-brane matrix background no matter where the D0-branes are located. Our numerical results are inconsistent with a local gas of D-branes. If this persists in the fully quantum regime, the results of calculations based on models of such gases are suspect. The setup is maximally non-local, but it looks as if the dynamics lives effectively in $1 + 1$ dimensions.

9.4 Locating the Horizon

Up to this point we have made a very strong claim about our thermal matrix configurations; that they are holographically dual to black holes. We have used the thermal properties, power spectra, and chaotic dynamics of these configurations to make our arguments, but black holes have many other properties. They have mass and entropy. They possess metric data responsible for interactions with other objects in their vicinity, for example stable and unstable orbits. The most defining characteristic of black holes is that they possess event horizons and a singularity behind it. Our matrix configurations should possess this property and we will use the results of the previous section to argue that they do.

We propose to place the horizon of the black hole exactly at the interface between the gapless region and the gapped region shown in Figure 9.2. This is potentially different than the proposal in [186]. Consider a string suspended between a probe D-brane at fixed position and a black hole. The energy carried by such a string is given by $\int_{r_0}^{r_D} T(r)\sqrt{g_{tt}g_{rr}}\,dr$ where $T(r)$ is the local string tension at r, r_0 is the horizon, and r_D is the position of the brane. This is finite for typical black holes since the black hole horizon is at finite distance. In the limit $r_D \to r_0$ we get that the energy of such a string goes to zero. In our setup, the fermionic energies connecting the probe to the matrix configuration have this same behavior. Also, the presence of a large number of massless modes appearing at the edge of the gapless region indicates that wiggles on a string also get redshifted and produce a large number of string states with small energies. This is analogous to strings spreading when reaching the horizon [192].

A natural question to ask is if we can integrate out the modes connecting the probe to the matrix configuration and extract an effective action for the probe. This is how gravitational interactions and forces between objects are captured in the BFSS matrix model [107] (see [132, 116] for a systematic treatment). In our case the answer to this question is yes, for fermions, away from the gapless region.

If we reintroduce $\hbar$ and call an eigenvalue of (9.7) ω, the energy of such a fermionic mode is $\hbar|\omega|$. The light fermion modes become thermally active when

$\hbar|\omega| < kT$. In classical physics all the fermions are active, yet we will assume that the system is cold enough so that most fermions are not active. After taking the limit where N is large with $\hbar$ constant, and rescaling X so that the matrix configuration is of finite size in the probe coordinates, the light fermions become active exactly when we enter the gapless region. The approximation where we can integrate out the off-diagonal degrees of freedom connecting a probe to the black hole breaks down exactly at the putative horizon. This puts further into question the paradigm that black holes be treated as D-brane gases.

The breakdown of effective field theory of a configuration plus a probe, considered as an observer, further suggests that physics has changed dramatically on crossing the horizon (see however [193]). The fourth postulate of [194] was that no drama occurs when crossing the horizon. Removing this postulate to restore consistency suggested the existence of a firewall. We see that the BFSS matrix model provides a physical model for the firewall.

This in itself does not give a proof that firewalls exist. There could be some other physical effect on the probe that comes from understanding the bosonic degrees of freedom that forces us to put the horizon elsewhere, as in [186]. Bosonic instabilities might be realized only via parametric resonance and would require a full time dependent treatment to be understood.

Our analysis so far has been done for our stringy black holes of Chapter 8. For such black holes the horizon and the singularity are on top of each other in string units. The $1 + 1$ dimensional effective physics could be associated with the singularity rather than with the horizon. This can be remedied with fully quantum simulations [189, 190].

Physics at the black hole singularity is also argued to be effectively $1 + 1$ dimensional in the causal dynamical triangulation program, since the effective UV structure of gravity has a different dimension [195] (see also [196]).

Also note that this picture, although similar in spirit to the fuzzball picture [178], is distinct. The known fuzzball solutions are geometric (non-singular solutions of supergravity) and they stretch all the way to the horizon. Microphysics in these setups is essentially gravitational. In our case the inside of the black hole gets replaced by non-geometric, non-local objects whose effective dimension is different than that of the ambient space.

The presence of an effective $1 + 1$ dimensional field theory starting at the horizon is also reminiscent of ideas espoused by Carlip [197] and suggests that the additional entropy added to the black hole when the probe is absorbed can be computed using Cardy's formula.

9.5 Discussion

The BFSS and BMN matrix models are of particular interest because of their dual gravitational interpretation. Though quantum effects are crucial to the emergent gravitational dynamics in general, we have argued that at high temperatures the classical dynamics of these matrix models do encode certain dual gravitational phenomena, including black holes, albeit in a stringy regime. As such, a direct comparison with supergravity solutions is not possible, but we can look for and have found some qualitative agreement.

The first level of correspondence is between black holes, broadly defined to include large stringy corrections, and equilibrium thermal states in these models. This thermodynamic correspondence was referred to in both of the seminal papers on BFSS matrix theory and AdS / CFT [107, 13] and subsequently investigated and verified in many situations. As a first step toward a more detailed correspondence, we have presented evidence here that the approximate analytic structure we find in the power spectra of certain observables at large N could be the remnant of the quasinormal modes of supergravity black holes. This is suggested by the numerical data, where the results we find on the real axis seem to be well approximated by functions that, when analytically continued, would have branch cuts in the complex plane. These could be an approximation of a sequence of roughly evenly spaced poles.

Reflecting on what we have accomplished here, we have made a modest attempt at reconciling gravitational dynamics in holographic setups with the theory of chaotic dynamical systems. We have argued that these types of analyses do cover interesting black holes in the stringy regime. We have barely scratched the surface of what can be computed and analyzed and it would be interesting to pursue this further to improve our understanding of holography. The simulations of the classical dynamics provide new ways to address questions about black holes in simple systems where the numerical computations are easily implemented. It is also important to understand how to move away from the correspondence limit, which would mean quantum dynamics starts becoming important and the dynamics of fermions starts affecting the results. In such setups the tools of quantum chaos will play an increasingly important role. This is closely related to the question of whether at low temperatures it is the fermionic degrees of freedom that dominate, or if they only play a marginal role in most of the dynamical regimes of interest.

We were able to show that the surfaces constructed using the techniques of Chapter 7 could be used to analyze numerical data from classical simulations of matrix models. We were able to make contact with conjectures about the structure of black hole interiors as made from brane-antibrane systems. We were also able to show that with the Hanany-Witten effect, the fermions created on these surfaces could be used to stop a probe D0-brane particle in a simple model. Thus it is clear that these modes can give us a handle on black hole dynamics that do not require much effort.

Extending the techniques of Chapter 7 to the full BFSS matrix model revealed the persistence of a gapped and a gapless region for a D0-brane probe interacting with a background matrix configuration. We used the spectral dimension during the transition to show that there exists a locus of points in $\mathbb{R}^9$ where the effective field theory of the fermion modes connecting the probe to the configuration breaks down. We propose placing a horizon at this locus, although we concede that this may be premature. Since the black holes in question are hot and stringy, the locus may be sitting on the singularity and not the horizon. Additionally the bosonic excitations in that region may also provide an explanation for the breakdown of the effective theory. We leave this for future work.

Chapter 10

Adding Angular Momentum

The BMN matrix model has exact, supersymmetric solutions with zero energy [60]. These matrix configurations are characterized by all adjoint representations of $\mathfrak{su}(2)$. They have an interpretation as giant gravitons [19]. The spectrum of fluctuations around these solutions is known [129] (see also [135] for an alternative derivation of the spectrum) and one can argue that there is a large tower of protected states that are available to study [198]. Unfortunately, the nonlinear structure of the classical solutions keep this tower of BPS states unknown.

It is expected that adding angular momentum to the fuzzy sphere states can induce topology changes from a sphere to a torus [112]. In this Chapter we investigate this topology transition with a special family of matrix solutions at finite angular momentum. We devote most of our attention to constructing these solutions. Once the solutions are found, the geometry of the corresponding fuzzy membrane is analyzed using the techniques of Chapter 7.

10.1 The Hamiltonian and the Ansatz

The $SO(3)$ BMN matrix model is the matrix model (D.1) restricted to the bosonic $SO(3)$ sector. We label the three $N \times N$ Hermitian matrices $X^{1,2,3}$, or alternatively $X,\ Y,\ Z$. The conjugate momentum matrices are $P_{1,2,3}$, and $P_{X,Y,Z}$ respectively. The Hamiltonian for this restricted system is given by

$$H = \frac{1}{2}\mathrm{Tr}(P_1^2 + P_2^2 + P_3^2) + \frac{1}{2}\mathrm{Tr}\left(\sum_{j=1}^{3}(X^j + i\epsilon_{jmn}X^m X^n)^2\right) \tag{10.1}$$

The system possesses a $U(N)$ gauge symmetry where X^i and P_i both transform in the adjoint, $X^i \to UX^iU^{-1}$ and $P_i \to UP_iU^{-1}$. The presentation of the Hamiltonian (10.1) is in the gauge $A_0 = 0$. The generators of gauge transformations are the matrix of functions on phase space given by

$$\mathfrak{G} = i\sum_{j=1}^{3}[X^j, P_j] \tag{10.2}$$

The dynamics need to be supplemented by the Gauss' law constraint $\mathfrak{G} = 0$. The system also enjoys an $SO(3)$ symmetry of rotations of the matrices $X,\ Y,\ Z$ into each other. The generator of angular momentum along the Z direction is

$$J = L_Z = \mathrm{Tr}(XP_Y - YP_X) \tag{10.3}$$

with similar expressions for the other two $SO(3)$ generators. Lastly, the equations of motion are

$$\dot{X}^j = \frac{\partial H}{\partial P^j} = P_j, \tag{10.4}$$

$$\dot{P}_j = -\frac{\partial H}{\partial X^j} = -X^j - 3i\epsilon^{jmn}X^m X^n - [[X^j, X^m], X^m] \tag{10.5}$$

The solutions with $H = 0$ are given by fuzzy spheres. These are solutions of the equations

$$[X^i, X^j] = i\epsilon^{ijk}X^k \tag{10.6}$$

The solutions to these equations are characterized by direct sums of the adjoint matrices for irreducible representations of $\mathfrak{su}(2)$. For these solutions we have $P_1,\ P_2,\ P_3 = 0$ and thus are classically gauge invariant according to (10.2). These solutions carry no angular momentum as $\vec{L} = 0$ identically.

The Hamiltonian also satisfies a BPS inequality bound, where $H \geq |J|$ (details can be found in [199]). Solutions that saturate the bound will be called extremal or BPS. This follows from writing the Hamiltonian as a sum of squares in a slightly different way

$$\begin{aligned} H = \mathrm{Tr}\Bigg(\frac{1}{2}P_3^2 + \frac{1}{2}(P_1 \pm (X_2 + i\epsilon_{231}[X^3, X^1]))^2 \\ + \frac{1}{2}(P_2 \mp (X_1 + i\epsilon_{123}[X^2, X^3]))^2 + \frac{1}{2}(X_3 + i\epsilon_{312}[X^1, X^2])^2\Bigg) \pm J \end{aligned} \tag{10.7}$$

The cross terms between $X_2,\ P_1$ and $X_1,\ P_2$ in the squares generate a copy of J that needs to be subtracted. The cross terms with P_1 and $[X^3, X^1]$ lead to something that does not automatically cancel for generic matrices, but after a bit of reshuffling can be shown to be proportional to

$$X^3([X^1, P^1] + [X^2, P^2]) \tag{10.8}$$

and we recognize the Gauss' law constraint starting to arise. After imposing the full Gauss' law constraint, we get $\mathrm{Tr}(X^3[X^3, P^3])$ that does vanish identically.

The BPS bound is not directly related to supersymmetry. Instead it is derived from the conformal group in four dimensions, where one can show based on unitarity arguments that $E \geq J$ by requiring that $K = P^\dagger$, where P, K are the generators of translations and special conformal transformations on $S^3 \times \mathbb{R}$. This bound asserts that the dimension of operators is greater than the spin and is usually saturated for free theories, or nearly free theories at leading order in perturbation theory. This should be lifted in general theories (see [200] for a recent discussion). However, the bound does show up in studying supersymmetric BPS states [201, 202] for the full BMN matrix model. This bound descends to any classical solution of Yang-Mills theory which is a conformal field theory at the classical level.

Now we construct solutions to (10.4) and (10.5) with non-zero J. We define the matrices

$$X^+ = \frac{1}{2}(X + iY), \quad X^- = \frac{1}{2}(X - iY) \tag{10.9}$$

$$X = X^+ + X^-, \quad Y = -i(X^+ - X^-) \tag{10.10}$$

We will make an ansatz for a solution more general than the fuzzy spheres

$$X^+(t) = \begin{pmatrix} 0 & a_1 \exp(i\omega_1 t) & 0 & \dots \\ 0 & 0 & a_2 \exp(i\omega_2 t) & \dots \\ \ddots & \ddots & \ddots & \vdots \\ 0 & \dots & 0 & a_{N-1} \exp(i\omega_{N-1} t) \\ a_N \exp(i\omega_N t) & 0 & \dots & 0 \end{pmatrix} \tag{10.11}$$

with a_i constants, and $X^-(t) = (X^+(t))^\dagger$ (this is the transpose complex conjugate). At the same time we also take

$$Z(t) = \mathrm{diag}(z_1, \dots, z_N) \tag{10.12}$$

independent of time and real. We will explain the origin of this ansatz in the following section. Notice that all fuzzy sphere ground states are solutions of this kind already, with $\omega_i = 0$, and some of the $a_i = 0$. Gauge transformations that commute with Z allow us to vary the relative phases of the a_i. Therefore we can assume that they are real, and a common phase can be translated away by choosing the starting time appropriately. This ansatz is different to those that have been studied before [199] (previous works also look for solutions of the BMN and BFSS matrix model where more than three matrices are oscillating [203, 203, 204]). Other time dependent solutions can be found in [205, 206, 207], but again, these involve more matrices being turned on. In particular, we allow for multiple frequencies to arise in the ansatz, rather than just one. This does not affect fact that the system is rigidly rotating. One can use a gauge transformation to make the frequencies the same, but one pays the price that A_0, the connection in the time direction, becomes non-trivial. This is actually very useful for the BPS states, where $A_0 \propto Z$ [201].

The method of solving the equations is then to first solve for the conjugate momenta by using equation (10.4). Then, we solve the Gauss' law constraint (10.2) to relate the ω_i to each other. These can then be substituted into the angular momentum equation (10.3), so that we can express the ω_i in terms of the total angular momentum $L_z = J$ and the a_i. One can then show that the system of equations of motion (10.5) reduces consistently to an algebraic set of real equations for the $a_i,\ z_i$ and that it has as many unknowns as there are variables. One therefore expects to generally find a discrete (possibly empty) set of solutions to the equations. We will show eventually that this set of solutions is non-empty for all J.

10.1.1 Relation to SYM and $\mathcal{N} = 1^*$

The BMN Hamiltonian (10.1) also arises from sphere reductions of four dimensional Yang-Mills into a $S^3 \times \mathbb{R}$ [109] and from the $\mathcal{N} = 1^*$ theory. The relation to Yang Mills on $S^3 \times \mathbb{R}$ is as follows. Consider that the round three sphere is also the group manifold of $SU(2)$, and has an $SU(2) \times SU(2)$ isometry group by acting with the group on the left and on the right. We can use a basis of left invariant one-forms under $SU(2)$, $e^{1,2,3}$ and write the spatial part of the connection connection as follows

$$A = A_i e^i \tag{10.13}$$

where the A_i are now Lie-algebra valued functions on S^3. Requiring that the allowed configurations are invariant under left actions of the group, we have that A_i becomes position independent and is just a constant Hermitian matrix. The Mauer-Cartan equations for the one forms e^i then give us that

$$dA + A \wedge A = A_i de^i + [A_i, A_j] e^i \wedge e^j \tag{10.14}$$

whereas the electric fields will give

$$D_t A \simeq (D_t A_i) dt \wedge e^i \tag{10.15}$$

Because of the large amount of symmetry preserved, we are led to a consistent truncation of the SYM lagrangian. We then identify $A_i \simeq X_i$ and $P^i \simeq D_t A_i$. The Legendre transform of the Lagrangian for $SU(2)$ invariant fields will give rise to the same BMN Hamiltonian.

The $\mathcal{N} = 1^*$ field theories are obtained from $\mathcal{N} = 4$ SYM after an $SO(3)$ invariant mass deformation of the superpotential. The $\mathcal{N} = 4$ SYM Lagrangian can be characterized by having three chiral matter superfields $\phi^{1,2,3}$ in the adjoint of $SU(N)$, and a super potential of the form

$$W = \mathrm{Tr}(\phi^1 \phi^2 \phi^3 - \phi^3 \phi^2 \phi^1) \tag{10.16}$$

The full potential has an $SO(6)$ R-symmetry invariance, of which only an $SU(3)$ symmetry is manifest in terms of $\mathcal{N} = 1$ super fields.

The$\mathcal{N} = 1^*$ deformation adds the super potential mass term

$$\delta W = -\frac{i}{2} M \mathrm{Tr}\left(\sum_{k=1}^{3} (\phi^k)^2\right) \tag{10.17}$$

The factor of i is a choice of convention, as the phase of M can be changed by a global R-charge rotation of the ϕ. This preserves an $SO(3)$ global symmetry from the R-charge, but the theory can confine in the infrared in some of its vacua. For this theory, the classical vacua are given by fuzzy spheres, or $\mathfrak{su}(2)$ representations [208] (see also [209] for the characterization of the vacua at strong coupling). The potential for the ϕ fields is given by

$$V(\phi) = \sum_{k=1}^{3} \left|[\phi^\ell, \phi^m]\epsilon_{\ell m}{}^{k} + iM\phi^k\right|^2 + \left(\sum_{k=1}^{3} [\phi^k, \bar{\phi}^k]\right)^2 \tag{10.18}$$

where the first term is the F-term and the last term comes from the D-terms of Yang-Mills. The theory also has a parity transformation that sends the superfield $\phi^i \to \bar{\phi}^i$. This is a symmetry of $\mathcal{N} = 4$ SYM if the theta angle of the field theory vanishes. The scalar potential is invariant under this transformation. We can choose to look for configurations that are classically parity invariant. In that case, we only preserve the real part of ϕ^i, while the imaginary part is removed. This parity transformation commutes with the $SO(3)$ symmetry group, but not the full $SU(3)$.

With this constraint on the fields, the potential term arising from the D-terms automatically vanishes. Moreover, the potential for $V(\phi)$ becomes the BMN potential after factoring out the dimensionful constant from the fields ϕ. A translation invariant classical solution of the $\mathcal{N} = 1^*$ field theory with parity invariance can be understood as a classical solution of the $SO(3)$ BMN matrix model. The angular momentum of the BMN matrix model solutions becomes a charge density for a global symmetry of the field theory. This is a charge density in a four dimensional $\mathcal{N} = 1$ field theory, so it is not a charge density for a central charge. The solutions are to be regarded as non-supersymmetric, but in the classical limit they are controlled by the same dynamics as the $SO(3)$ BMN matrix model. The quantum corrections will be different. The structure of solutions will then be described by the (parity invariant) phase diagram for the weakly coupled $\mathcal{N} = 1^*$ field theory at finite charge density. This in turn can be understood as a phase diagram for a (top-down) holographic superconductor [210].

10.2 Symmetry Considerations

A natural question to ask is if we can find rotationally invariant configurations of the $SO(3)$ BMN matrix model around the Z axis that rotate uniformly without changing the shape of the configuration and while being small perturbations of a single fuzzy sphere. After all, this is how the giant torus configurations in supergravity are constructed [112]. It turns out that the answer is no.

The way to see this is as follows. Assume that Z is a Hermitian matrix with eigenvalues that are non-degenerate. A configuration will be rotationally invariant around the Z-axis if a naive rotation of the matrices into each other can be undone with a gauge transformation. This is the same way that the method of images works for D-branes on orbifolds when considering a discrete subset of the rotation group [90] (this is also the mechanism for rotational invariance of monopole solutions in nonabelian gauge theories [211, 212]).

That is, for any angle θ can we find a unitary matrix $U(\theta)$ such that

$$\begin{aligned} U(\theta)ZU^{-1}(\theta) &= Z \\ U(\theta)XU^{-1}(\theta) &= X\cos(\theta) - Y\sin(\theta) \\ U(\theta)YU^{-1}(\theta) &= Y\cos(\theta) + X\sin(\theta) \end{aligned} \tag{10.19}$$

Because Z has non-degenerate eigenvalues, the first equation tells us that U must be diagonal in the same basis that Z is (they commute with each other). We gauge transform to such a basis without loss of generality. The angle θ will be identified with the time evolution itself later on. The uniform rotation motion of the configuration requires that Z is time independent, so that $\dot{Z} = 0$.

Let $|1\rangle, \ldots, |N\rangle$ denote the eigenvectors of Z. We rewrite the last two equations of (10.19) in terms of the general matrix $X^+ = X + iY$ and its adjoint. The matrix X^+ is unconstrained. Then we have that

$$U(\theta)X^+U^{-1}(\theta) = \exp(i\theta)X^+ \tag{10.20}$$

Using a general expression for $X^+|m\rangle = X^+_{mn}|n\rangle$, and $U \simeq \mathrm{diag}(\exp(i\theta_i))$ we find that X^+_{mn} transforms under conjugation by U as

$$X^+_{mn} \to \exp(i(\theta_m - \theta_n))X^+_{mn} \tag{10.21}$$

which can only be equal to $\exp(i\theta)X_{mn}$ if $\theta_m - \theta_n = \theta \mod (2\pi)$ or if $X^+_{mn} = 0$. Picking θ arbitrarily small, we can only satisfy $\theta_m - \theta_n = \theta$ for some of the components, and because θ is very small, we can arrange the kets $|n\rangle$ such that the θ_n are strictly decreasing as we increase n. This shows that $U(1)$ invariance requires X^+_{mn} to be upper triangular with zeros on the diagonal. Now, comparing with the fuzzy sphere solutions, X^+ actually must border the diagonal. That is, we find that the solutions must be of the form

$$X^+ = \begin{pmatrix} 0 & |a_1|\exp(i\phi_1) & 0 & \dots \\ 0 & 0 & |a_2|\exp(i\phi_2) & \ddots \\ \vdots & \ddots & \ddots & \vdots \\ 0 & \dots & 0 & |a_{N-1}|\exp(i\phi_{N-1}) \\ 0 & 0 & \dots & 0 \end{pmatrix} \tag{10.22}$$

where the a_i are some as of yet unspecified numbers that depend on time, and both X^+X^- and X^-X^+ are diagonal and rotationally invariant themselves. Thus if a configuration is rotating uniformly we find that the only possible solution has the $|a_i|$ being constant, and all the dynamics will be in the phases $\phi_i(t)$. Inserting these expressions in the Gauss' law constraints, we find that

$$|a_i|^2\dot{\phi}_i - |a_{i+1}|^2\dot{\phi}_{i+1} = 0 \tag{10.23}$$

for all i. We then have that $\dot{\phi}_{N-1} = 0$ and from there, $\dot{\phi}_i = 0$ for all i. The solutions are thus static and carry no angular momentum. Since we want to turn on angular momentum, we need to relax the rotational invariance around the Z-axis of the configuration.

The obvious idea is to look for the maximal discrete subgroup of rotations that can actually be preserved if we can not have a full $SO(2)$ symmetry. Let us assume that we turn on an X_{mn} which is not one of the above. The matrix U that implements the constraint (10.20) for X^+ defined in (10.22) is diagonal and up to a global phase it is equal to

$$U = \mathrm{diag}[\exp(-i\theta), \exp(-2i\theta), \exp(-3i\theta)\dots\exp(-Ni\theta)] \tag{10.24}$$

We then have that $n\theta - m\theta = \theta \mod (2\pi)$, or equivalently, that $(m+1-n)\theta = 0 \mod (2\pi)$. This tells us that we can preserve a $\mathbb{Z}_{m+1-n}$ subgroup of the $SO(2)$ rotations if we turn on this particular X_{mn}. If we want to maximize this group, we find that we must take $m = N$ and $n = 1$, where we get an $\mathbb{Z}_N$ subgroup of the rotation group to be invariant. None of the other X_{mn} that are not already turned on are neutral under this subgroup. We can self-consistently set them to zero by symmetry arguments; if an initial solution for $X,\ P$ respects the symmetry, $\mathbb{Z}_N$ invariance will guarantee that no symmetry breaking can occur afterwards. We are therefore led to a general ansatz for X^+ which can still have arbitrary time dependence

$$X^+ = \begin{pmatrix} 0 & |a_1|\exp(i\phi_1) & 0 & \dots \\ 0 & 0 & |a_2|\exp(i\phi_2) & \ddots \\ \vdots & \ddots & \ddots & \vdots \\ 0 & \dots & 0 & |a_{N-1}|\exp(i\phi_{N-1}) \\ |a_N|\exp(i\phi_N) & 0 & \dots & 0 \end{pmatrix} \tag{10.25}$$

Now we want to insist that the only motion that the system undergoes is rigid rotation, so that the $|a_i|$ are necessarily constant, but the ϕ_i can vary in time. Substituting this in Gauss' law shows that all the motions in the angles are related to each other by $|a_i|^2\dot{\phi}_i - |a_{i+1}|^2\dot{\phi}_{i+1} = 0$ cyclically. Furthermore, one can show that $L_z = \frac{1}{2}\sum_i |a_i|^2\dot{\phi}_i = J$ which is a conserved quantity. Putting these two pieces of information together shows that the phases ϕ_i have constant time derivatives which we call ω_i. This leads us to the general form of the ansatz described in equations (10.11) and (10.12).

Notice also that the ansatz we have made has an additional remnant discrete $\hat{\mathbb{Z}}_N$ symmetry on the variables $a_i,\ z_i$, where we send $|a_k|\exp(i\phi_k) \to |a_{k+1}|\exp(i\phi_{k+1})$ and $z_k \to z_{k+1}$ cyclically. That is, any solution of the equations can be permuted to a new solution using this symmetry. This is a subset of the gauge freedom of the original system, where we permute the eigenvalues of a Hermitian matrix. In D0 brane dynamics this permutation symmetry is associated to the permutation statistics of D-branes [107]. This symmetry can also be understood if we orbifold the matrix problem by the original $\mathbb{Z}_N$ symmetry we identified via the rules of [90]. In the orbifold theory by an abelian symmetry, it is expected that one has a dual quantum symmetry $\hat{\mathbb{Z}}_N$ that permutes the nodes of the corresponding quiver theory [84]. Gauging this dual quantum symmetry restores the original theory in a straightforward way [122]. There is a second symmetry where we reverse the order of the $|a_i|,\ z_i$ and also change the sign of the z_i. This acts essentially as reflection on the Z-axis, so that when we combine it with time reversal, we can still spin in the same direction. These two symmetries form a dihedral group with $2N$ elements and it will be useful for analyzing the set of solutions of the ansatz.

Notice that if a discrete subgroup of the quantum symmetry is left unbroken, this implies that there is an enhanced unbroken gauge group so long as it is not just the spatial reflection symmetry. For example, if the $\hat{\mathbb{Z}}_N$ is unbroken (we find some solutions of this type), the unbroken gauge group turns out to be $U(1)^N$. The solution can be interpreted as N D0 branes separated from each other in a $\mathbb{Z}_N$ symmetric pattern of rotations around the origin, just like one would expect from the method of images in an orbifold.

10.3 The Solutions as a Set of Critical Points

The equations of motion that follow from the Hamiltonian (10.1) come in two different sets. First, we have that

$$\dot{X}^j = P_j \tag{10.26}$$

We can solve these immediately given the ansatz for the X. We find that $P_Z = 0$ and that

$$P_X = \dot{X} = i\Omega X^+ - iX^-\Omega \tag{10.27}$$

$$P_Y = \dot{Y} = \Omega X^+ + X^-\Omega \tag{10.28}$$

where the matrix Ω of angular velocities is given by

$$\Omega = \mathrm{diag}(\omega_1, \omega_2, \ldots, \omega_N) \tag{10.29}$$

This way we find that

$$P_X X - X P_X = (i\Omega X^+ - iX^-\Omega)(X^+ + X^-) - (X^+ + X^-)(i\Omega X^+ - iX^-\Omega) \tag{10.30}$$

$$P_Y Y - Y P_Y = (\Omega X^+ + X^-\Omega)(-i(X^+ - X^-)) - (-i(X^+ - X^-))(\Omega X^+ + X^-\Omega) \tag{10.31}$$

Adding these two, we find that the terms with two X^+ or two X^- cancel each other, so that the Gauss' law constraint reads

$$\mathfrak{G} = 2i\Omega X^+ X^- - 4iX^-\Omega X^+ + 2iX^+X^-\Omega \tag{10.32}$$

A straightforward computation shows that this is a diagonal matrix and that it is equal to

$$\mathfrak{G} = 4i\,\mathrm{diag}(|a_i|^2\omega_i - |a_{i+1}|^2\omega_{i+1}) \tag{10.33}$$

To satisfy the Gauss law constraint, we need that $\mathfrak{G} = 0$ identically. Hence we find that $|a_i|^2\omega_i$ is independent of i.

Similarly, we find that the angular momentum is written as

$$J = \mathrm{Tr}((X^+ + X^-)(\Omega X^+ + X^-\Omega) - (-iX^+ + iX^-)(i\Omega X^+ - iX^-\Omega)) \tag{10.34}$$

and similarly, the terms with two copies of X^+ or X^- cancel even before taking the trace. We find that

$$J = 2\mathrm{Tr}(X^+X^-\Omega + X^-\Omega X^+) = 2\mathrm{Tr}(\mathrm{diag}(\omega_i|a_i|^2 + \omega_{i-1}|a_{i-1}|^2)) \tag{10.35}$$

Now, notice that because of Gauss' law constraint, all the $\omega_i|a_i|^2$ are equal to each other. Thus, even before taking the trace, the matrix version of J is proportional to the identity. We can interpret this as having uniform density of angular momentum per unit D0-brane of the corresponding fuzzy membrane. We use this to find that

$$J = 4N\omega_i|a_i|^2 \tag{10.36}$$

so that we can substitute

$$\omega_i = \frac{J}{4N|a_i|^2} \tag{10.37}$$

Knowing the $|a_i|$, the z_i and J, we can evaluate the energy by substituting the above results in the Hamiltonian (10.1). The result for the kinetic energy is

$$\begin{aligned} E_{kin}(J,|a_i|) &= \frac{1}{2}\mathrm{Tr}(P_X^2+P_Y^2) = \frac{1}{2}\mathrm{Tr}(P_X+iP_Y)(P_X-iP_Y) && (10.38)\\ &= \frac{4}{2}\mathrm{Tr}(\Omega X^+X^-\Omega) && (10.39)\\ &= 2\sum_{i=1}^{N}|a_i|^2\omega_i^2 = \frac{1}{8N^2}\sum_{i=1}^{N}\frac{J^2}{|a_i|^2} && (10.40)\end{aligned}$$

What is important to realize is that this looks very similar to an angular momentum centrifugal potential, where each particle (associated to the radial variable a_i) has the same angular momentum J/N and the same mass (in this case the mass would be interpreted as 4). To specify the full problem, we need to evaluate the potential energy as well. A straightforward, though rather tedious procedure shows that

$$V(|a_i|,z_i) = \sum_{i=1}^{N}\frac{1}{2}[z_i+2|a_{i-1}|^2-2|a_i|^2]^2 + 2(1+z_{i+1}-z_i)^2|a_i|^2 \tag{10.41}$$

where the i are defined modulo N. We denote the full energy of a configuration $(J,\ |a_i|,\ z_i)$ by

$$\mathcal{E}(J, |a_i|, z_i) = E_{kin}(J, |a_i|) + V(|a_i|, z_i) \tag{10.42}$$

When we consider the energy function $\mathcal{E}(J, |a_i|, z_i)$ and recall that $P_Z = 0$ in our ansatz, it is straightforward to notice that the equations of motion of the Z variables are exactly the equations that extremize $\mathcal{E}$ as a function of the z_i keeping the other variables fixed. Namely, that $\partial_{z_i}\mathcal{E} = 0$. This suggests that to look for solutions of the original problem we set out to do with our ansatz, it is enough to consider the extrema of the energy function $\mathcal{E}$ at fixed J. Indeed, any solution of the ansatz that solves the equations of motion of the Hamiltonian (10.1) are going to be extrema of the energy function $\mathcal{E}$ and vice versa, any extremum of the energy function can be shown to give a solution of the equations of motion derived from the $SO(3)$ BMN Hamiltonian.

The essence of the proof is that when we take the derivatives of the kinetic energy with respect to the $|a_i|$ we find that

$$\partial_{|a_i|} E_{kin} = -\frac{J^2}{4N^2|a_i|^3} = -4\omega_i^2|a_i| \tag{10.43}$$

and these can be assembled into $\dot{P}_X = \ddot{X}, \dot{P}_Y = \ddot{Y}$. Then we need to compare this expression to the derivatives of the potential

$$\partial_{|a_i|} V \tag{10.44}$$

which can be assembled into the right hand side of the Hamilton's equations for

(10.1). The two sets of equations can be shown to be the same set when we remove the time dependent phases $\exp(i\omega_i t)$.

The potential is a sum of 'nearest neighbor' terms and it is a sum of squares. As a function of the z_i it is quadratic. Therefore if we fix the $|a_i|$, we can solve for the z_i via a linear set of equations, and these equations are independent of J. The quadratic form that appears in front of the z_i is of the form $\delta_{ij} + U_{ij}$ where U is a non-negative matrix. Therefore it is always invertible.

The kinetic energy is also a sum of squares. Therefore the energy function is bounded from below. Notice that when $J \neq 0$, and as we take $|a_i| \to 0$ the energy diverges at $|a_i| = 0$. Also, when we take the $|a_i| \to \infty$ the potential grows quadratically in the $|a_i|$, and if we solve for the z_i in this limit, they are bounded. Therefore we expect that generically the potential grows quartically at infinity. The only time when this does not happen is when we take a double scaling limit where $|a_i|^2 = \Lambda \to \infty$ independent of i. In this case one has that the $z_i \to 0$ and the potential grows only like Λ^2.

Considering the configuration space as the set of open intervals $|a_i| \in (0, \infty)$ (since after all we can solve for the z_i given the a_i), we have that the domain of interest is an open ball (it is diffeomorphic to $(0,1)^N$), and the potential function diverges on all the boundary, while it is finite (and indeed analytic) in the interior. This shows that the energy function has at least one minimum. Moreover, if we compactify the boundary of the configuration space by adding one point at infinity, we get a configuration space which is compact and has the topology of a sphere. The point at infinity realizes the maximum of the energy function continuously [1].

---

[1] We can always map the energy function from $[0, \infty)$ to $[0, 1]$ by using $\tanh(\mathcal{E})$ for example.

Notice that

$$\partial_{|a_i|}\mathcal{E}_J(|a_i|) = \partial_{|a_i|}\mathcal{E}(J, z_i(a_i), a_i)|_z + \partial_{z_j}\mathcal{E}(J, z_i(a_i), a_i)\frac{\partial z_j}{\partial |a_i|} = \partial_{|a_i|}\mathcal{E}(J, z_i(a_i), a_i)|_z \tag{10.45}$$

since the z_i solve the $\partial_{z_j}\mathcal{E}(J, z_i(a_i), a_i) = 0$ equations. Any critical point of the original $\mathcal{E}(J, a_i, z_i)$ will give rise to a critical point of $\mathcal{E}_J(|a_i|)$ and vice versa. In our original ansatz where we have $3N$ variables, given by a_i, ω_i, z_i, we have managed to reduce the problem to a set of algebraic equations in N variables, the a_i themselves.

For the purpose of analyzing configurations, the function $\mathcal{E}_J(|a_i|)$ where we fix the J and have already solved for the z_i will be thought of as a Morse function on this topological sphere (the reader unfamiliar with Morse theory should look at [213, 214], and the lecture notes by Hutchins are very approachable [215]). The main reason for using Morse theory is that it utilizes and analyzes the set of critical points of a function, and from this set the topology of the manifold can be reconstructed. For us, the topology is already known (it is a sphere), but the set of critical points is not. The set of critical points and gradient flows between them gives a model for the cohomology of the manifold, which in our case is known. Given a set of critical points we can ask if the set is consistent with the topology of the manifold. If it is not, we are missing critical points. Also, as J changes, the set of critical points can change dimension and how these changes can happen is understood in general. In our case, because of the extra symmetries of the potential, the critical points will exhibit also a representation of the symmetry group.

10.4 The case of 2×2 matrices

The case of $N = 2$ is the simplest we can analyze given the structure of our ansatz that is not completely trivial. The matrices take the form

$$X^+ = \begin{pmatrix} 0 & |a_1| \exp(i\omega_1 t) \\ |a_2| \exp(i\omega_2 t) & 0 \end{pmatrix}, \quad Z = \begin{pmatrix} z_1 & 0 \\ 0 & z_2 \end{pmatrix} \tag{10.46}$$

When we compute the equations that the z_i must satisfy for fixed a_i, J, we find that

$$0 = z_1 + |a_1|^2(-6 + 4z_1 - 4z_2) + |a_2|^2(-6 + 4z_1 - 4z_2) \tag{10.47}$$

$$0 = z_2 + |a_1|^2(-6 + 4z_2 - 4z_1) + |a_2|^2(-6 + 4z_2 - 4z_1) \tag{10.48}$$

Summing the two, we find that $z_1 + z_2 = 0$. We can substitute this result back to find that

$$z_{1,2} = \pm \frac{6(|a_1|^2 - |a_2|^2)}{1 + 8|a_1|^2 + 8|a_2|^2} \tag{10.49}$$

At this point it becomes clear that the expressions simplify if we consider the two variables $P = |a_1|^2 + |a_2|^2$ and $Q = |a_1|^2 - |a_2|^2$. This is because P is even with respect to the $\mathbb{Z}_2$ symmetry $|a_1| \leftrightarrow |a_2|$, and Q is odd. Thus, the symmetry algebra acts simply on the variables P and Q themselves. We find then that

$$\mathcal{E}(J, z_i(|a_i|), |a_i|) = \frac{J^2}{16P - 16Q} + \frac{J^2}{16(P + Q)} + \frac{32(P-1)Q^2}{8P + 1} + 2P \tag{10.50}$$

When we compute the equations that P, Q must satisfy, obtained by considering $\partial_{P,Q}E = 0$, it is convenient to eliminate the J dependence of one algebraic combination of these. After a bit of work, this is accomplished by considering

$$2PQ\partial_P E + (P^2+Q^2)\partial_Q E = \frac{4(4P-1)Q\left(32P^3-4P^2+P\left(32Q^2-1\right)+16Q^2\right)}{(8P+1)^2} \tag{10.51}$$

Notice that this factorizes, so there are three branches. One where $Q = 0$ identically, one where $P = 1/4$ identically and another one where

$$Q^2 = \frac{-32P^3+4P^2+P}{16(2P+1)} \tag{10.52}$$

which is positive only if $P \leq 1/4$.

Let us analyze the first one. We can substitute $Q = 0$ in E, to find that

$$E = \frac{J^2}{8P} + 2P \tag{10.53}$$

And the minimum occurs for $P \to J/4$ (here we have taken $J > 0$, and obviously P is positive since it is a sum of squares). We can then evaluate that for this solution

$$E = J \tag{10.54}$$

in the limit $J \to 0$, this solution reduces to the trivial solution where all matrices are identically zero. For the second solution, we take $P = 1/4$, and we find similarly that

$$E = \frac{J^2+\left(1-16Q^2\right)^2}{2-32Q^2} \tag{10.55}$$

which is of similar form if we use the variable $x = 1 - 16Q^2$ (this is, of the form $Ax + Bx^{-1}$). Again, the minimum occurs when

$$Q = \frac{\sqrt{1-J}}{4} \tag{10.56}$$

and we also find that $E = J$ identically. This is the solution where we choose to take $Q > 0$. There is a similar solution with $Q < 0$ that is a $\mathbb{Z}_2$ reflection of this solution. When $J \to 0$, this is the standard fuzzy sphere of 2×2 matrices. When $J \to 1$, this matches our other solution with $Q = 0$. The three solutions meet at $J = 1$. Beyond $J = 1$ this solution does not exist anymore.

In the third branch, we have that

$$E = \frac{2J^2(2P+1)}{(4P+1)(16P-1)} - 4P^2 + 9P - \frac{9P}{2P+1} \tag{10.57}$$

and it is easy to solve for J as a function of P (essentially solving $\partial_P E = 0$), giving us

$$J^2 = \frac{(1-P)P\left(64P^2+12P-1\right)^2}{(2P+1)^2(8P+1)} \tag{10.58}$$

So that we end up with a parametric solution $J(P)$, rather than the other way around. This can be inverted numerically. This only makes sense if $J^2 \geq 0$, so that necessarily $P \leq 1$, and remember also that $1/4 \geq P \geq 0$ from the reality of Q. But moreover, $|Q| \leq P$, and this restricts P to be bigger than $1/16$. Notice that when $J \to 0$, there are various values of P that can arise as roots. The only one that is new corresponds to $P = 1/16$. This is a fuzzy sphere at half radius. This can be easily understood if we make an ansatz of spherical symmetry for a saddle point. In this case the matrices $X,\ Y,\ Z$ are all proportional to the corresponding Pauli matrices with proportionality constant r. Because the energy for a static configuration is quartic in the matrices, and we have that $E = 0$ at $r = 0$ and $E = 0$ at $r = 1$, and always $E \geq 0$, then the energy must be proportional to $r^2(1-r)^2$. This has a maximum at $r = 1/2$, which is the sphere at half radius. This solution also matches the solution at $Q = 0$ that we already had when we set $P = 1/4$. There is similarly a reflected solution with $Q < 0$, where we take the other square root branch cut of equation (10.52). The new solution of the fuzzy sphere at half radius migrates to higher angular momentum as we increase P from $1/16$ to $1/4$ and is a saddle point. Therefore it has Morse index one. This solution and the one that is reflected by taking $Q \to -Q$ can cancel the two minima from the BPS solution as they meet at $J = 1$ with the trivial solution that has $Z = 0$ throughout.

The full set of solutions is depicted in Figure 10.1. There we can see that for low angular momenta there are five critical points. Three are minima and two are saddles with Morse index one. The saddles and two of the minima are reflected into each other by the $\mathbb{Z}_2$ symmetry, and one minimum is at the fixed point. The two saddles and two of the minima annihilate each other when $J = 1$. Because the minima that annihilate with the saddles are BPS, the saddles need to approach the extremal limit and thus must touch the fixed point set, because one can not descend further from the saddle to the fixed point otherwise.

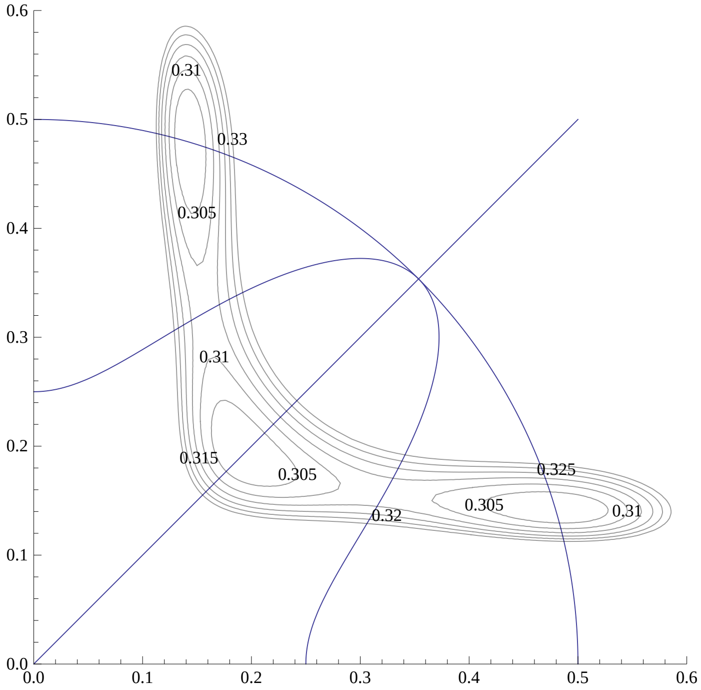

Figure 10.1: Parametric plot of the solutions for a_1, a_2 derived either from equation (10.52), from $P = 1/4$ or from the solution $Q = 0$ with $a_1 = a_2$. Superposed we find level sets of the energy function at $J = 0.3$, with the energy levels shown, and we see that the curves pass through the critical points of the energy function.

10.5 The case of 3×3 matrices

The equations that the a_i and z_i need to satisfy can be directly derived from (10.43) and (10.41). We have not been able to solve them algebraically in general, although there is one trivial solution with $z_i = 0$ and all a_i equal to each other. This solution exists for any value of the angular momentum (and actually all values of N as well). Our strategy for solving the problem is to start with known solutions at $J = 0$ and perturb them numerically slowly by varying J until a new solution near the old one is found. Because the solutions are saddle points of the energy function, which is considered as a Morse function, small perturbations of the function preserve the saddles in general. These are saddles for any J until a subset of the saddles collides. A saddle with index m can be annihilated by a saddle of index $m+1$ or $m-1$ [2].

The obvious solutions at $J = 0$ are the fuzzy sphere vacua. For any such fuzzy sphere with $k \times k$ matrices, we can also find an unstable fuzzy sphere at half size, which is analogous to the one we found for 2×2 matrices. We can then combine these solutions together into new solutions. The reason for this is that in any fuzzy sphere for $k \times k$ matrices we have $|a_k|^2 = 0$ and the matrix is upper triangular. This is true regardless of if the fuzzy sphere is stable or unstable. We can then mix and match these solutions and put them in some order. For 3×3 matrices this does not matter as there are not too many ways of partitioning 3 into integers, but the strategy works in general for other values of N. The value $J = 0$ is technically a singularity of the family of Morse functions because the fuzzy sphere vacua end up with some $a_i = 0$, and we argued before that these points need to be identified with each other in the one point compactification of the open intervals $|a_i| \in (0, \infty)$ to get a sphere topology. Numerically, we can start with these solutions and perturb entries that start at zero by a small amount, while at the same time turning on a small amount of angular momentum. All solutions persist under this procedure, so we can safely describe them by taking the limit $J \to 0$. We also need to count them with multiplicity, because we have our dihedral group of (quantum) symmetries that let us find new solutions of the a_i by permuting them clockwise, or by reflection. This is described in Table 10.1 If we take the solutions as above and we compute the Morse polynomial with just

---

[2] Recall that the index of a critical point is number of negative eigenvalues of the Hessian at that point.

Splitting	Stability	Morse Index	Multiplicity	Unbroken Quantum Symmetry
1+1+1	S, S, S	0	1	D_3
2+1	S, S	0	3	$\mathbb{Z}_2$
2+1	U, S	1	3	$\mathbb{Z}_2$
3	S	0	3	$\mathbb{Z}_2$
3	U	2	3	$\mathbb{Z}_2$

Table 10.1: Table of sphere solutions. The splitting indicates the size of matrices of the fuzzy spheres, S, U indicates if they are stable BMN vacua, or unstable spheres at half size, the Morse index is the number of negative modes of the Hessian (after perturbing by a small j, and the multiplicity is the number of copies of the solution that are obtained from using the group symmetry actions on a given solution.

these solutions, we find that

$$M_{trial}(t) = 1 + 3 + 3t + 3 + 3t^2 + t^3 = 7 + 3t + 3t^2 + t^3 \tag{10.59}$$

where the last entry (the one for t^3) corresponds to the maximum of the energy function at infinity. The Poincare series of the three sphere is

$$P(t) = 1 + t^3 \tag{10.60}$$

The Morse inequalities require that $M_{trial}(t) - P(t) = (1+t)Q(t)$ where Q should be a polynomial with positive integer coefficients. In particular we should have that $M(-1) = P(-1)$. This is not the case. This indicates that we are missing critical points of the energy function. Since all the solutions above have an enhanced $U(1)$ rotation symmetry, it makes sense to look for solutions with such a rotation symmetry for more saddles. We do this graphically in Figure 10.2. In the figure the z_i have already been solved for, but the $|a_i|$ are variables.

We see from the figure that there are additional saddles that are not reflection

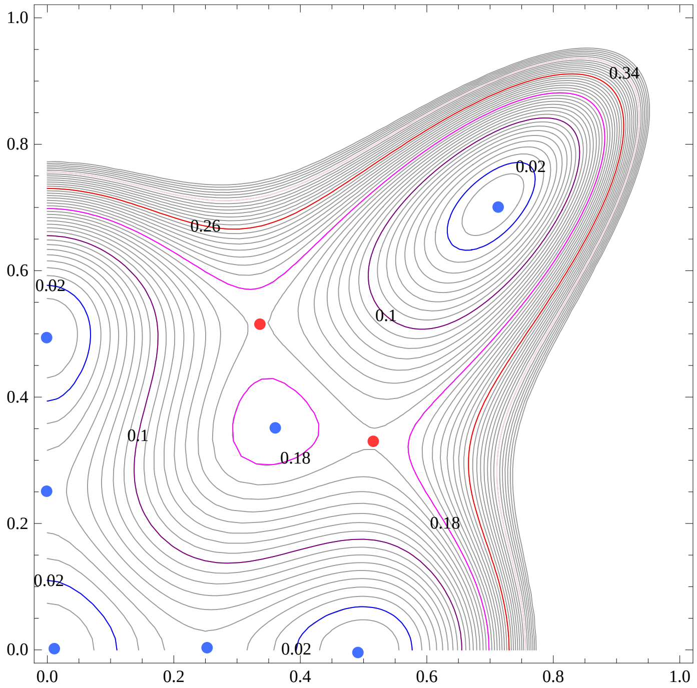

Figure 10.2: Energy function at $J = 0$, $|a_3| = 0$. The axis indicate $|a_1|$, $|a_2|$, and the colored contours have their energy values indicated. The solid dots indicate approximate positions for the various saddles. The solid dots in red indicate new saddles that do not arise from collections of round fuzzy spheres.

symmetric with respect to the diagonal, nor are they on the edges of the graph. These new saddles have index 1, and the orbit under the symmetry group produces 6 saddles in total, and no unbroken symmetry. These would add an additional $6t$ to $M_{trial}(t)$. With this additional set of solutions we find that

$$M(t) = 1 + t^3 + (1 + t)(6 + 3t) \tag{10.61}$$

and now we satisfy the Morse inequalities. This means that it is consistent if these are all the saddle points and we are not missing any.

We have not found any other saddle point numerically at $J = 0$. If they exist they should have all three $|a_i| \neq 0$. It is possible to use this information to show that no such saddle can exist, and not just for $N = 3$ but for all N.

The energy function is given by

$$\mathcal{E}(J, |a_i|, z_i) = \frac{J^2}{8N^2} \sum_{i=1}^{N} \frac{1}{|a_i|^2} + \sum_{i=1}^{N} \frac{1}{2}(z_i + 2|a_{i-1}|^2 - 2|a_i|^2)^2 + 2(1 + z_{i+1} - z_i)^2 |a_i|^2 \tag{10.62}$$

The equations of motion for the a_i yield

$$\frac{J^2}{4N^2|a_i|^3} = 4|a_i| \left((1 + z_{i+1} - z_i)^2 + (z_{i+1} - z_i) + 2(-|a_{i-1}|^2 + 2|a_i|^2 - |a_{i+1}|^2)\right) \tag{10.63}$$

Next we suppose that $|a_i| \neq 0$ for all i at $J = 0$. The first term of (10.63) vanishes and we may divide the rest by $4|a_i|$. We are left with

$$0 = (1 + z_{i+1} - z_i)^2 + (z_{i+1} - z_i) + 2(-|a_{i-1}|^2 + 2|a_i|^2 - |a_{i+1}|^2) \tag{10.64}$$

Summing over all i we have

$$0 = N + \sum_{i=1}^{N} (z_{i+1} - z_i)^2 \tag{10.65}$$

Since the summation is non-negative and N is positive, we have reached a contradiction. Thus $|a_i| = 0$ for at least one i at $J = 0$.

The equation of motion for the z_i yields.

$$0 = z_i - 4|a_i|^2 \left(\frac{3}{2} + z_{i+1} - z_i\right) + 4|a_{i-1}|^2 \left(\frac{3}{2} + z_i - z_{i-1}\right) \tag{10.66}$$

Summing these equations yields a traceless condition, $\sum_i z_i = 0$. This had to be true because $\dot{P}_Z = 0$ and the trace of the matrix model is just a harmonic oscillator.

This feature has the following implication. When we perturb away from $J = 0$, the $|a_j|^2$ will be modified very slightly (at order J^2), but for the one that begins at zero $|a_\ell|^2$ it is different. In the kinetic term we will have a singular term, so that the energy function will look like

$$\mathcal{E}(J) \simeq \mathcal{E}(0) + \alpha |a_\ell|^2 + \frac{J^2}{8N^2|a_\ell|^2} \tag{10.67}$$

and clearly the $|a_\ell|$ that minimize this are such that $|a_\ell|^2 \simeq J/\sqrt{8N^2\alpha}$. When we plug this into the energy function we find that there is always a term linear in J. This means that the fuzzy configuration built with our ansatz can never be considered as a rigid body; for rigid bodies the energy goes like J^2, where the coefficient of proportionality depends on the moment of inertia. The fuzzy configurations rotate by turning on wave-like excitations on the sphere. This is exactly as expected for a membrane.

A presentation of the solutions found at $J = 0$ for 3×3 matrices, followed as we change J is shown in Figure 10.3. As shown in the figure, there are many phase transitions. The one marked A corresponds to two saddles of index one and one saddle of index 2 merging into a single saddle of index 1. This is repeated in three different locations due to the symmetry operations. The unbroken symmetry of the incoming saddles of index one changes from all symmetry broken to a saddle with a $\mathbb{Z}_2$ symmetry unbroken. It also shows that the saddle of index

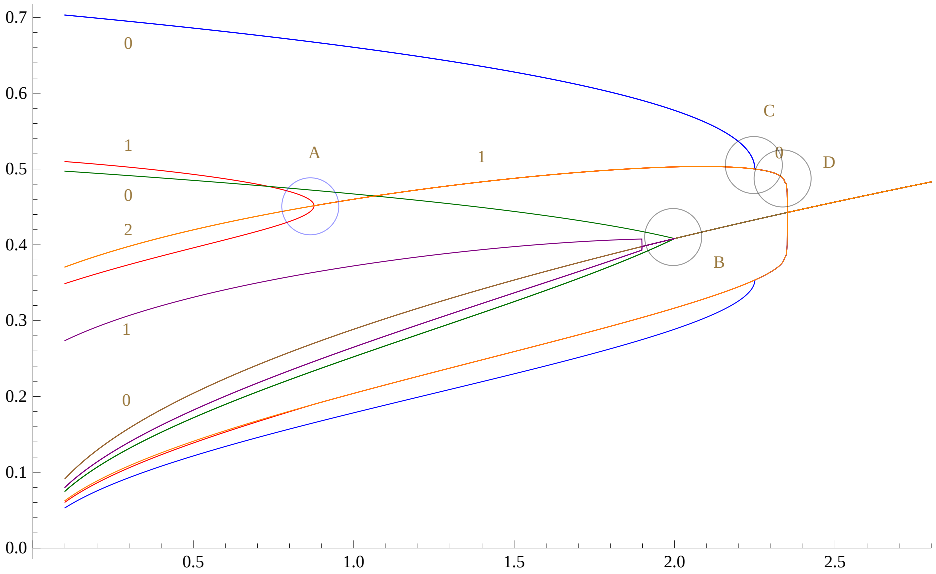

Figure 10.3: Phase diagram of solutions as a function of J on the abscissa, and the $|a_i|$ are plotted on the ordinate. We follow the solutions slightly perturbed from $J = 0$. Shown are the values of the $|a_i|$. Different solutions for $|a_1|$, $|a_2|$, $|a_3|$ are colored differently, but all values are shown in the same color for the same solution. The numbers attached to saddles are the Morse index. Phase transitions where solutions merge or end are shown as A, B, C, D. The ones that are not marked below the maximal symmetry solution are C, D also.

one ends smoothly and without corners. Actually this is what is expected in general: saddles should end smoothly and without corners as we pass through critical values of J. The phase transition marked as C is inconsistent as shown: a single saddle of index zero and a saddle of index one can not annihilate into a saddle of index zero (this would violate the Morse inequalities). This means that there is a solution missing. Similarly, in phase transition D, the line actually ends. The vertical line down is an artifact of joining the numerical solutions, and instabilities of the numerical method when the Hessian is degenerate. This solution ending also indicates a missing solution, because of inconsistency with the Morse inequalities. Finally, at the transition B we see that a set of three saddles of index zero and index one merge with the saddle with all symmetries unbroken. Although this is in principle allowed, it is not smoothed out like in transition A, or as one would expect from transition C once a solution is found. We can conjecture that the solutions that correspond to the green and purple lines in the figure actually continue to the other side. Because of the way solutions are merging and the dihedral symmetry being restored, transition B is a multi-critical point. It is natural to believe that the solutions that are continued end on the other inconsistent transitions. They should have also an unbroken $\mathbb{Z}_2$ symmetry each and come in three copies. Because of the unbroken $\mathbb{Z}_2$ symmetry, two of the $|a_i|$ should be equal to each other. This makes it possible to guess the solutions by looking at energy contours in a two dimensional plot where we set $|a_3| = |a_2|$ a bit after the transition at $J \simeq 2.1$. We should be looking for a BD line of index one (it's the only way we can cancel a solution of index zero). The green line actually saturates the BPS inequality, and this should persist in the analytic continuation to the right. This indicates that there should be a saddle of index zero joining BC. This process is depicted in Figure 10.4. Once we include the new saddles after this point, we can complete the phase diagram in Figure 10.5. What we see from the figure is that first, there is a maximal angular momentum after which there is only one solution, and this solution preserves the maximal dihedral symmetry. Second, the trajectory of the maximal sphere goes through a phase transition at a finite J before reaching this maximal angular momentum. We have checked that after the first transition the solution stops being extremal (BPS), even though it is a local minimum. This means that the corresponding phase can be considered metastable from energetic considerations.

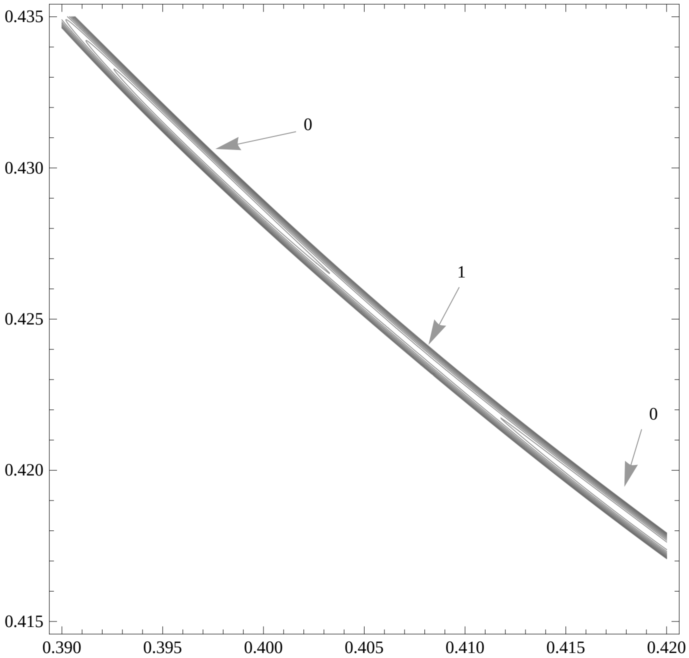

Figure 10.4: Energy contours in $|a_1|$, $|a_2| = |a_3|$ at $J = 2.1$. The saddles are hard to see. The energy contours have energies starting at $E = 2.1$ and spaced at $\delta E = 2 \times 10^{-7}$ showing ten contours.

At the maximal angular momentum, it becomes classically unstable. The jump from the metastable to the stable configuration is a first order transition, but at the place where it changes from being BPS to being non-BPS, we have coexistence of a second order phase transitions and a first order phase transition with the same energy. This degeneracy is expected to be lifted by quantum corrections. At small $\hbar$ we expect that the phase diagram has the same structure we have shown, because it is controlled by topological aspects of a Morse function. This is similar to the transition found in [216], where studying spherical D-brane configurations, beyond the maximal giant graviton there is a non-BPS metastable D-brane solution that continues for a while with larger R-charge (this branch was first found in [72], but the stability analysis was not done), and the family of solutions ends in a

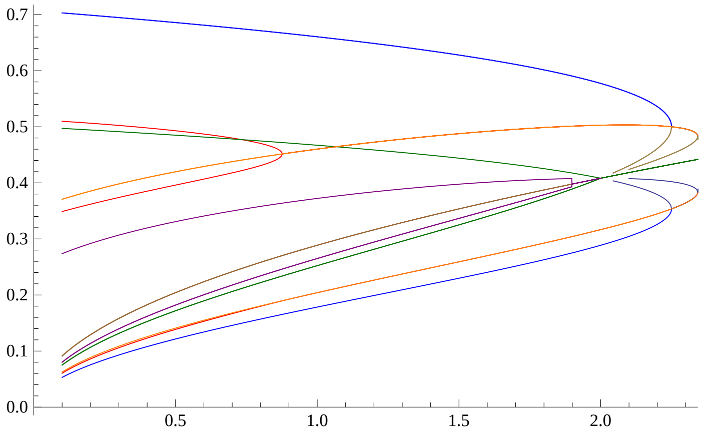

Figure 10.5: Full phase diagram of solutions as a function of J on the abscissa, and the $|a_i|$ of a single solution are plotted on the ordinate.

transition that should take us to another branch. This transition should be where the metastability is lost.

10.6 Other Examples

Our next task is to understand how to go beyond $N = 3$. Armed with the information that at least one of the $|a_i|$ needs to be zero at $J = 0$, we can begin by looking at saddles for smaller N and fit them into saddles for N by either bordering by zeros, or by taking direct sums of solutions for smaller N such that the rank adds up to N. We choose these saddles to have $|a_k| = 0$ for the entry on the first row at the bottom corner. These will all fit the ansatz where X^+ is upper triangular, bordering the diagonal, and with a zero in the bottom corner. This actually always produces correct solutions at $J = 0$. From equation (10.66), we find that for the values of $|a_i|$ such that $|a_i| = 0$, z_i only depends on the previous ones, and therefore decouples from z_{i+1}, and similarly z_{i+1} will be related to z_{i+2},

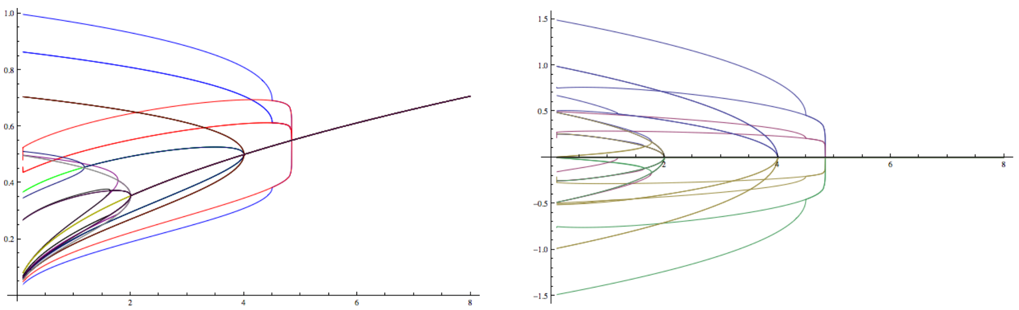

Figure 10.6: On the left, partial phase diagram of 4 × 4 solutions as a function of J on the abscissa, and the $|a_i|$ of a single solution plotted on the ordinate in the same color. Notice the similarity of the transitions to the ones for 3 × 3 matrices in Figure 10.3. On the right, we evaluate also the z_i values for the given solution of the $|a_i|$. The figure is not symmetric under $z_i \to -z_i$ which indicates that many of the phases are not 'parity invariant' with respect to the dihedral discrete symmetry group.

but not the other ones. Secondly, the equations for $|a_i|$ are trivially satisfied in this case because of the $|a_i|$ appearing in front of it in equation (10.63). The rest of the equations are satisfied if they were satisfied for smaller values of N. This gives us an ample trove of solutions with which we can explore the phase diagram. This is explicitly shown in Figure 10.6. The same structure appears qualitatively. There is a maximal angular momentum beyond which only the trivial solution exists, and it ends in a first order phase transition with a metastable phase. Because there are many more solutions at $J = 0$ at each N (the number is bounded below at least by twice the partitions of N), the full phase diagram is more complicated as we increase N, and it is clear from the Morse analysis that we are missing quite a number of saddles. Although two new solutions always exists for any N, the maximal fuzzy sphere and the sphere at half size, one can expect in general that there are quite a number of intrinsically new (indecomposable) solutions that appear at any N.

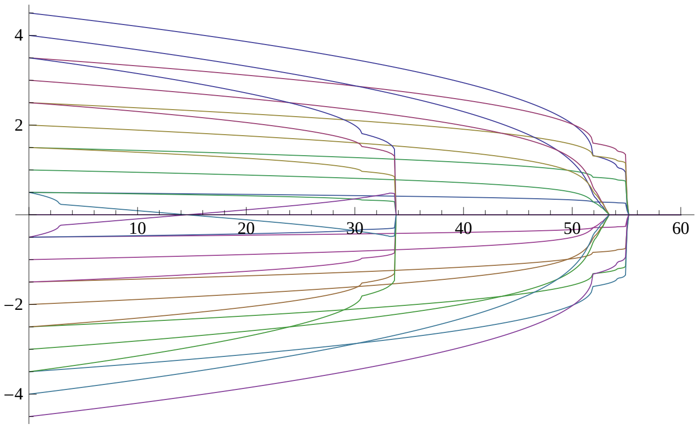

Figure 10.7: We evaluate $z_i(J)$ for three different solutions of 10×10 matrices, the maximal fuzzy sphere, a near maximal fuzzy sphere bordered by zero, and a solution for a fuzzy sphere of spin $7/2 \oplus 1/2$.

For illustration purposes, we also show some of the solutions for 10×10 matrices in Figure 10.7. This shows the procedure for building up solutions by bordering by zero or adding up previous solutions in more detail. It is clear that the full phase diagram is quite complicated, some of the solutions ending in first order phase transitions, and some others ending in what appear to be multi-critical points. Here we basically show that the problem is amenable to computer calculations. We should point out that for larger N we do not have a good strategy to search for the intrinsically new solutions yet. The graphical method that worked for $N = 3$ is unsuited for higher dimensions, as we can not visualize the data.

10.7 Large N

An interesting way to proceed to large N is the following. Since the energy function in equation (10.41) is of nearest neighbor type, we can think of it as a discretized integral of an energy density. Indeed, this is what the interpretation of the solutions as of matrix mechanics as discretized membranes indicates we should be doing [105, 106]. With that in mind, we want to replace $z_i \to \tilde{z}(\theta)$ and the same for $|a_i|^2 \to |\tilde{a}|^2(\theta)$, where θ is a periodic coordinate with period one, rather than a discrete set with N elements. We basically take $i \simeq N\theta$. Then expressions of nearest neighbor differences get replaced by derivatives $z_{i+1} - z_i \to N^{-1}\partial_\theta \tilde{z}$. We also need to remember that the maximal fuzzy spheres are of size N when we have N D0-branes, and we want to rescale this out of the energy. Therefore, we write $z_i \simeq Nz(\theta)$, and $|a_i|^2 \simeq N^2|a|^2(\theta)$ and $\sum_i = N\int d\theta$. When we do this, we find that

$$V_{pot} = V(|a_i|, z_i) \to N^3 \int d\theta \left[\frac{1}{2}\left(z - 2\partial_\theta|a|^2\right)^2 + 2\left(1 + \partial_\theta z\right)^2 |a|^2\right] \tag{10.68}$$

and similarly, the terms that contain angular momentum, when we rescale $J \to N^3\tilde{j}$, give us

$$E_{kin} = N^3 \int d\theta \frac{\tilde{j}^2}{8|a(\theta)|^2} \tag{10.69}$$

The point is that in this rescaling, we get a common factor of N^3 in front of the energy that can be dropped to obtain a classical membrane energy which is independent of N. The value of N can effectively be changed by changing the periodicity of θ without changing the energy density further. We use the relation $N_{tot} = N\int d\theta$ to convert the changing period of θ into a different value of N, and we can always change scales by taking $\theta \to \alpha\theta$, $z \to \alpha z$ and $|a|^2 \to \alpha^2|a|^2$. The energy function also has a $\mathbb{Z}_2$ symmetry where we change $z \to -z$ and $\theta \to -\theta$.

The energy function is now a local integral of the functions z, a and their derivatives. The condition to be a critical point of the effective energy is a pair of differential equations, one for z and one for a that come from the variational principle. A complete set of initial conditions requires specifying $z(0),\ a^2(0),\ \partial_\theta z(0),\ \partial_\theta a^2(0)$. These can be evolved in θ, but the trajectories need to be periodic with a fixed prescribed period (which we are choosing to be set equal to one). This effectively quantizes the set of possible solutions so that they are discrete.

The system is translation invariant in θ and so there is a trivial one parameter family of solutions that is obtained by translation. This becomes a $U(1)$ symmetry that was only realized as a $\mathbb{Z}_N$ quantum symmetry at finite N, and which is spontaneously broken on most of the solutions. Because $|a^2|$ is bounded for interesting solutions, we can always start out from a place where $\partial_\theta |a|^2 = 0$.

The fuzzy spheres at zero energy appear at $\tilde{\jmath} = 0$, and are at the zeros of V_{pot}. These occur at

$$\partial_\theta z = -1 \tag{10.70}$$

$$\partial_\theta |a|^2 = \frac{1}{2} z \tag{10.71}$$

and satisfy a first order set of equations (typical of BPS states), rather than the usual second order equations. At finite N, the Z matrix for fuzzy spheres is the matrix of spins in an N dimensional representation of $\mathfrak{su}(2)$. Consecutive matrix elements differ by 1 and so the equation for $z(\theta)$ is capturing this effect. If we start from $z = 0$ at $\theta = 0$ (so that $z(\theta) = -\theta$), and $|a|^2(0) = a^2_{max}$, it is straightforward to integrate these and find that

$$\partial_\theta |a|^2 = -\frac{1}{2}\theta \tag{10.72}$$

so that

$$|a|^2(\theta) = a_{max}^2 - \theta^2/4 \tag{10.73}$$

We hit $a^2(\theta_0) = 0$ at some finite value of θ_0. This is a singular point in the differential equation system because the effective derivative term squared for z vanishes at this point. We are allowed to have large jumps in z at this point because there is no energy cost to it. This way we recover that the set of possible ground states is a collection of fuzzy spheres. Quantization then requires that each of these have an integer amount of D0 brane charge. This is reminiscent of the LLM droplet picture [77], where quantization of the area arises from a Dirac quantization condition. Notice that the solution can also be written as

$$|a|^2(\theta) = a_{max}^2 - z^2(\theta) \tag{10.74}$$

which gives $|a|^2 + |z^2| =$ const, as one expects from a sphere written in cylindrical coordinates (the additional angle is associated to the $\mathbb{Z}_N \to S^1$ rotational invariance of the set of solutions we are considering in the large N limit).

At this point, going beyond the BPS solutions, we want to change perspective and think of the variable θ as a time coordinate, and the effective energy function we had before as a Lagrangian whose variational principle gives some non-trivial equations of motion. Using this change of point of view, we see that the Lagrangian has a (repulsive towards infinity and the origin of $|a|^2$ when $\tilde{j} \neq 0$) potential of the form

$$V_{eff} \simeq -\frac{1}{2}|z|^2 - 2|a|^2 - \frac{\tilde{j}^2}{8|a|^2} \tag{10.75}$$

there is a non-trivial curved metric

$$ds^2 = 4(d|a|^2)^2 + 4|a|^2 dz^2 \tag{10.76}$$

with translation symmetry in z and a non-trivial magnetic potential associated to the one form

$$\mathcal{A} = -2zd|a|^2 + 4|a|^2 dz \tag{10.77}$$

which in these coordinates produces a constant magnetic field. Notice however, that because the metric is curved, the magnetic field per unit normalized area actually changes and becomes weak when $|a|^2$ gets large. The magnetic field will try to bend trajectories into confining circular orbits, but it has to compete with a repulsive potential that tries to destabilize the system. Also, the metric has a scaling symmetry where $|a|^2 \to \gamma^2|a|^2,\ z \to \gamma z$. The metric is also positively curved away from $|a|^2 = 0$, which is a singularity. If we think of the z as an angle coordinate and the $|a|^2$ as a radial variable, then the curvature wants to repel geodesics from hitting $|a|^2 = 0$.

The obvious critical point of the equations of motion where nothing moves is at the maximum of the potential and is in unstable equilibrium. This produces a periodic orbit for any period. Other periodic orbits need to be found by trial and error, and once a sufficiently approximate solution of the periodicity condition is found it is possible to zoom into it.

Particularly simple examples of this search can be performed if the solutions are reflection symmetric under $z \to -z$. Then the solution can be characterized by the value of $|a|^2(\theta_0)$, when $z(\theta_0) = 0$, and the condition for symmetry forces

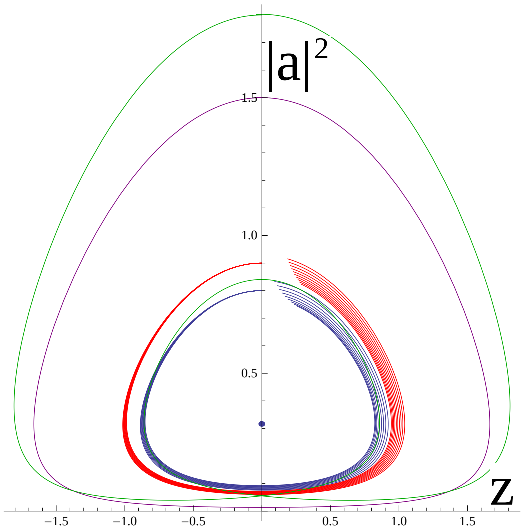

Figure 10.8: Parametric plots of $(z(\theta),\ |a|^2(\theta))$ for various initial conditions at fixed value of $\tilde{\jmath}^2 = 0.1$. We show a BPS trajectory in purple, and examples of scanning over parameters to find periodic trajectories in blue and red. The fixed point is marked. The green solution which was found by scanning winds twice around the fixed point and it is not BPS.

$\partial_\theta |a^2|(\theta_0) = 0$. We can then move the velocity of $\partial_\theta z(\theta_0) = \xi$ as a scanning parameter. Some examples of this procedure are depicted in Figure 10.8.

When the orbit returns to $z(\theta_1) = 0$ at some later time (not necessarily the first time around), we can then compute $\kappa = \partial_\theta |a|^2(\theta_1)$ from solving the equations of motion, and as we scan over ξ we look for sign changes in κ. We can then zoom in for the parameter ξ that solves the periodicity condition. The point of intersection can be the same one as before or it can be different. If it is different we double the time of this half orbit, and it becomes periodic.

It is also interesting to study the first order differential equations that arise for states that saturate the BPS inequality at finite J. These equations are given by

$$\partial_\theta z = -1 + \frac{\tilde{\jmath}}{4|a|^2} \tag{10.78}$$

$$\partial_\theta |a|^2 = \frac{1}{2} z \tag{10.79}$$

and are obtained from requiring the vanishing of the squares in equation (10.7) after substituting our ansatz. These can in turn be derived from a variational principle for an auxiliary Lagrangian of the form

$$L = \dot{q}^2 - q + \frac{\tilde{\jmath}}{4} \log q \tag{10.80}$$

where $q = |a|^2$, and z plays the role of the canonical conjugate of q (namely $z = 2\dot{q} = p_q$). The effective one dimensional potential $\mathcal{U}(q) = q - \frac{\tilde{\jmath}}{4} \log q$ is bounded from below and goes to infinity at $q \to 0$ and also at $q \to \infty$, so it produces automatically closed periodic orbits without self intersections. There is also only one minimum at $q = \tilde{\jmath}/4$.

These trajectories are interpreted geometrically as multiply wrapped tori that wrap the same torus, where the wrapping number is the number of times we have to go around the orbit so that the period matches the number of D0-branes.

The period of the orbit can be calculated using standard techniques as follows

$$\Theta = \oint \frac{dq}{\dot{q}} \propto \oint \frac{dq}{z} \tag{10.81}$$

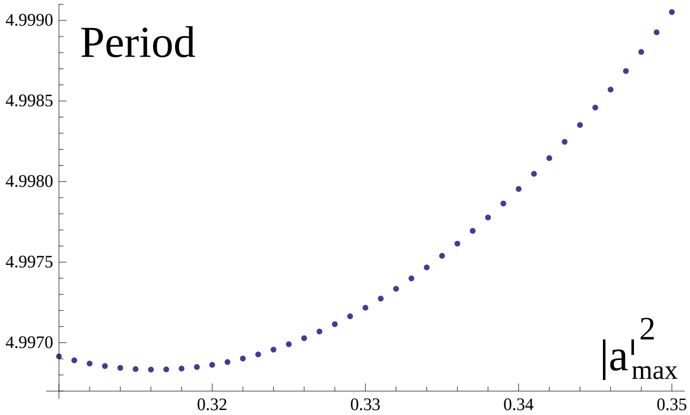

Figure 10.9: Period of an orbit as a function of $|a|^2_{max}$ at $z = 0$, and at fixed $\tilde{\jmath}^2 = 0.1$.

The integral is over a periodic orbit characterized by the parametric equation

$$\mathcal{W} = \dot{q}^2 + q - \frac{\tilde{\jmath}}{4}\log(q) = z^2 + q - \frac{\tilde{\jmath}}{4}\log(q) \tag{10.82}$$

where $\mathcal{W}$ is a constant of integration (the energy associated to the Lagrangian function L). This solves for z as a function of q readily. Indeed, the parameter $\mathcal{W}$ this way defines a curve with a differential, and then Θ is the period integral over the differential. We have to be careful with this interpretation since the curve is real analytic and not a complex curve. More general solutions for the BPS states in the continuum limit were found in [202], and they similarly show up with various logarithms [3].

Because $\mathcal{U}(q)$ has a non-trivial third derivative about the minimum, it is possible to show that the period for orbits very near the fixed point have a decreasing period as we go away from the fixed point, and for large orbits, the period increases again. This is depicted in Figure 10.9.

---

[3] The variable W in their work is related to q in ours, with $q \simeq W^2$.

Since we need to fix the period to fix the number of D0-branes, while we are allowed to vary $\tilde{\jmath}$, this shows that for some values of $\tilde{\jmath}$ there is more than one non-trivial solution (the trivial fixed point orbit can have any period we want it to). The larger solution is interpreted as a fat torus which in principle can become very large as we decrease $\tilde{\jmath}$ going smoothly to the fuzzy spheres in the limit $\tilde{\jmath} \to 0$ while the small one is a thin torus that gets thinner and disappears into the trivial solution at finite $\tilde{\jmath}$.

As we increase $\tilde{\jmath}$, we increase the period of the orbits near the fixed point, as well as the minimal period. Eventually the period is too long and the BPS solutions with the fixed period we want disappear. This behavior can already be seen for the phase diagram of 3×3 matrices in Figure 10.5, where one of the new family of minima joining transitions B, C in Figure 10.3 plays the role of the small torus solution whereas the maximal fuzzy sphere family plays the role of the large torus. This phenomenon can happen for any multiply wound torus in the same way. At the transition C two BPS minima end together by joining with a saddle and becoming a non-BPS minimum. Hence, it would not be captured by the BPS solutions we are finding.

10.8 Topology Change

Now that we have the solutions for the matrix ansatz, even if computed numerically, we can analyze the geometry of the resulting matrix configurations as membranes using the ideas developed in Chapter 7. The main calculational tool we use is the effective Hamiltonian (7.7). We characterize the brane probe by the vector $\vec{\xi} \in \mathbb{R}^3$. Again, the effective Hamiltonian is given by

$$\hat{\mathcal{H}}(\vec{\xi}) = \sum_{i=1}^{3} (X_i - \xi_i \mathbf{1}_{N\times N}) \otimes \sigma^i \tag{10.83}$$

A zero eigenvalue occurs at $\vec{\xi}$ exactly when $\det(\hat{\mathcal{H}}(\xi)) = 0$. At this place, the determinant changes sign. We can therefore plot the level set $\det(\hat{\mathcal{H}}(\xi)) = 0$ and standard numerical algorithms can be used to determine this locus. Since this is a polynomial equation in real variables, the corresponding surface is algebraic in nature. In contrast, for the BPS solutions at large N, we get a surface that also contains the log function in equation (10.82). In this sense, there is a measurable finite departure from the finite N and the infinite N limit. We can think of this procedure as measuring quantum geometry corrections to large N. The most glaring one is that the rotation symmetry group of the solution is reduced from $U(1)$ to $\mathbb{Z}_N$, so the matrix solutions are lumpy, and the lumpiness is non-perturbative in N; we get exactly N lumps.

Our goal stated at the beginning of the paper is to analyze the topology transition from a sphere to a torus. As we discussed in Section 10.7, the topology change at large N is instantaneous as soon as we turn on a non-zero value of the angular momentum $\tilde{\jmath}$. As seen for the BPS trajectory in Figure 10.8, this proceeds by forming a very thin funnel between the north pole and the south pole. This funnel represents a condensate of strings, as the picture of [112] suggests we should have. From here we ask a few natural questions. The first one is if the topology change is apparent as a phase transition in the bosonic set of degrees of freedom, that is, if we have to go beyond a phase transition in Figures 10.5, 10.6, or 10.7.

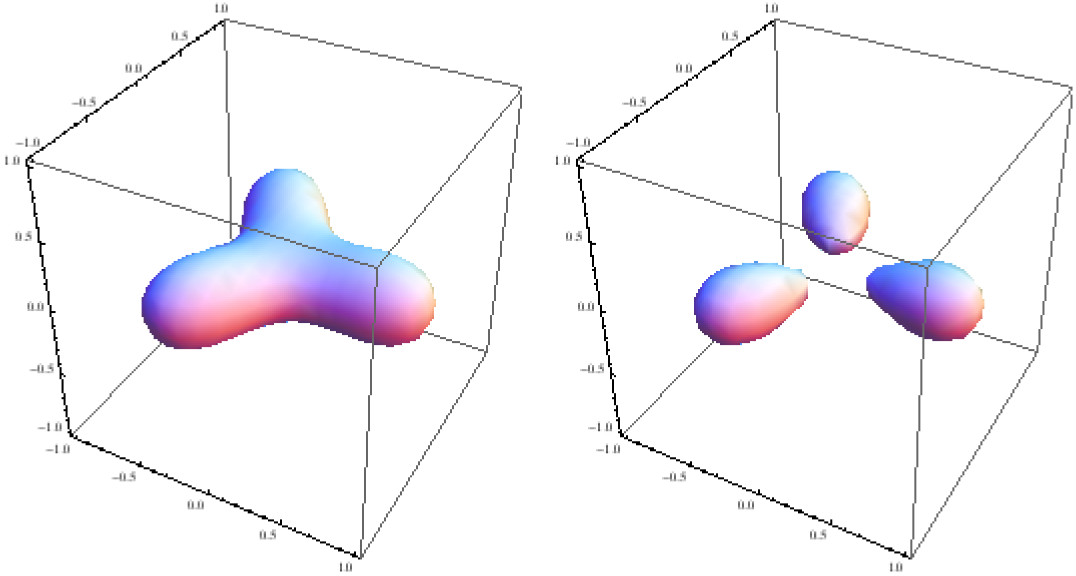

Figure 10.10: Transition from a deformed sphere to three small spheres for the case of 3×3 matrices. The values are at $J \simeq 1.9$ and $J \simeq 1.99$ for the maximal sphere.

The second question is if the transition is instantaneous or not. Lastly we ask what happens also when the torus gets very thin (as suggested by the thin ring solution in the continuum limit).

We do not find tori for either 2×2 or 3×3 matrices. This is shown in Figure 10.10. The transition in topology is from a single sphere to three different small spheres. This can be understood as a transition from a membrane to a collection of separated D0-branes that have been puffed up a little bit from having some off-diagonal excitations, rather than pure D0-branes where the ansatz is diagonal. Incidentally, in the trivial configuration one can show that Z commutes with X^+ and X^- and they actually commute with each other. This represents a collection of separated D0-branes, because the matrices can be diagonalized simultaneously. This is the same type of interpretation as in the BFSS matrix theory [107].

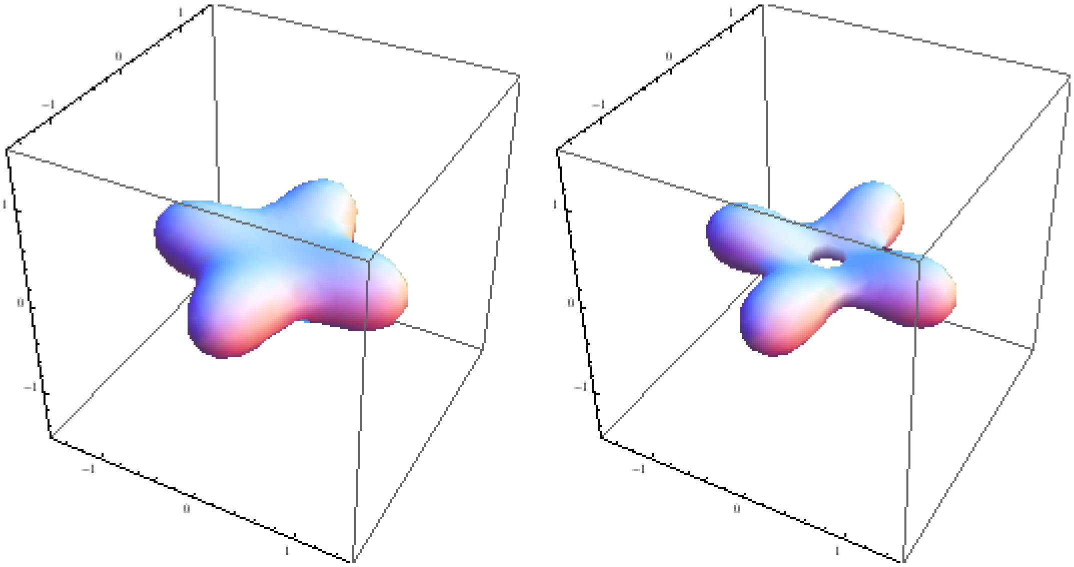

Figure 10.11: Transition from a very distorted sphere to a very distorted tours for 4 × 4 matrices. The values are at $J \simeq 4.24$ and $J \simeq 4.31$ for the maximal sphere.

The topology transition depicted in Figure 10.10 occurs before any singularity of the phase diagram in Figure 10.3 is encountered, but for the values of J given, it is close to the transition. The same procedure for the case of 4 × 4 matrices is depicted in Figure 10.11 where we see a sphere transitioning to a torus near the phase transition for the maximal sphere, but before it. We saw a very similar phase transition in Section 7.3.2. After all, the deformations there take the same form as our ansatz here. The only difference is that the deformation is controlled by the equations of motion. That is, the deformation is not arbitrary and these tori are present in the phase space of the BMN matrix model.

From these examples it should be clear that as far as the bosonic degrees of freedom are concerned, the change of topology from a sphere to a torus is smooth. Moreover, it does not occur immediately as in the large N limit. The fermions do detect the topology change. The tori that are obtained this way for the maximal sphere for such small values of N are very distorted. This should improve as we increase N.

One could also analyze the geometry and topology in terms of the ideas of fuzzy Riemann surfaces found in [130, 127]. For the analysis of topology, one uses properties of the eigenvalues of Z interpreted as a Morse function. This only works for very large N. As far as the geometry is concerned, we find that the finite matrices for some sufficiently classical states (at sufficiently large N again) would give rise to fuzzy approximations to (10.82) for some values of W, where $q \simeq (X^+X^-)$ is interpreted as a matrix and is a normal ordered form of the product. These solutions are not algebro-geometric in nature because of the logarithm. In this case q and Z commute and can be thought of as classical variables on the torus that can be constrained by an equation. Deviations from satisfying the precise equation $W = z^2 + q - 1/4\tilde{\jmath}\log(q)$ for fixed W should then be interpreted as "quantum corrections" in $1/N$. These are not quantum due to a non-trivial value of the Planck constant $\hbar$, but instead should be thought of as quantum corrections to geometry due to the discrete nature of the D0-brane charge. These corrections are due to the small size of the M-theory circle in the DLCQ limit [217]. Here we take the DLCQ of the plane wave geometry.

10.9 Discussion

We have analyzed a particularly simple set of periodic classical solutions of the $SO(3)$ sector of the BMN matrix model. The solutions are periodic in time modulo gauge transformations. They are also required to preserve the maximal discrete subgroup of rotations along the axis of rotation that is allowed by the discreteness of the matrices, namely a $\mathbb{Z}_N$. At large N, a $U(1)$ of rotations is recovered, so if the solutions have a continuous limit, they go to a rotationally invariant configuration. Not all solutions are not supersymmetric. As a consequence, the rotations that are turned on are not a central charge of the theory. There is, however, a BPS inequality that the solutions must satisfy, relating their energy to the angular momentum. Some solutions saturate the inequality, and they have a simpler set of equations that need to be satisfied.

The rigidly rotating solutions can be understood in terms of a system of algebraic equations. These are in one to one correspondence with critical points of an energy function. Solutions found at zero angular momentum correspond not only to the vacua of the matrix model, made of concentric fuzzy spheres, but also other various unstable saddle points. These all survive when we turn on the angular momentum. Excitating angular motion in the configurations always leads to a term in the on-shell energy proportional to the angular momentum, rather than starting at the square of angular momentum. This indicates that even though the configurations are rotating rigidly, the matrix object can not be thought of as a rigid body.

Both the finite N and large N results suggest that there is a maximal angular momentum beyond which there is only one phase. This should scale like N^3. This phase when interpreted geometrically corresponds to the brane dissociating into a collection of D0-branes arranged symmetrically on a circle.

The phase diagram of solutions is rather complicated in general and we found it very useful to use Morse theory to find all the solutions, at least for low values of N. The full pattern for a given N has many more saddles than the ones for smaller N. Any solution that is found for lower values of N at $J = 0$ can be combined with other such solutions to build solutions at a given N for $J = 0$. These becomes seeds for a family of such solutions at finite J. Moreover, for every N there are new solutions. Some of them we are aware of, like the maximal fuzzy sphere or a maximal fuzzy sphere at half radius. We do not have a systematic way to search for the other ones. The parameter space grows in dimension proportional to N making it increasingly difficult to find them. Understanding this pattern in general should be very interesting.

At large N, the particular family of solutions we have considered reduces to a variational problem for critical points of a local integral. The saddle point equations reduce to finding periodic solutions of a pair of coupled second order differential equations, while the BPS ones reduce to solving a coupled set of non-linear first order differential equations. It is only solutions with the right period that can be used. The period fixes the D0-brane charge of the configuration.

We also found that the topology change from a sphere to a (sometimes multiply wound) torus happens instantaneously in the large N limit, but not so at finite N. Here it is delayed. Moreover, the shape of the fuzzy membranes can be very deformed from a circular torus. The effects that lead to that deformation are suppressed at large N. It should be interesting to investigate this in more detail. The breaking of the symmetry is due to the discretization of the D0-brane charge into matrices. In the fuzzy geometry it is a purely classical effect. However, in the continuum large N limit, this is supposed to arise from quantum effects that are responsible for the quantization of the D0-brane charge. It is often the case that quantum effects on D-brane field theories can be captured geometrically, like beta functions being captured by brane bending [218, 219]. In this case we find that the discretization that appears in matrix theory introduces symmetry breaking effects that are not apparent in the continuum limit, and they would not appear in perturbation theory.

It should also be interesting to understand supersymmetry breaking effects better in these solutions and in particular the corrections due to zero point energy. This depends on the full theory, as we found that the $SO(3)$ BMN system of classical equations arises in various different contexts. Such answers depend on the context.

Another interesting possibility to examine is that the $SO(3)$ sector of the BMN matrix model is also part of the description of the discrete lightcone quantization of the membrane in the Penrose limit of $AdS_4 \times S^7$ [60], or its orbifolds. In particular, one can consider the ABJM model [220] in the appropriate sector that takes us to the Penrose limit. The natural candidates to consider are D0-brane states, which are dual to monopole operators. The spectrum of fluctuations around such objects have been analyzed in [221, 222, 223, 224] and they have many fluctuations that are supersymmetric and saturate the BPS bound. It should be interesting to try to turn on rotations in AdS_4 for such states and see if the extremal solutions we have found can be mapped to them at weak coupling as well. This should help to understand how the D0-brane theory of the matrix model and the ABJM field theory in the presence of monopole states are related to each other.

Chapter 11

Conclusions

Locality and geometry must appear as exact concepts in the classical limit of a quantum theory of gravity. As evident by the existence of black holes and singularities in the classical theory, it is not clear that these notions appear at all in the quantum theory. Gauge / gravity duality is a powerful tool that allows us to use the gauge theory as a probe of locality and geometry in the gravity theory. We explored both locality and geometry in the planar limit of AdS / CFT correspondence and through the classical dynamics of large N gauged matrix models.

In the context of AdS / CFT, we explored the physics of open strings stretched between giant gravitons. We explained how to build the operators dual to giant gravitons and their stringy excitations. To make connections with the classical sigma model, the giant graviton operators were delocalized using a collective coordinate. The delocalized giants have indefinite angular momentum, or R-charge, and can be seen as a coherent state of giant gravitons with definite R-charge. The collective coordinate can be mapped to its dual position on the S^5 in the string theory. Open strings ending these giants have a description in terms of Cuntz oscillator chains. The dynamics of the open string / giant graviton system is given by the one-loop dilatation operator to leading order which becomes a Hamiltonian like operator for the Cuntz system. Taking coherent states of the Cuntz chains, we were able to build the ground state of the Cuntz Hamiltonian explicitly and find its energy. Going to second order in perturbation, or to three-loop order in the gauge theory, we were able to find the first order correction to the ground state and the second order correction to the energy. We found that the energy of the open string was consistent with a fully relativistic dispersion relation to third order in the 't Hooft coupling.

We believe the dispersion relation to hold to all orders in perturbation theory due to the existence of a central charge extension of the supersymmetry algebra left unbroken by the giant graviton system. The central charge is given exactly by the distance between the giant gravitons and plays the role of the mass of the open string ground state. In particular, the open string is like a W boson on the Coulomb branch of the $\mathcal{N} = 4$ SYM theory living on the worldvolume of the giant gravitons. The open string is revealing how locality and geometry arise on the worldvolume of the giant graviton.

We then asked what are the geometric duals of β deformations of $\mathcal{N} = 4$ SYM? We answered this question by extending the open string dispersion relation for $\beta = 0$ to arbitrary β using integrability arguments. The base case is $\beta = 0$ and describes how the gauge theory is dual to string theory on an $AdS_5 \times S^5$ background. For nonzero β, the dual geometric background changes based on the number theoretic properties of β.

Matrix models gave us a different perspective on how geometry is realized in gauge / gravity duality. Were able to extract two dimensional surfaces embedded in three dimensional space given three Hermitian matrices even at finite N. These surfaces are closed and oriented. We found that the membranes behave like D2-branes by showing that these surfaces carry the information of a line bundle on them with a connection.

We then studied thermalization in the classical evolution of matrix models. For a particular set of initial conditions, we were able to generate a microcanonical ensemble of thermal matrix configurations. We measured the temperature, made tests of the virial theorem, and analyzed their power spectra. We found N-independent hydrodynamic behavior for the power spectra of various observables and large N factorization for correlators. We argued that the thermal matrix configurations were holographically dual to black holes and develops tools to determine where the horizon may lie.

Lastly, we added angular momentum to classical configurations of the matrix models and studied their topologies using our own techniques for generating surfaces from matrices. We found that transitions from spheres to tori were smooth as we increased the angular momentum. Studying the thermalization of these matrix models in the presence of angular momentum is work in progress, but we plan to understand how dynamics affect the topology encoded in these classical thermal configurations.

We have only scratched the surface when it comes to understanding how locality and geometry arise in the context gauge theories. We specifically looked at emerging strings and branes and clearly, there is still a great deal of work to be done.

Appendix A

Conventions and Relations for the Lie Algebra of $U(N)$

We use the following conventions for the generators of $U(N)$. These are the same as those used in [29].

$$\mathrm{Tr}(T^A T^B) = \delta^{AB}, \quad (T^A)^{\alpha}{}_{\beta}(T^A)^{\gamma}{}_{\delta} = \delta^{\alpha}{}_{\delta}\delta^{\gamma}{}_{\beta} \tag{A.1}$$

where $A,\ B$ run from 1 to N^2 and repeated indices indicate summation. These relations can be used to prove the fusion / fission rules

$$\mathrm{Tr}(AT^A)\mathrm{Tr}(BT^A) = \mathrm{Tr}(AB), \quad \mathrm{Tr}(AT^A BT^A) = \mathrm{Tr}(A)\mathrm{Tr}(B) \tag{A.2}$$

The following relations are relevant to computing the order N^2 boundary contribution to the two loop Hamiltonian. If W is a field in the SYM then we may expand it as $X = X^A T^A$ and its derivative as $\partial_X = T^A \partial_{X^A}$. Using this fact and the relations

$$(\partial_Z)^a{}_b \det(Z-\lambda) = \det(Z-\lambda)\left(\frac{1}{Z-\lambda}\right)^a{}_b \tag{A.3}$$

$$(\partial_Z)^a{}_b \left(\frac{1}{Z-\lambda}\right)^c{}_d = -\left(\frac{1}{Z-\lambda}\right)^a{}_d \left(\frac{1}{Z-\lambda}\right)^c{}_b \tag{A.4}$$

we have the following fusion / fission rules

$$\mathrm{Tr}(A\partial_Z)\det(Z-\lambda) = \det(Z-\lambda)\mathrm{Tr}\left(A\frac{1}{Z-\lambda}\right) \tag{A.5}$$

$$\mathrm{Tr}(A\partial_Z)\mathrm{Tr}\left(B\frac{1}{Z-\lambda}\right) = -\mathrm{Tr}\left(A\frac{1}{Z-\lambda}B\frac{1}{Z-\lambda}\right) \tag{A.6}$$

$$\mathrm{Tr}\left(A\partial_Z B\frac{1}{Z-\lambda}\right) = -\mathrm{Tr}\left(A\frac{1}{Z-\lambda}\right)\mathrm{Tr}\left(B\frac{1}{Z-\lambda}\right) \tag{A.7}$$

where it is assumed that A and B are independent of Z.

When computing the boundary terms at two loop order, we need to collect terms into a derivative with respect to λ so that we then pull down its conjugate. In order to do this we need the relations

$$\begin{aligned}
&\partial_\lambda\left[\det(Z-\lambda)\mathrm{Tr}\left(\frac{1}{Z-\lambda}A\right)\right] = \\
&\qquad \det(Z-\lambda)\left[\mathrm{Tr}\left(\frac{1}{(Z-\lambda)^2}A\right) - \mathrm{Tr}\left(\frac{1}{Z-\lambda}\right)\mathrm{Tr}\left(\frac{1}{Z-\lambda}A\right)\right]
\end{aligned} \tag{A.8}$$

$$\begin{aligned}
&\partial_\lambda^2\left[\det(Z-\lambda)\mathrm{Tr}\left(\frac{1}{Z-\lambda}A\right)\right] = \\
&\qquad \det(Z-\lambda)\left[2\mathrm{Tr}\left(\frac{1}{(Z-\lambda)^3}A\right) - 2\mathrm{Tr}\left(\frac{1}{Z-\lambda}\right)\mathrm{Tr}\left(\frac{1}{(Z-\lambda)^2}A\right)\right. \\
&\qquad\qquad \left. - \left[\mathrm{Tr}\left(\frac{1}{(Z-\lambda)^2}\right) - \mathrm{Tr}\left(\frac{1}{Z-\lambda}\right)\mathrm{Tr}\left(\frac{1}{Z-\lambda}\right)\right]\mathrm{Tr}\left(\frac{1}{Z-\lambda}A\right)\right]
\end{aligned} \tag{A.9}$$

where A is a matrix that does not depend on λ.

Appendix B

Cuntz Algebra and Hamiltonians

B.1 Cuntz Oscillators

The Cuntz algebra is a q-deformation of the harmonic oscillator algebra in the limit $q \to 0$. One has a lowering operator a and a raising operator $a^\dagger$. There is a zero occupation state $|0\rangle$ satisfying $a\,|0\rangle = 0$. The defining relations are

$$aa^\dagger = I, \quad a^\dagger a = I - P_0 \tag{B.1}$$

and lead to the commutation relation

$$[a, a^\dagger] = P_0 \tag{B.2}$$

with P_0 the projection onto the zero occupation state. Higher occupation states are obtained by acting with the raising operator, $|n\rangle = (a^\dagger)^n\,|0\rangle$. The commutation relation (3.14) implies the simple action of the ladder operators

$$a^\dagger\,|n\rangle = |n+1\rangle\,, \quad a\,|n\rangle = |n-1\rangle \tag{B.3}$$

with $n > 0$ for the second relation. Negative occupation numbers are not allowed.

We can extend these Cuntz oscillators to act on individual sites of our multi-occupation number states by defining $a_i = I^{\otimes^{i-1}} \otimes a \otimes I^{\otimes^{k-i}}$ and likewise for $a_i^\dagger$ and the projection operator P_{0i}. We now have the commutation relation

$$[a_i, a_j^\dagger] = \delta_{ij} P_{0i} \tag{B.4}$$

A generic state in the occupation number basis is represented as

$$|n_1, n_2, \ldots, n_k\rangle_k = (a_1^\dagger)^{n_1} \cdots (a_k^\dagger)^{n_k} |0\rangle_k \tag{B.5}$$

Coherent states can be build from a set of complex numbers $\{z_i\}_{i=1}^k$ that satisfy

$$a_i |z_1, \ldots, z_k\rangle = z_i |z_1, \ldots, z_k\rangle \tag{B.6}$$

For a single Cuntz oscillator we have $a|z\rangle = z|z\rangle$ for some complex number z. Solving for $|z\rangle$ yields

$$|z\rangle = N_z \sum_{n=0}^{\infty} z^n (a^\dagger)^n |0\rangle \tag{B.7}$$

Normalizing the coherent states gives the normalization factor

$$N_z = \frac{1}{\sqrt{1 - |z|^2}} \tag{B.8}$$

If we want to the coherent states to have finite norm, then z should lie in the complex unit disk. The state $|z_1, \ldots, z_k\rangle$ is obtained by tensoring the single Cuntz coherent states with appropriate collective coordinate.

Because $aa^\dagger = I$, all operators can (and should) naturally be written as linear combinations of objects in normal ordered form $\hat{S}_{kn} = (a^\dagger)^k a^n$. It is easy to show that

$$\hat{S}_{nn} = (a^\dagger)^n a^n = 1 - \sum_{m=0}^{n-1} P_m \tag{B.9}$$

where P_m is the projector onto the state with occupation number m. The occupation number operator is given by

$$\hat{N} = \sum_{n=1}^{\infty} \hat{S}_{nn} = \hat{N}^\dagger \tag{B.10}$$

One has $[\hat{N}_i, a_i^\dagger] = a_i^\dagger$ and consequently $\hat{N}_i \left|n_1, \ldots, n_k\right\rangle_k = n_i \left|n_1, \ldots, n_k\right\rangle_k$.

B.2 Closed Cuntz Hamiltonians

For closed Cuntz chains, the Cuntz operators are cyclically identified, $a_i \equiv a_{i+k}$. The Hamiltonians for the closed Cuntz chain are given up to order λ^3 by

$$H_{\text{closed}} = \sum_{\ell=0}^{\infty} \left(\frac{\lambda}{4\pi^2}\right)^{\ell} H_{\text{closed},\ell} \tag{B.11}$$

$$H_{\text{closed},0} = \hat{N} + k \tag{B.12}$$

$$H_{\text{closed},1} = \frac{1}{2} \sum_{i=1}^{k} (a_{i+1}^\dagger - a_i^\dagger)(a_{i+1} - a_i) \tag{B.13}$$

$$\begin{aligned} H_{\text{closed},2} = -\frac{1}{8} \sum_{i=1}^{k} &(a_{i+1}^\dagger - a_i^\dagger)^2 (a_{i+1} - a_i)^2 \\ &+ (a_{i+1}^\dagger - 2a_i^\dagger + a_{i-1}^\dagger) P_{0i} (a_{i+1} - 2a_i + a_{i-1}) \end{aligned} \tag{B.14}$$

$$\begin{aligned}H_{\text{closed},3} = \frac{1}{16}\sum_{i=1}^{k}&(a^\dagger_{i+1}-a^\dagger_i)^3(a_{i+1}-a_i)^3 + v_a^{i\dagger}M_{ab}P_{0i}v_b^i \\ &+ (a^\dagger_{i+2}-3a^\dagger_{i+1}+3a^\dagger_i-a^\dagger_{i-1})P_{0i+1}P_{0i}(a_{i+2}-3a_{i+1}+3a_i-a_{i-1})\end{aligned} \tag{B.15}$$

where

$$v_a^i = (a_{i+1}a_{i+1},\ a_{i+1}a_i,\ a_{i+1}a_{i-1},\ a_ia_i,\ a_ia_{i-1},\ a_{i-1}a_{i-1}) \tag{B.16}$$

$$M_{ab} = \begin{pmatrix} 4 & -8 & 2 & 2 & 0 & 0 \\ -8 & 15 & -3 & -3 & -1 & 0 \\ 2 & -3 & 1 & 1 & -3 & 2 \\ 2 & -3 & 1 & 1 & -3 & 2 \\ 0 & -1 & -3 & -3 & 15 & -8 \\ 0 & 0 & 2 & 2 & -8 & 4 \end{pmatrix} \tag{B.17}$$

B.3 Open Cuntz Hamiltonians

The Hamiltonians for the open Cuntz chain are given up to order λ^3 by

$$H_{\text{open}} = \sum_{\ell=0}^{\infty}\left(\frac{\lambda}{4\pi^2}\right)^\ell H_{\text{open},\ell} \tag{B.18}$$

$$H_{\text{open},0} = k+1 \tag{B.19}$$

$$H_{\text{open},1} = \frac{1}{2}\sum_{i=0}^{k}(a^\dagger_{i+1}-a^\dagger_i)(a_{i+1}-a_i) \tag{B.20}$$

$$\begin{aligned}H_{\text{open},2} = &-\frac{1}{8}\sum_{i=0}^{k}(a^\dagger_{i+1}-a^\dagger_i)^2(a_{i+1}-a_i)^2 \\ &-\frac{1}{8}\sum_{i=1}^{k}(a^\dagger_{i+1}-2a^\dagger_i+a^\dagger_{i-1})P_{0i}(a_{i+1}-2a_i+a_{i-1})\end{aligned} \tag{B.21}$$

$$H_{\text{open},3} = \frac{1}{16}\sum_{i=0}^{k}(a_{i+1}^\dagger - a_i^\dagger)^3(a_{i+1} - a_i)^3 + \frac{1}{16}\sum_{i=1}^{k} v_a^{i\dagger} M_{ab} P_{0i} v_b^i$$
$$+ \frac{1}{16}\sum_{i=1}^{k-1}(a_{i+2}^\dagger - 3a_{i+1}^\dagger + 3a_i^\dagger - a_{i-1}^\dagger)P_{0i+1}P_{0i}(a_{i+2} - 3a_{i+1} + 3a_i - a_{i-1}) \tag{B.22}$$

where

$$v_a^i = (a_{i+1}a_{i+1},\ a_{i+1}a_i,\ a_{i+1}a_{i-1},\ a_ia_i,\ a_ia_{i-1},\ a_{i-1}a_{i-1}) \tag{B.23}$$

$$M_{ab} = \begin{pmatrix} 4 & -8 & 2 & 2 & 0 & 0 \\ -8 & 15 & -3 & -3 & -1 & 0 \\ 2 & -3 & 1 & 1 & -3 & 2 \\ 2 & -3 & 1 & 1 & -3 & 2 \\ 0 & -1 & -3 & -3 & 15 & -8 \\ 0 & 0 & 2 & 2 & -8 & 4 \end{pmatrix} \tag{B.24}$$

and the operators a_0, $a_0^\dagger$, a_{k+1}, $a_{k+1}^\dagger$ are ordinary c-numbers

$$a_0 = \xi_1, \quad a_0^\dagger = \bar{\xi}_1, \quad a_{k+1} = \xi_2, \quad a_{k+1}^\dagger = \bar{\xi}_2 \tag{B.25}$$

Appendix C

Proof of First Order Ground State Correction

Here we show that (4.59) solves (4.53). One has

$$(H_{\text{open},0} - E_0^{(0)})\left|\Omega^{(1)}\right\rangle$$

$$= \frac{1}{8}(\Delta z)^2 \sum_{i=0}^{k}(A_{i+1}^{(1)\dagger} - A_i^{(1)\dagger})(A_{i+1}^{(1)} - A_i^{(1)})\left(\sum_{j=1}^{k}\sum_{n=2}^{\infty} z_j^{n-2}A_j^{(n)\dagger}\left|\Omega^{(0)}\right\rangle\right) \tag{C.1}$$

$$= -\frac{1}{8}(\Delta z)^2 \sum_{i=1}^{k}\sum_{j=1}^{k}\sum_{n=2}^{\infty} z_j^{n-2}(A_{i+1}^{(1)\dagger} - 2A_i^{(1)\dagger} + A_{i-1}^{(1)\dagger})A_i A_j^{(n)\dagger}\left|\Omega^{(0)}\right\rangle \tag{C.2}$$

$$= -\frac{1}{8}(\Delta z)^2 \sum_{i=1}^{k}\sum_{j=1}^{k}\sum_{n=2}^{\infty} z_j^{n-2}(A_{i+1}^{(1)\dagger} - 2A_i^{(1)\dagger} + A_{i-1}^{(1)\dagger}) \times (A_j^{(n)\dagger}A_i + \delta_{ij}A_j^{(n-1)\dagger}P_{0j})\left|\Omega^{(0)}\right\rangle \tag{C.3}$$

$$= -\frac{1}{8}(\Delta z)^2 \sum_{j=1}^{k}\sum_{n=2}^{\infty} z_j^{n-2}(A_{j+1}^{(1)\dagger} - 2A_j^{(1)\dagger} + A_{j-1}^{(1)\dagger})A_j^{(n-1)\dagger}(1 - z_j a_j^\dagger)\left|\Omega^{(0)}\right\rangle \tag{C.4}$$

$$= -\frac{1}{8}(\Delta z)^2 \sum_{j=1}^{k}\left(\sum_{n=1}^{\infty} z_j^{n-1}(A_{j+1}^{(1)\dagger} - 2A_j^{(1)\dagger} + A_{j-1}^{(1)\dagger})A_j^{(n)\dagger}\left|\Omega^{(0)}\right\rangle\right.$$

$$-\sum_{n=2}^{\infty} z_j^{n-1}(A_{j+1}^{(1)\dagger} - 2A_j^{(1)\dagger} + A_{j-1}^{(1)\dagger})A_j^{(n)\dagger} \left|\Omega^{(0)}\right\rangle\Bigg) \tag{C.5}$$

$$= -\frac{1}{8}(\Delta z)^2 \sum_{j=1}^{k}(A_{j+1}^{(1)\dagger} - 2A_j^{(1)\dagger} + A_{j-1}^{(1)\dagger})A_j^{(1)\dagger} \left|\Omega^{(0)}\right\rangle \tag{C.6}$$

$$= \frac{1}{4}(\Delta z)^2 \left(\sum_{j=1}^{k} A_j^{(2)\dagger} - \sum_{j=1}^{k-1} A_j^{(1)\dagger}A_{j+1}^{(1)\dagger} - \sum_{j=1}^{k} \bar{z}_j A_j^{(1)\dagger}\right) \left|\Omega^{(0)}\right\rangle \tag{C.7}$$

$$= -(H_{\text{open},1} - E_1^{(1)}) \left|\Omega^{(0)}\right\rangle \tag{C.8}$$

To go from (C.6) to (C.7) we used the relation $A_j^{(1)\dagger}A_j^{(1)\dagger} = A_j^{(2)\dagger} - \bar{z}A_j^{(1)\dagger}$.

Appendix D

BFSS and BMN model conventions

The BFSS and BMN matrix models are systems of gauged quantum mechanics. Each has nine bosonic matrices ϕ^i and sixteen component spinors Ψ transforming in the adjoint of $U(N)$. There is also a non-dynamical $\mathfrak{u}(N)$ valued gauge connection A_0. Their actions listed here are taken from [60, 129, 135] using a mix of conventions:

$$S_{\text{BMN}} = S_{\text{BFSS}} + S_{\text{mass}} \tag{D.1}$$

$$\begin{aligned}S_{\text{BFSS}} = \frac{1}{g^2}\int dt\,\text{Tr}\Bigg[&\sum_{j=1}^{9}\frac{1}{2(2R)}(D_0\phi^j)^2 + \frac{i}{2}\Psi^\dagger D_0\Psi + \frac{(2R)}{4}\sum_{j,k=1}^{9}[\phi^j,\phi^k]^2\\ &+\sum_{j=1}^{9}\frac{1}{2}(2R)(\Psi^\dagger\gamma^j[\phi^j,\Psi])\Bigg]\end{aligned} \tag{D.2}$$

$$\begin{aligned}S_{\text{mass}} = \int dt\,\text{Tr}\Bigg[&\frac{1}{2(2R)}\left(-\left(\frac{\mu}{3}\right)^2\sum_{j=1}^{3}(\phi^j)^2 - \left(\frac{\mu}{6}\right)^2\sum_{j=4}^{9}(\phi^j)^2\right)\\ &-\frac{i}{2}\left(\frac{\mu}{4}\right)\Psi^\dagger\gamma_{123}\Psi - i\frac{\mu}{3}\sum_{j,k,l=1}^{3}\epsilon_{jkl}\phi^j\phi^k\phi^l\Bigg]\end{aligned} \tag{D.3}$$

where $D_0\phi^i = \partial_t\phi^i - i[A_t, \phi^i]$ is the covariant derivative with respect to A_0. The $\gamma_{i\ldots}$ are the nine dimensional gamma matrices. The $U(N)$ gauge symmetry is generated by

$$G = i\sum_{i=1}^{9}[\phi^i, D_0\phi^i] + 2\{\Psi^{\dagger\alpha}, \Psi_\alpha\} \tag{D.4}$$

where $D_0\phi^i$ is the momentum conjugate to ϕ^i. The fermion representation we choose to work in is not explicitly real, and so we use $\Psi^\dagger$ instead of Ψ^T (see Appendix E).

For the purposes of this thesis, it is convenient to rescale the mass μ by three $\mu \to 3\mu'$ and then the fields and time to remove the mass scale μ' and the length scale R from the action via

$$\phi \to \frac{\mu'}{2R}\phi, \quad \Psi \to \left(\frac{\mu'}{2R}\right)^{3/2}\Psi, \quad t \to \frac{t}{\mu'} \tag{D.5}$$

The action becomes

$$\begin{aligned}
S_{\mathrm{BMN}} &= S_{\mathrm{BFSS}} + S_{\mathrm{mass}} && \text{(D.6)}\\
S_{\mathrm{BFSS}} &= \frac{1}{g^2}\int dt\,\mathrm{Tr}\left[\sum_{j=1}^{9}\frac{1}{2}(D_0\phi^j)^2 + \frac{i}{2}\Psi^\dagger D_0\Psi + \frac{1}{4}\sum_{j,k=1}^{9}[\phi^j,\phi^k]^2\right.\\
&\qquad\left. + \sum_{j=1}^{9}\frac{1}{2}(\Psi^\dagger\gamma^j[\phi^j,\Psi])\right] && \text{(D.7)}\\
S_{\mathrm{mass}} &= \frac{1}{g^2}\int dt\,\mathrm{Tr}\left[\frac{1}{2}\left(-\sum_{j=1}^{3}(\phi^j)^2 - \frac{1}{4}\sum_{j=4}^{9}(\phi^j)^2\right)\right.\\
&\qquad\left. - \frac{i}{2}\left(\frac{3}{4}\right)\Psi^\dagger\gamma_{123}\Psi - i\sum_{j,k,l=1}^{3}\epsilon_{jkl}\phi^j\phi^k\phi^l\right] && \text{(D.8)}
\end{aligned}$$

with

$$\frac{1}{g^2} = \frac{{\mu'}^3}{(2R)^3} \tag{D.9}$$

In the $A_0 = 0$ gauge, the covariant time derivatives become ordinary time derivatives. Relabel the ϕ^j by X^I. Define $X^i = \phi^i$ for $i = 1, 2, 3$ and $Y^a = \phi^a$ for $a = 1, \ldots, 6$. The bosonic action takes the form

$$S_B = \frac{1}{2g^2} \int dt \, \mathrm{Tr} \left[(\dot{X}^i)^2 + (\dot{Y}^a)^2 - (X^i)^2 - \frac{1}{4}(Y^a)^2 - 2i\epsilon_{ijk} X^i X^j X^k - \frac{1}{2}[X^I, X^J]^2 \right] \tag{D.10}$$

The fermionic action becomes

$$S_F = \frac{1}{g^2} \int dt \, \mathrm{Tr} \left[\frac{i}{2} \Psi^\dagger \dot{\Psi} - \frac{i}{2} \left(\frac{3}{4} \right) \Psi^\dagger \gamma_{123} \Psi + \frac{1}{2} \Psi^\dagger \gamma^I [X^I, \Psi] \right] \tag{D.11}$$

This is how the action is written in [135].

Appendix E

Fermion Decomposition

This section comes from Appendix A of reference [129]. Decompose the sixteen component spinor as

$$\begin{aligned} SO(16) &\to SO(6) \otimes SO(3) \simeq SU(4) \otimes SU(2) \\ \mathbf{16} &\to (\mathbf{4} \otimes \mathbf{2}) \oplus (\bar{\mathbf{4}} \otimes \bar{\mathbf{2}}) \\ \Psi &\to \psi_{I\alpha}, \psi^{\dagger J\beta} \end{aligned} \tag{E.1}$$

where I, J are fundamental $SU(4)$ indices and α, β are fundamental $SU(2)$ indices. The spinors obey the reality condition

$$(\psi^{\dagger})^{I\alpha} = \tilde{\psi}^{I\alpha} \tag{E.2}$$

which allow us to write the spinors in the stacked form

$$\Psi \to \begin{pmatrix} \psi_{I\alpha} \\ \epsilon_{\alpha\beta}\psi^{\dagger I\beta} \end{pmatrix} \tag{E.3}$$

The matrices g^a_{IJ} are introduced to relate the inner product of $SU(4)$ to the vector of $SO(6)$ which satisfy

$$g^a(g^\dagger)^b + g^b(g^\dagger)^a = 2\delta^{ab} \tag{E.4}$$

The gamma matrices are then written as

$$\gamma^i = \begin{pmatrix} -\sigma^i \otimes 1 & 0 \\ 0 & \sigma^i \otimes I \end{pmatrix}, \quad \gamma^a = \begin{pmatrix} 0 & 1 \otimes g^a \\ 1 \otimes (g^a)^\dagger & 0 \end{pmatrix} \tag{E.5}$$

The terms in the Lagrangian then decompose as

$$\frac{i}{2}\Psi^\dagger D_0 \Psi \rightarrow i\psi^{\dagger I\alpha} D_0 \psi_{I\alpha} \tag{E.6}$$

$$\frac{i}{2}\Psi^\dagger \gamma_{123} \Psi \rightarrow \psi^{\dagger I\alpha} \psi_{I\alpha} \tag{E.7}$$

$$\frac{1}{2}\Psi^\dagger \gamma^i [X^i, \Psi] \rightarrow -\psi^{\dagger I\alpha} \sigma^{i\beta}_{\alpha} [X^i, \psi_{I\beta}] \tag{E.8}$$

$$\frac{1}{2}\Psi^\dagger \gamma^a [X^a, \Psi] \rightarrow \frac{1}{2}\epsilon_{\alpha\beta}\psi^{\dagger I\alpha} g^a_{IJ} [Y^a, \psi^{\dagger J\beta}] - \frac{1}{2}\epsilon^{\alpha\beta}\psi_{I\alpha}(g^\dagger)^{aIJ}[Y^a, \psi_{J\beta}] \tag{E.9}$$

The fermionic part of the action (in the $A_t = 0$ gauge) may then be written as

$$\begin{aligned} S_F = \frac{1}{g^2}\int dt\, \mathrm{Tr}\Big[& i\psi^{\dagger I\alpha}\dot{\psi}_{I\alpha} - \frac{3}{4}\psi^{\dagger I\alpha}\psi_{I\alpha} - \psi^{\dagger I\alpha}\sigma^{i\beta}_{\alpha}[X^i, \psi_{I\beta}] \\ & + \frac{1}{2}\epsilon_{\alpha\beta}\psi^{\dagger I\alpha} g^a_{IJ}[Y^a, \psi^{\dagger J\beta}] - \frac{1}{2}\epsilon^{\alpha\beta}\psi_{I\alpha}(g^\dagger)^{aIJ}[Y^a, \psi_{J\beta}]\Big] \end{aligned} \tag{E.10}$$

Notice that the coupling to the X variables uses just the Pauli matrices after this decomposition. Also, a ψ spinor is always paired with its conjugate. If we perform orbifolds that are chiral, this structure remains, but the other mass terms that do not preserve four dimensional chirality might be eliminated.

Appendix F

Fermionic Modes Between Displaced Fuzzy Spheres

For the calculations of Section 7.4 we want to consider computing fermionic modes between two fuzzy spheres in the BMN matrix model that have been displaced as described in [135]. We want to restrict to a chiral projection of the modes between two such fuzzy spheres. We will first set up some conventions for the fermionic modes of a single fuzzy sphere. Then we work with the more general problem.

F.1 Diagonal Fermionic Modes

This section is essentially a repeat of Section 5.2 of [129] using the conventions of [135].

The $SU(4)$ indices are dropped as they do not come into play at all during the following calculation. We take the following conventions for the spherical harmonics and the angular momentum generators:

$$[L^3, Y_{lm}] = mY_{lm} \qquad\qquad [L^3, Y_{lm}^\dagger] = -mY_{lm}^\dagger \tag{F.1}$$

$$[L^+, Y_{lm}] = \Lambda_-^{lm} Y_{lm+1} \qquad [L^+, Y_{lm}^\dagger] = -\Lambda_+^{lm} Y_{lm-1}^\dagger \tag{F.2}$$

$$[L^-, Y_{lm}] = \Lambda_+^{lm} Y_{lm-1} \qquad [L^-, Y_{lm}^\dagger] = -\Lambda_-^{lm} Y_{lm+1}^\dagger \tag{F.3}$$

where $L^\pm = L_1 \pm i L_2$. The spherical harmonics are normalized such that $\mathrm{Tr}(Y_{lm}^\dagger Y_{l'm'}) = \frac{1}{2}\delta_{ll'}\delta_{mm'}$. The constants $\Lambda_\pm^{\ell m}$ are defined as

$$\Lambda_+^{lm} = \sqrt{(l+m)(l-m+1)}, \quad \Lambda_-^{lm} = \sqrt{(l-m)(l+m+1)} \tag{F.4}$$

$$\Lambda_+^{l-l} = 0, \quad \Lambda_-^{ll} = 0, \quad \Lambda_+^{lm+1} = \Lambda_-^{lm} \tag{F.5}$$

We expand the fermions as

$$\psi_\alpha = \sum_{lm} \psi_\alpha^{lm} Y_{lm} \tag{F.6}$$

The potential in the presence of the bosonic VEV's becomes

$$\begin{aligned}
V_F - \frac{3}{4}\mathrm{Tr}(\psi^{\dagger\alpha}\psi_\alpha) \\
&= \mathrm{Tr}\left[\psi^{\dagger\alpha}\sigma_\alpha^{i\beta}[L^i, \psi_{I\beta}]\right] \\
&= \mathrm{Tr}\left[\psi^{\dagger+}\left([L^3, \psi_+] + [L^-, \psi_-]\right) + \psi^{\dagger-}\left([L^+, \psi_+] - [L^3, \psi_-]\right)\right] \\
&= \mathrm{Tr}\left[\psi^{\dagger+}\sum_{lm}\left(m\psi_+^{lm} Y_{lm} + \Lambda_+^{lm}\psi_-^{lm} Y_{lm-1}\right)\right. \\
&\qquad\qquad \left. + \psi^{\dagger-}\sum_{lm}\left(\Lambda_-^{lm}\psi_+^{lm} Y_{lm+1} - m\psi_-^{lm} Y_{lm}\right)\right] \\
&= \frac{1}{2}\sum_{lmm'}\left[\psi_+^{\dagger lm'}\left(m\psi_+^{lm}\delta_{m'm} + \Lambda_+^{lm}\psi_-^{lm}\delta_{m'm-1}\right)\right. \\
&\qquad\qquad \left. + \psi_-^{\dagger lm'}\left(\Lambda_-^{lm}\psi_+^{lm}\delta_{m'm+1} - m\psi_-^{lm}\delta_{m'm}\right)\right]
\end{aligned}$$

$$= \frac{1}{2} \sum_{lmm'} \begin{pmatrix} \psi_+^{\dagger lm'} & \psi_-^{\dagger lm'} \end{pmatrix} \begin{pmatrix} m & \Lambda_+^{lm} \delta_{m'm-1} \\ \Lambda_-^{lm} \delta_{m'm+1} & -m \end{pmatrix} \begin{pmatrix} \psi_+^{lm} \\ \psi_-^{lm} \end{pmatrix} \tag{F.7}$$

The eigenvalues of the matrix plus 3/4 give the mass spectrum. Note that $-l \leq m,\ m' \leq l$. The δ's tell us that this matrix has $2l$ two by two blocks and two one by one blocks where $m,\ m' = l$ and $m,\ m' = -l$. Each of the one by one blocks yield the eigenvalue l. The $2l$ two by two blocks can be parametrized according to m from $-l$ to $l-1$. They are given by

$$\begin{pmatrix} m & \Lambda_+^{lm+1} \\ \Lambda_-^{lm} & -(m+1) \end{pmatrix} = \begin{pmatrix} m & \Lambda_-^{lm} \\ \Lambda_-^{lm} & -(m+1) \end{pmatrix} \tag{F.8}$$

The eigenvalues are given by the characteristic equation

$$0 = (m-\lambda)(-m-1-\lambda) - (l-m)(l+m+1) = (\lambda - l)(\lambda + l + 1)$$

Thus the eigenvalues are l and $-(l+1)$. This means that the mass spectrum is $M = 3/4 + l$ with degeneracy of $2l+2$ and $M = -(l+1/4)$ with degeneracy $2l$. Note that there are two more positive eigenvalues than negative eigenvalues.

F.2 Off-diagonal modes

Here we follow the procedure of the previous section and that in [135]. Expand the off diagonal modes in fuzzy monopole harmonics

$$\psi_\alpha = \sum_{lm} \begin{pmatrix} 0 & \delta\psi_\alpha^{lm} Y_{lm} \\ (\delta\tilde{\psi}_\alpha^{lm}) Y_{lm}^\dagger & 0 \end{pmatrix} \tag{F.9}$$

The following commutators are necessary

$$\begin{aligned} [X^3, \psi_\alpha] &= \sum_{lm} \begin{pmatrix} 0 & \delta\psi_\alpha^{lm} [L^3, Y_{lm}] \\ (\delta\tilde{\psi}_\alpha^{lm}) [L^3, Y_{lm}^\dagger] & 0 \end{pmatrix} \\ &\quad + b \left[\begin{pmatrix} 0 & 0 \\ 0 & 1 \end{pmatrix}, \begin{pmatrix} 0 & \delta\psi_\alpha^{lm} Y_{lm} \\ (\delta\tilde{\psi}_\alpha^{lm}) Y_{lm}^\dagger & 0 \end{pmatrix} \right] \\ &= \sum_{lm} \begin{pmatrix} 0 & (m-b)\delta\psi_\alpha^{lm} Y_{lm} \\ -(m-b)(\delta\tilde{\psi}_\alpha^{lm}) Y_{lm}^\dagger & 0 \end{pmatrix} \end{aligned} \tag{F.10}$$

$$\begin{aligned} [X^+, \psi_\alpha] &= \sum_{lm} \begin{pmatrix} 0 & \delta\psi_\alpha^{lm} [L^+, Y_{lm}] \\ (\delta\tilde{\psi}_\alpha^{lm}) [L^+, Y_{lm}^\dagger] & 0 \end{pmatrix} \\ &= \sum_{lm} \begin{pmatrix} 0 & \Lambda_-^{lm} \delta\psi_\alpha^{lm} Y_{lm+1} \\ -\Lambda_+^{lm} (\delta\tilde{\psi}_\alpha^{lm}) Y_{lm-1}^\dagger & 0 \end{pmatrix} \end{aligned} \tag{F.11}$$

$$\begin{aligned} [X^-, \psi_\alpha] &= \sum_{lm} \begin{pmatrix} 0 & \delta\psi_\alpha^{lm} [L^-, Y_{lm}] \\ (\delta\tilde{\psi}_\alpha^{lm}) [L^-, Y_{lm}^\dagger] & 0 \end{pmatrix} \\ &= \sum_{lm} \begin{pmatrix} 0 & \Lambda_+^{lm} \delta\psi_\alpha^{lm} Y_{lm-1} \\ -\Lambda_-^{lm} (\delta\tilde{\psi}_\alpha^{lm}) Y_{lm+1}^\dagger & 0 \end{pmatrix} \end{aligned} \tag{F.12}$$

Substituting these expressions into the potential, taking the chiral projection and finally taking the trace we have

$$V_F - \frac{3}{4}\mathrm{Tr}(\psi^{\dagger\alpha}\psi_\alpha) = \begin{pmatrix} \psi^{\dagger+lm'} & \psi^{\dagger-lm'} \end{pmatrix} \begin{pmatrix} m-b & \Lambda_+^{lm}\delta_{m'm-1} \\ \Lambda_-^{lm}\delta_{m'm+1} & -(m-b) \end{pmatrix} \begin{pmatrix} \psi_+^{lm} \\ \psi_-^{lm} \end{pmatrix} \tag{F.13}$$

This essentially produces the same matrix system as for the diagonal modes except with different diagonal elements. Also, half spin objects are allowed as when we decompose into the tensor product we can get different spins. There is a one by one block with $\lambda = l - b$, another with $\lambda = l + b$, and $2l$ two by two blocks. The matrix for these blocks is

$$\begin{pmatrix} m-b & \Lambda_-^{lm} \\ \Lambda_-^{lm} & -(m+1-b) \end{pmatrix} \tag{F.14}$$

with $-l \leq m \leq l-1$. The eigenvalues λ satisfy

$$\begin{aligned} 0 &= -(m-b-\lambda)(m+1-b+\lambda) - (l-m)(l+m-1) \\ &= \lambda^2 + \lambda - l(l+1) - b(b-1) + 2mb \end{aligned} \tag{F.15}$$

Solving for λ gives

$$\lambda = -\frac{1}{2} \pm \sqrt{(l-m)(l+m+1) + (b-m-1/2)^2} \tag{F.16}$$

Thus the full modes are with $-l \leq m \leq l-1$ (each with degeneracy two):

$$m = \frac{1}{4} \pm \sqrt{(l-m)(l+m+1)+(b-m-1/2)^2} \tag{F.17}$$

We also have two other modes corresponding to the one by one blocks of the mass matrix: $m = 3/4 + l \pm b$. These yield zero modes for the right value of b. That is, we have zero modes when

$$b = \pm(l+3/4) \tag{F.18}$$

for the modes with the greatest angular momentum in the z direction for a given value of ℓ. These zero modes are correlated with the modes that become tachyonic for bosons in the same type of configurations found in [135]. They are objects of maximal spin fixing ℓ.

Appendix G

Measuring the Temperature

Here we derive the relation between the temperature of a system with constraints and the second moments of its degrees of freedom. Consider a system with $2D$ degrees of freedom $\vec{x}$, $\vec{p}$ with the standard kinetic energy, potential $V(\vec{x})$, and k constraints $C^i(\vec{x},\vec{p}) = 0$ with each C^i linear in the momenta. The canonical partition function is given by

$$\mathcal{Z} = \int d^D x d^D p \prod_{i=1}^{k} \delta(C_i(\vec{x},\vec{p})) \exp\left[-\beta\left(\frac{1}{2}|\vec{p}|^2 + V(\vec{x})\right)\right] \tag{G.1}$$

We scale the momenta by a parameter $\sqrt{\gamma}$ and then rescale the δ functions by the inverse of that parameter. Since the constraints are linear in the momenta

$$\mathcal{Z} = \gamma^{(D-k)/2} \int d^D x d^D p \prod_{i=1}^{k} \delta(C_i(\vec{x},\vec{p})) \exp\left[-\beta\left(\frac{\gamma}{2}|\vec{p}|^2 + V(\vec{x})\right)\right] \tag{G.2}$$

The partition function is independent of γ since all we have done is rescaled the momenta. Differentiating we have

$$\begin{aligned}0 = \frac{\partial \mathcal{Z}}{\partial \gamma} = \frac{D-k}{2\gamma}\gamma^{(D-k)/2} \int d^D x d^D p \prod_{i=1}^{k} \delta(C_i(\vec{x}, \vec{p})) \exp\left[-\beta\left(\frac{\gamma}{2}|\vec{p}|^2 + V(\vec{x})\right)\right] \\ - \frac{\beta}{2}\gamma^{(D-k)/2} \int d^D x d^D p \, |\vec{p}|^2 \prod_{i=1}^{k} \delta(C_i(\vec{x}, \vec{p})) \exp\left[-\beta\left(\frac{\gamma}{2}|\vec{p}|^2 + V(\vec{x})\right)\right]\end{aligned} \tag{G.3}$$

Letting $\gamma = 1$ we have

$$0 = \frac{D-k}{2}\mathcal{Z} - \frac{\beta}{2}\mathcal{Z}\langle|\vec{p}|^2\rangle \Rightarrow (D-k)T = \langle|\vec{p}|^2\rangle \tag{G.4}$$

In order to measure the temperature properly, we must subtract off the number of constraints from the degrees of freedom.

Bibliography

[1] E. Dzienkowski, *Excited States of Open Strings From $\mathcal{N} = 4$ SYM*, arXiv:1507.0159.

[2] D. Berenstein, E. Dzienkowski, and R. Lashof-Regas, *Spinning the Fuzzy Sphere*, arXiv:1506.0172.

[3] D. Berenstein and E. Dzienkowski, *Giant gravitons and the emergence of geometric limits in beta-deformations of $\mathcal{N} = 4$ SYM*, *JHEP* **1501** (2015) 126, [arXiv:1408.3620].

[4] D. Berenstein and E. Dzienkowski, *Numerical Evidence for Firewalls*, arXiv:1311.1168.

[5] D. Berenstein and E. Dzienkowski, *Open spin chains for giant gravitons and relativity*, *JHEP* **1308** (2013) 047, [arXiv:1305.2394].

[6] C. T. Asplund, D. Berenstein, and E. Dzienkowski, *Large N classical dynamics of holographic matrix models*, *Phys.Rev.* **D87** (2013), no. 8 084044, [arXiv:1211.3425].

[7] D. Berenstein and E. Dzienkowski, *Matrix embeddings on flat R^3 and the geometry of membranes*, *Phys. Rev.* **D86** (2012) 086001, [arXiv:1204.2788].

[8] S. Hawking, *Breakdown of Predictability in Gravitational Collapse*, *Phys.Rev.* **D14** (1976) 2460–2473.

[9] J. Polchinski, *String Theory*, vol. 1. Cambridge University Press, 1998. Cambridge Books Online.

[10] J. Polchinski, *String Theory*, vol. 2. Cambridge University Press, 1998. Cambridge Books Online.

[11] C. Rovelli, *Loop quantum gravity: the first twenty five years*, *Class.Quant.Grav.* **28** (2011) 153002, [arXiv:1012.4707].

[12] J. Ambjorn, A. Goerlich, J. Jurkiewicz, and R. Loll, *Quantum Gravity via Causal Dynamical Triangulations*, arXiv:1302.2173.

[13] J. M. Maldacena, *The Large N limit of superconformal field theories and supergravity*, *Int.J.Theor.Phys.* **38** (1999) 1113–1133, [hep-th/9711200].

[14] I. Bena, J. Polchinski, and R. Roiban, *Hidden symmetries of the AdS(5) x S**5 superstring*, *Phys.Rev.* **D69** (2004) 046002, [hep-th/0305116].

[15] N. Beisert, C. Ahn, L. F. Alday, Z. Bajnok, J. M. Drummond, *et. al.*, *Review of AdS/CFT Integrability: An Overview*, *Lett.Math.Phys.* **99** (2012) 3–32, [arXiv:1012.3982].

[16] D. Berenstein and S. A. Cherkis, *Deformations of N=4 SYM and integrable spin chain models*, *Nucl.Phys.* **B702** (2004) 49–85, [hep-th/0405215].

[17] P. Basu and L. A. Pando Zayas, *Chaos Rules out Integrability of Strings in* $AdS_5 \times T^{1,1}$, *Phys.Lett.* **B700** (2011) 243–248, [arXiv:1103.4107].

[18] D. Berenstein, *Large N BPS states and emergent quantum gravity*, *JHEP* **0601** (2006) 125, [hep-th/0507203].

[19] J. McGreevy, L. Susskind, and N. Toumbas, *Invasion of the giant gravitons from Anti-de Sitter space*, *JHEP* **0006** (2000) 008, [hep-th/0003075].

[20] E. Witten, *Baryons and branes in anti-de Sitter space*, *JHEP* **9807** (1998) 006, [hep-th/9805112].

[21] S. S. Gubser and I. R. Klebanov, *Baryons and domain walls in an N=1 superconformal gauge theory*, *Phys.Rev.* **D58** (1998) 125025, [hep-th/9808075].

[22] A. Mikhailov, *Giant gravitons from holomorphic surfaces*, *JHEP* **0011** (2000) 027, [hep-th/0010206].

[23] D. Berenstein, C. P. Herzog, and I. R. Klebanov, *Baryon spectra and AdS /CFT correspondence*, *JHEP* **0206** (2002) 047, [hep-th/0202150].

[24] R. G. Leigh and M. J. Strassler, *Exactly marginal operators and duality in four-dimensional N=1 supersymmetric gauge theory*, *Nucl.Phys.* **B447** (1995) 95–136, [hep-th/9503121].

[25] O. Lunin and J. M. Maldacena, *Deforming field theories with U(1) x U(1) global symmetry and their gravity duals*, *JHEP* **0505** (2005) 033, [hep-th/0502086].

[26] N. Beisert and R. Roiban, *Beauty and the twist: The Bethe ansatz for twisted N=4 SYM*, *JHEP* **0508** (2005) 039, [hep-th/0505187].

[27] K. Zoubos, *Review of AdS/CFT Integrability, Chapter IV.2: Deformations, Orbifolds and Open Boundaries*, *Lett.Math.Phys.* **99** (2012) 375–400, [arXiv:1012.3998].

[28] S. Frolov, R. Roiban, and A. A. Tseytlin, *Gauge-string duality for superconformal deformations of N=4 super Yang-Mills theory*, *JHEP* **0507** (2005) 045, [hep-th/0503192].

[29] N. Beisert, C. Kristjansen, and M. Staudacher, *The Dilatation operator of conformal N=4 superYang-Mills theory*, *Nucl.Phys.* **B664** (2003) 131–184, [hep-th/0303060].

[30] N. Beisert and M. Staudacher, *The N=4 SYM integrable super spin chain*, *Nucl.Phys.* **B670** (2003) 439–463, [hep-th/0307042].

[31] N. Beisert and M. Staudacher, *Long-range psu(2,2—4) Bethe Ansatze for gauge theory and strings*, *Nucl.Phys.* **B727** (2005) 1–62, [hep-th/0504190].

[32] N. Beisert, V. Kazakov, K. Sakai, and K. Zarembo, *Complete spectrum of long operators in N=4 SYM at one loop*, *JHEP* **0507** (2005) 030, [hep-th/0503200].

[33] S. Frolov and A. A. Tseytlin, *Multispin string solutions in AdS(5) x S**5*, *Nucl.Phys.* **B668** (2003) 77–110, [hep-th/0304255].

[34] J. Plefka, *Spinning strings and integrable spin chains in the AdS/CFT correspondence*, *Living Rev.Rel.* **8** (2005) 9, [hep-th/0507136].

[35] M. Kruczenski, J. Russo, and A. A. Tseytlin, *Spiky strings and giant magnons on S**5*, *JHEP* **0610** (2006) 002, [hep-th/0607044].

[36] H.-Y. Chen, N. Dorey, and K. Okamura, *Dyonic giant magnons*, *JHEP* **0609** (2006) 024, [hep-th/0605155].

[37] D. M. Hofman and J. M. Maldacena, *Giant Magnons*, *J.Phys.* **A39** (2006) 13095–13118, [hep-th/0604135].

[38] N. Dorey, *Magnon Bound States and the AdS/CFT Correspondence*, *J.Phys.* **A39** (2006) 13119–13128, [hep-th/0604175].

[39] D. Berenstein, *Giant gravitons: a collective coordinate approach*, *Phys.Rev.* **D87** (2013), no. 12 126009, [arXiv:1301.3519].

[40] V. Balasubramanian, M. Berkooz, A. Naqvi, and M. J. Strassler, *Giant gravitons in conformal field theory*, *JHEP* **0204** (2002) 034, [hep-th/0107119].

[41] V. Balasubramanian, M.-x. Huang, T. S. Levi, and A. Naqvi, *Open strings from N=4 superYang-Mills*, *JHEP* **0208** (2002) 037, [hep-th/0204196].

[42] D. Berenstein, *Shape and holography: Studies of dual operators to giant gravitons*, *Nucl.Phys.* **B675** (2003) 179–204, [hep-th/0306090].

[43] S. Corley, A. Jevicki, and S. Ramgoolam, *Exact correlators of giant gravitons from dual N=4 SYM theory*, *Adv.Theor.Math.Phys.* **5** (2002) 809–839, [hep-th/0111222].

[44] R. de Mello Koch, J. Smolic, and M. Smolic, *Giant Gravitons - with Strings Attached (I)*, *JHEP* **0706** (2007) 074, [hep-th/0701066].

[45] R. de Mello Koch, J. Smolic, and M. Smolic, *Giant Gravitons - with Strings Attached (II)*, *JHEP* **0709** (2007) 049, [hep-th/0701067].

[46] D. Bekker, R. de Mello Koch, and M. Stephanou, *Giant Gravitons - with Strings Attached. III.*, *JHEP* **0802** (2008) 029, [arXiv:0710.5372].

[47] J. Cuntz, *Simple c^*-algebras generated by isometries*, *Comm. Math. Phys.* **57** (1977), no. 2 173–185.

[48] F. Fiamberti, A. Santambrogio, C. Sieg, and D. Zanon, *Wrapping at four loops in N=4 SYM*, *Phys.Lett.* **B666** (2008) 100–105, [arXiv:0712.3522].

[49] C. Sieg, *Superspace computation of the three-loop dilatation operator of N=4 SYM theory*, *Phys.Rev.* **D84** (2011) 045014, [arXiv:1008.3351].

[50] D. Berenstein, D. H. Correa, and S. E. Vazquez, *Quantizing open spin chains with variable length: An Example from giant gravitons*, *Phys.Rev.Lett.* **95** (2005) 191601, [hep-th/0502172].

[51] D. Berenstein and S. E. Vazquez, *Giant magnon bound states from strongly coupled N=4 SYM*, *Phys.Rev.* **D77** (2008) 026005, [arXiv:0707.4669].

[52] D. Berenstein, *On the central charge extension of the N=4 SYM spin chain*, arXiv:1411.5921.

[53] D. Berenstein, D. H. Correa, and S. E. Vazquez, *All loop BMN state energies from matrices*, *JHEP* **0602** (2006) 048, [hep-th/0509015].

[54] Y. Hatsuda and K. Okamura, *Emergent classical strings from matrix model*, *JHEP* **0703** (2007) 077, [hep-th/0612269].

[55] V. Balasubramanian, D. Berenstein, B. Feng, and M.-x. Huang, *D-branes in Yang-Mills theory and emergent gauge symmetry*, *JHEP* **0503** (2005) 006, [hep-th/0411205].

[56] R. d. M. Koch, G. Mashile, and N. Park, *Emergent Threebrane Lattices*, *Phys.Rev.* **D81** (2010) 106009, [arXiv:1004.1108].

[57] R. de Mello Koch, G. Kemp, and S. Smith, *From Large N Nonplanar Anomalous Dimensions to Open Spring Theory*, *Phys.Lett.* **B711** (2012) 398–403, [arXiv:1111.1058].

[58] D. J. Gross, A. Mikhailov, and R. Roiban, *Operators with large R charge in N=4 Yang-Mills theory*, *Annals Phys.* **301** (2002) 31–52, [hep-th/0205066].

[59] A. Santambrogio and D. Zanon, *Exact anomalous dimensions of N=4 Yang-Mills operators with large R charge*, *Phys.Lett.* **B545** (2002) 425–429, [hep-th/0206079].

[60] D. E. Berenstein, J. M. Maldacena, and H. S. Nastase, *Strings in flat space and pp waves from N=4 superYang-Mills*, *JHEP* **0204** (2002) 013, [hep-th/0202021].

[61] N. Beisert, *The SU(2—2) dynamic S-matrix*, *Adv.Theor.Math.Phys.* **12** (2008) 945–979, [hep-th/0511082].

[62] J. Dai, R. Leigh, and J. Polchinski, *New Connections Between String Theories*, *Mod.Phys.Lett.* **A4** (1989) 2073–2083.

[63] E. Witten and D. I. Olive, *Supersymmetry Algebras That Include Topological Charges*, *Phys.Lett.* **B78** (1978) 97.

[64] N. Seiberg and E. Witten, *Electric - magnetic duality, monopole condensation, and confinement in N=2 supersymmetric Yang-Mills theory*, *Nucl.Phys.* **B426** (1994) 19–52, [hep-th/9407087].

[65] J. Minahan and K. Zarembo, *The Bethe ansatz for N=4 superYang-Mills*, *JHEP* **0303** (2003) 013, [hep-th/0212208].

[66] L. Dolan, C. R. Nappi, and E. Witten, *A Relation between approaches to integrability in superconformal Yang-Mills theory*, *JHEP* **0310** (2003) 017, [hep-th/0308089].

[67] D. Berenstein, D. H. Correa, and S. E. Vazquez, *A Study of open strings ending on giant gravitons, spin chains and integrability*, *JHEP* **0609** (2006) 065, [hep-th/0604123].

[68] D. M. Hofman and J. M. Maldacena, *Reflecting magnons*, *JHEP* **0711** (2007) 063, [arXiv:0708.2272].

[69] D. Berenstein and D. Trancanelli, *S-duality and the giant magnon dispersion relation*, *Eur.Phys.J.* **C74** (2014) 2925, [arXiv:0904.0444].

[70] S. R. Das, A. Jevicki, and S. D. Mathur, *Vibration modes of giant gravitons*, *Phys.Rev.* **D63** (2001) 024013, [hep-th/0009019].

[71] J. Polchinski, *Dirichlet Branes and Ramond-Ramond charges*, *Phys.Rev.Lett.* **75** (1995) 4724–4727, [hep-th/9510017].

[72] M. T. Grisaru, R. C. Myers, and O. Tafjord, *SUSY and goliath*, *JHEP* **0008** (2000) 040, [hep-th/0008015].

[73] A. Hashimoto, S. Hirano, and N. Itzhaki, *Large branes in AdS and their field theory dual*, *JHEP* **0008** (2000) 051, [hep-th/0008016].

[74] D. Berenstein, *A Toy model for the AdS / CFT correspondence*, *JHEP* **0407** (2004) 018, [hep-th/0403110].

[75] D. Berenstein, *Strings on conifolds from strong coupling dynamics, part I*, *JHEP* **0804** (2008) 002, [arXiv:0710.2086].

[76] D. E. Berenstein and S. A. Hartnoll, *Strings on conifolds from strong coupling dynamics: Quantitative results*, *JHEP* **0803** (2008) 072, [arXiv:0711.3026].

[77] H. Lin, O. Lunin, and J. M. Maldacena, *Bubbling AdS space and 1/2 BPS geometries*, *JHEP* **0410** (2004) 025, [hep-th/0409174].

[78] N. Beisert, *The Analytic Bethe Ansatz for a Chain with Centrally Extended su(2—2) Symmetry*, *J.Stat.Mech.* **0701** (2007) P01017, [nlin/0610017].

[79] M. Spradlin and A. Volovich, *Dressing the Giant Magnon*, *JHEP* **0610** (2006) 012, [hep-th/0607009].

[80] C. Kalousios, M. Spradlin, and A. Volovich, *Dressing the giant magnon II*, *JHEP* **0703** (2007) 020, [hep-th/0611033].

[81] R. de Mello Koch and S. Ramgoolam, *A double coset ansatz for integrability in AdS/CFT*, *JHEP* **1206** (2012) 083, [arXiv:1204.2153].

[82] M. R. Douglas and N. A. Nekrasov, *Noncommutative field theory*, *Rev.Mod.Phys.* **73** (2001) 977–1029, [hep-th/0106048].

[83] M. R. Douglas, *D-branes and discrete torsion*, hep-th/9807235.

[84] D. Berenstein and R. G. Leigh, *Discrete torsion, AdS / CFT and duality*, *JHEP* **0001** (2000) 038, [hep-th/0001055].

[85] F. Elmetti, A. Mauri, S. Penati, A. Santambrogio, and D. Zanon, *Real versus complex beta-deformation of the N=4 planar super Yang-Mills theory*, *JHEP* **0710** (2007) 102, [arXiv:0705.1483].

[86] N. Bobev and R. Rashkov, *Multispin Giant Magnons*, *Phys.Rev.* **D74** (2006) 046011, [hep-th/0607018].

[87] D. V. Bykov and S. Frolov, *Giant magnons in TsT-transformed AdS(5) x S**5*, *JHEP* **0807** (2008) 071, [arXiv:0805.1070].

[88] J. Fokken, C. Sieg, and M. Wilhelm, *The complete one-loop dilatation operator of planar real β-deformed $\mathcal{N} = 4$ SYM theory*, *JHEP* **1407** (2014) 150, [arXiv:1312.2959].

[89] G. Arutyunov, M. de Leeuw, and S. J. van Tongeren, *Twisting the Mirror TBA*, *JHEP* **1102** (2011) 025, [arXiv:1009.4118].

[90] M. R. Douglas and G. W. Moore, *D-branes, quivers, and ALE instantons*, hep-th/9603167.

[91] S. Gukov, M. Rangamani, and E. Witten, *Dibaryons, strings and branes in AdS orbifold models*, *JHEP* **9812** (1998) 025, [hep-th/9811048].

[92] N. Dorey, T. J. Hollowood, and S. P. Kumar, *S duality of the Leigh-Strassler deformation via matrix models*, *JHEP* **0212** (2002) 003, [hep-th/0210239].

[93] D. Berenstein, V. Jejjala, and R. G. Leigh, *Noncommutative moduli spaces, dielectric tori and T duality*, *Phys.Lett.* **B493** (2000) 162–168, [hep-th/0006168].

[94] F. Ferrari, M. Moskovic, and A. Rovai, *Examples of Emergent Type IIB Backgrounds from Matrices*, *Nucl.Phys.* **B872** (2013) 184–212, [arXiv:1301.3738].

[95] D. Kutasov, J. Marklof, and G. W. Moore, *Melvin models and diophantine approximation*, *Commun.Math.Phys.* **256** (2005) 491–511, [hep-th/0407150].

[96] M. Pirrone, *Giants On Deformed Backgrounds*, *JHEP* **0612** (2006) 064, [hep-th/0609173].

[97] E. Imeroni and A. Naqvi, *Giants and loops in beta-deformed theories*, *JHEP* **0703** (2007) 034, [hep-th/0612032].

[98] R. de Mello Koch, N. Ives, J. Smolic, and M. Smolic, *Unstable giants*, *Phys.Rev.* **D73** (2006) 064007, [hep-th/0509007].

[99] S. Frolov, *Lax pair for strings in Lunin-Maldacena background*, *JHEP* **0505** (2005) 069, [hep-th/0503201].

[100] D. Berenstein, *Reverse geometric engineering of singularities*, *JHEP* **0204** (2002) 052, [hep-th/0201093].

[101] C. Walton, *Representation theory of three-dimensional Sklyanin algebras*, *Nucl.Phys.* **B860** (2012) 167–185, [arXiv:1107.2953].

[102] N. Beisert and R. Roiban, *The Bethe ansatz for Z(S) orbifolds of N=4 super Yang-Mills theory*, *JHEP* **0511** (2005) 037, [hep-th/0510209].

[103] A. Gadde and L. Rastelli, *Twisted Magnons*, *JHEP* **1204** (2012) 053, [arXiv:1012.2097].

[104] E. Witten, *Bound states of strings and p-branes*, *Nucl.Phys.* **B460** (1996) 335–350, [hep-th/9510135].

[105] J. Hoppe, *Quantum theory of a massless relativistic surface and a two-dimensional bound state problem.* PhD thesis, MIT, 1982.

[106] B. de Wit, J. Hoppe, and H. Nicolai, *On the Quantum Mechanics of Supermembranes*, *Nucl.Phys.* **B305** (1988) 545.

[107] T. Banks, W. Fischler, S. Shenker, and L. Susskind, *M theory as a matrix model: A Conjecture*, *Phys.Rev.* **D55** (1997) 5112–5128, [hep-th/9610043].

[108] R. C. Myers, *Dielectric branes*, *JHEP* **9912** (1999) 022, [hep-th/9910053].

[109] N. Kim, T. Klose, and J. Plefka, *Plane wave matrix theory from N=4 superYang-Mills on R x S**3*, *Nucl.Phys.* **B671** (2003) 359–382, [hep-th/0306054].

[110] G. Policastro, D. T. Son, and A. O. Starinets, *The Shear viscosity of strongly coupled N=4 supersymmetric Yang-Mills plasma*, *Phys.Rev.Lett.* **87** (2001) 081601, [hep-th/0104066].

[111] P. Kovtun, D. T. Son, and A. O. Starinets, *Viscosity in strongly interacting quantum field theories from black hole physics*, *Phys.Rev.Lett.* **94** (2005) 111601, [hep-th/0405231].

[112] T. Nishioka and T. Takayanagi, *Fuzzy Ring from M2-brane Giant Torus*, *JHEP* **0810** (2008) 082, [arXiv:0808.2691].

[113] T. Banks, N. Seiberg, and S. H. Shenker, *Branes from matrices*, *Nucl.Phys.* **B490** (1997) 91–106, [hep-th/9612157].

[114] H. Steinacker, *Emergent Geometry and Gravity from Matrix Models: an Introduction*, *Class.Quant.Grav.* **27** (2010) 133001, [arXiv:1003.4134].

[115] D. N. Kabat and W. Taylor, *Linearized supergravity from matrix theory*, *Phys.Lett.* **B426** (1998) 297–305, [hep-th/9712185].

[116] W. Taylor and M. Van Raamsdonk, *Multiple D0-branes in weakly curved backgrounds*, *Nucl.Phys.* **B558** (1999) 63–95, [hep-th/9904095].

[117] K. Millar, W. Taylor, and M. Van Raamsdonk, *D particle polarizations with multipole moments of higher dimensional branes*, hep-th/0007157.

[118] W. Taylor, *M(atrix) theory: Matrix quantum mechanics as a fundamental theory*, *Rev.Mod.Phys.* **73** (2001) 419–462, [hep-th/0101126].

[119] D. N. Kabat and W. Taylor, *Spherical membranes in matrix theory*, *Adv.Theor.Math.Phys.* **2** (1998) 181–206, [hep-th/9711078].

[120] S. Kachru and E. Silverstein, *4-D conformal theories and strings on orbifolds*, *Phys.Rev.Lett.* **80** (1998) 4855–4858, [hep-th/9802183].

[121] M. R. Douglas, B. R. Greene, and D. R. Morrison, *Orbifold resolution by D-branes*, *Nucl.Phys.* **B506** (1997) 84–106, [hep-th/9704151].

[122] D. Berenstein and R. G. Leigh, *Resolution of stringy singularities by noncommutative algebras*, *JHEP* **0106** (2001) 030, [hep-th/0105229].

[123] M. B. Hastings and T. A. Loring, *Almost commuting matrices, localized wannier functions, and the quantum hall effect*, *Journal of Mathematical Physics* **51** (2010), no. 1 –, [arXiv:0910.5490].

[124] R. Delgadillo-Blando and D. O'Connor, *Matrix geometries and Matrix Models*, *JHEP* **1211** (2012) 057, [arXiv:1203.6901].

[125] H. Steinacker, *Quantized gauge theory on the fuzzy sphere as random matrix model*, *Nucl.Phys.* **B679** (2004) 66–98, [hep-th/0307075].

[126] M. B. Hastings and T. A. Loring, *Topological insulators and c-algebras: Theory and numerical practice*, *Annals of Physics* **326** (2011), no. 7 1699 – 1759, [arXiv:1012.1019]. July 2011 Special Issue.

[127] J. Arnlind, M. Bordemann, L. Hofer, J. Hoppe, and H. Shimada, *Fuzzy Riemann surfaces*, *JHEP* **0906** (2009) 047, [hep-th/0602290].

[128] J. Arnlind, M. Bordemann, L. Hofer, J. Hoppe, and H. Shimada, *Noncommutative riemann surfaces by embeddings in* $\mathbb{R}^3$, *Communications in Mathematical Physics* **288** (2009), no. 2 403–429, [arXiv:0711.2588].

[129] K. Dasgupta, M. M. Sheikh-Jabbari, and M. Van Raamsdonk, *Matrix perturbation theory for M theory on a PP wave*, *JHEP* **0205** (2002) 056, [hep-th/0205185].

[130] H. Shimada, *Membrane topology and matrix regularization*, *Nucl.Phys.* **B685** (2004) 297–320, [hep-th/0307058].

[131] H. Shimada, *beta-deformation for matrix model of M-theory*, *Nucl.Phys.* **B813** (2009) 283–314, [arXiv:0804.3236].

[132] W. Taylor and M. Van Raamsdonk, *Supergravity currents and linearized interactions for matrix theory configurations with fermionic backgrounds*, *JHEP* **9904** (1999) 013, [hep-th/9812239].

[133] A. Chatzistavrakidis, H. Steinacker, and G. Zoupanos, *Intersecting branes and a standard model realization in matrix models*, *JHEP* **1109** (2011) 115, [arXiv:1107.0265].

[134] M. Berkooz, M. R. Douglas, and R. G. Leigh, *Branes intersecting at angles*, *Nucl.Phys.* **B480** (1996) 265–278, [hep-th/9606139].

[135] D. Berenstein and D. Trancanelli, *Dynamical tachyons on fuzzy spheres*, *Phys.Rev.* **D83** (2011) 106001, [arXiv:1011.2749].

[136] A. Hanany and E. Witten, *Type IIB superstrings, BPS monopoles, and three-dimensional gauge dynamics*, *Nucl.Phys.* **B492** (1997) 152–190, [hep-th/9611230].

[137] N. Itzhaki, J. M. Maldacena, J. Sonnenschein, and S. Yankielowicz, *Supergravity and the large N limit of theories with sixteen supercharges*, *Phys.Rev.* **D58** (1998) 046004, [hep-th/9802042].

[138] J. L. Karczmarek and K. H.-C. Yeh, *Noncommutative spaces and matrix embeddings on flat* R^{2n+1}, arXiv:1506.0718.

[139] M. H. de Badyn, J. L. Karczmarek, P. Sabella-Garnier, and K. H.-C. Yeh, *Emergent geometry of membranes*, arXiv:1506.0203.

[140] J. L. Boersema and T. A. Loring, *K-Theory for Real C*-algebras via Unitary Elements with Symmetries*, arXiv:1504.0328.

[141] M. Berkooz and M. R. Douglas, *Five-branes in M(atrix) theory*, *Phys.Lett.* **B395** (1997) 196–202, [hep-th/9610236].

[142] C. Pedder, J. Sonner, and D. Tong, *The Berry Phase of D0-Branes*, *JHEP* **0803** (2008) 065, [arXiv:0801.1813].

[143] M. Srednicki, *Chaos and quantum thermalization*, *Phys. Rev. E* **50** (Aug, 1994) 888–901, [cond-mat/9403051].

[144] M. R. Douglas, D. N. Kabat, P. Pouliot, and S. H. Shenker, *D-branes and short distances in string theory*, *Nucl.Phys.* **B485** (1997) 85–127, [hep-th/9608024].

[145] D. Berenstein and R. Corrado, *M(atrix) theory in various dimensions*, *Phys.Lett.* **B406** (1997) 37–43, [hep-th/9702108].

[146] K. Becker, M. Becker, J. Polchinski, and A. A. Tseytlin, *Higher order graviton scattering in M(atrix) theory*, *Phys.Rev.* **D56** (1997) 3174–3178, [hep-th/9706072].

[147] E. P. Verlinde, *On the Origin of Gravity and the Laws of Newton*, *JHEP* **1104** (2011) 029, [arXiv:1001.0785].

[148] C. Asplund, D. Berenstein, and D. Trancanelli, *Evidence for fast thermalization in the plane-wave matrix model*, *Phys.Rev.Lett.* **107** (2011) 171602, [arXiv:1104.5469].

[149] D. Frenkel and B. Smit, *Understanding Molecular Simulation.* Academic Press, Inc., Orlando, FL, USA, 2nd ed., 2001.

[150] K.-P. Ho and J. M. Kahn, *Statistics of group delays in multimode fiber with strong mode coupling, supplement*, *Journal of Lightwave Technology* **29** (2011) 3119–3128, [arXiv:1104.4527].

[151] F. Bornemann, *Traceless gue: Four centered fermions*, Jan, 2012. `http://mathoverflow.net/questions/87019`.

[152] S. Catterall and T. Wiseman, *Black hole thermodynamics from simulations of lattice Yang-Mills theory*, *Phys.Rev.* **D78** (2008) 041502, [arXiv:0803.4273].

[153] M. Hanada, Y. Hyakutake, J. Nishimura, and S. Takeuchi, *Higher derivative corrections to black hole thermodynamics from supersymmetric matrix quantum mechanics*, *Phys.Rev.Lett.* **102** (2009) 191602, [arXiv:0811.3102].

[154] P. Riggins and V. Sahakian, *On black hole thermalization, D0 brane dynamics, and emergent spacetime*, *Phys.Rev.* **D86** (2012) 046005, [arXiv:1205.3847].

[155] G. Z. Baseyan, S. G. Matinyan, and G. K. Savvidi *JETP Lett.* **29** (1979) 585.

[156] B. Chirikov and D. Shepelyansky, *Stochastic Oscillation of Classical Yang-Mills Fields. (In Russian)*, *JETP Lett.* **34** (1981) 163–166.

[157] I. Y. Aref'eva, P. Medvedev, O. Rytchkov, and I. Volovich, *Chaos in M(atrix) theory*, *Chaos Solitons Fractals* **10** (1999) 213–223, [hep-th/9710032].

[158] S. G. Matinyan, G. Savvidy, and N. Ter-Arutunian Savvidy, *Stochasticity of Classical Yang-Mills Mechanics and Its Elimination by Higgs Mechanism. (In Russian)*, *JETP Lett.* **34** (1981) 590–593.

[159] S. R. Das and S. D. Mathur, *Comparing decay rates for black holes and D-branes*, *Nucl.Phys.* **B478** (1996) 561–576, [hep-th/9606185].

[160] I. R. Klebanov, *World volume approach to absorption by nondilatonic branes*, *Nucl.Phys.* **B496** (1997) 231–242, [hep-th/9702076].

[161] K. D. Kokkotas and B. G. Schmidt, *Quasinormal modes of stars and black holes*, *Living Rev.Rel.* **2** (1999) 2, [gr-qc/9909058].

[162] E. Berti, V. Cardoso, and A. O. Starinets, *Quasinormal modes of black holes and black branes*, *Class.Quant.Grav.* **26** (2009) 163001, [arXiv:0905.2975].

[163] R. Konoplya and A. Zhidenko, *Quasinormal modes of black holes: From astrophysics to string theory*, *Rev.Mod.Phys.* **83** (2011) 793–836, [arXiv:1102.4014].

[164] C. Manderfeld, J. Weber, and F. Haake, *Classical versus quantum time evolution of (quasi-) probability densities at limited phase-space resolution*, *Journal of Physics A: Mathematical and General* **34** (2001), no. 46 9893.

[165] J. P. Eckmann and D. Ruelle, *Ergodic theory of chaos and strange attractors*, *Rev. Mod. Phys.* **57** (Jul, 1985) 617–656.

[166] G. 't Hooft, *A Planar Diagram Theory for Strong Interactions*, *Nucl.Phys.* **B72** (1974) 461.

[167] E. Witten, *Baryons in the 1/n Expansion*, *Nucl.Phys.* **B160** (1979) 57.

[168] L. G. Yaffe, *Large n Limits as Classical Mechanics*, *Rev.Mod.Phys.* **54** (1982) 407.

[169] D. Berenstein, R. Cotta, and R. Leonardi, *Numerical tests of AdS/CFT at strong coupling*, *Phys.Rev.* **D78** (2008) 025008, [arXiv:0801.2739].

[170] D. Berenstein and H. Nastase, *On light cone string field theory from superYang-Mills and holography*, hep-th/0205048.

[171] D. Marolf and S. F. Ross, *Plane waves: To infinity and beyond!*, *Class.Quant.Grav.* **19** (2002) 6289–6302, [hep-th/0208197].

[172] P. Gaspard, *Hamiltonian dynamics, nanosystems, and nonequilibrium statistical mechanics*, *Physica A: Statistical Mechanics and its Applications* **369** (2006), no. 1 201 – 246. Fundamental Problems in Statistical Physics Proceedings of the 11th International Summerschool on 'Fundamental problems in statistical physics', September 4–17, 2005, Leuven, Belgium 11th International Summerschool on 'Fundamental problems in statistical physics'.

[173] S. Catterall and T. Wiseman, *Towards lattice simulation of the gauge theory duals to black holes and hot strings*, *JHEP* **0712** (2007) 104, [arXiv:0706.3518].

[174] K. N. Anagnostopoulos, M. Hanada, J. Nishimura, and S. Takeuchi, *Monte Carlo studies of supersymmetric matrix quantum mechanics with sixteen supercharges at finite temperature*, *Phys.Rev.Lett.* **100** (2008) 021601, [arXiv:0707.4454].

[175] S. Catterall and G. van Anders, *First Results from Lattice Simulation of the PWMM*, *JHEP* **1009** (2010) 088, [arXiv:1003.4952].

[176] G. T. Horowitz and A. Strominger, *Black strings and P-branes*, *Nucl.Phys.* **B360** (1991) 197–209.

[177] G. T. Horowitz and J. Polchinski, *A Correspondence principle for black holes and strings*, *Phys.Rev.* **D55** (1997) 6189–6197, [hep-th/9612146].

[178] S. D. Mathur, *The Fuzzball proposal for black holes: An Elementary review*, *Fortsch.Phys.* **53** (2005) 793–827, [hep-th/0502050].

[179] E. Brzin, C. Itzykson, G. Parisi, and J. B. Zuber, *Planar diagrams*, *Comm. Math. Phys.* **59** (1978), no. 1 35–51.

[180] P. K. Kovtun and A. O. Starinets, *Quasinormal modes and holography*, *Phys.Rev.* **D72** (2005) 086009, [hep-th/0506184].

[181] D. Marolf and M. Rangamani, *Causality and the AdS Dirichlet problem*, *JHEP* **1204** (2012) 035, [arXiv:1201.1233].

[182] N. Iqbal and H. Liu, *Universality of the hydrodynamic limit in AdS/CFT and the membrane paradigm*, *Phys.Rev.* **D79** (2009) 025023, [arXiv:0809.3808].

[183] R. Florido, J. M. Martín-González, and J. M. Gomez Llorente, *Locating pollicott-ruelle resonances in chaotic dynamical systems: A class of numerical schemes*, *Phys. Rev. E* **66** (Oct, 2002) 046208.

[184] P. Gaspard, *Chaos, Scattering and Statistical Mechanics.* Cambridge University Press, 1998. Cambridge Books Online.

[185] U. H. Danielsson, A. Guijosa, and M. Kruczenski, *Brane anti-brane systems at finite temperature and the entropy of black branes*, *JHEP* **0109** (2001) 011, [hep-th/0106201].

[186] D. N. Kabat and G. Lifschytz, *Tachyons and black hole horizons in gauge theory*, *JHEP* **9812** (1998) 002, [hep-th/9806214].

[187] A. Almheiri, D. Marolf, J. Polchinski, D. Stanford, and J. Sully, *An Apologia for Firewalls*, *JHEP* **1309** (2013) 018, [arXiv:1304.6483].

[188] S. B. Giddings and Y. Shi, *Effective field theory models for nonviolent information transfer from black holes*, *Phys.Rev.* **D89** (2014), no. 12 124032, [arXiv:1310.5700].

[189] N. Iizuka, D. Kabat, S. Roy, and D. Sarkar, *Black Hole Formation at the Correspondence Point*, *Phys.Rev.* **D87** (2013) 126010, [arXiv:1303.7278].

[190] T. Wiseman, *On black hole thermodynamics from super Yang-Mills*, *JHEP* **1307** (2013) 101, [arXiv:1304.3938].

[191] V. Kaplunovsky and M. Weinstein, *SPACE-TIME: ARENA OR ILLUSION?*, *Phys.Rev.* **D31** (1985) 1879.

[192] L. Susskind, *String theory and the principles of black hole complementarity*, *Phys.Rev.Lett.* **71** (1993) 2367–2368, [hep-th/9307168].

[193] G. Horowitz, A. Lawrence, and E. Silverstein, *Insightful D-branes*, *JHEP* **0907** (2009) 057, [arXiv:0904.3922].

[194] A. Almheiri, D. Marolf, J. Polchinski, and J. Sully, *Black Holes: Complementarity or Firewalls?*, *JHEP* **1302** (2013) 062, [arXiv:1207.3123].

[195] J. Ambjorn, J. Jurkiewicz, and R. Loll, *Spectral dimension of the universe*, *Phys.Rev.Lett.* **95** (2005) 171301, [hep-th/0505113].

[196] S. Carlip, *The Small Scale Structure of Spacetime*, arXiv:1009.1136.

[197] S. Carlip, *Logarithmic corrections to black hole entropy from the Cardy formula*, *Class.Quant.Grav.* **17** (2000) 4175–4186, [gr-qc/0005017].

[198] K. Dasgupta, M. M. Sheikh-Jabbari, and M. Van Raamsdonk, *Protected multiplets of M theory on a plane wave*, *JHEP* **0209** (2002) 021, [hep-th/0207050].

[199] J. Hoppe and K.-M. Lee, *New BPS configurations of BMN matrix theory*, *JHEP* **0806** (2008) 041, [arXiv:0712.3616].

[200] S. Hellerman, D. Orlando, S. Reffert, and M. Watanabe, *On the CFT Operator Spectrum at Large Global Charge*, arXiv:1505.0153.

[201] D.-s. Bak, *SUPERSYMMETRIC BRANES IN THE MATRIX MODEL OF A PP WAVE BACKGROUND*, *Phys.Rev.* **D67** (2003) 045017, [hep-th/0204033].

[202] D. Bak, S. Siwach, and H.-U. Yee, *1/2 BPS geometries of M2 giant gravitons*, *Phys.Rev.* **D72** (2005) 086010, [hep-th/0504098].

[203] J. Arnlind and J. Hoppe, *Classical solutions in the BMN matrix model*, hep-th/0312166.

[204] J. Arnlind, J. Hoppe, and S. Theisen, *Spinning membranes*, *Phys.Lett.* **B599** (2004) 118–128.

[205] H. Steinacker, *Split noncommutativity and compactified brane solutions in matrix models*, *Prog.Theor.Phys.* **126** (2011) 613–636, [arXiv:1106.6153].

[206] A. P. Polychronakos, H. Steinacker, and J. Zahn, *Brane compactifications and 4-dimensional geometry in the IKKT model*, *Nucl.Phys.* **B875** (2013) 566–598, [arXiv:1302.3707].

[207] H. C. Steinacker, *Spinning squashed extra dimensions and chiral gauge theory from N=4 SYM*, *Nucl.Phys.* **B896** (2015) 212–243, [arXiv:1411.3139].

[208] C. Vafa and E. Witten, *A Strong coupling test of S duality*, *Nucl.Phys.* **B431** (1994) 3–77, [hep-th/9408074].

[209] N. Dorey, *An Elliptic superpotential for softly broken N=4 supersymmetric Yang-Mills theory*, *JHEP* **9907** (1999) 021, [hep-th/9906011].

[210] S. A. Hartnoll, C. P. Herzog, and G. T. Horowitz, *Building a Holographic Superconductor*, *Phys.Rev.Lett.* **101** (2008) 031601, [arXiv:0803.3295].

[211] G. 't Hooft, *Magnetic Monopoles in Unified Gauge Theories*, *Nucl.Phys.* **B79** (1974) 276–284.

[212] A. M. Polyakov, *Particle Spectrum in the Quantum Field Theory*, *JETP Lett.* **20** (1974) 194–195.

[213] E. Witten, *Supersymmetry and Morse theory*, *J.Diff.Geom.* **17** (1982) 661–692.

[214] Y. Matsumoto, *An Introduction to Morse Theory (Translations of Mathematical Monographs, Vol 208).* American Mathematical Society, Providence, Rhode Island, 2002.

[215] M. Hutchings, *Lecture notes on morse homology (with an eye towards floer theory and pseudoholomorphic curves)*, (Fall 2002). Available at `https://math.berkeley.edu/~hutching/`.

[216] J. Armas, T. Harmark, N. A. Obers, M. Orselli, and A. V. Pedersen, *Thermal Giant Gravitons*, *JHEP* **1211** (2012) 123, [arXiv:1207.2789].

[217] N. Seiberg, *Why is the matrix model correct?*, *Phys.Rev.Lett.* **79** (1997) 3577–3580, [hep-th/9710009].

[218] L. Randall, Y. Shirman, and R. von Unge, *Brane boxes: Bending and beta functions*, *Phys.Rev.* **D58** (1998) 105005, [hep-th/9806092].

[219] R. G. Leigh and M. Rozali, *Brane boxes, anomalies, bending and tadpoles*, *Phys.Rev.* **D59** (1999) 026004, [hep-th/9807082].

[220] O. Aharony, O. Bergman, D. L. Jafferis, and J. Maldacena, *N=6 superconformal Chern-Simons-matter theories, M2-branes and their gravity duals*, *JHEP* **0810** (2008) 091, [arXiv:0806.1218].

[221] D. Berenstein and D. Trancanelli, *Three-dimensional N=6 SCFT's and their membrane dynamics*, *Phys.Rev.* **D78** (2008) 106009, [arXiv:0808.2503].

[222] D. Berenstein and J. Park, *The BPS spectrum of monopole operators in ABJM: Towards a field theory description of the giant torus*, *JHEP* **1006** (2010) 073, [arXiv:0906.3817].

[223] S. Kim and K. Madhu, *Aspects of monopole operators in N=6 Chern-Simons theory*, *JHEP* **0912** (2009) 018, [arXiv:0906.4751].

[224] S. Kovacs, Y. Sato, and H. Shimada, *Membranes from monopole operators in ABJM theory: Large angular momentum and M-theoretic AdS_4/CFT_3*, *PTEP* **2014** (2014), no. 9 093B01, [arXiv:1310.0016].